doi.org/10.26434/chemrxiv.12485786.v1

Redox-neutral Photocatalytic C-H Carboxylation of Arenes and Styrenes with CO2

Matthias Schmalzbauer, Thomas D. Svejstrup, Florian Fricke, Peter Brandt, Magnus J. Johansson, Giulia Bergonzini, Burkhard Koenig

Submitted date: 16/06/2020 • Posted date: 17/06/2020

Citation information: Schmalzbauer, Matthias; Svejstrup, Thomas D.; Fricke, Florian; Brandt, Peter; Johansson, Magnus J.; Bergonzini, Giulia; et al. (2020): Redox-neutral Photocatalytic C-H Carboxylation of Arenes and Styrenes with CO2. ChemRxiv. Preprint. https://doi.org/10.26434/chemrxiv.12485786.v1

Carbon dioxide (CO_2) is an attractive one-carbon (C1) building block in terms of sustainability and abundance. However, its low reactivity limits applications in organic synthesis as typically high-energy reagents are required to drive transformations. Here, we present a redox-neutral C–H carboxylation of arenes and styrenes using a photocatalytic approach. Upon blue-light excitation, the anthrolate anion photocatalyst is able to reduce many aromatic compounds to their corresponding radical anions, which react with CO_2 to afford carboxylic acids. High-throughput screening and computational analysis suggest that a correct balance between electron affinity and nucleophilicity of substrates is essential. This novel methodology enables the carboxylation of numerous aromatic compounds, including many that are not tolerated in classical carboxylation chemistry. Over 50 examples of C–H functionalizations using CO_2 or ketones illustrate a broad applicability. The method opens new opportunities for late-stage C–H carboxylation and valorization of common arenes.

File list (2)

Redox-neutral Photocatalytic C–H Carboxylation of Arenes and Styrenes with CO_2

Matthias Schmalzbauer,[1,5] Thomas D. Svejstrup,[2,5] Florian Fricke,[1] Peter Brandt,[2] Magnus J. Johansson,[2,3] Giulia Bergonzini,[2,*] and Burkhard König[1,4,**]

[1]Faculty of Chemistry and Pharmacy, University of Regensburg, Germany
[2]Medicinal Chemistry, Research and Early Development Cardiovascular, Renal and Metabolism, BioPharmaceuticals R&D, AstraZeneca, Gothenburg, Sweden
[3]Department of Organic Chemistry, Stockholm University, Stockholm 10691, Sweden
[4]Lead Contact
[5]These authors contributed equally
*Correspondence: giulia.bergonzini@astrazeneca.com
**Correspondence: burkhard.koenig@ur.de

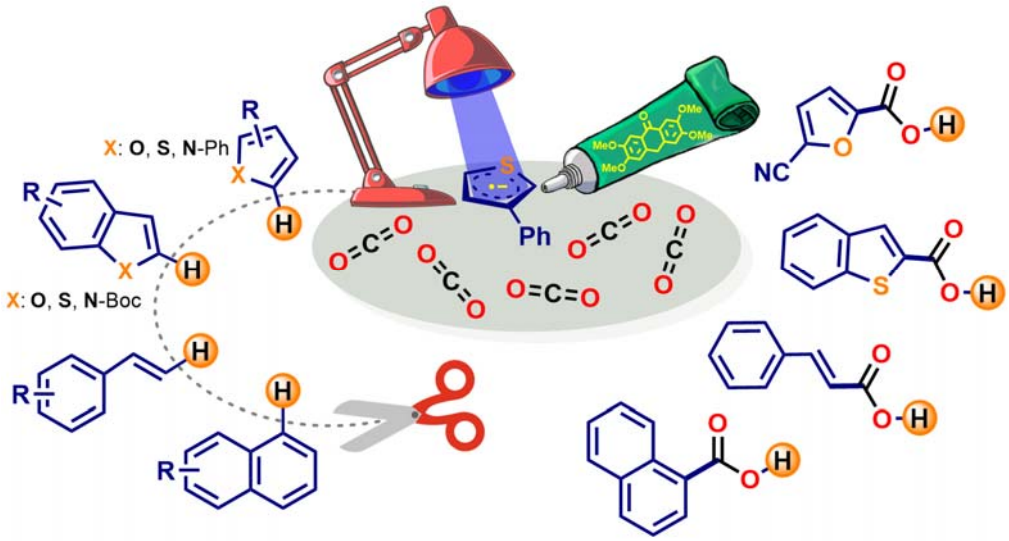

Abstract: Carbon dioxide (CO_2) is an attractive one-carbon (C1) building block in terms of sustainability and abundance. However, its low reactivity limits applications in organic synthesis as typically high-energy reagents are required to drive transformations. Here, we present a redox-neutral C−H carboxylation of arenes and styrenes using a photocatalytic approach. Upon blue-light excitation, the anthrolate anion photocatalyst is able to reduce many aromatic compounds to their corresponding radical anions, which react with CO_2 to afford carboxylic acids. High-throughput screening and computational analysis suggest that a correct balance between electron affinity and nucleophilicity of substrates is essential. This novel methodology enables the carboxylation of numerous aromatic compounds, including many that are not tolerated in classical carboxylation chemistry. Over 50 examples of C−H functionalizations using CO_2 or ketones illustrate a broad applicability. The method opens new opportunities for late-stage C−H carboxylation and valorization of common arenes.

Keywords: Photocatalysis, carbon dioxide, carboxylation, C−H functionalization, radical anion, carboxylic acid, 9-anthrone, styrene, heteroarenes

INTRODUCTION

Photosynthesis, the most important photobiological process on our planet, allows photoautotrophs to store energy in form of chemical bonds by absorbing sunlight. Driven by that energy, CO_2 is captured from the atmosphere and serves as carbon feedstock for the organisms to build up sugars and biomass in the Calvin cycle.[1]

Electrochemical and catalytic dihydrogen reductions of carbon dioxide have been developed in the field of renewable energy storage.[2–4] However, the use of CO_2 as a C1 building block in organic synthesis has received far less attention despite resembling the principle of biological carbon fixing process the most.[5] The high thermodynamic stability and kinetic inertness of CO_2 require the use of stoichiometric amounts of reactive reaction partners such as Grignard reagents or organolithium compounds for chemical conversion.[6] Aiming for a better efficiency and an increased atom economy, a variety of catalytic carboxylation methods have been developed. These processes make use of readily available aryl bromides which undergo carboxylation with CO_2 in the presence of catalytic $Pd(OAc)_2$, as reported by Martín and Correa.[7] Daugulis showed that Cu(I) catalyzes the carboxylation of aryl iodides.[8] Tsuji and co-workers applied $NiCl_2(PPh_3)_2$ to carboxylate more inert aryl and vinyl chlorides under 1 atm CO_2 at room temperature.[9] The reaction scope was extended to sulfonates,[10] ester derivatives,[11,12] allylic alcohols,[13] benzylic ammonium salts,[14] arylsulfonium salts[15] and unsaturated hydrocarbons.[16–20] However, all these systems require stoichiometric reducing reagents based on Et_2Zn, $AlMe_3$, Mn and Zn powder or prefunctionalized starting materials.[21] Electrical current may also be used to drive reductive carboxylation chemistry. Buckley and co-workers reported the regioselective hydrocarboxylation of styrenes using a non-sacrificial electrode system.[22] Ackermann *et al.* showed that allyl chlorides derived from cinnamyl chloride are carboxylated in presence of a cobalt catalyst.[23] Concomitantly, difunctionalizations of alkenes *via* radical addition and subsequent reduction were reported affording thio-,[24] carbo-[25–27] phosphono-[28] or silylcarboxylation[27] products.

Non-catalytic $C(sp^2)$−H carboxylations typically require stoichiometric amounts of either strong bases, such as NaH[29] or LiO^tBu,[30,31] or Lewis acids, like AlX_3 (X = Br, Cl),[32–35] Me_2AlCl[36] and $EtAlCl_2$[37,38] to activate CO_2. Transition metal-catalyzed directed $C(sp^2)$−H carboxylation reactions have been reported with Au,[39] Cu[39,40] and Rh[41] complexes.[42] Moreover, direct carboxylation of non-activated $C(sp^2)$−H was reported in molten alkali carbonate salts under elevated temperatures (>200 °C) and high CO_2 pressure.[43,44]

More recently, photoredox catalysis has been applied in the field of carboxylation chemistry. Photocatalytic carboxylation of aryl-[45,46] and alkyl-halides[46] were the first transformations to be reported, followed by direct C−H carboxylation of alkynes[47] and styrenes.[48,49] These methods utilize a dual catalytic approach consisting of a photocatalyst and an *in situ* generated low-valent transition metal complex enabled by an excess amount of a sacrificial electron donor. Visible-light mediated benzylic C−H carboxylation was recently reported by the use of 4CzIPN and an organo-silanethiol HAT reagent which allowed to generate carbanions.[50]

Direct UV-light excitation of polyaromatic hydrocarbons in presence of sacrificial amines and CO_2 was reported to yield the corresponding carboxylic acids.[51,52] Jamison employed *p*-terphenyl, which forms a radical anion upon UV-light excitation in the presence of amines.[53] The *p*-terphenyl radical anion is capable of the kinetically slow one-electron reduction of CO_2 to its radical anion, which is used in the hydrocarboxylation of styrenes (see Scheme 1). Murakami and co-workers employed UV-excited xanthone as hydrogen-atom-transfer (HAT) reagent in combination with a Cu complex or a Ni catalyst to carboxylate allylic[54] and benzylic[55] C(sp^3)–H respectively.

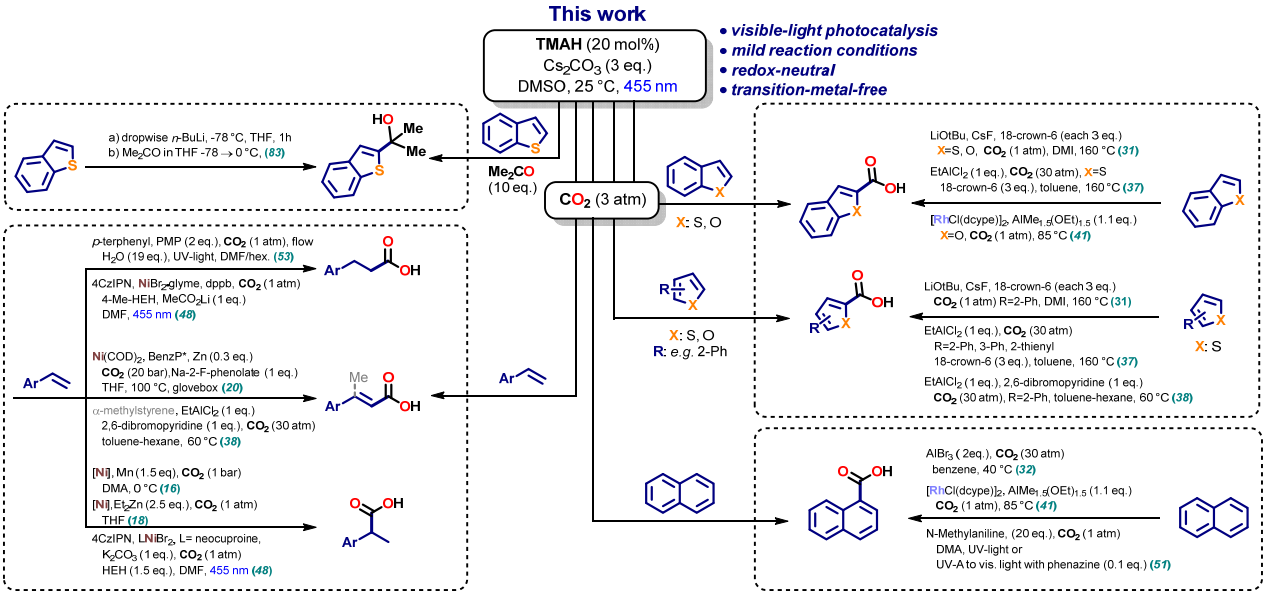

Scheme 1. Overview of representative literature procedures for the direct C–H carboxylation with CO_2 or hydroxyalkylation with acetone considering the herein discussed substrate classes.

However, despite the great progress achieved in thermal and photochemical carboxylation methods, the efficient redox-neutral carboxylation of C(sp^2)–H in arenes, heteroarenes and alkenes remains challenging. Here, we report a mechanistically different catalytic approach in which aromatic compounds are converted into their radical anions by photoinduced single-electron transfer (SET) from a visible-light excited anthrolate anion. The generated nucleophilic arene radical anions react with CO_2 to provide (hetero)aromatic carboxylic- and cinnamic acids.

RESULTS & DISCUSSION

Recently, we showed that upon photoexcitation, the anionic form of commercially available 9-anthrone and derivatives (Scheme 2 and Figure S6, Supplemental Information) readily generate strong reductants capable of activating aryl chlorides.[56] While comparing reported reduction potentials of various aromatic compounds, we noticed that many arenes lay within the range of the approximated excited state oxidation potential of the strongest

photo-reductant 2,3,6,7-tetramethoxyanthracen-9(10*H*)-one (**TMAH**) [E_{ox} (**TMA**$^{\bullet}$/**TMA**$^{-*}$) = −2.92 V *vs.* SCE] shown in that series. We thus envisioned a direct activation of arenes *via* radical anion formation, which may subsequently react with CO_2 to form aromatic carboxylic acids. Strong carbon nucleophiles (*e.g.* organolithium and -magnesium reagents)[57–60] or carbanions are well known to react with CO_2. By contrast, aromatic radical anions formed in the presence of alkali metal have always been considered poor nucleophiles,[61] yet still showed reactivity towards CO_2.[62,63] With a strongly reducing photoredox catalyst in hand and inspired by early literature reports, we questioned if a similar reactivity of aromatic radical anions towards carbon dioxide can be obtained under much milder photocatalytic conditions.

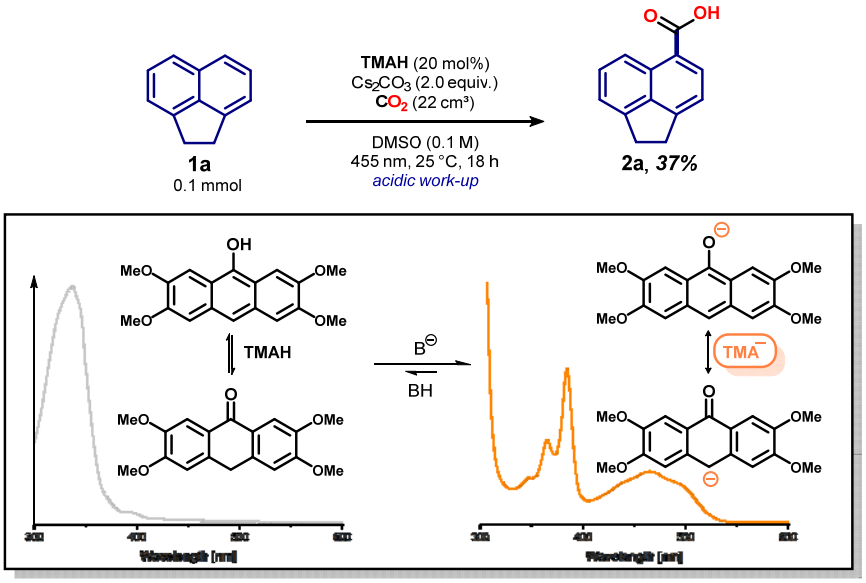

Scheme 2. (top) Photocatalytic C−H carboxylation of acenaphthene **1a**; (bottom) Base-promoted formation of TMA^{-} and the influence on the absorption spectrum.

Initial experiments and optimization

We chose acenaphthene (**1a**, Scheme 2) as a model substrate and applied the established combination of **TMAH** as the photocatalyst and cesium carbonate as the base. To our delight, after 18 hours of irradiation with blue LED light and acidic work-up, the desired carboxylic acid **2a** could be isolated in 37% yield as a single regioisomer. Encouraged by this first result we run an intensive screening of the reaction conditions (Table 1). During the optimization studies, we observed that the reaction outcome was dependent on the amount of Cs_2CO_3. The use of less than 3 equivalents of base led to significantly lower product yield (entry 2) while more equivalents of Cs_2CO_3 reduced the yield (entry 3). A lower catalyst loading reduced the overall amount of base required, while the carboxylated product **2a** was still obtained in good yield (entry 4-5). K_2CO_3, although being scarcely soluble in DMSO, was also able to promote the carboxylation reaction and useful product yields were obtained in combination with crown-ether (entry 6). Monitoring the reaction progress over time (Figure S8, Supplemental

Information) showed that the reaction was not complete after 6 hours (entry 7). An overpressure of CO_2 was found to be beneficial for the reaction outcome (entries 8 and 9). The solubility of CO_2 is reported to be higher in DMF compared to DMSO, yet better yield was obtained in the latter (entry 10).[64] When using green light (535 nm), a reduced product yield was obtained (entry 11), which can be explained by both weaker catalyst absorption and LED radiant flux. Control experiments revealed that all reagents and light are crucial, as no product was detected in the absence of either photocatalyst, cesium carbonate, carbon dioxide or light (entry 12-15).

Table 1. Optimized reaction conditions and effects upon deviation.

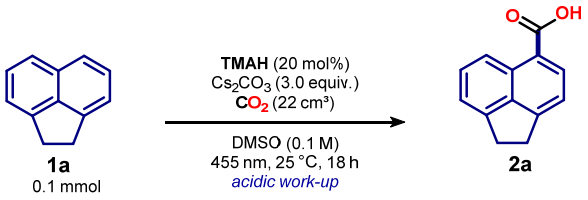

Entry	Deviations from optimized conditions	Yield 2a [%][a]
1	**none**	**68**[b]
2	Cs_2CO_3 (2 equiv.)	37[b]
3	Cs_2CO_3 (4 equiv.)	59
4	**TMAH** (5 mol%), Cs_2CO_3 (2 equiv.)	54
5	**TMAH** (10 mol%), Cs_2CO_3 (2 equiv.)	60
6[c]	**TMAH** (10 mol%), K_2CO_3 instead of Cs_2CO_3, 18-crown-6	47
7	6 hours instead of 18 hours	44
8	no CO_2 pressure (1 atm)	37
9	11 cm³ CO_2 instead of 22 cm³	48
10	DMF instead of DMSO	35
11[d]	535 nm instead of 455 nm	29
12	no **TMAH**	n.d.
13	no Cs_2CO_3	n.d.
14	N_2 (1 atm) instead of CO_2	n.d.
15[e]	no light	n.d.

Optimized reaction conditions: **1a** (0.1 mmol), **TMAH** (20 mol%) and Cs_2CO_3 (0.3 mmol) were added to a 5 mL crimp top vial equipped with a stirring bar. The vial was sealed, evacuated and backfilled with CO_2 (5×). Degassed, anhydrous DMSO (1 mL) was added *via* syringe. The septum was further sealed with Parafilm® and gaseous CO_2 (22 cm³) was added to the headspace *via* syringe. While stirring, the reaction was irradiated from the bottom side (blue LED, 455 ± 15 nm) and constant temperature was maintained by an aluminum cooling block and a water-cooling circuit. For complete optimization table, please see Table S1, Supplemental Information. n.d. = not detected. [a] Product yield was determined after acidic work-up by crude ^{1}H-NMR with an internal standard. [b] Combined isolated yield of four reactions. [c] Crown ether 18-crown-6 (1 equiv.) was added to the reaction. [d] Radiant flux is lowered by a factor of 8 compared to 455 nm LED (see Supplemental Information). [e] Reaction mixture was stirred in the dark.

Substrate scope of the carboxylation reaction

With the optimized reaction conditions in hand (*cf.*, Table 1), we explored the scope of this novel transformation. Naphthalene derivatives were investigated, as their reported potentials are in a feasible range (−2.49 up to −2.65 V *vs.* SCE)[65] for reduction by the photocatalyst (Scheme 3). We were pleased to see that unsubstituted as well as substituted naphthalene derivatives were converted to the corresponding aromatic carboxylic acids (**2b-g**) and could be isolated in useful yields. The regioselectivity of the reaction was found to be affected by strong electron-donating groups (−OMe **2c**, −NMe_2 **2d**) in the C1-position giving selectively 5-naphtoic acids as single regioisomers. In contrast, the directing effect of electronically neutral substituents (−Me, **2e**) was minor and led to a mixture of 4- and 5-naphtoic acid. Remarkably, carboxylation in the C8-position was not observed. Notably, unprotected hydroxyl groups (**2f**, **2g**) were tolerated. Utilizing 1-naphthol (**1f**) led to the formation of two regioisomers of the corresponding acid in 2- and 4-position. 2,7-Dihydroxynaphthalene (**1g**) reacted smoothly under our reaction conditions to yield the corresponding 1-naphtoic acid **2g** as a single regioisomer. Quinoline (**1h**), isoquinoline or quinazoline, although quenching the photoexcited state of the catalyst, failed to yield any product.

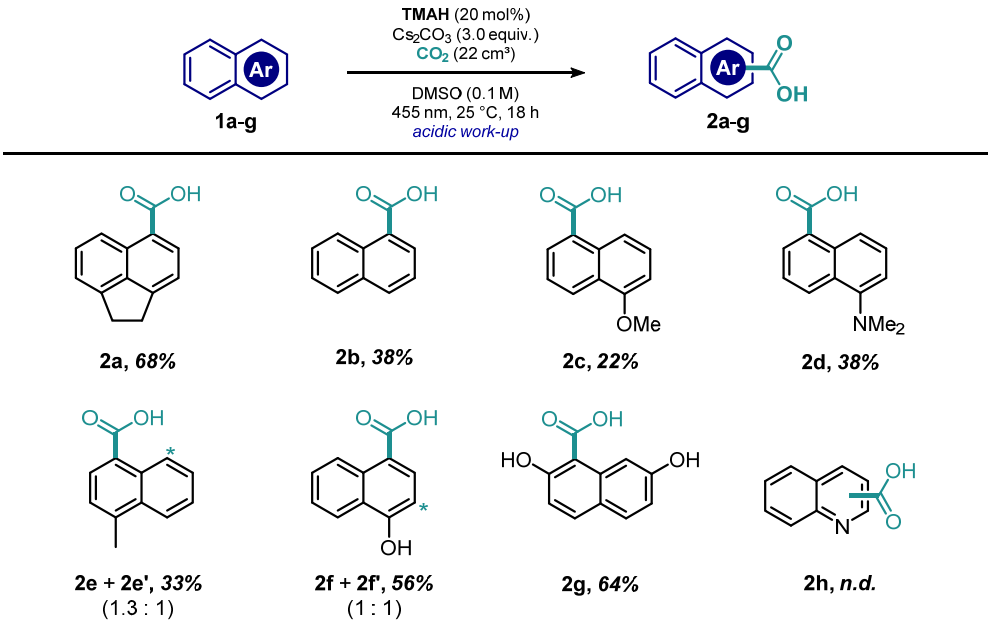

Scheme 3. Substrate scope for the carboxylation of naphthalene derivatives.

Pleasingly, many other heteroaromatic compounds were suitable substrates for our carboxylation method (Scheme 4). Thiophenes, bearing electron-deficient (**3a-d**, **3f**, **3i-k**) and -neutral (**3e**, **3g-h**, **3l-n**) substituents smoothly converted into the corresponding thiophenecarboxylic acids **4a-n** in good to excellent yield. Remarkably, a broad range of functional groups including ketones, esters, amides, $-CH_2CO_2Me$, $-CH_2CN$, phenyl-, trimethylsilyl-,

nitrile were tolerated. However, unfunctionalized thiophene could not be activated by the photocatalyst (see Figure S11b, Supplemental Information). Due to the mild nature of this reaction, we were pleased to see that regioselectivity was maintained even with substrates containing acidic C–H (**4c**, **4j**) or active methylene groups (**4g**-**h**). This is in contrast to reported base promoted methods that are usually selective for the most acidic position of the substrates and that fail in the presence of sensitive functionalities.

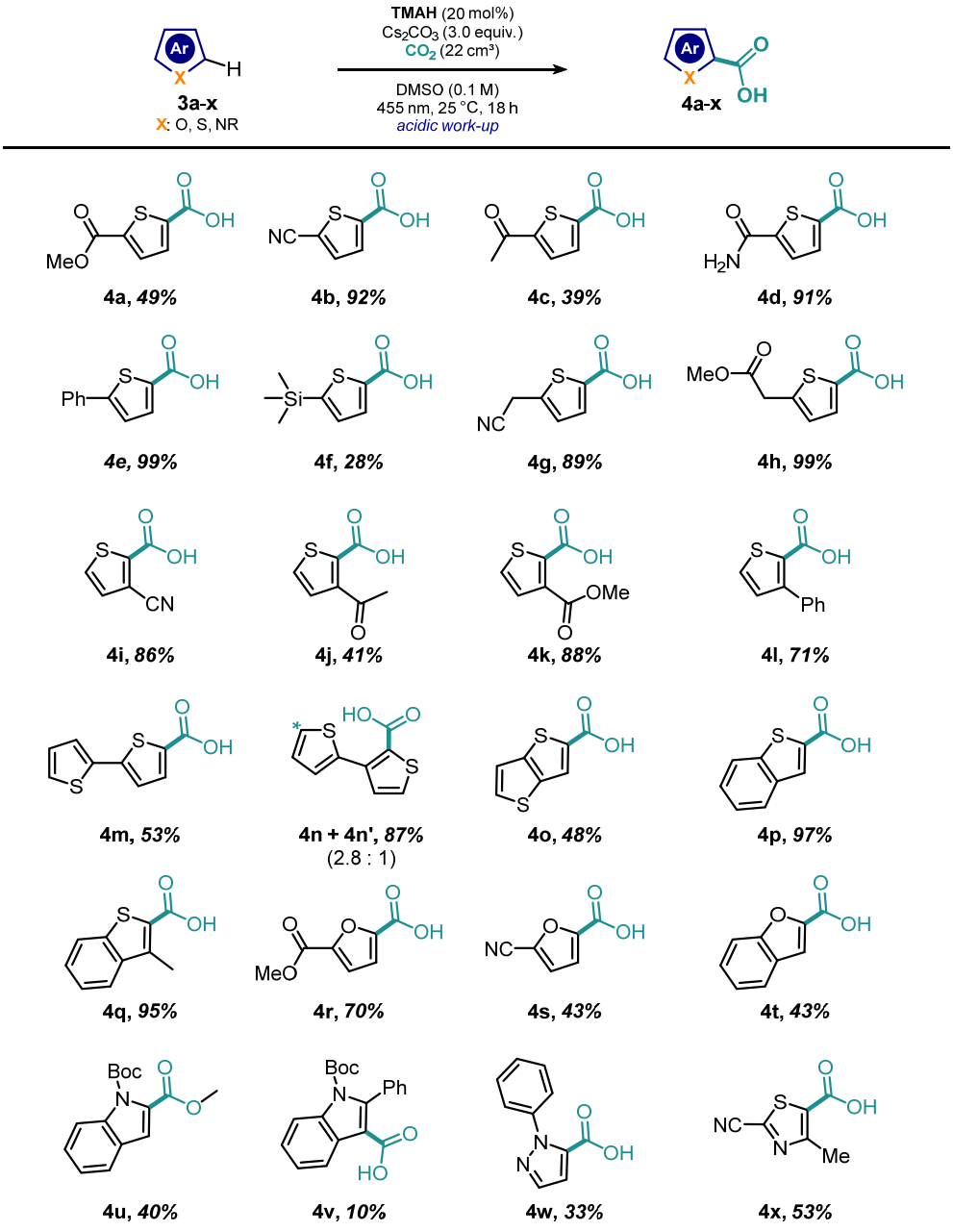

Scheme 4. Substrate scope for the carboxylation of 5-membered (hetero)arenes.

Our procedure allowed for the conversion of methyl thiophene-2-carboxylate to 5-(methoxycarbonyl)thiophene-2-carboxylic acid (**4a**) in one step, providing a much shorter route than by using other reported methods [Scheme 5, A(i)].[66] Moreover, our method allowed the synthesis of 5-carboxy-2-acetylthiophene (**4c**), an important building block for the synthesis of the alpha/beta blocker arotinolol,[67] in one step from 1-(thiophen-2-yl)ethan-1-one (**3c**). This is significantly shorter than well-established synthetic routes [Scheme 5, A(ii)].[68] Remarkably, we also found that 3-substituted thiophenes were exclusively carboxylated in the 2-position (**4i-l**) which highlights the excellent regioselectivity of this reaction. In comparison, a previous literature report on the lithiation of 3-phenylthiophene (**3l**) and subsequent carboxylation led to a mixture of **4l** and **4l'** (Scheme 5, B).[69] Perfect regioselectivity was also observed for the photocatalyzed carboxylation of 1-phenylpyrazole where only **4w** was obtained. In this case, due to the chelating effect of nitrogen, the use of organometallic reagents leads to product mixtures (*n*-BuLi)[70] or to an inverse regioselectivity (EtMgBr)[71] (Scheme 5, C).This photocatalyzed carboxylation method could also be extended to benzothiophenes (**4p-q**), furans (**4r-s**), benzofuran **4t**, Boc-protected indoles (**4u-v**) and thiocarbazole **4x**. Non-protected 1*H*-indoles however, were carboxylated at the nitrogen atom, as reported in literature.[30]

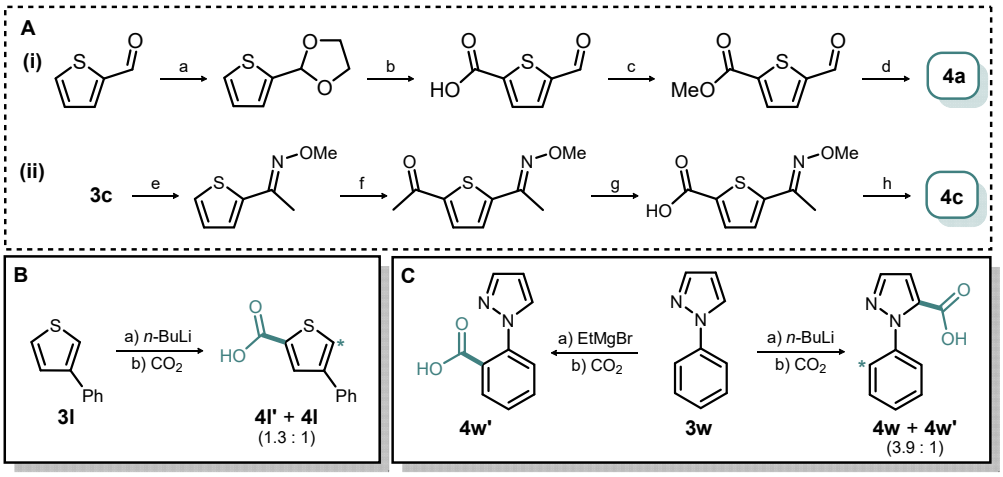

Scheme 5. Commonly applied synthetic routes to obtain products **4a** and **4c** (A). Regioselectivity of organometallic carboxylation (B+C).

(A) Reported four-step synthesis for compound **4a** (i)[66] and **4c** (ii)[68]; conditions: (a) ethane-1,2-diol, Al_2O_3, CCl_4, Δ, 48 h; (b) *n*-BuLi, THF, −78 °C, then CO_2 followed by H_2SO_4 (10%); (c) MeI, Na_2CO_3, DMF, 20 °C, 48 h; (d) Jones reagent; (e) $MeONH_2{\cdot}HCl$, Na_2CO_3, H_2O, MeOH, AcOH (pH 5), Δ, 3 h; (f) $ZnCl_2$, $CHCl_3$, Ac_2O, 100 °C, 12 h, r.t., aq. HCl (20%) (g) MeOH, aq. NaOCl (5.5%), 70 °C, 4 h, r.t., HCl conc.; (h) aq. HCl, 65 °C, 12 h.

(B) *n*-BuLi promoted carboxylation of **3l** leads to a mixture of regioisomers.

(C) Organometallic methods for carboxylation of 1-phenylpyrazole. Due to the chelating effect of nitrogen, the use of organometallic reagents causes a mixture of regioisomers (*n*-BuLi) or leads to an inversion of regioselectivity (EtMgBr) yielding benzoic acid **4w'** as single product.

Noteworthy, modifying the conditions during the reaction work-up of **4r** allowed the formation of either 2,5-furandicarboxylic acid (FDCA) or dimethyl 2,5-furandicarboxylate (DMFDC, see Scheme S4, Supplemental Information). Both are important monomers for the manufacture of polyesters derived from biomass, including

polyethylene furandicarboxylate (PEF), a potential large-scale substitute for fossil-based polyethylene terephthalate (PET).[72,73] Lignocellulose is converted into furfural on an industrial scale[74] and catalytic follow-up procedures have been reported to yield methyl furoate quantitatively.[75,76] Starting from methyl furan-2-carboxylate **3r**, our procedure offers a new one-step synthetic route to form lignocellulose-derived monomers. Remarkably, all examined heterocycles were carboxylated at the five-membered ring in α-position (except **4v**, where the α-position is blocked) to the heteroatom. Contrarily, hydroxybenzothiophene **6a** or condensed heterocycles such as indazoles (**6b-c**) and pyrazolo[1,5-*a*]pyridine (**6d**) showed exclusive selectivity for the six-membered ring (Scheme 6, A). With mild carboxylation conditions in hand, we postulated that this methodology could be applied for the late-stage functionalization of biologically active molecules. To this end, a Boc-protected thiophene analogue of propranolol, a well-established beta blocker bearing a free hydroxyl group in the side chain, was subjected to our reaction conditions. Pleasantly, regioselective carboxylation was successfully achieved to provide **6e**, albeit in modest yield.

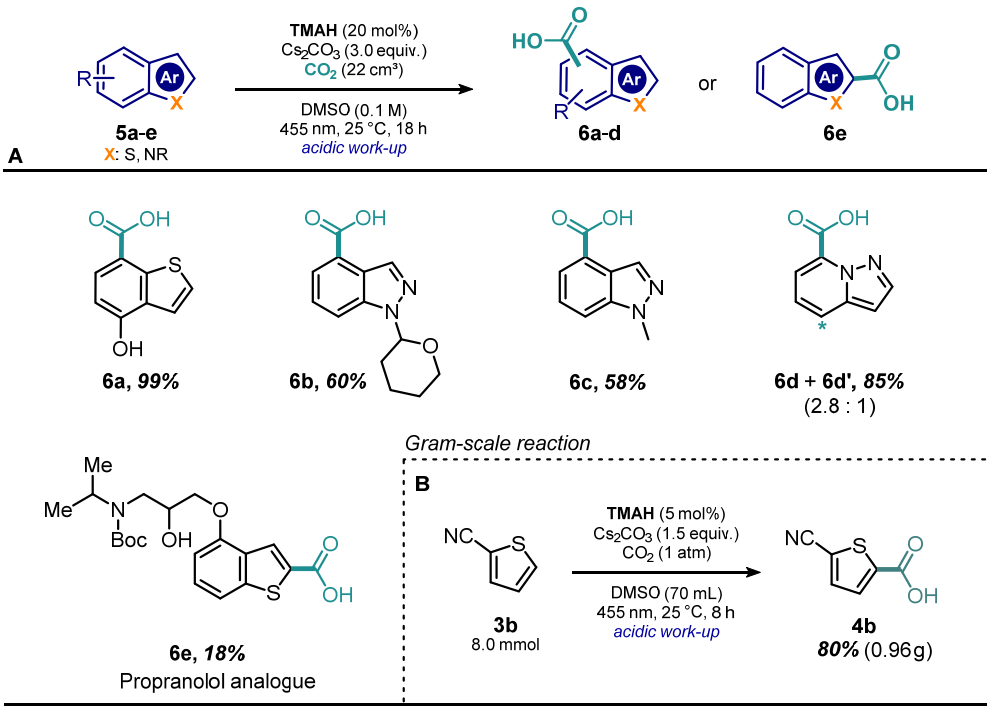

Scheme 6. (A) Substrate scope for the carboxylation of (hetero)arenes on the six-membered ring and example of late-stage functionalization. (B) Reaction conditions for the gram-scale carboxylation of **3b**.

To demonstrate the scalability of our reaction, we repeated the synthesis of **4b** on a gram-scale. 2-Cyanothiophene **3b** was reacted in a custom-built glass reactor (see Figure S2, Supplemental Information) with a reduced amount of both **TMAH** (5 mol%) and cesium carbonate (1.5 equiv.) in DMSO (Scheme 6B). Remarkably, as working with CO_2 overpressure was not possible with this reaction vessel, a gentle stream of CO_2 was sufficient to obtain the product in good yield.

We then questioned whether our photocatalytic system could be further utilized for the direct carboxylation of other stabilized sp^2-hybridized carbon atoms. To this end, we examined styrene derivatives (Scheme 7) and we were delighted to see that under the presented redox-neutral conditions only the corresponding *trans*-cinnamic acids were obtained. Our protocol thus provides a complementary method to previous net-reductive approaches where excess of sacrificial reductant or electrical current yielded hydrocarboxylated products (*cf.*, Scheme 1).[22,48,53] Despite the limitation posed by competing polymerization reactions, a variety of vinyl benzenes could be converted into *trans*-cinnamic acid derivatives **8b-l** (Scheme 7), which find applications in the food industry, material science[77] and cosmetics.[78] While styrene derivatives bearing electron-donating substituents (**7d-f**, **7h**) reacted smoothly, the reaction with the electron-poor 4-(trifluoromethyl)styrene resulted in low product yield. 4-Cyanostyrene (**7n**) or methyl-4-vinylbenzoate (**7o**) were not suitable substrates under these conditions. As the electron transfer from the excited photocatalyst to an electron-poor styrene is thermodynamically favored, we postulated that electron-withdrawing groups stabilize the negative charge and reduce the nucleophilicity of the corresponding radical anion. When using α-methylstyrene, we observed the formation of 3-aryl-3-butenoic acid **8m** in favor of the thermodynamically more stable α,β-unsaturated acid **8m'**.[38]

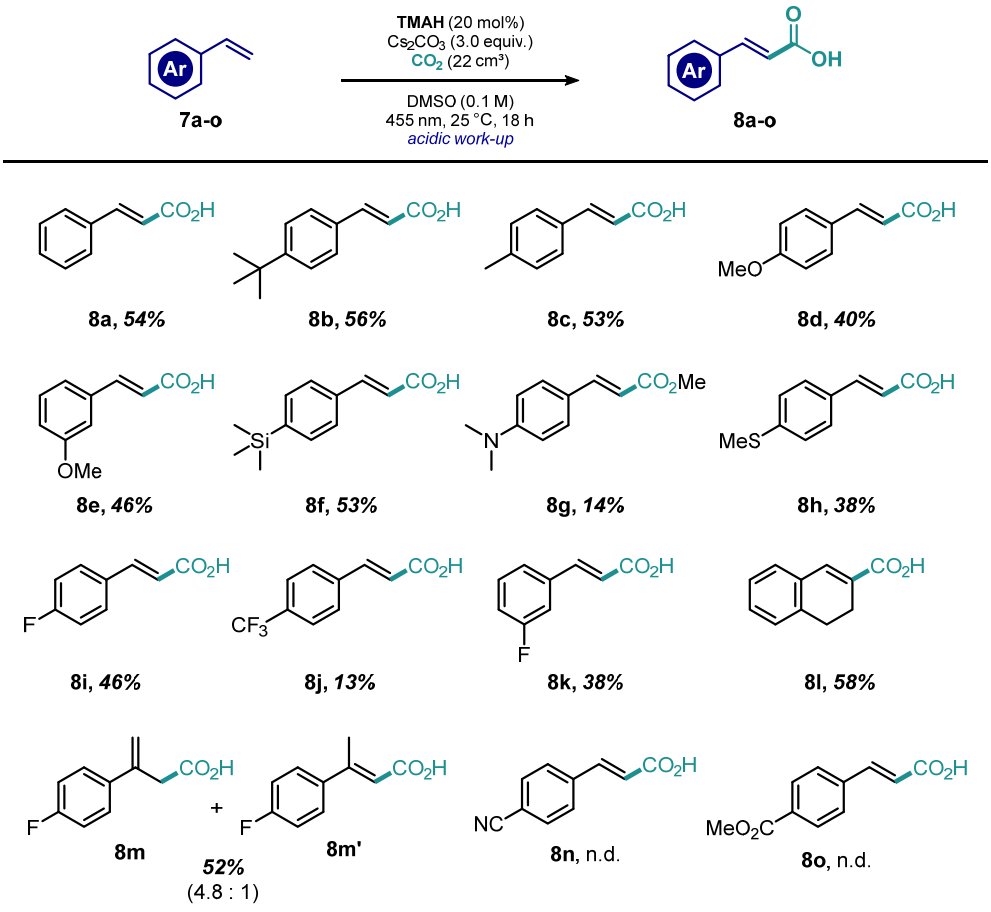

Scheme 7. Substrate scope for the carboxylation of styrene derivatives.

Mechanistic Insights

We propose a photoinduced single-electron transfer (SET) from the excited **TMA**$^{-*}$ to the substrate as the first step. The excited photocatalyst **TMA**$^{-*}$ is strongly emissive and its luminescence decay follows first-order kinetics (see Figure S4a-b and Figure S5, Supplemental Information). In presence of chosen (hetero)arenes (*cf.,* Scheme 4) as well as styrenes (*cf.,* Scheme 7) we observed a decrease in the luminescence lifetime of **TMA**$^{-*}$. Based on the obtained data, a Stern-Volmer plot was derived (see Figure S11a-b, Supplemental Information). The luminescence lifetime of **TMA**$^{-*}$ in a CO_2-saturated solution of DMSO remains almost unchanged, indicating that CO_2 is not reduced by the photocatalyst. Reduction of CO_2 by SET to achieve carbon-bond formation has been reported, but it requires reagents such as *p*-terphenyl radical anion[53,79]. Although a direct reduction of CO_2 (−2.21 V *vs.* SCE in DMF)[80] by **TMA**$^{-*}$ is thermodynamically feasible, we assume a kinetic barrier preventing the formation of the bent CO_2 radical anion within the excited state lifetime of **TMA**$^{-*}$. Thus, we ascertained that the productive pathway is dominated by the formation of an aromatic radical anion, which subsequently reacts with CO_2 *via* nucleophilic addition. In order to get further insight into the reaction mechanism, we tested other electrophiles than CO_2. We decided to use ketones for this study, as single-electron reduction from the excited photocatalyst to the ketone would give a ketyl radical anion. In sharp contrast to the radical anion of CO_2, ketyl radical anions are considered as electron-rich species acting as single-electron reductants rather than forming C-C bonds *via* radical reactions.[81] When benzo[*b*]thiophene (**3p**, Scheme 8) was reacted with acetone (**9a**), the corresponding tertiary alcohol adduct **9pa** was formed in good yield. The luminescence lifetime of **TMA**$^{-*}$ remains unchanged upon titration with acetone (−2.84 V *vs.* SCE in DMF)[82] and thus, the formation of a ketyl radical anion is unlikely (Figure S11d, Supplemental Information). Remarkably, similar transformations require very harsh reaction conditions (−78 °C, excess of *n*-BuLi) and are not viable in a one-pot procedure.[83] Moderate yield of the resulting tertiary alcohol were also obtained using cyclic ketone **9b** and non-conjugated enone **9c** as electrophiles.

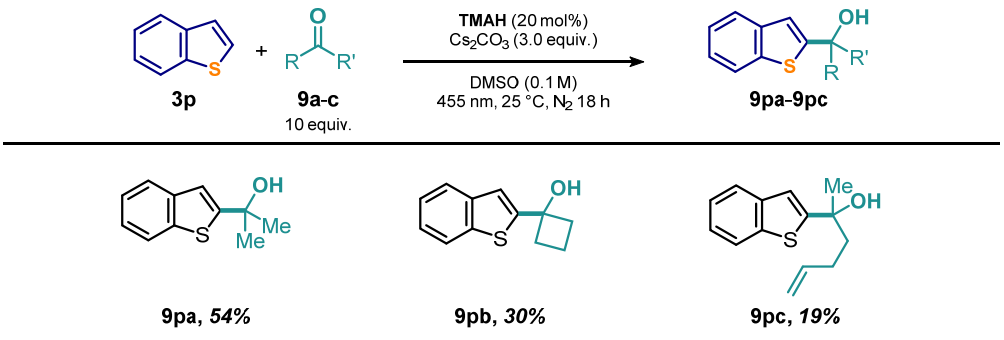

Scheme 8. Mechanistic investigations: Probing the possibility of other electrophiles as viable candidates for reactivity with aromatic radical anions.

In addition, we performed deuterium-labeling experiments using D_2O and ^tBuOD respectively. Upon formation of the nucleophilic arene radical anion, we envisioned a fast acid-base reaction followed by reoxidation and deprotonation to yield a mixture of H and D in the substrate (see Scheme S3, Supplemental Information). However, as water in the reaction mixture was found to be detrimental and protic solvents were shown to inhibit the reaction (*cf.,* Table S1, Supplemental Information), only small amounts of incorporated deuterium were detected using benzothiophene **3q** (Table S3, Supplemental Information). Based on the aforementioned results we propose the following reaction mechanism for the photocatalytic C−H carboxylation of (hetero)arenes (Scheme 9). In the presence of a base, the pre-catalyst **TMAH** is chemically activated by deprotonation to form an anionic species **TMA**$^-$, indicated by the solution colour change. Upon irradiation with visible light (455 nm) a strongly-reducing excited anion **TMA**$^{-*}$ is formed. The excited state is then quenched by the arene **I** *via* SET to afford the radical of the photocatalyst **TMA**$^{\cdot}$ and the electron rich radical anion of the arene (**II**). The Mulliken spin population for each aromatic sp^2-hybridized carbon, indicative of reactivity towards CO_2, is shown for the benzothiophene radical anion (**II**). In the bond-forming step CO_2 is attacked by **II** to generate a radical carboxylate **III** as an intermediate. The catalytic cycle is closed *via* SET to recapture the active catalyst **TMA**$^-$ followed by re-aromatization of the cationic arene **IV** upon deprotonation. Despite the weakly oxidizing nature of the photocatalyst, the electron transfer from **III** to **TMA**$^{\cdot}$ may be driven by the stabilization energy gained upon re-aromatization of **IV**. It remains to be shown if this re-aromatization occurs *via* electron transfer and subsequent deprotonation as proposed, or *via* a direct H-atom abstraction by the oxidized photocatalyst.

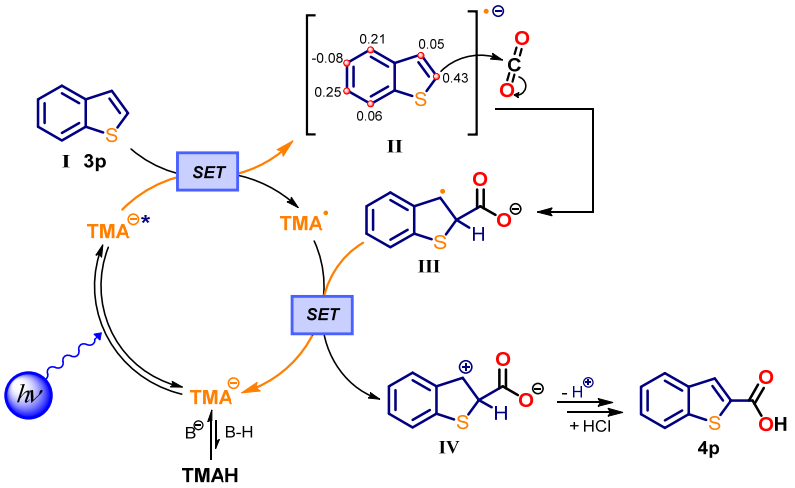

Scheme 9. Proposed mechanism for the C−H carboxylation of (hetero)arenes exemplified by the carbxoxylation of benzothiophene.

During the exploration of the substrate scope, we found that several aromatic compounds that quench the excited state of the photocatalyst did not undergo carboxylation (see Figure S11c, Supplemental Information). While some functional groups are understandably not tolerated under our reaction conditions, such as aromatic halides

(these may undergo fast mesolytic bond-cleavage to form aryl radicals) or highly electrophilic moieties, we were surprised that only certain radical anions were reacting with CO_2. In order to determine the required electronic characteristics for reactivity and to improve our insight regarding functional group tolerance, high-throughput screening (HTS) of various arenes containing a large array of functionalities and differing in complexity was carried out (see Figure S9, Supplemental Information). The analysis of the HTS outcome indicates that aldehydes, halides (with the exception of fluorine), aliphatic amines, 6-membered N-heterocycles and nitro groups are not compatible with the reaction conditions. Beyond functional group interference, the applicability of our methodology is related to the arene electron affinity and the nucleophilicity of the resulting radical anion. Arenes may be able to accept an electron with ease, but the radical anion formed may not be nucleophilic enough to add to CO_2. Conversely, some aromatic radical anions may be highly nucleophilic, but their formation may be beyond the reductive capabilities of the photocatalyst or a functional group present may be reduced instead. The estimated electron affinities of the arenes, and the Mulliken spin population and charges for the arene radical anions were derived from DFT calculations. The importance of a correct balance of electron affinity of the arene and the nucleophilicity of the aromatic radical anion for a successful reaction is illustrated in Schemes S12a-d (Supplemental Information). The regioselectivity is generally well predicted by comparing the Mulliken spin population for the aromatic carbons in each substrate.

Conclusion

We have developed a mild, direct, redox-neutral and transition-metal-free insertion of CO_2 into non-prefunctionalized $C(sp^2)$−H bonds, leading to an efficient method for producing valuable aromatic carboxylic acids and *trans*-cinnamic acids in a single operation. A reaction performed on gram-scale demonstrated the scalability of this carboxylation method, while ketones could be used as alternative electrophiles to CO_2 yielding tertiary alcohols. The scope of the reaction can be predicted by DFT-estimated reduction potential of the substrates and nucleophilicity of the intermediate arene radical anions. These findings may open new opportunities for atom-economic and energy efficient use of CO_2 as a C1 building block in the chemical processing of aromatic hydrocarbons, as well as for developing new photocatalytic late-stage functionalizations of drug-like compounds.

Experimental Procedures

Full experimental procedures are provided in the Supplemental Information

Supplemental Information

Supplemental Information can be found online.

Acknowledgments

We thank Dr. Rudolf Vasold for GC measurements, Ernst Lautenschlager for his help regarding laboratory equipment and Regina Hoheisel for cyclic voltammetry measurements. M.S. thanks Marie-Sofie Dürr & Andreas Ratzenböck for their assistance. The Physical and Analytical Chemistry team at AstraZeneca is kindly acknowledged for their help with NMR and HRMS analyses of compounds. T.D.S., P.B., M.J.J. and G.B. acknowledge Dr. Malin Lemurell, AstraZeneca and the AstraZeneca PostDoc program for their financial support. This project has received funding from the European Research Council (ERC) under the European Union's Horizon 2020 Research and Innovation Programme (grant agreement No. 741623).

Author Contributions

M.S. developed the catalytic system, optimized the reaction, isolated the compounds **2a-d**, **4a-f**, **4i-t**, **4v-w**, **8a-m**, **9pa-pc**, designed and carried out the gram-scale reaction and conducted all experiments to investigate the reaction mechanism. T.D.S. designed and performed the high-throughput-screening and isolated compounds **2f-g**, **4g-h**, **4u**, **4x**, **6a-e**. F.F. prepared compounds and isolated compound **2e**. M.S. and T.D.S. wrote the manuscript and Supplemental Information with input from all of the authors. P.B. conducted the computational studies. M.J.J., G.B. and B.K. supervised the project.

Declaration of Interests

The authors declare no competing interests. T.D.S., P.B., M.J.J., G.B. are employees and shareholders of AstraZeneca.

References

1. Hou, H.J.M., Najafpour, M.M., Moore, G.F., and Allakhverdiev, S.I. (2017). Photosynthesis: Structures, mechanisms, and applications (Springer International Publishing).
2. Nitopi, S., Bertheussen, E., Scott, S.B., Liu, X., Engstfeld, A.K., Horch, S., Seger, B., Stephens, I.E.L., Chan, K., Hahn, C., et al. (2019). Progress and Perspectives of Electrochemical CO_2 Reduction on Copper in Aqueous Electrolyte. Chem. Rev. *119*, 7610–7672.
3. Küngas, R. (2020). Electrochemical CO_2 Reduction for CO Production: Comparison of Low- and High-Temperature Electrolysis Technologies. J. Electrochem. Soc. *167*, 044508.
4. Nielsen, D.U., Hu, X.M., Daasbjerg, K., and Skrydstrup, T. (2018). Chemically and electrochemically catalysed conversion of CO_2 to CO with follow-up utilization to value-added chemicals. Nat. Catal. *1*, 244–254.
5. Liu, Q., Wu, L., Jackstell, R., and Beller, M. (2015). Using carbon dioxide as a building block in organic synthesis. Nat. Commun. *6*, 5933.
6. Correa, A., and Martín, R. (2009). Metal-Catalyzed Carboxylation of Organometallic Reagents with Carbon Dioxide. Angew. Chem. Int. Ed. *48*, 6201–6204.

7. Correa, A., and Martín, R. (2009). Palladium-Catalyzed Direct Carboxylation of Aryl Bromides with Carbon Cioxide. J. Am. Chem. Soc. *131*, 15974–15975.

8. Tran-Vu, H., and Daugulis, O. (2013). Copper-Catalyzed Carboxylation of Aryl Iodides with Carbon Dioxide. ACS Catal. *3*, 2417–2420.

9. Nogi, K., Tsuji, Y., Terao, J., Xu, T., and Fujihara, T. (2012). Nickel-Catalyzed Carboxylation of Aryl and Vinyl Chlorides Employing Carbon Dioxide. J. Am. Chem. Soc. *134*, 9106–9109.

10. Liu, Y., Cornella, J., and Martin, R. (2014). Ni-Catalyzed Carboxylation of Unactivated Primary Alkyl Bromides and Sulfonates with CO_2. J. Am. Chem. Soc. *136*, 11212–11215.

11. Correa, A., León, T., and Martin, R. (2014). Ni-Catalyzed Carboxylation of C(sp^2)- and C(sp^3)-O Bonds with CO_2. J. Am. Chem. Soc. *136*, 1062–1069.

12. Moragas, T., Cornella, J., and Martin, R. (2014). Ligand-Controlled Regiodivergent Ni-Catalyzed Reductive Carboxylation of Allyl Esters with CO_2. J. Am. Chem. Soc. *136*, 17702–17705.

13. Mita, T., Higuchi, Y., and Sato, Y. (2015). Highly Regioselective Palladium-Catalyzed Carboxylation of Allylic Alcohols with CO_2. Chem. Eur. J. *21*, 16391–16394.

14. Moragas, T., Gaydou, M., and Martin, R. (2016). Nickel-Catalyzed Carboxylation of Benzylic C−N Bonds with CO_2. Angew. Chem. Int. Ed. *55*, 5053–5057.

15. Yanagi, T., Somerville, R.J., Nogi, K., Martin, R., and Yorimitsu, H. (2020). Ni-Catalyzed Carboxylation of C(sp^2)-S Bonds with CO_2: Evidence for the Multifaceted Role of Zn. ACS Catal. *10*, 2117–2123.

16. Gaydou, M., Moragas, T., Juliá-Hernández, F., and Martin, R. (2017). Site-Selective Catalytic Carboxylation of Unsaturated Hydrocarbons with CO_2 and Water. J. Am. Chem. Soc. *139*, 12161–12164.

17. Michigami, K., Mita, T., and Sato, Y. (2017). Cobalt-Catalyzed Allylic C(sp^3)-H Carboxylation with CO_2. J. Am. Chem. Soc. *139*, 6094–6097.

18. Williams, C.M., Johnson, J.B., and Rovis, T. (2008). Nickel-Catalyzed Reductive Carboxylation of Styrenes Using CO_2. J. Am. Chem. Soc. *130*, 14936–14937.

19. Tortajada, A., Ninokata, R., and Martin, R. (2018). Ni-Catalyzed Site-Selective Dicarboxylation of 1,3-Dienes with CO_2. J. Am. Chem. Soc. *140*, 2050–2053.

20. Huguet, N., Jevtovikj, I., Gordillo, A., Lejkowski, M.L., Lindner, R., Bru, M., Khalimon, A.Y., Rominger, F., Schunk, S.A., Hofmann, P., et al. (2014). Nickel-Catalyzed Direct Carboxylation of Olefins with CO_2: One-Pot Synthesis of α,β-Unsaturated Carboxylic Acid Salts. Chem. Eur. J. *20*, 16858–16862.

21. Yang, Y., and Lee, J.W. (2019). Toward ideal carbon dioxide functionalization. Chem. Sci. *10*, 3905–3926.

22. Alkayal, A., Tabas, V., Montanaro, S., Wright, I.A., Malkov, A. V., and Buckley, B.R. (2020). Harnessing Applied Potential: Selective β-Hydrocarboxylation of Substituted Olefins. J. Am. Chem. Soc. *142*, 1780–1785.

23. Ang, N.W.J., de Oliveira, J.C.A., and Ackermann, L. (2020). Electro-Reductive Cobalt-Catalyzed Carboxylation: Cross-Electrophile Electro-coupling with Atmospheric CO_2. Angew. Chem. Int. Ed., doi.org/10.1002/anie.202003218.

24. Ye, J.-H., Miao, M., Huang, H., Yan, S.-S., Yin, Z.-B., Zhou, W.-J., and Yu, D.-G. (2017). Visible-Light-Driven Iron-Promoted Thiocarboxylation of Styrenes and Acrylates with CO_2. Angew. Chem. Int. Ed. *56*, 15416–15420.

25. Wang, H., Zhou, C., Li, G., Wang, H., Gao, Y., Zhou, C., and Li, G. (2020). Visible-Light-Driven Reductive Carboarylation of Styrenes with CO_2 and Aryl Halides. J. Am. Chem. Soc. *142*, 8122–8129.

26. Yatham, V.R., Shen, Y., and Martin, R. (2017). Catalytic Intermolecular Dicarbofunctionalization of Styrenes with CO_2 and Radical Precursors. Angew. Chem. Int. Ed. *56*, 10915–10919.

27. Hou, J., Ee, A., Cao, H., Ong, H.-W., Xu, J.-H., and Wu, J. (2018). Visible-Light-Mediated Metal-Free Difunctionalization of Alkenes with CO_2 and Silanes or C(sp^3)−H Alkanes. Angew. Chem. Int. Ed. *57*, 17220–17224.

28. Fu, Q., Bo, Z.Y., Ye, J.H., Ju, T., Huang, H., Liao, L.L., and Yu, D.G. (2019). Transition metal-free phosphonocarboxylation of alkenes with carbon dioxide via visible-light photoredox catalysis. Nat. Commun. *10*, 1–9.

29. Luo, J., Preciado, S., Xie, P., and Larrosa, I. (2016). Carboxylation of Phenols with CO_2 at Atmospheric Pressure. Chem. Eur. J. *22*, 6798–6802.

30. Yoo, W.J., Capdevila, M.G., Du, X., and Kobayashi, S. (2012). Base-Mediated Carboxylation of Unprotected Indole

Derivatives with Carbon Dioxide. Org. Lett. *14*, 5326–5329.

31. Shigeno, M., Hanasaka, K., Sasaki, K., Nozawa-Kumada, K., and Kondo, Y. (2019). Direct Carboxylation of Electron-Rich Heteroarenes Promoted by LiO-*t*Bu with CsF and [18]Crown-6. Chem. Eur. J. *25*, 3235–3239.

32. Suzuki, Y., Hattori, T., Okuzawa, T., and Miyano, S. (2002). Lewis Acid-Mediated Carboxylation of Fused Aromatic Compounds with Carbon Dioxide. Chem. Lett., 102–103.

33. Nemoto, K., Yoshida, H., Suzuki, Y., Morohashi, N., and Hattori, T. (2006). Beneficial Effect of TMSCl in the Lewis Acid-mediated Carboxylation of Aromatic Compounds with Carbon Dioxide. Chem. Lett. *35*, 820–821.

34. Nemoto, K., Yoshida, H., Egusa, N., Morohashi, N., and Hattori, T. (2010). Direct Carboxylation of Arenes and Halobenzenes with CO_2 by the Combined Use of $AlBr_3$ and R_3SiCl. J. Org. Chem. *75*, 7855–7862.

35. Olah, G.A., Török, B., Joschek, J.P., Bucsi, I., Esteves, P.M., Rasul, G., and Prakash, G.K.S. (2002). Efficient Chemoselective Carboxylation of Aromatics to Arylcarboxylic Acids with a Superelectrophilically Activated Carbon Dioxide-Al_2Cl_6/Al System. J. Am. Chem. Soc. *124*, 11379–11391.

36. Nemoto, K., Onozawa, S., Egusa, N., Morohashi, N., and Hattori, T. (2009). Carboxylation of indoles and pyrroles with CO_2 in the presence of dialkylaluminum halides. Tetrahedron Lett. *50*, 4512–4514.

37. Nemoto, K., Onozawa, S., Konno, M., Morohashi, N., and Hattori, T. (2012). Direct Carboxylation of Thiophenes and Benzothiophenes with the Aid of $EtAlCl_2$. Bull. Chem. Soc. Jpn. *85*, 369–371.

38. Tanaka, S., Watanabe, K., Tanaka, Y., and Hattori, T. (2016). $EtAlCl_2$/2,6-Disubstituted Pyridine-Mediated Carboxylation of Alkenes with Carbon Dioxide. Org. Lett. *18*, 2576–2579.

39. Boogaerts, I.I.F., Fortman, G.C., Furst, M.R.L., Cazin, C.S.J., and Nolan, S.P. (2010). Carboxylation of N-H/C-H Bonds Using N-heterocyclic Carbene Copper(I) Complexes. Angew. Chem. Int. Ed. *49*, 8674–8677.

40. Zhang, L., Cheng, J., Ohishi, T., and Hou, Z. (2010). Copper-Catalyzed Direct Carboxylation of C-H Bonds with Carbon Dioxide. Angew. Chem. Int. Ed. *49*, 8670–8673.

41. Suga, T., Mizuno, H., Takaya, J., and Iwasawa, N. (2014). Direct carboxylation of simple arenes with CO_2 through a rhodium-catalyzed C-H bond activation. Chem. Commun. *50*, 14360–14363.

42. Hong, J., Li, M., Zhang, J., Sun, B., and Mo, F. (2019). C-H Bond Carboxylation with Carbon Dioxide. ChemSusChem *12*, 6–39.

43. Banerjee, A., Dick, G.R., Yoshino, T., and Kanan, M.W. (2016). Carbon dioxide utilization via carbonate-promoted C-H carboxylation. Nature *531*, 215–219.

44. Kudo, K., Shima, M., Kume, Y., Ikoma, F., Mori, S., and Sugita, N. (1995). Carboxylation of Cesium 2-Naphthoate in the Alkali Metal Molten Salts of Carbonate and Formate with CO_2 under High Pressure. J. Jpn. Petrol. Inst. *38*, 40–47.

45. Shimomaki, K., Murata, K., Martin, R., and Iwasawa, N. (2017). Visible-Light-Driven Carboxylation of Aryl Halides by the Combined Use of Palladium and Photoredox Catalysts. J. Am. Chem. Soc. *139*, 9467–9470.

46. Meng, Q.-Y., Wang, S., and König, B. (2017). Carboxylation of Aromatic and Aliphatic Bromides and Triflates with CO_2 by Dual Visible-Light-Nickel Catalysis. Angew. Chem. Int. Ed. *56*, 13426–13430.

47. Hou, J., Ee, A., Feng, W., Xu, J.H., Zhao, Y., and Wu, J. (2018). Visible-Light-Driven alkyne hydro-/carbocarboxylation using CO_2 via iridium/cobalt dual catalysis for divergent heterocycle synthesis. J. Am. Chem. Soc. *140*, 5257–5263.

48. Meng, Q.Y., Wang, S., Huff, G.S., and König, B. (2018). Ligand-Controlled Regioselective Hydrocarboxylation of Styrenes with CO_2 by Combining Visible Light and Nickel Catalysis. J. Am. Chem. Soc. *140*, 3198–3201.

49. Murata, K., Numasawa, N., Shimomaki, K., Takaya, J., and Iwasawa, N. (2017). Construction of a visible light-driven hydrocarboxylation cycle of alkenes by the combined use of Rh(I) and photoredox catalysts. Chem. Commun. *53*, 3098–3101.

50. Meng, Q.-Y., Schirmer, T.E., Berger, A.L., Donabauer, K., and König, B. (2019). Photocarboxylation of Benzylic C–H Bonds. J. Am. Chem. Soc. *141*, 11393–11397.

51. Tagaya, H., Onuki, M., Tomioka, Y., Wada, Y., Karasu, M., and Chiba, K. (1990). Photocarboxylation of Naphthalene in the Presence of Carbon Dioxide and an Electron Donor. Bull. Chem. Soc. Jpn. *63*, 3233–3237.

52. Minabe, M., Isozumi, K., Kawai, K., and Yoshida, M. (1988). An Observation on Carboxylation of 4*H*-Cyclopenta[*def*]phenanthrene. Bull. Chem. Soc. Jpn. *61*, 2063–2066.

53. Seo, H., Liu, A., and Jamison, T.F. (2017). Direct β-Selective Hydrocarboxylation of Styrenes with CO_2 Enabled by Continuous Flow Photoredox Catalysis. J. Am. Chem. Soc. *139*, 13969–13972.

54. Ishida, N., Masuda, Y., Uemoto, S., and Murakami, M. (2016). A Light/Ketone/Copper System for Carboxylation of Allylic C−H Bonds of Alkenes with CO_2. Chem. Eur. J. *22*, 6524–6527.

55. Ishida, N., Masuda, Y., Imamura, Y., Yamazaki, K., and Murakami, M. (2020). Carboxylation of Benzylic and Aliphatic C-H bonds with CO_2 Induced by Light/Ketone/Nickel. J. Am. Chem. Soc. *141*, 19611–19615.

56. Schmalzbauer, M., Ghosh, I., and König, B. (2019). Utilising excited state organic anions for photoredox catalysis: Activation of (hetero)aryl chlorides by visible light-absorbing 9-anthrolate anions. Faraday Discuss. *215*, 364–378.

57. Mutule, I., and Suna, E. (2005). Arylzinc species by microwave assisted Grignard formation-transmetallation sequence: Application in the Negishi coupling. Tetrahedron *61*, 11168–11176.

58. Hussey, A.S. (1951). The Carbonation of Grignard Reagent Solutions. J. Am. Chem. Soc. *73*, 1364–1365.

59. Nagaki, A., Takahashi, Y., and Yoshida, J. (2014). Extremely Fast Gas/Liquid Reactions in Flow Microreactors: Carboxylation of Short-Lived Organolithiums. Chem. Eur. J. *20*, 7931–7934.

60. Polyzos, A., O'Brien, M., Petersen, T.P., Baxendale, I.R., and Ley, S. V. (2011). The Continuous-Flow Synthesis of Carboxylic Acids using CO_2 in a Tube-In-Tube Gas Permeable Membrane Reactor. Angew. Chem. Int. Ed. *50*, 1190–1193.

61. Holy, N.L. (1974). Reactions of the Radical Anions and Dianions of Aromatic Hydrocarbons. Chem. Rev. *74*, 243–277.

62. Schlenk, W., and Bergmann, E. (1928). Forschungen auf dem Gebiete der alkaliorganischen Verbindungen. I. Über Produkte der Addition von Alkalimetal an mehrfache Kohlenstoff-Kohlenstoff-Bindungen. Justus Liebigs Ann. Chem. *463*, 1–97.

63. Walker, J.F., and Scott, N.D. (1938). Sodium Naphthalene. II. Preparation and Properties of Dihydronaphthalene Dicarboxylic Acids. J. Am. Chem. Soc. *60*, 951–955.

64. Gennaro, A., Isse, A.A., and Vianello, E. (1990). Solubility and electrochemical determination of CO_2 in some dipolar aprotic solvents. J. Electroanal. Chem. *289*, 203–215.

65. Montalti, M., Credi, A., Prodi, L., and Gandolfi, M.T. (2006). Handbook of Photochemisty 3rd ed. (CRC Press).

66. Mahboobi, S., Dove, S., Sellmer, A., Winkler, M., Eichhorn, E., Pongratz, H., Ciossek, T., Baer, T., Maier, T., and Beckers, T. (2009). Design of Chimeric Histone Deacetylase- and Tyrosine Kinase-Inhibitors: A Series of Imatinib Hybrides as Potent Inhibitors of Wild-Type and Mutant BCR-ABL, PDGF-Rβ, and histone deacetylases. J. Med. Chem. *52*, 2265–2279.

67. Hara, Y., Sato, E., Miyagishi, A., Aisaka, A., and Hibino, T. (1978). Synthesis and β-Adrenergic Blocking Action of a New Thiazolylthiopropanolamine Derivative. J. Pharm. Sci. *67*, 1334–1335.

68. Liu, H., Tang, H., Yang, D., and Ji, Q. (2011). Synthesis of Arotinolol Hydrochloride. Chinese J. Pharm. *42*, 641–644.

69. Gschwend, H.W., and Rodriguez, H.R. (1979). Heteroatom-Facilitated Lithiations. In Organic Reactions (John Wiley & Sons, Inc.), pp. 1–360.

70. Alley, P.W., and Shirley, D.A. (1958). The Metalation of 1-Phenyl- and 1-Methylpyrazole with *n*-Butyllithium. J. Am. Chem. Soc. *80*, 6271–6274.

71. Marxer, A., and Siegrist, M. (1974). Über die Umsetzung von 1-Phenylpyrazol mit Äthylmagnesiumbromid. 8. Mitteilung über Grignard -Reaktionen. Helv. Chim. Acta *57*, 1988–2000.

72. Banella, M.B., Bonucci, J., Vannini, M., Marchese, P., Lorenzetti, C., and Celli, A. (2019). Insights into the Synthesis of Poly(ethylene 2,5-Furandicarboxylate) from 2,5-Furandicarboxylic Acid: Steps toward Environmental and Food Safety Excellence in Packaging Applications. Ind. Eng. Chem. Res. *58*, 8955–8962.

73. Sousa, A.F., Vilela, C., Fonseca, A.C., Matos, M., Freire, C.S.R., Gruter, G.J.M., Coelho, J.F.J., and Silvestre, A.J.D. (2015). Biobased polyesters and other polymers from 2,5-furandicarboxylic acid: A tribute to furan excellency. Polym. Chem. *6*, 5961–5983.

74. Lange, J.-P., van der Heide, E., van Buijtenen, J., and Price, R. (2012). Furfural-A Promising Platform for Lignocellulosic Biofuels. ChemSusChem *5*, 150–166.

75. Cho, A., Byun, S., Cho, J.H., and Kim, B.M. (2019). AuPd-Fe_3O_4 Nanoparticle-Catalyzed Synthesis of Furan-2,5-dimethylcarboxylate from 5-Hydroxymethylfurfural under Mild Conditions. ChemSusChem *12*, 2310–2317.

76. Zhou, H., Hong, S., Zhang, H., Chen, Y., Xu, H., Wang, X., Jiang, Z., Chen, S., and Liu, Y. (2019). Toward biomass-based

single-atom catalysts and plastics: Highly active single-atom Co on N-doped carbon for oxidative esterification of primary alcohols. Appl. Catal. B-Environ. *256*, 117767.

77. Fonseca, A.C., Lima, M.S., Sousa, A.F., Silvestre, A.J., Coelho, J.F.J., and Serra, A.C. (2019). Cinnamic acid derivatives as promising building blocks for advanced polymers: Synthesis, properties and applications. Polym. Chem. *10*, 1696–1723.

78. Gunia-Krzyżak, A., Słoczyńska, K., Popiół, J., Koczurkiewicz, P., Marona, H., and Pękala, E. (2018). Cinnamic acid derivatives in cosmetics: current use and future prospects. Int. J. Cosmet. Sci. *40*, 356–366.

79. Seo, H., Katcher, M.H., and Jamison, T.F. (2017). Photoredox activation of carbon dioxide for amino acid synthesis in continuous flow. Nat. Chem. 9, 453–456.

80. Lamy, E., Nadjo, L., and Saveant, J.M. (1977). Standard potential and kinetic parameters of the electrochemical reduction of carbon dioxide in dimethylformamide. J. Electroanal. Chem. *78*, 403–407.

81. Xia, Q., Dong, J., Song, H., and Wang, Q. (2018). Visible-Light Photocatalysis of the Ketyl Radical Coupling Reaction. Chem. Eur. J. *25*, 2949–2961.

82. Fuchigami, T., Inagi, S., and Atobe, M. eds. (2014). Appendix B. In Fundamentals and Applications of Organic Electrochemistry (John Wiley & Sons Ltd), pp. 217–222.

83. Raghu, M., Grover, J., and Ramasastry, S.S. V. (2016). Cyclopenta[*b*]annulation of Heteroarenes by Organocatalytic γ′[C(sp^3)−H] Functionalization of Ynones. Chem. Eur. J. *22*, 18316–18321.

Supplemental Information

Redox-neutral Photocatalytic C–H Carboxylation of Arenes and Styrenes with CO_2

Matthias Schmalzbauer,[1,5] Thomas D. Svejstrup,[2,5] Florian Fricke,[1] Peter Brandt,[2] Magnus J. Johansson,[2,3] Giulia Bergonzini,[2,*] and Burkhard König[1,4,**]

[1]Faculty of Chemistry and Pharmacy, University of Regensburg, Germany
[2]Medicinal Chemistry, Research and Early Development Cardiovascular, Renal and Metabolism, BioPharmaceuticals R&D, AstraZeneca, Gothenburg, Sweden
[3]Department of Organic Chemistry, Stockholm University, Stockholm 10691, Sweden
[4]Lead Contact
[5]These authors contributed equally
*Correspondence: giulia.bergonzini@astrazeneca.com
**Correspondence: burkhard.koenig@ur.de

Table of contents

1 - General Experimental Details 2

2 - Catalyst Synthesis and Physicochemical Properties 5

2.1 - Synthesis of the Photocatalyst 5

2.2 - Spectroscopic and Photochemical Characteristics 6

3 - Substrate Synthesis 13

4 - Carboxylation Reactions 17

4.1 - Reaction Optimization 17

4.2 - Substrate Scope 20

5 - Spectra 43

6 - Mechanistic Studies 96

6.1 - General Procedure for High-throughput Screening of Arenes 96

6.2 - Deuterium Labeling Experiments 96

6.3 - Time-resolved Luminescence Quenching studies 101

6.4 - Computational Analysis 104

7 - Miscellaneous 109

7.1 - Synthetic route towards FDCA and DMFDC 109

7.2 - Carboxylation of biphenyl 109

7.3 - Unsuccessful Substrates 110

8 - References 111

1 - General Experimental Details

All required fine chemicals were purchased from commercial suppliers (abcr, Acros, Alfa Aesar, Fluka, Fluorochem, Merck, Sigma Aldrich, TCI) and were used directly without purification unless stated otherwise. All air and moisture sensitive reactions were carried out under nitrogen atmosphere using standard Schlenk manifold technique. Anhydrous DMSO was used directly from the bottle or dried using activated 4Å molecular sieves. ^{1}H and ^{13}C Nuclear Magnetic Resonance (NMR) spectra were acquired at room temperature with field strengths as indicated and were referenced to $CDCl_3$ (7.26 and 77.16 ppm for ^{1}H and ^{13}C respectively), DMSO-d6 (2.50 and 39.52 for ^{1}H and ^{13}C respectively) or CD_3OD (3.31 and 49.0 ppm for ^{1}H and ^{13}C respectively). ^{1}H-NMR coupling constants are reported in Hertz and refer to apparent multiplicities and not true coupling constants. Data are reported as follows: chemical shift, multiplicity (s = singlet, bs = broad singlet, d = doublet, t = triplet, q = quartet, qi = quintet, sx = sextet, sp = septet, m = multiplet, dd = doublet of doublets, etc.), coupling constants, integration, proton assignment (determined by 2D NMR experiments: COSY, HSQC and HMBC) where possible. ^{13}C-NMR assignment was aided using DEPT 135 techniques (DEPT = distortion less enhancement by polarization transfer) to distinguish CH_2 groups from CH and CH_3 groups and to assign quaternary carbon atoms (C_q). ^{19}F-NMR spectra were recorded for compounds containing fluorine atoms.

Analytical TLC was performed on silica gel coated aluminium sheets (Merck, TLC Silica gel 60 F_{254}) Compounds were visualized by exposure to UV-light (254 or 366 nm) or by dipping the plates in staining solutions (permanganate stain, bromocresol green stain, ceric ammonium molybdate stain) followed by heating. Flash column chromatography was performed using Merck Silica Gel 60 (40–63 µm) & Medium pressure liquid chromatography (MPLC) was performed on a Grace Reveleris® X2 from Büchi with built-in UV-detector and fraction collector using Biotage® sfär silica HC D 20 µm column cartridges or on a Biotage® Isolera One flash purification system using flash silica gel. All mixed solvent eluents are reported as v/v solutions. High resolution mass spectrometry (HRMS) were performed at the Central Analytical Laboratory of the University of Regensburg. Mass spectra were recorded on a Finnigan MAT 95, ThermoQuest Finnigan TSQ 7000, Finnigan MAT SSQ 710 A or Agilent Q-TOF 6540 UHD instrument and a Waters Acquity UPLC system equipped with Waters PDA, sample manager, sample organiser, column oven and Waters Xevo QTOF mass spectrometer. Photoreactions in regular scale were irradiated with blue LEDs (OSRAM Oslon SSL 80 royal-blue, λ = 455 nm (± 15), average radiant flux 232 ± 23 mW, 2.9 V, 350 mA) or green LEDs (λ = 535 nm, average radiant flux, 29 ± 5 mW) and were exposed to light from the flat bottom side of the vial. The temperature of the reaction mixtures was controlled by a water-cooling circuit consisting of an aluminium cooling block connected to a thermostat (Figure S1). An exemplary reaction in larger scale was carried out in a

custom-built glass reactor which upon vigorous stirring generates a thin film of the reaction mixture between the reaction vessel and an attached cold finger. A hose which was dipped in the solution provided CO_2 gas from the cylinder. The reaction vessel was surrounded by blue LED arrays (OSRAM Oslon SSL 80 LT-2010, λ = 451 nm, 700 mA) generating a total radiant flux of 12 W (Figure S2). For the high-throughput screening experiments, Kessil PR160L 456 nm LEDs were used. Cyclic voltammetry measurements were performed with a three-electrode system consisting of a glassy carbon working electrode, a platinum wire counter electrode and a silver wire as a reference electrode. Data was processed on a potentiostat PGSTAT302N from Metrohm Autolab. Prior to the measurement the solvent DMSO (dry) was degassed with argon and TBATFB (0.1M) was added as supporting electrolyte. All experiments were performed under argon atmosphere. Ferrocene was used as an internal reference. Measurements were performed at a scan rate of 0.05 Vs^{-1}. Potentials are reported against saturated calomel electrode (SCE) as reference. UV-Vis measurements were performed on an Agilent Cary 4000 UV-Vis Spectrophotometer. Prior to measurements a solvent blank was recorded and subtracted. Precision cells (1×1 cm) made of quartz SUPRASIL® from Hellma® Analytics were used. Luminescence measurements were performed on a Horiba® Scientific FluoroMax-4 instrument using the above-mentioned quartz cells. Luminescence lifetime measurements were performed on a Horiba® Scientific DeltraPro™ fluorescence lifetime system using a 452 nm laser diode from Horiba® Scientific DeltaDiode™ as excitation source and above-mentioned quartz cells. The instrument response function (IRF) was determined prior to measurements by using colloidal silica (LUDOX®) in water.

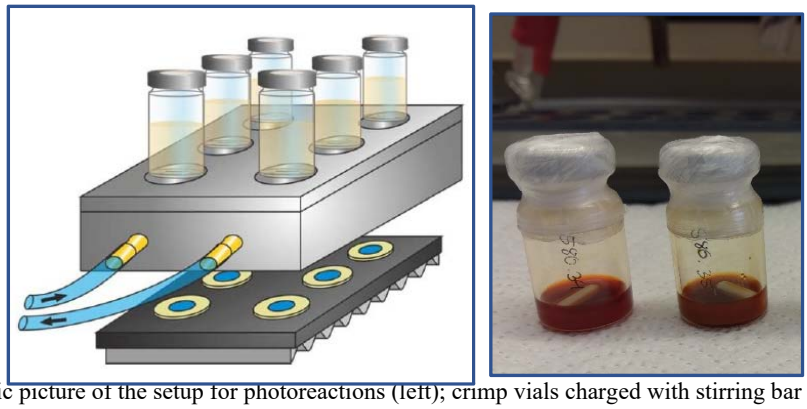

Figure S1. Schematic picture of the setup for photoreactions (left); crimp vials charged with stirring bar and reaction mixture and sealed with aluminium crimp seal with septum and Parafilm®

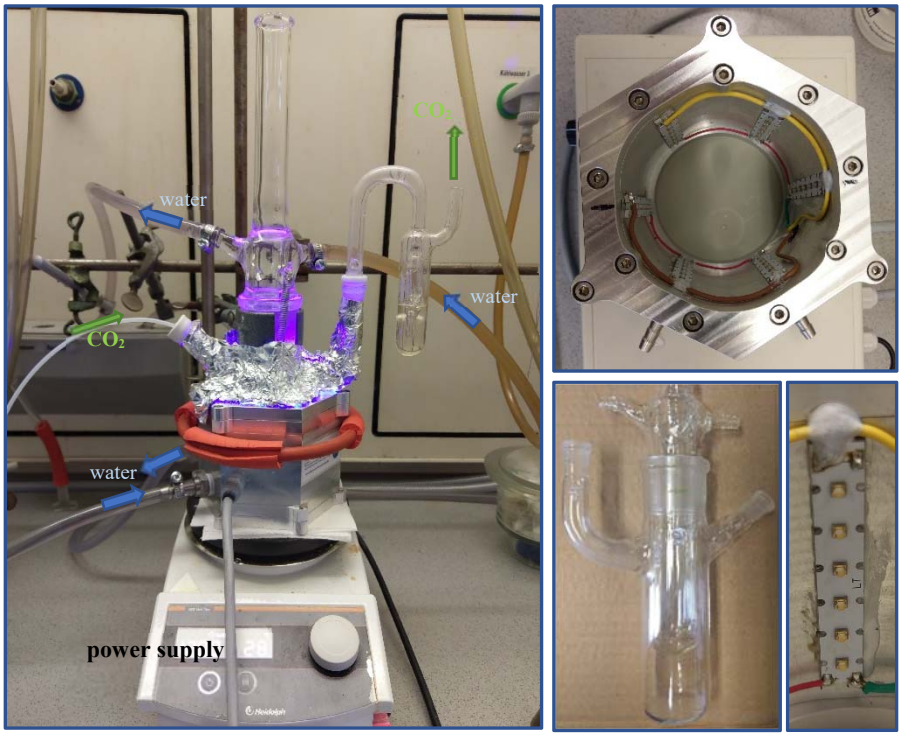

Figure S2. Custom-built glass reactor for upscaling of the photocatalytic carboxylation reaction.

2 - Catalyst Synthesis and Physicochemical Properties

2.1 - Synthesis of the Photocatalyst

2,3,6,7-tetramethoxyanthracen-9(10*H*)-one **TMAH** was synthesized in three steps with an overall yield of 33%. The catalyst in its neutral form is a bench stable compound and can be stored easily.

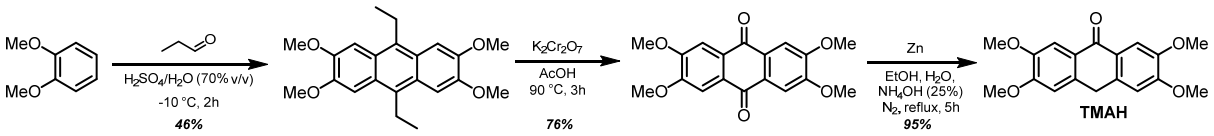

Scheme S1. Overview of the synthetic steps in the synthesis of the used photocatalyst **TMAH**; overall yield 33% (3 steps).

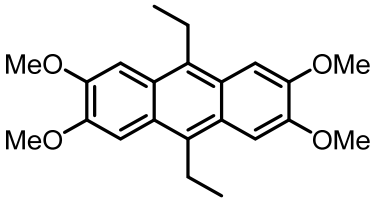

Synthesis of 9,10-diethyl-2,3,6,7-tetramethoxyanthracene: Referring to literature known procedures[1,2], a 250 mL round bottom flask equipped with stirring bar was charged with H_2SO_4 (70 mL, 70% v/v in H_2O) and veratrole (12.8 mL, 0.1 mol, 1 equiv.) and the resulting mixture was cooled to -10 °C. Under vigorous stirring, propanal (14.3 mL, 0.2 mol, 2 equiv.) was added dropwise *via* a syringe pump within 2 hrs. Care was taken, that the reaction temperature during addition of aldehyde was kept below 0 °C. The reaction mixture was poured into ice water (ca. 500 mL) and the resulting precipitate was filtered off and washed with water. The filter cake was dried over night by lyophilization and was washed in boiling EtOH. The precipitate was filtered off, washed with EtOH and dried under vacuo to give the title compound (8.06 g, 23 mmol, 46%) as pale-yellow powder. **^{1}H-NMR** (400 MHz, Chloroform-*d*) δ 7.41 (s, 4H), 4.07 (s, 12H), 3.47 (q, J = 7.6 Hz, 4H), 1.44 (t, J = 7.6 Hz, 6H). **^{13}C-NMR** (101 MHz, $CDCl_3$) δ 149.0 (C_q), 130.7 (C_q), 125.1 (C_q), 102.4, 55.8, 22.0 (CH_2), 14.6.

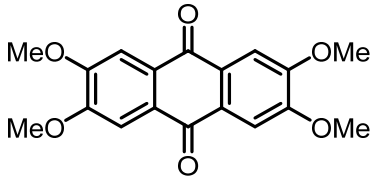

Synthesis of 2,3,6,7- tetramethoxy-9,10-anthraquinone: According to a literature known procedure[3] a 500 mL round bottom flask was charged with 9,10-diethyl-2,3,6,7-tetramethoxyanhtracene (8.0 g, 22.6 mmol, 1 equiv.) and $K_2Cr_2O_7$ (33.2 g, 113 mmol, 5 equiv.) and the solids were suspended in glacial acetic acid (270 mL). The resulting mixture was heated to 90 °C for 3 hrs. After the mixture was cooled

to ambient temperature the yellow precipitate was filtered off and washed several times with water to remove excess of $K_2Cr_2O_7$. The filter cake was freeze-dried and finally washed with Et_2O and dried in vacuo to afford the title compound as yellow powder (5.67 g, 17.3 mmol, 76%), which was used without further purification for the next step. **^{1}H-NMR** (300 MHz, Chloroform-*d*) δ 7.68 (s, 4H), 4.07 (s, 12H). **^{13}C-NMR** (101 MHz, $CDCl_3$) δ 182.1(C_q), 153.6 (C_q), 128.6 (C_q), 108.5, 56.7.

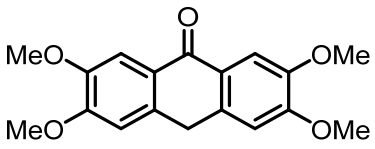

Synthesis of 2,3,6,7-tetramethoxyanthracen-9(10H)-one (**TMAH**): Referring to a literature known procedure[4] a 500 mL Schlenk flask equipped with stirring bar and condenser was charged with 2,3,6,7-tetramethoxy-9,10-anthraquinone (5.60 g, 17.1 mmol, 1 equiv) and zinc dust (3.40 g, 52.0 mmol, 3.1 equiv.). The flask was set under N_2 atmosphere and a mixture of aq. ammonia solution (135 mL, 25%), EtOH (135 mL) and water (135 mL) was added. The resulting mixture was refluxed for 5 hrs under N_2 atmosphere and vigorous stirring. The mixture was allowed to cool to ambient temperature and was poured in ice water (ca. 1 L). Conc. HCl (150 mL) was added to dissolve excess zinc and the mixture was stirred overnight. The turbid solution was filtered and the residue was washed several times with water and was freeze-dried to yield **TMAH** as pale-yellow powder (5.10 g, 16.2 mmol, 95%). **^{1}H-NMR** (400 MHz, Chloroform-*d*) δ 7.79 (s, 2H), 6.82 (s, 2H), 4.15 (s, 2H), 3.98 (d, J = 7.3 Hz, 12H). **^{13}C-NMR** (101 MHz, $CDCl_3$) δ 182.4 (C_q), 153.1 (C_q), 148.6 (C_q), 135.1 (C_q), 125.4 (C_q), 109.7, 108.5, 56.2, 32.0 (CH_2). Data in accordance with the literature.[3]

2.2 - Spectroscopic and Photochemical Characteristics

The properties of the used photocatalyst (PC) were investigated in various spectroscopic experiments.

2.2.1 - UV-Vis absorption

The absorption of the photocatalyst was recorded in dry, degassed DMSO (50µM) by using a quartz cuvette (1×1 cm) with septum screw cap. The cuvette was degassed *in vacuo* and backfilled with N_2 (5×) before the solvent and the catalyst solution were added *via* syringe. In presence of cesium carbonate, a distinct absorption band arises in the visible range of the spectrum (Figure S3). This process can also be followed by naked eye, as the solution turns from colorless into yellow.

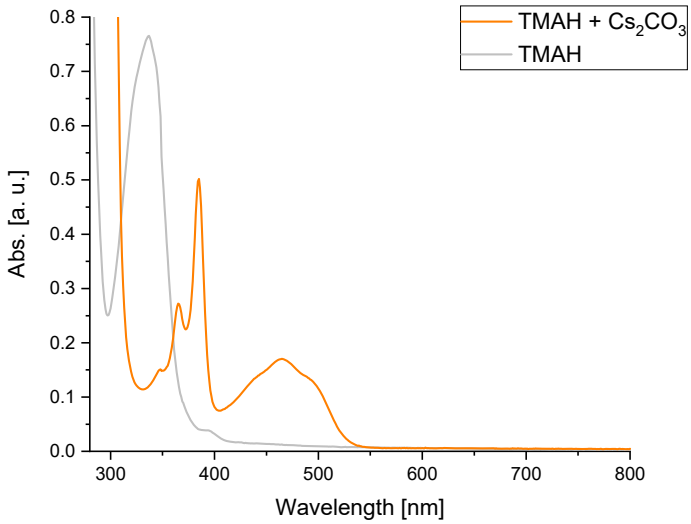

Figure S3. UV-vis spectra of (PC) in DMSO and in presence and absence of cesium carbonate.

2.2.2 - Emission spectra

The emission spectrum of the photocatalyst was recorded in dry, degassed DMSO in presence of cesium carbonate by using a quartz cuvette (1×1 cm) with septum screw cap. The cuvette was degassed *in vacuo* and backfilled with N_2 (5×) before the solvent and the catalyst solution were added *via* syringe. The excitation wavelength was set to 420 nm (entrance-/exit slit 1 nm) and the emission was measured starting from 450 nm to 800 nm (Increment 1 nm, entrance-/exit slit 2 nm). Relative intensities are plotted for absorption and emission (Figure S4a). To determine the intersection between normalized symmetrical absorption- and emission spectra, relative intensities for the lowest energy absorption band ($\lambda > 400$ nm) were calculated and plotted (Figure S4b).

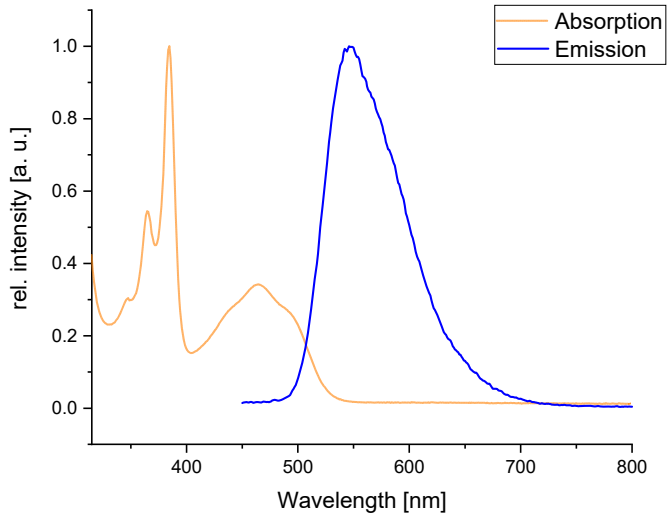

Figure S4a: Superimposed absorption and emission spectra of the photocatalyst in DMSO and in presence of cesium carbonate

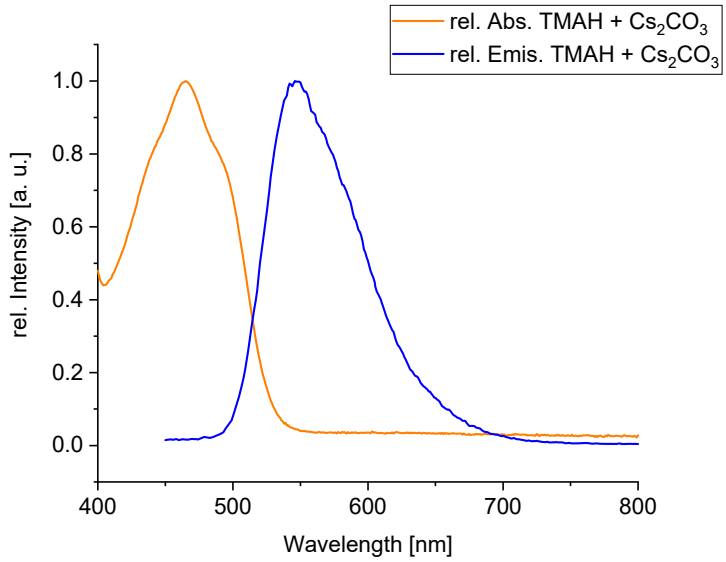

Figure S5b: Superimposed normalized absorption- and emission spectra of the photocatalyst in DMSO and in presence of cesium carbonate with an intersection at λ_{isec} = 514 nm.

2.2.3 - Excited state lifetime

The luminescence lifetime of the PC was recorded in dry, degassed DMSO in presence of cesium carbonate by using a quartz cuvette (1×1 cm) with septum screw cap. The cuvette was degassed *in vacuo* and backfilled with N_2 (5×) before the solvent and the catalyst solution were added *via* syringe. For excitation of the sample, a 452 nm laser diode was used and an optical longpass filter (cut-on wavelength

500 nm) was installed before the detection unit. The time range for the measurement was set to 400 ns. The experimental data were fitted with a mono-exponential function.

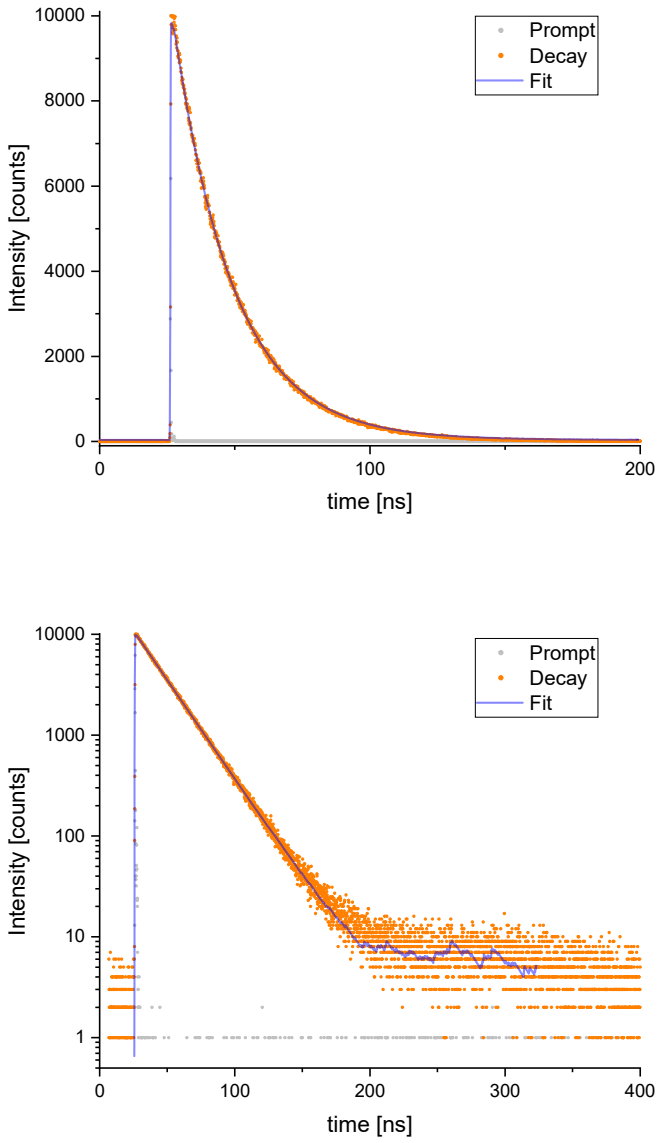

Figure S6. Luminescence decay of the excited photocatalyst with fit function in a linear plot (top) and logarithmic plot (bottom).

According to the parameters of the single-exponential fit function, a luminescence lifetime of 22.08 ns (CHISQ = 1.416859) was found.

2.2.4 - ^{1}H-NMR spectroscopy of TMAH

Proton NMR spectra of **TMAH** were recorded in absence and presence of Cs_2CO_3 (Figure S6a-b) in dried, degassed DMSO-d6. For the measurement in presence of base, a NMR tube with septum and screw-cap was used and the spectra was recorded under N_2 atmosphere. Integration over the NMR signals in presence of Cs_2CO_3 confirms the quantitative formation of the anionic species **TMA$^-$**.

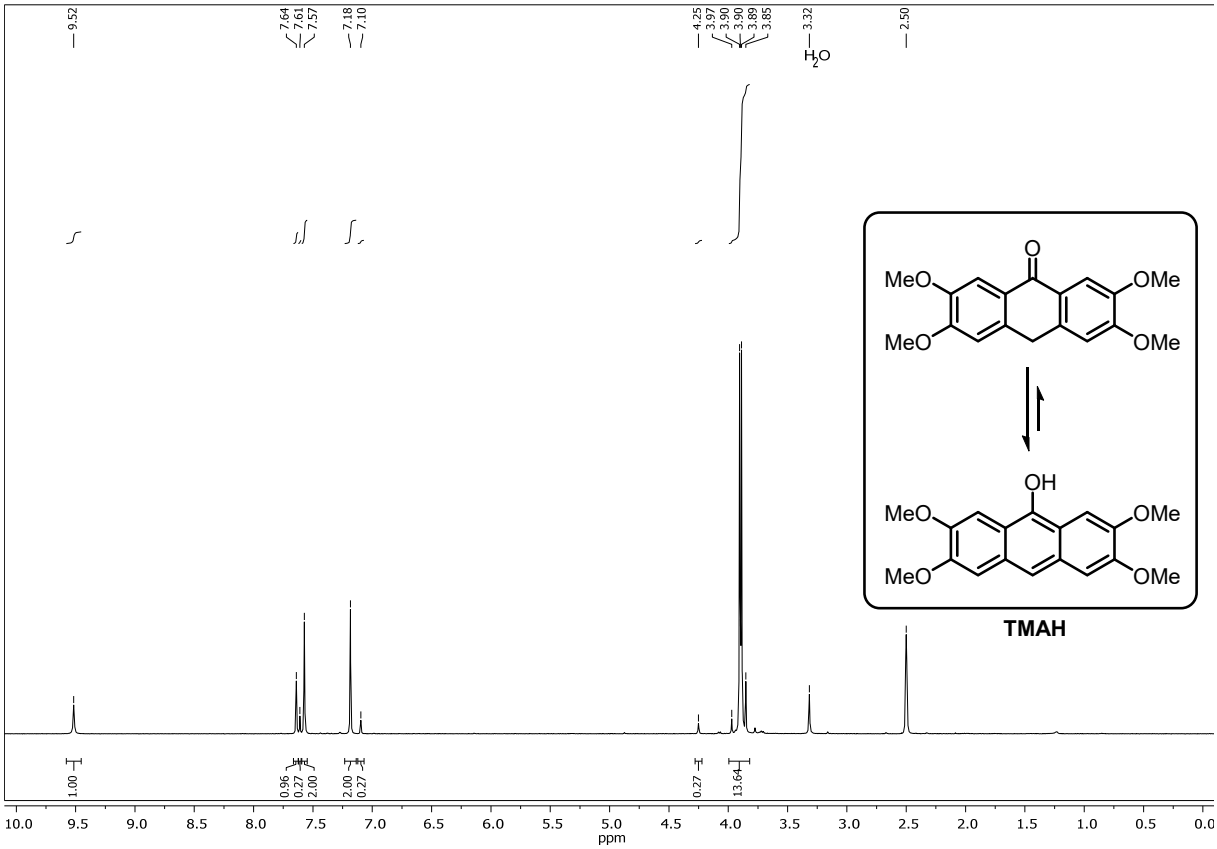

Figure S7a. ^{1}H-NMR of **TMAH** in DMSO-d6. The keto-enol tautomerism causes two sets of signals; The peak at 3.32 ppm is caused by residual water in the sample.

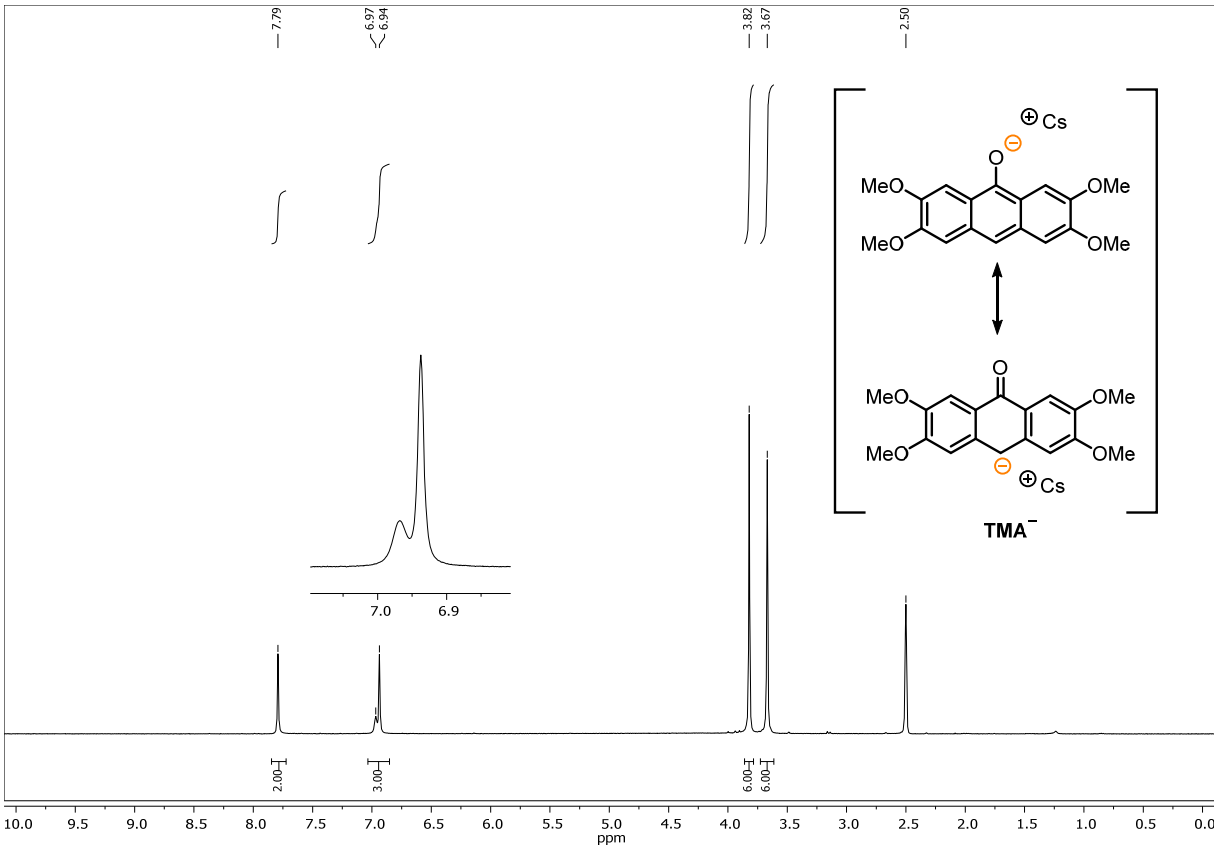

Figure S6b. ^{1}H-NMR of **TMAH** in presence of Cs_2CO_3 (6 eq.) in DMSO-d6.

2.2.5 - Ground state and excited state potential

The ground state potential of the photocatalyst was investigated by cyclic voltammetry. In presence of 1,1,3,3-tetramethylguanidine the anionic photocatalyst was oxidized (Figure S7) upon sweeping to positive potentials. Obtained potentials vs. Fc^{+}/Fc were converted to potentials against SCE.[5] The estimated excited state oxidation potential (E^{*}_{ox} = −2.92 V vs. SCE) of the photocatalyst was determined according to the free enthalpy change of PET (neglecting the solvent-dependent electrostatic work term) as described in literature[6,7] by taking the excited state energy ($E_{0,0}$ = 2.41 eV, λ_{isec} = 514 nm) and the converted ground state potential ($E_{p,ox}$ = −0.51 V vs. SCE) into account.

$$E^{*}_{ox} = E_{p,ox} - E_{0,0} + \omega$$

The obtained value for E^{*}_{ox} is based on following approximations: (a) As reported in literature,[8,9] the single electron oxidation of an organic anion causes an irreversible peak in the cyclic voltammogram and an accurate value for the ground state oxidation potential is not accessible. Thus, for the anionic photocatalyst the peak potential $E_{p,ox}$ obtained for this irreversible process (Figure S7) was used to determine the excited state potential. (b) The excited state energy $E_{0,0}$ can be estimated in a number of ways. When using the wavelength at the luminescence maximum $\lambda_{emis,max}$ (546 nm) an underestimation of $E_{0,0}$ is likely.[6] Furthermore, it is possible to use the midpoint between the absorption maximum of the

most red shifted absorption band and the emission maximum (506 nm). The most common way to determine $E_{0,0}$ is by taking the intersection between symmetric normalized absorption- and emission spectra (Figure S4b, $\lambda_{isec} = 514$ nm) which was used for the calculation herein. (c) The solvent-dependent electrostatic work term ω contributes little to the free enthalpy change of PET when working in polar solvents like DMSO and hence was omitted in the calculation.

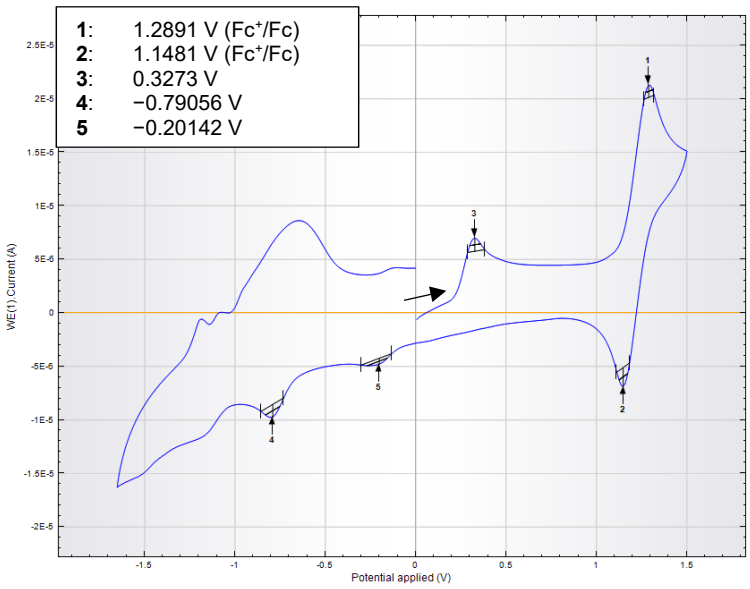

Figure S7. Cyclic voltammetry of the photocatalyst was recorded in anhydrous, degassed DMSO, in presence of 1,1,3,3-tetramethylguandine as base and ferrocene (peaks 1, 2) as internal reference.

3 - Substrate Synthesis

Methyl 2-(thiophen-2-yl)acetate (3h)

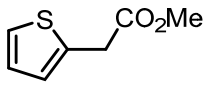

To a solution of 2-thiopheneacetic acid (123 mg, 0.2 mmol) in methanol (2 mL) was added conc. H_2SO_4 (2 drops) and the reaction was heated at reflux for 4 h. The solution was cooled, diluted with water (20 mL) and extracted with diethyl ether (3×20 mL). The combined organics were washed with brine (2×50 mL), dried via a phase separator and concentrated *in vacuo*. Purification by column chromatography on silica gel eluting with heptane:EtOAc (9:1) gave the title compound as a colorless oil (125 mg, 92%). **^{1}H-NMR** (400 MHz, $CDCl_3$) δ 7.22 (dd, *J* = 4.9, 1.4 Hz, 1H), 6.98–6.95 (m, 2H), 3.85 (s, 2H), 3.73 (s, 3H); **^{13}C-NMR** (100 MHz, $CDCl_3$) δ 171.2, 135.3, 127.2, 127.1, 125.4, 52.6, 35.5. Data in accordance with the literature.[10]

***tert*-Butyl (3-(benzo[*b*]thiophen-4-yloxy)-2-hydroxypropyl)(isopropyl)carbamate (5e)**

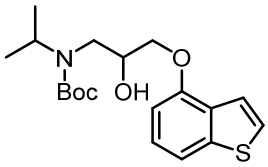

1-(Benzo[*b*]thiophen-4-yloxy)-3-(isopropylamino)propan-2-ol (239 mg, 0.9 mmol), triethylamine (0.377 ml, 2.70 mmol), and di-*tert*-butyl dicarbonate (0.236 g, 1.08 mmol) were added to a 50 mL round bottom flask. DCM (25 mL) was added and the mixture stirred at room temperature for 2 h. Water (25 mL) was subsequently added and the layers were separated. The organic layer was washed brine (2 x 25 mL) with then dried *via* a phase separator and concentrated *in vacuo*. Purification by column chromatography on silica gel eluting with heptane:EtOAc (9:1) gave the title compound as a yellow/orange oil (151 mg, 45%). R_f 0.56 [petrol–EtOAc (9:1)]; **^{1}H-NMR** (400 MHz, DMSO) δ 7.66 (d, *J* = 5.4 Hz, 1H), 7.53 (dd, *J* = 10.5, 2.3 Hz, 2H), 7.30 (t, *J* = 8.0 Hz, 1H), 6.84 (d, *J* = 7.9 Hz, 1H), 5.76 (s, 1H), 5.17 (d, *J* = 5.2 Hz, 1H), 4.23 – 3.89 (m, 4H), 3.54 – 3.22 (m, 1H), 1.38 (s, 9H), 1.24 – 1.01 (m, 6H). **^{13}C-NMR** (125 MHz, DMSO) δ 156.4, 155.2, 141.5, 131.1, 130.0, 128.9, 123.2, 121.1, 109.1, 80.3, 71.5, 68.2, 49.0, 45.5, 28.3, 19.5.

***tert*-Butyl 2-phenyl-1*H*-indole-1-carboxylate (3v)**

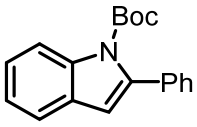

The compound was synthesized according to a literature known procedure.[11] In a flame dried 100 mL Schlenk flask under N_2 atmosphere equipped with stirring bar, $(Boc)_2O$ (1.20 g, 5.50 mmol, 1.1 equiv.) was added to a solution of 2-phenylindole (0.966 g, 5.0 mmol, 1 equiv.) and 4-(*N*,*N*-dimethylamino)pyridine in dry MeCN (30 mL). The resulting mixture was stirred at room temperature for 24 h and was then concentrated *in vacuo*. After the addition of water, the mixture was extracted with EtOAc (3×). The combined organic layers were washed with brine, dried over Na_2SO_4, filtered and concentrated under reduced pressure. The crude material was purified by flash silica gel column chromatography using a mixture of hexanes/EtOAc to provide the title compound as white solid (1.40 g, 4.8 mmol, 96%). **^{1}H-NMR** (400 MHz, Chloroform-*d*) δ 8.27 – 8.20 (m, 1H), 7.59 – 7.54 (m, 1H), 7.46 – 7.31 (m, 6H), 7.27 (td, *J* = 7.6, 0.9 Hz, 1H), 6.57 (s, 1H), 1.32 (s, 9H). **^{13}C-NMR** (101 MHz, $CDCl_3$) δ 150.3 (C_q), 140.6 (C_q), 137.6 (C_q), 135.1 (C_q), 129.3 (C_q), 128.9, 127.9, 127.7, 124.4, 123.0, 120.6, 115.3, 110.0, 83.5 (C_q), 27.7.

Thieno[2,3-*d*]pyrimidine (3y)

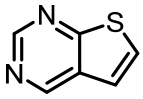

Based on a literature reported procedure for dehalogenation of aromatic compounds[12], a 5 mL crimp vial equipped with stirring bar was charged with 4-chlorothieno[2,3-*d*]pyrimidine (17.1 mg, 0.1 mmol, 1 equiv.) and 10-phenylphenothiazine (2.8 mg, 0.01 mmol, 10 mol%) and sealed with an aluminium crimp seal with septum. The vial was degassed and flushed with N_2 and tributylamine (119 µL, 0.5 mmol, 5 equiv.), formic acid (18.9 µL, 0.5 mmol, 5 equiv.) and dry MeCN (1 mL) were added. The reaction mixture was degassed by freeze-pump-thaw cycles (3×) and backfilled with N_2. The crimp vial was irradiated from the bottom side with 365 nm LED light for 22 hrs and a constant reaction temperature (25°C) was maintained by employing a water-cooling circuit connected to a thermostat. For isolation of the compound, 10 reactions were combined. The reactions were quenched by adding water and brine and the resulting mixture was extracted with EtOAc (3×). The combined organic layers were dried over Na_2SO_4, filtered and concentrated *in vacuo*. Purification was accomplished by flash silica gel chromatography using a mixture of hexanes/EtOAc as eluents and subsequent recrystallization from hexanes to afford the title compound as pale-yellow needles (31.8 mg, 0.23 mmol, 23%). **^{1}H-NMR** (400

MHz, Chloroform-*d*) δ 9.16 (s, 1H), 9.10 (s, 1H), 7.57 (d, *J* = 6.0 Hz, 1H), 7.36 (d, *J* = 6.0 Hz, 1H). Data in accordance with the literature.[13]

2-(Thiophen-3-yl)pyridine (**3z**)

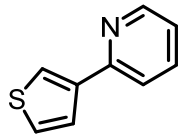

Following a literature known procedure[14] a 10 mL crimp vial was charged with 3-thienylboronic acid (130 mg, 1.01 mmol, 1.2 equiv.), K_2CO_3 (326 mg, 2.36 mmol, 2.8 equiv.), $[Pd(PPh_3)_2Cl_2]$ (29.6 mg, 0.042 mmol, 0.05 equiv.), DME (2.5 mL) and water (1.17 mL). The vial was sealed with an aluminium crimp seal with septum and argon was bubbled through the solution for 10 minutes. Bromopyridine (81 µL, 0.842 mmol, 1 equiv.) was added *via* syringe and the reaction was stirred in a pre-heated heating block for 18 hrs at 80 °C. The reaction was allowed to cool to ambient temperature, was quenched by adding water and was extracted with EtOAc (3×). The combined organic layers were washed with brine, dried over Na_2SO_4, filtered and concentrated *in vacuo*. The crude product was purified by flash silica gel column chromatography using a mixture of hexanes/EtOAc and was obtained as colorless oil (127 mg, 0.79 mmol, 94%). **^{1}H-NMR** (400 MHz, Chloroform-*d*) δ 8.62 (ddd, *J* = 4.9, 1.8, 0.9 Hz, 1H), 7.90 (dd, *J* = 3.0, 1.3 Hz, 1H), 7.70 (td, *J* = 7.7, 1.8 Hz, 1H), 7.66 (dd, *J* = 5.0, 1.3 Hz, 1H), 7.62 (dt, *J* = 8.0, 1.1 Hz, 1H), 7.40 (dd, *J* = 5.0, 3.0 Hz, 1H), 7.17 (ddd, *J* = 7.4, 4.9, 1.2 Hz, 1H). **^{13}C-NMR** (101 MHz, $CDCl_3$) δ 153.7 (C_q), 149.8, 142.3 (C_q), 136.8, 126.4, 126.3, 123.6, 121.9, 120.4.

***N*,*N*-Dimethyl-4-vinylaniline** (**7g**)

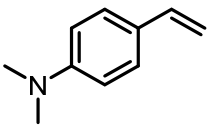

According to a literature known procedure[15] a flame-dried 250 mL Schlenk flask was charged under N_2 atmosphere with methyltriphenylphosphonium bromide (14.4 g, 40.3 mmol, 1 equiv.) and dry THF (60 mL). The suspension was cooled to 0 °C and *n*-BuLi (1.6M in hexane, 25.2 mL, 40.3 mmol, 1 equiv.) was slowly added *via* syringe and the resulting mixture was stirred for 1 h. A solution of 4-(*N*,*N*-dimethylamino)benzaldehyde (6.02 g, 40.3 mmol, 1 equiv.) in dry THF (20 mL) was added dropwise and the reaction was further stirred at 0 °C for 1 h and at ambient temperature for 18 hrs. The reaction was quenched by adding sat. aq. NH_4Cl (30 mL) and the resulting mixture was extracted with DCM (3×20 mL) and the combined organic layers were dried over Na_2SO_4, filtered and concentrated *in vacuo*. Purification by vacuum distillation (0.8 mbar, 75 °C) afforded the title compound as yellowish oil

(4.70 g, 31.9 mmol, 79%). **^{1}H-NMR** (300 MHz, Chloroform-*d*) δ 7.37 – 7.27 (m, 2H), 6.75 – 6.58 (m, 3H), 5.55 (dd, *J* = 17.6, 1.1 Hz, 1H), 5.03 (dd, *J* = 10.9, 1.1 Hz, 1H), 2.97 (s, 6H). **^{13}C-NMR** (75 MHz, $CDCl_3$) δ 150.4 (C_q), 136.7, 127.3, 126.3 (C_q), 112.5, 109.5 (CH_2), 40.7.

Methyl(4-vinylphenyl)sulfane (**7h**)

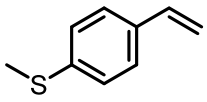

According to a literature known procedure[15] a flame-dried 250 mL Schlenk flask was charged under N_2 atmosphere with methyltriphenylphosphonium bromide (14.1 g, 39.5 mmol, 1 equiv.) and dry THF (60 mL). The suspension was cooled to 0 °C and *n*-BuLi (1.6M in hexane, 30 mL, 48 mmol, 1.2 equiv.) was slowly added *via* syringe and the resulting mixture was stirred for 1 h. 4-(Methylthio)benzaldehyde (5.24 mL, 38.4 mmol, 1 equiv.) was added dropwise *via* syringe and the reaction mixture was stirred for further 2.5 h at 0 °C. After dilution with THF (20 mL) the reaction was stirred at ambient temperature overnight and was quenched by adding sat. aq. NH_4Cl (20 mL). The crude mixture was extracted with DCM (3×20 mL) and the combined organic layers were dried over Na_2SO_4, filtered and concentrated *in vacuo*. Purification by flash silica gel chromatography (hexanes/MTBE) afforded the title compound as colorless liquid (4.04 g, 26.9 mmol, 68%). **^{1}H-NMR** (400 MHz, Chloroform-*d*) δ 7.37 – 7.32 (m, 2H), 7.25 – 7.20 (m, 2H), 6.69 (dd, *J* = 17.6, 10.9 Hz, 1H), 5.73 (dt, *J* = 17.6, 0.9 Hz, 1H), 5.23 (dt, *J* = 10.8, 0.9 Hz, 1H), 2.50 (s, 3H). **^{13}C-NMR** (101 MHz, $CDCl_3$) δ 138.1 (C_q), 136.3, 134.6 (C_q), 126.7, 126.7, 113.3 (CH_2), 15.9.

4 - Carboxylation Reactions

4.1 - Reaction Optimization

4.1.1 - General Procedure for the Reaction Optimization – GP1

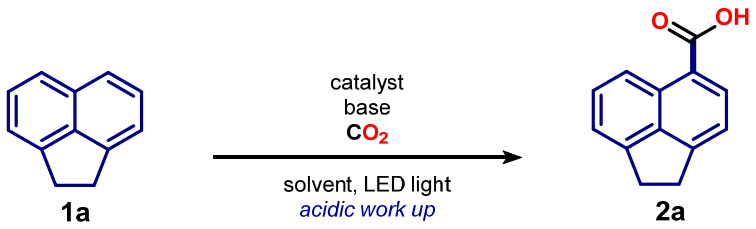

To a dry flat-bottomed crimp vial (5 mL) equipped with stirring bar, was added acenaphthene (**1a**, 0.1-0.2 mmol, 1 equiv.) and photocatalyst (5-20 mol%, Scheme S2). Base (if solid) was quickly added and the vial was sealed with a Supelco aluminium crimp seal with septum (PTFE/butyl). The vial was then evacuated and refilled with CO_2 (5×) *via* syringe needle. The reaction mixture was dissolved in the solvent (dry and degassed by bubbling with N_2) and base (if liquid) was added *via* syringe. The vial was sealed with two layers of Parafilm® and then had gaseous CO_2 added *via* a Luer Lock Monoject™ (20 ccm) syringe, into the head space. The vial was then stirred and irradiated from the bottom side and a constant reaction temperature (0 °C or 25 °C) was maintained by employing a cooling circuit connected to a thermostat. After 18 hrs the reaction was transferred with aq. NaOH (0.1M) into a centrifuge tube and was washed with Et_2O (2×) to remove left over starting material or non-polar side products. The aqueous layer was acidified by adding aq. HCl (2M) and was extracted with EtOAc (3×). The combined organic layers were dried over Na_2SO_4, filtered and concentrated *in vacuo*. As internal standard a stock solution of 1,3,5-trimethoxybenzene in DMSO-d6 (0.7 mL, 42.9 mM) was added and the mixture was analyzed by ^{1}H-NMR spectroscopy. The ^{1}H-NMR yield was determined by integration over product signals and internal standard signals.

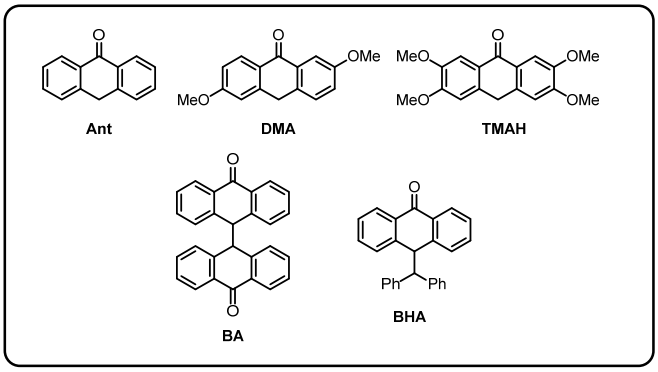

Scheme S2. Tested 9-anthrone based derivatives for the optimization of the carboxylation reaction; 9-anthrone (**Ant**), 2,6-dimethoxyanthracen-9(10*H*)-one (**DMA**), 2,3,6,7-tetramethoxyanthracen-9(10*H*)-one (**TMAH**), bianthronyl (**BA**), 10-benzhydryl-anthrone (**BHA**).

Table S1. Optimization of the photocatalyzed aromatic C-H carboxylation.

entry	PC (mol%)	base (eq.)	solvent	λ [nm]	V(CO_2) added [ccm]	NMR yield [%]
1	**Ant** (20)	Cs_2CO_3 (2)	DMSO	455	22	n.d.[a]
2	**DMA** (20)	Cs_2CO_3 (2)	DMSO	455	22	n.d.
3	**TMA** (20)	Cs_2CO_3 (2)	DMSO	455	22	37[b]
4	**BA** (20)	Cs_2CO_3 (2)	DMSO	455	22	trace
5	**BHA** (20)	Cs_2CO_3 (2)	DMSO	455	22	n.d.
6	**TMAH** (20)	Cs_2CO_3 (1)	DMSO	455	22	1
7	**TMAH** (20)	Cs_2CO_3 (3)	DMSO	455	22	68[b]
8	**TMAH** (20)	Cs_2CO_3 (4)	DMSO	455	22	59
9	**TMAH** (5)	Cs_2CO_3 (2)	DMSO	455	22	54
10	**TMAH** (10)	Cs_2CO_3 (2)	DMSO	455	22	60
11	**TMAH** (10)	Cs_2CO_3 (3)	DMSO	455	22	56
12[c]	**TMAH** (20)	Cs_2CO_3 (3)	DMSO	455	22	52
13	**TMAH** (20)	Na_2CO_3 (2)	DMSO	455	22	1
14	**TMAH** (20)	K_2CO_3 (2)	DMSO	455	22	17
15	**TMAH** (10)	K_2CO_3 (3)	DMSO	455	22	25
16[c]	**TMAH** (10)	K_2CO_3 (3)	DMSO	455	22	47
17[c]	**TMAH** (20)	K_2CO_3 (3)	DMSO	455	22	38
18	**TMAH** (20)	$(NH_4)_2CO_3$ (3)	DMSO	455	22	2
19	**TMAH** (20)	Cs pivalate (3)	DMSO	455	22	6
20	**TMAH** (20)	K_3PO_4 (3)	DMSO	455	22	trace
21	**TMAH** (20)	$(NBu_4)H_2PO_4$ (3)	DMSO	455	22	7
22	**TMAH** (20)	DBU (3)	DMSO	455	22	28
23	**TMAH** (20)	TMG (3)	DMSO	455	22	22
24	**TMAH** (20)	BTMG (3)	DMSO	455	22	25
25	**TMAH** (20)	Cs_2CO_3 (3)	DMF	455	22	35
26	**TMAH** (20)	Cs_2CO_3 (3)	DMA	455	22	12
27	**TMAH** (20)	Cs_2CO_3 (3)	NMP	455	22	14
28	**TMAH** (20)	Cs_2CO_3 (3)	^{i}PrOH	455	22	n.d.
29	**TMAH** (20)	Cs_2CO_3 (3)	DCM	455	22	n.d.
30	**TMAH** (20)	Cs_2CO_3 (3)	acetone	455	22	trace
31	**TMAH** (20)	Cs_2CO_3 (3)	DMSO	400	22	14
32	**TMAH** (20)	Cs_2CO_3 (3)	DMSO	535	22	29
33	**TMAH** (20)	Cs_2CO_3 (3)	DMSO	white[d]	22	27
34	**TMAH** (20)	Cs_2CO_3 (3)	DMSO	455[e]	22	23
35	**TMAH** (20)	Cs_2CO_3 (3)	DMSO	455[f]	22	56
36[g]	**TMAH** (20)	Cs_2CO_3 (3)	DMSO/DMF (1:1)	455	22	17
37	**TMAH** (20)	Cs_2CO_3 (3)	DMSO	455	-[h]	37
38	**TMAH** (20)	Cs_2CO_3 (3)	DMSO	455	11	48
39[i]	**TMAH** (20)	Cs_2CO_3 (3)	DMSO	455	22	39
40[j]	**TMAH** (20)	Cs_2CO_3 (3)	DMSO	455	22	51
41[k]	**TMAH** (20)	Cs_2CO_3 (3)	DMSO	455	22	13
42[l]	**TMAH** (20)	Cs_2CO_3 (3)	DMSO	455	22	34
43[m]	**TMAH** (20)	Cs_2CO_3 (3)	DMSO	455	22	49
44[n]	**TMAH** (20)	Cs_2CO_3 (3)	DMSO	455	22	57
45[o]	**TMAH** (20)	Cs_2CO_3 (3)	DMSO	455	22	52

All reactions, if not otherwise stated, were run following GP1: [a] product was not detected; [b] isolated yield following GP2a; [c] reaction was run with 18-crown-6 (1 equiv.); [d] cold white LED; [e] fan-cooled high-power LED setup (7 W) was used. Due to inefficient cooling, the reaction temperature was significantly elevated; [f] water-cooled high-power LED setup (1.4 W) was used. DMSO was saturated with CO_2 by bubbling gas through the solvent; [g] reaction was run at 0 °C; [h] reaction was run without pressure (1 atm) of CO_2; [i] reaction was run with 0.2 mmol of substrate; [j] concentration was changed to 0.05 M (0.1 mmol substrate in 2 mL DMSO); [k] reaction with chloro(pyridine)bis(dimethylglyoximato)cobalt(III) (5 mol%); [l] reaction with *p*-terphenyl (5 mol%); [m] reaction with *p*-quaterphenyl (5 mol%); [n] reaction with (^{i}Pr)$_3$SiSH (10 mol%); [o] reaction with 1,4-cyclohexadiene (20 mol%).

4.1.2 - Kinetic profile of the aromatic carboxylation reaction

Under the optimized conditions the kinetic profile of the reaction was monitored within the first six hours of the reaction (Figure S8). Reactions were run following GP1.

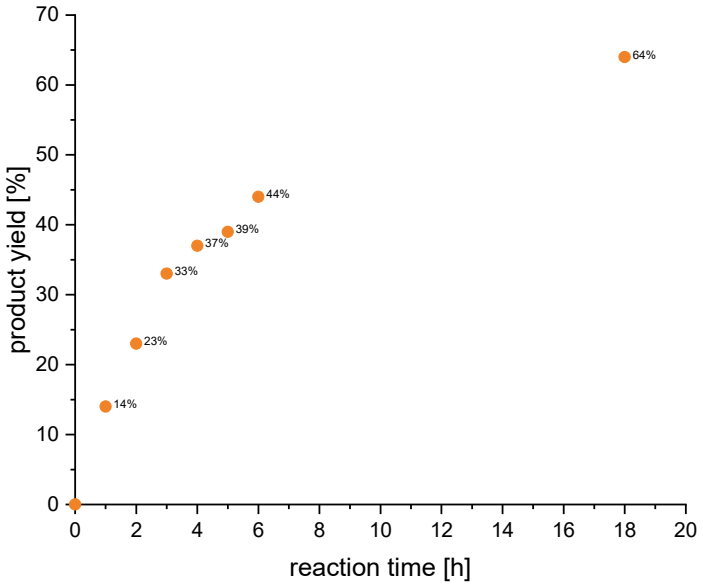

Figure S8. The progress of the carboxylation reaction was monitored within the first six hours.

4.1.3 - Control reactions

Conducted control experiments revealed that all compounds and light are crucial for product formation (Table S2). To exclude a base promoted carboxylation reaction, substrates **3c** & **3j** possessing acidic C-H bonds were tested in absence of catalyst and light and upon work-up, the respective products **4c** & **4j** could not be detected. Substrates **3b** and **3p** gave excellent yields of the respective carboxylation products following GP2a. No product was formed in absence of light and catalyst, demonstrating the photocatalytic nature of this reaction.

Table S2. Control reactions

entry	PC (mol%)	Substrate	base (eq.)	λ [nm]	V(CO_2) added [ccm]	Product	NMR yield [%]
1	-	**1a**	Cs_2CO_3 (3)	455	22	**2a**	n.d.[a]
2	**TMAH** (20)	**1a**	-	455	22	**2a**	n.d.
3	**TMAH** (20)	**1a**	Cs_2CO_3 (3)	455	no CO_2[b]	**2a**	n.d.
4	**TMAH** (20)	**1a**	Cs_2CO_3 (3)	dark[c]	22	**2a**	n.d.
5	-	**3b**[d]	Cs_2CO_3 (3)	dark	22	**4b**	n.d.
6	-	**3c**[e]	Cs_2CO_3 (3)	dark	22	**4c**	n.d.
7	-	**3j**[f]	Cs_2CO_3 (3)	dark	22	**4j**	n.d.
8	-	**3p**[g]	Cs_2CO_3 (3)	dark	22	**4p**	n.d.

All reactions, if not otherwise stated, were run following GP1: [a] product was not detected; [b] reaction was run under N_2 atmosphere; [c] reaction was stirred in the dark; [d] reaction was run following GP1 using **3b** (0.1 mmol) as substrate; [e] reaction was run following GP1 using **3c** (0.1 mmol) as substrate; [f] reaction was run following GP1 using **3j** (0.1 mmol) as substrate; [g] reaction was run following GP1 using **3p** (0.1 mmol) as substrate.

4.2 - Substrate Scope

General Procedure for Carboxylation of Hetero(arenes) and Styrenes– GP2a

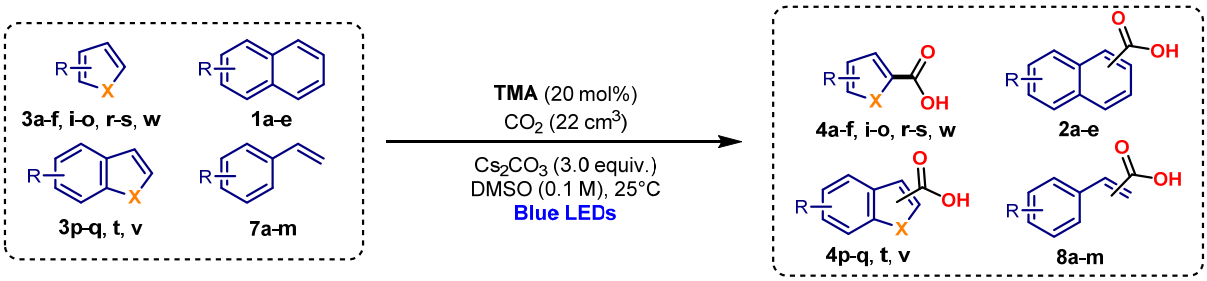

To a dry flat-bottomed crimp vial (5 mL) equipped with stirring bar, was added the arene (if solid) (0.1 mmol) and 2,3,6,7-tetramethoxyanthracen-9(10*H*)-one (6.3 mg, 0.02 mmol, 20 mol%). Cs_2CO_3 (98 mg, 3 equiv.) was quickly added and the vial was sealed with a Supelco aluminium crimp seal with septum (PTFE/butyl). The vial was then evacuated and refilled with CO_2 (5×) *via* syringe needle. The reaction mixture was dissolved in DMSO (1 mL, dry and degassed by bubbling with N_2) and the arene (0.1 mmol) (if liquid) was added *via* syringe. The vial was sealed with two layers of Parafilm® and then had gaseous CO_2 added *via* a Luer Lock Monoject™ (20 ccm) syringe, into the head space. The vial was then irradiated from the bottom side with blue LED light and a constant reaction temperature (25°C) was maintained by employing a water-cooling circuit connected to a thermostat. After 18 hrs of reaction time the pressure was released. For product isolation, the reaction mixtures of 4 reactions run in parallel were combined and transferred with water and Et_2O into a separating funnel. The ether layer was extracted with water (3×) and the combined aqueous layers were acidified with aq. HCl (2M) to adjust to an acidic pH. The aqueous layer was extracted with EtOAc (3×) and the combined EtOAc layers were dried over Na_2SO_4, filtered and concentrated *in vacuo*. The crude material was purified by silica flash column chromatography using mixtures of hexanes and ethyl acetate with 0.5% HOAc (v/v) as eluents.

General Procedure for Carboxylation of Arenes – GP2b (no glovebox)

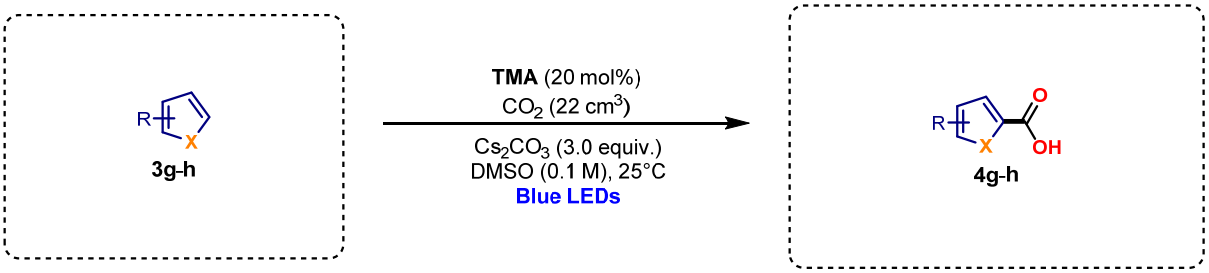

To a dry flat-bottomed crimp vial (5 mL) equipped with stirring bar, was added the arene (if solid) (0.1 mmol) and 2,3,6,7-tetramethoxyanthracen-9(10*H*)-one (6.3 mg, 0.02 mmol, 20 mol%). Cs_2CO_3 (98 mg, 3 equiv.) was quickly added and the vial was sealed with a Supelco aluminium crimp seal with septum (PTFE/butyl). The vial was then evacuated and refilled with N_2 (3×) *via* syringe needle. The reaction mixture was dissolved in DMSO (1 mL, dry and degassed by bubbling with N_2) and the arene (0.1 mmol) (if liquid) was added *via* syringe. The reaction mixture then had gaseous CO_2 (22 cm^3) added *via* a gastight Hamilton® syringe, into the head space of the vial. The vial was then irradiated from the bottom side with blue light and a constant reaction temperature (25°C) was maintained by employing a water-cooling circuit connected to a thermostat. After the designated time the reactions were extracted *via* an acid base wash. The combined organic layers were dried over Na_2SO_4, filtered and concentrated *in vacuo*.

General Procedure for Carboxylation of Arenes – GP2c (glovebox)

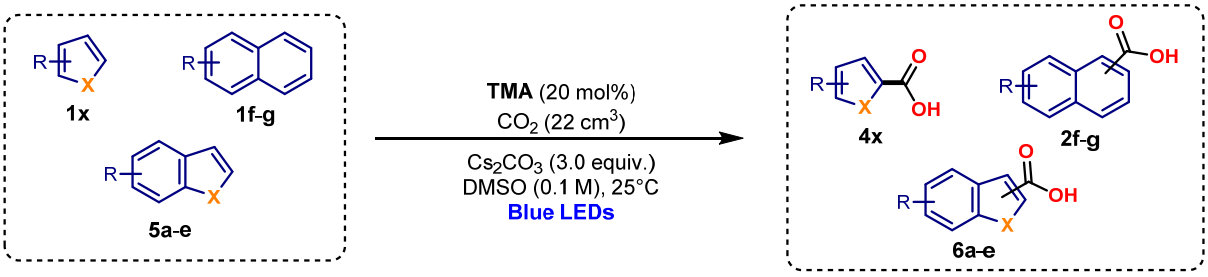

To a dry microwave vial (5 mL) equipped with stirring bar, was added the arene (if solid) (0.1 mmol) and 2,3,6,7-tetramethoxyanthracen-9(10H)-one (6.3 mg, 0.02 mmol, 20 mol%). The vials were sealed and transferred to a glovebox after the vial had evacuated and refilled with N_2 (×3) within the antechamber via syringe. Cs_2CO_3 (98 mg, 3 equiv.) and DMSO (1 mL) was added and the vial was sealed with a Supelco aluminium crimp seal with septum (PTFE/butyl). The vials were removed from the glovebox and the arene (0.1 mmol) (if liquid) was added via syringe. The reaction mixture then had gaseous CO_2 (22 cm^3) added via a gastight Hamilton® syringe, into the head space of the vial. The vial was then irradiated from two sides by two kessil lamps (vials approximately 6 cm away from the light source) with fans placed in front of the vials for cooling (temperatures measured via IR ranged between 25-30 °C). After 18 hrs. the irradiation was stopped and the vials were decapped quenched with aq. HCl (1 mL, 0.3M) and monitored by LCMS and ^{1}H NMR. Reactions were filtered of any solids and purified directly *via* prep-HPLC.

General Procedure for the substitution reaction of benzo[*b*]thiophene with ketones– GP3

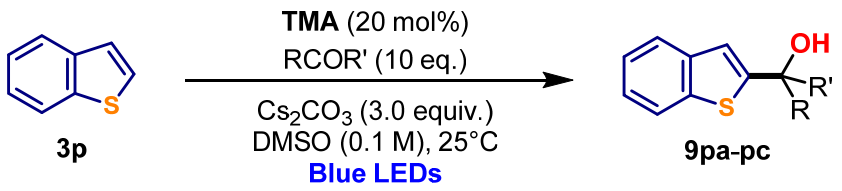

To a dry flat-bottomed crimp vial (5 mL) equipped with stirring bar, was added the benzo[*b*]thiophene (13.4 mg, 0.1 mmol, 1 equiv.) and 2,3,6,7-tetramethoxyanthracen-9(10*H*)-one (6.3 mg, 0.02 mmol, 20 mol%). Cs_2CO_3 (98 mg, 0.3 mmol, 3 equiv.) was quickly added and the vial was sealed with a Supelco aluminium crimp seal with septum (PTFE/butyl). The vial was then evacuated and refilled with N_2 (5×) *via* syringe needle. The reaction mixture was dissolved in DMSO (1mL, dry and degassed by bubbling with N_2) and the ketone (1.0 mmol, 10 equiv.) was added *via* syringe. The vial was then irradiated from the bottom side with blue LED light and a constant reaction temperature (25°C) was maintained by employing a water-cooling circuit connected to a thermostat. After 18 hrs the reaction was quenched by adding water. For product isolation, the reaction mixtures of 4 reactions run in parallel were combined and transferred with water and EtOAc into a separating funnel. The reaction mixture was extracted with EtOAc (3×) and the combined organic layers were dried over Na_2SO_4, filtered and concentrated *in vacuo*. The crude material was purified by silica flash column chromatography using mixtures of hexanes and ethyl acetate as eluents.

1,2-Dihydroacenaphthylene-5-carboxylic acid (2a)

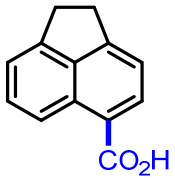

Following GP2a, acenaphthene (0.4 mmol) gave **2a** (68%) as a pale orange solid; **^{1}H-NMR** (400 MHz, Chloroform-*d*) δ 8.74 (d, *J* = 8.5 Hz, 1H), 8.45 (d, *J* = 7.3 Hz, 1H), 7.63 (dd, *J* = 8.6, 6.9 Hz, 1H), 7.37 (dd, *J* = 12.2, 7.1 Hz, 2H), 3.45 (s, 4H). **^{1}H-NMR** (400 MHz, DMSO-d_6) δ 12.85 (bs, 1H), 8.60 (d, *J* = 8.5 Hz, 1H), 8.22 (d, *J* = 7.3 Hz, 1H), 7.57 (dd, *J* = 8.6, 6.9 Hz, 1H), 7.36 (t, *J* = 6.6 Hz, 2H), 3.35 (s, 4H). **^{13}C-NMR** (101 MHz, DMSO) δ 168.3 (C_q), 152.5 (C_q), 146.2 (C_q), 139.1 (C_q), 132.9, 129.8 (C_q), 129.6, 122.3 (C_q), 121.6, 119.9, 118.6, 29.9. **HRMS** (EI+): calculated *m/z* for $C_{13}H_{10}O_2$ [$M^{+\bullet}$] 198.06753; found 198.06722. Data in accordance with the literature.[16]

1-Naphthoic acid (2b)

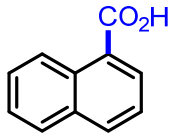

Following GP2a, naphthalene (0.3 mmol) gave **2b** (38%) as a white solid; **^{1}H-NMR** (400 MHz, DMSO-d_6) δ 13.13 (bs, 1H), 8.86 (d, *J* = 8.5 Hz, 1H), 8.20 – 8.10 (m, 2H), 8.02 (d, *J* = 7.7 Hz, 1H), 7.70 – 7.52 (m, 3H). **^{13}C-NMR** (101 MHz, DMSO) δ 168.6 (C_q), 133.5 (C_q), 132.9, 130.7 (C_q), 129.8, 128.6, 127.7 (C_q), 127.5, 126.2, 125.5, 124.9. **HRMS** (EI+): calculated *m/z* for $C_{11}H_8O_2$ [$M^{+\bullet}$] 172.05188; found 172.05143. Data in accordance with the literature.[17]

5-Methoxy-1-naphthoic acid (2c)

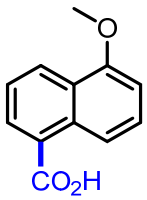

Following GP2a, 1-methoxynaphthalene (0.4 mmol) gave **2c** (22%) as a pale yellow solid; **^{1}H-NMR** (400 MHz, DMSO-d_6) δ 12.95 (bs, 1H), 8.45 – 8.35 (m, 2H), 8.13 (dd, *J* = 7.2, 1.3 Hz, 1H), 7.60 – 7.51 (m, 2H), 7.05 (d, *J* = 7.8 Hz, 1H), 3.99 (s, 3H). **^{13}C-NMR** (101 MHz, DMSO) δ 168.8 (C_q), 154.9 (C_q),

131.6 (C_q), 130.0, 127.8, 127.7 (C_q), 126.1, 125.3 (C_q), 124.2, 117.5, 104.7, 55.7. **HRMS** (EI+): calculated *m/z* for $C_{12}H_{10}O_3$ [$M^{+\bullet}$] 202.06245; found 202.06283. Data in accordance with the literature.[18]

5-(Dimethylamino)-1-naphthoic acid (2d)

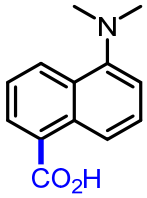

Following GP2a, 1-dimethylaminonaphthalen (0.4 mmol) gave **2d** (38%) as a yellow solid; **^{1}H-NMR** (400 MHz, DMSO-d_6) δ 13.04 (bs, 1H), 8.43 (dd, *J* = 15.9, 8.6 Hz, 2H), 8.08 (dd, *J* = 7.1, 1.0 Hz, 1H), 7.54 (ddd, *J* = 18.0, 8.6, 7.3 Hz, 2H), 7.19 (d, *J* = 7.3 Hz, 1H), 2.82 (s, 6H). **^{13}C-NMR** (101 MHz, DMSO) δ 168.9 (C_q), 151.0 (C_q), 132.0 (C_q), 129.3, 128.6 (C_q), 128.5 (C_q), 128.4, 127.4, 124.0, 120.0, 114.4, 45.0. **HRMS** (ESI+): calculated *m/z* for $C_{13}H_{14}NO_2$ [$(M+H)^+$] 216.1019; found 216.1022.

4-Methyl-1-naphtoic acid (2e) & 5-Methyl-1-naphtoic acid (2e')

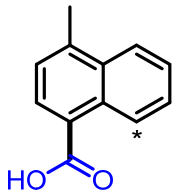

Following GP2a, 1-methylnaphthalene (0.1 mmol) gave **2e** (19%) and **2e'** (14%) as a beige solid. **2e:2e'** = 1.3:1. The ratio of products was determined by ^{1}H-NMR analysis. **HRMS** (EI+): calculated *m/z* for $C_{12}H_{10}O_2$ [$M^{+\bullet}$] 186.06753; found 186.06731.

Data for **2e**: **^{1}H-NMR** (300 MHz, Chloroform-*d*) δ 9.22 – 9.13 (m, 1H), 8.34 (d, *J* = 7.5 Hz, 1H), 8.13 – 8.05 (m, 1H), 7.73 – 7.50 (m, 2H), 7.41 (d, *J* = 7.5 Hz, 1H), 2.78 (s, 3H). **^{1}H-NMR** (400 MHz, DMSO-d_6) δ 13.06 (bs, 1H), 9.00 – 8.88 (m, 1H), 8.11 (m, 1H), 8.06 (d, *J* = 7.4 Hz, 1H), 7.68 – 7.58 (m, 2H), 7.44 (d, *J* = 7.0 Hz, 1H), 2.70 (s, 3H). **^{13}C-NMR** (101 MHz, DMSO) δ 168.7, 139.7, 132.4, 130.9, 129.8, 127.2, 126.1, 126.0, 125.9, 125.7, 124.7, 19.6. Data in accordance with literature.[19,20]

Data for **2e'**: **^{1}H-NMR** (300 MHz, CD_3OD) δ 8.95 (d, *J* = 8.8 Hz, 1H), 8.40 (dd, *J* = 7.3, 1.3 Hz, 1H), 8.30 (dt, *J* = 8.5, 1.1 Hz, 1H), 7.71 – 7.51 (m, 2H), 7.41 (d, *J* = 7.5 Hz, 1H), 2.75 (s, 3H).**^{1}H-NMR** (400 MHz, DMSO-d_6) δ 13.06 (bs, 1H), 8.67 (d, *J* = 8.6 Hz, 1H), 8.25 (d, *J* = 8.5 Hz, 1H), 8.14 – 8.08 (m, 1H), 7.68 – 7.58 (m, 1H), 7.54 – 7.48 (m, 1H), 7.39 – 7.47 (m, 1H), 2.68 (s, 3H). **^{13}C-NMR** (101 MHz,

DMSO) δ 169.0, 134.5, 132.5, 130.8, 129.1, 128.7, 128.6, 127.1, 126.9, 124.8, 123.7, 19.5. Data in accordance with the literature.[21]

1-Hydroxy-4-naphthoic acid (2f) & 1-hydroxy-2-naphthoic acid (2f')

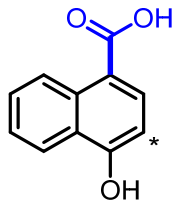

Following GP2c, 1-naphthol (0.1 mmol) gave **2f & 2f'** (56%) as an inseparable mixture (1:1), as a waxy solid. **^{1}H-NMR** (500 MHz, DMSO) δ 12.58 (s, 2H), 11.02 (s, 2H), 9.03 (d, *J* = 8.7 Hz, 1H), 8.23 (d, *J* = 7.7 Hz, 1H), 8.13 (d, *J* = 8.1 Hz, 1H), 7.87 (dd, *J* = 8.3, 1.0 Hz, 1H), 7.61 (ddd, *J* = 8.5, 6.8, 1.4 Hz, 1H), 7.50 (ddd, *J* = 8.2, 6.8, 1.2 Hz, 1H), 7.48 – 7.42 (m, 1H), 7.41 – 7.32 (m, 3H), 6.91 (d, *J* = 8.2 Hz, 1H), 6.87 (dd, *J* = 7.2, 1.3 Hz, 1H). **^{13}C-NMR** (126 MHz, DMSO) δ 171.88, 168.30, 157.80, 134.78, 133.04, 132.85, 128.74, 127.86, 126.98, 125.54, 125.08, 124.75, 124.56, 123.59, 122.43, 118.63, 116.69, 109.60, 106.95, 104.40. Data in accordance with the literature.[18,22]

2,7-dihydroxy-1-naphthoic acid (2g)

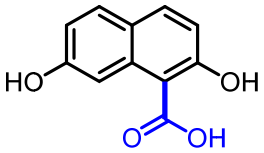

Following GP2c, naphthalene-2,7-diol (0.1 mmol) gave **2g** (64%) as a yellow solid. **^{1}H-NMR** (500 MHz, DMSO-d6) δ 12.43 (bs, 1H), 9.82 (s, 2H), 7.95 (s, 1H), 7.84 (d, *J* = 8.8 Hz, 1H), 7.68 (d, *J* = 8.8 Hz, 1H), 6.95-6.77 (m, 2H); **^{13}C-NMR** (126 MHz, DMSO-d6) δ 173.0, 161.8, 157.5, 135.1, 133.6, 130.5, 122.5, 115.1, 115.1 107.5, 105.8; **HRMS** (ESI+): calculated *m/z* for $C_{11}H_9O_4$ [$(M+H)^+$] 205.0495; found 205.0497.

5-(methoxycarbonyl)thiophene-2-carboxylic acid (4a)

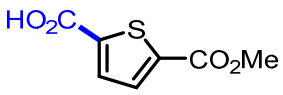

Following GP2a, methyl thiophene-2-carboxylate (0.4 mmol) gave **4a** (49%) as a white solid; **^{1}H-NMR** (400 MHz, DMSO-d6) δ 13.65 (bs, 1H), 7.78 (d, *J* = 3.9 Hz, 1H), 7.72 (d, *J* = 3.9 Hz, 1H), 3.85 (s, 3H).

^{13}C-NMR (101 MHz, DMSO) δ 162.3 (C_q), 161.4 (C_q), 140.4 (C_q), 137.5 (C_q), 133.7, 133.2, 52.7. **HRMS** (EI+): calculated *m/z* for $C_7H_6O_4S$ [$M^{+\bullet}$] 185.99813; found 185.99833. Data in accordance with the literature.[23]

5-Cyanothiophene-2-carboxylic acid (4b)

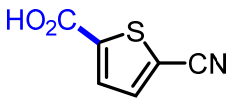

Following GP2a, thiophene-2-carbonitrile (0.4 mmol) gave **4b** (92%) as a pale yellow solid; **^{1}H-NMR** (400 MHz, DMSO-d_6) δ 13.98 (bs, 1H), 8.00 (d, J = 4.0 Hz, 1H), 7.79 (d, J = 4.0 Hz, 1H). **^{13}C-NMR** (101 MHz, DMSO) δ 161.5 (C_q), 141.7 (C_q), 139.5 (C_q), 132.9 (C_q), 113.6, 113.3. **HRMS** (EI+): calculated *m/z* for $C_6H_3NO_2S$ [$M^{+\bullet}$] 152.98790; found 152.98804. Data in accordance with the literature.[24]

5-Acetylthiophene-2-carboxylic acid (4c)

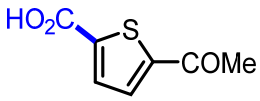

Following GP2a, 2-acetylthiophene (0.4 mmol) gave **4c** (39%) as a pale yellow solid; **^{1}H-NMR** (300 MHz, DMSO-d_6) δ 13.55 (bs, 1H), 7.92 (d, J = 4.0 Hz, 1H), 7.76 (d, J = 3.9 Hz, 1H), 2.58 (s, 3H). **^{13}C-NMR** (75 MHz, DMSO) δ 191.5 (C_q), 162.5 (C_q), 148.2 (C_q), 141.0 (C_q), 133.7, 133.6, 26.8. **HRMS** (EI+): calculated *m/z* for $C_7H_6O_3S$ [$M^{+\bullet}$] 170.00322; found 170.00333. Data in accordance with literature.[24]

5-Carbamoylthiophene-2-carboxylic acid (4d)

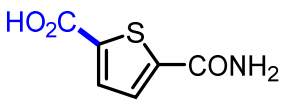

The title compound was prepared according to GP2a. Isolation of the compound was accomplished by employing C18 reversed-phase silica gel column chromatography using a mixture of water and acetonitrile as eluents. Thiophene-2-carboxamide (0.4 mmol) gave **4d** (91%) as a white solid; **^{1}H-NMR** (400 MHz, DMSO-d_6) δ 13.40 (bs, 1H), 8.17 (bs, 1H), 7.73 (d, J = 3.9 Hz, 1H), 7.69 (d, J = 3.9 Hz, 1H), 7.64 (bs, 1H). **^{13}C-NMR** (101 MHz, DMSO) δ 162.7 (C_q), 162.2 (C_q), 145.7 (C_q), 137.9 (C_q), 133.3, 128.9. **HRMS** (ESI+): calculated *m/z* for $C_6H_6O_3S$ [$(M+H)^+$] 172.0063; found 172.0065.

5-Phenylthiophene-2-carboxylic acid (4e)

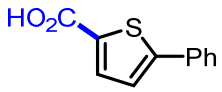

Following GP2a, 3-phenylthiophene (0.4 mmol) gave **4e** (99%) as a white solid; **^{1}H-NMR** (300 MHz, DMSO-d6) δ 13.18 (bs, 1H), 7.77 – 7.68 (m, 3H), 7.55 (d, *J* = 4.0 Hz, 1H), 7.49 – 7.33 (m, 3H). **^{13}C-NMR** (75 MHz, DMSO) δ 162.9 (C_q), 149.8 (C_q), 134.4, 133.4 (C_q), 132.9 (C_q), 129.3, 128.9, 125.9, 124.6. **HRMS** (ESI+): calculated *m/z* for $C_{11}H_9O_2S$ [$(M+H)^+$] 205.0318; found 205.0321. Data in accordance with the literature.[25]

5-(Trimethylsilyl)thiophene-2-carboxylic acid (4f)

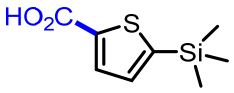

Following GP2a, trimethyl(thiophen-2-yl)silane (0.4 mmol) gave **4f** (28%) as a white solid; **^{1}H-NMR** (400 MHz, DMSO-d_6) δ 13.02 (bs, 1H), 7.75 (d, *J* = 3.5 Hz, 1H), 7.34 (d, *J* = 3.5 Hz, 1H), 0.31 (s, 9H). **^{13}C-NMR** (101 MHz, DMSO) δ 162.6 (C_q), 148.1 (C_q), 139.5 (C_q), 135.0, 133.9, −0.4. **HRMS** (EI+): calculated *m/z* for $C_8H_{12}O_2SiS$ [$M^{+\bullet}$] 200.03218; found 200.03162.

5-(cyanomethyl)thiophene-2-carboxylic acid (4g)

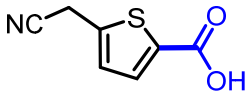

Following GP2b, 2-(thiophen-2-yl)acetonitrile (0.1 mmol) gave **4g** (89%) as a white soild. **^{1}H-NMR** (500 MHz,$CDCl_3$) δ 7.78 (d, *J* = 3.8 Hz, 1H), 7.13 (d, *J* =3.8 Hz, 1H), 3.96 (s, 2H); **^{13}C-NMR** (126 MHz, $CDCl_3$) δ 165.6 (C_q), 139.8 (C_q), 135.3, 133.2 (C_q), 128.3, 115.9 (C_q), 19.3 (CH_2); **HRMS** (ESI): calculated *m/z* for $C_7H_4NO_2S$ [$(M-H)^+$] 165.9968; found 165.9967.

5-(2-methoxy-2-oxoethyl)thiophene-2-carboxylic acid (4h)

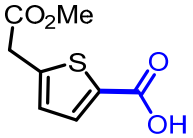

Following GP2b, methyl 2-(thiophen-2-yl)acetate (0.1 mmol) gave **4h** (99%) as a waxy solid. **^{1}H-NMR** (500 MHz, $CDCl_3$) δ 7.76 (d, *J* = 3.8 Hz, 1H), 6.99 (d, *J* = 3.8 Hz, 1H), 3.8 (s, 2H), 3.76 (s, 3H); **^{13}C-NMR** (126 MHz, $CDCl_3$) δ 170.0, 167.4, 144.5, 135.2, 132.2, 128.2, 52.7, 35.9; **HRMS** (ESI): calculated *m/z* for $C_8H_7O_4S$ [$(M-H)^+$] 199.0065; found 199.0065.

3-Cyanothiophene-2-carboxylic acid (**4i**)

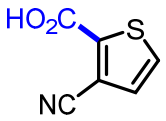

Following GP2a, thiophene-3-carbonitrile (0.4 mmol) gave **4i** (86%) as a pale yellow solid; **^{1}H-NMR** (300 MHz, DMSO-d_6) δ 14.12 (bs, 1H), 8.06 (d, *J* = 5.2 Hz, 1H), 7.62 (d, *J* = 5.1 Hz, 1H). **^{13}C-NMR** (75 MHz, DMSO) δ 160.7 (C_q), 141.9 (C_q), 133.9, 131.6, 114.1 (C_q), 113.0 (C_q). **HRMS** (ESI+): calculated *m/z* for $C_6H_4NO_2S$ [$(M+H)^+$] 153.9957; found 153.9957. Data in accordance with the literature.[26]

3-Acetylthiophene-2-carboxylic acid (**4j**)

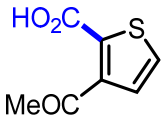

Following GP2a, 3-acetylthiophene (0.4 mmol) gave **4j** (41%) as a pale yellow solid; **^{1}H-NMR** (300 MHz, Acetonitrile-d_3) δ 7.78 (d, *J* = 5.4 Hz, 1H), 7.71 (d, *J* = 5.4 Hz, 1H), 2.73 (s, 3H). **^{1}H-NMR** (400 MHz, DMSO-d_6) δ 13.59 (bs, 1H), 7.85 (d, *J* = 5.0 Hz, 1H), 7.24 (d, *J* = 5.0 Hz, 1H), 2.50 (s, 3H). **^{13}C-NMR** (101 MHz, DMSO) δ 199.3 (C_q), 162.3 (C_q), 146.9 (C_q), 132.2 (C_q), 132.1, 128.1, 30.9. **HRMS** (EI+): calculated *m/z* for $C_7H_6O_3S$ [$M^{+\bullet}$] 170.00322; found 170.00304.

3-(Methoxycarbonyl)thiophene-2-carboxylic acid (**4k**)

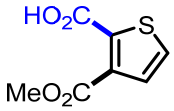

Following GP2a, methyl thiophene-2-carboxylate (0.4 mmol) gave **4k** (88%) as a white solid; **^{1}H-NMR** (400 MHz, DMSO-d_6) δ 13.53 (bs, 1H), 7.86 (d, *J* = 5.1 Hz, 1H), 7.31 (d, *J* = 5.1 Hz, 1H), 3.80 (s, 3H). **^{13}C-NMR** (101 MHz, DMSO) δ 164.8 (C_q), 161.9 (C_q), 136.8 (C_q), 134.5 (C_q), 131.8, 128.3, 52.5. **HRMS** (ESI+): calculated *m/z* for $C_7H_7O_4S$ [$(M+H)^+$] 187.0060; found 187.0059.

3-Phenylthiophene-2-carboxylic acid (4l)

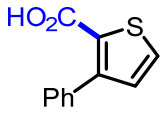

Following GP2a, 3-phenylthiophene (0.4 mmol) gave **4l** (71%) as a pale yellow solid; **^{1}H-NMR** (400 MHz, DMSO-d_6) δ 12.86 (bs, 1H), 7.85 (d, J = 5.0 Hz, 1H), 7.49 – 7.42 (m, 2H), 7.42 – 7.32 (m, 3H), 7.17 (d, J = 5.1 Hz, 1H). **^{13}C-NMR** (101 MHz, DMSO) δ 162.8 (C_q), 147.1 (C_q), 135.5 (C_q), 131.7, 131.0, 129.3, 128.1 (C_q), 127.7, 127.6. **HRMS** (ESI+): calculated *m/z* for $C_{11}H_9O_2S$ [$(M+H)^+$] 205.0318; found 205.0319. Data in accordance with the literature.[27]

[2,2'-Bithiophene]-5-carboxylic acid (4m)

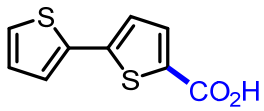

Following GP2a, 2,2'-bithiophene (0.4 mmol) gave **4m** (53%) as a pale yellow solid; **^{1}H-NMR** (400 MHz, DMSO-d_6) δ 13.15 (bs, 1H), 7.66 (d, J = 3.9 Hz, 1H), 7.62 (dd, J = 5.1, 1.1 Hz, 1H), 7.48 (dd, J = 3.7, 1.1 Hz, 1H), 7.34 (d, J = 3.9 Hz, 1H), 7.13 (dd, J = 5.1, 3.6 Hz, 1H). **^{13}C-NMR** (101 MHz, DMSO) δ 162.6 (C_q), 142.9 (C_q), 135.4 (C_q), 134.2, 132.5 (C_q), 128.6, 127.2, 125.9, 124.5. **HRMS** (ESI+): calculated *m/z* for $C_9H_7O_2S_2$ [$(M+H)^+$] 210.9882; found 210.9884. Data in accordance with the literature.[28]

[2,3'-Bithiophene]-2'-carboxylic acid (4n) & [2,3'-bithiophene]-5-carboxylic acid (4n')

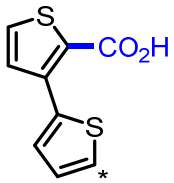

Following GP2a, 2,3'-bithiophene (0.4 mmol) gave **4n** (64%) as a white solid and **4n'** (23%) as a pale yellow solid. **4n**:**4n'** = 2.8:1.

Data for **4n**: **^{1}H-NMR** (400 MHz, Chloroform-*d*) δ 7.60 (dd, J = 3.7, 1.2 Hz, 1H), 7.56 (d, J = 5.2 Hz, 1H), 7.40 (dd, J = 5.1, 1.2 Hz, 1H), 7.27 (d, J = 5.2 Hz, 1H), 7.10 (dd, J = 5.1, 3.7 Hz, 1H). **^{1}H-NMR** (400 MHz, DMSO-d_6) δ 13.07 (bs, 1H), 7.84 (d, J = 5.2 Hz, 1H), 7.65 – 7.59 (m, 2H), 7.36 (d, J = 5.2

Hz, 1H), 7.11 (dd, J = 5.1, 3.7 Hz, 1H). **^{13}C-NMR** (101 MHz, DMSO) δ 162.8 (C_q), 138.7 (C_q), 135.9 (C_q), 131.3, 131.2, 129.0, 127.3, 127.2, 126.7 (C_q). **HRMS** (ESI+): calculated *m/z* for $C_9H_7O_2S_2$ [$(M+H)^+$] 210.9882; found 210.9883. Data in accordance with the literature.[29]

Data for **4n'**: **^{1}H-NMR** (400 MHz, DMSO-d_6) δ 7.93 (dd, J = 2.9, 1.4 Hz, 1H), 7.69 – 7.64 (m, 2H), 7.49 (dd, J = 5.0, 1.4 Hz, 1H), 7.44 (d, J = 3.8 Hz, 1H). **^{13}C-NMR** (101 MHz, DMSO) δ 162.9 (C_q), 144.7 (C_q), 134.3 (C_q), 134.0, 132.6 (C_q), 128.0, 126.0, 124.5, 122.4. Data in accordance with the literature.[30]

Thieno[3,2-*b*]thiophene-2-carboxylic acid (4o)

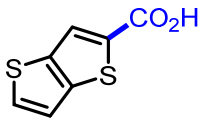

Following GP2a, thieno[3,2-*b*]thiophene (0.4 mmol) gave **4o** (48%) as a pale green solid; **^{1}H-NMR** (400 MHz, DMSO-d_6) δ 13.20 (bs, 1H), 8.11 (s, 1H), 7.92 (d, J = 5.3 Hz, 1H), 7.51 (d, J = 5.3 Hz, 1H). **^{13}C-NMR** (101 MHz, DMSO) δ 163.4 (C_q), 143.2 (C_q), 138.6 (C_q), 135.7 (C_q), 133.0, 126.1, 120.3. **HRMS** (ESI+): calculated *m/z* for $C_7H_5O_2S_2$ [$(M+H)^+$] 184.9725; found 184.9728. Data in accordance with the literature.[31]

Benzo[*b*]thiophene-2-carboxylic acid (4p)

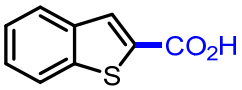

Following GP2a, benzo[*b*]thiophene (0.4 mmol) gave **4p** (97%) as a white solid; **^{1}H-NMR** (400 MHz, DMSO-d_6) δ 13.45 (bs, 1H), 8.11 (s, 1H), 8.06 – 7.96 (m, 2H), 7.54 –7.41 (m, 2H). **^{13}C-NMR** (101 MHz, DMSO) δ 163.5 (C_q), 141.3 (C_q), 138.7 (C_q), 134.8 (C_q), 130.2, 127.0, 125.7, 125.1, 123.0. **HRMS** (ESI+): calculated *m/z* for $C_9H_7O_2S$ [$(M+H)^+$] 179.0161; found 179.0163. Data in accordance with the literature.[32]

3-Methylbenzo[*b*]thiophene-2-carboxylic acid (4q)

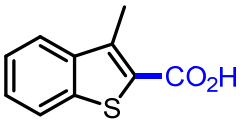

Following GP2a, 3-methylbenzo[*b*]thiophene (0.4 mmol) gave **4q** (95%) as a white solid; **^{1}H-NMR** (300 MHz, DMSO-d_6) δ 13.37 (bs, 1H), 8.01 – 7.88 (m, 2H), 7.55 – 7.41 (m, 2H), 2.70 (s, 3H). **^{13}C-NMR** (75 MHz, DMSO) δ 164.4 (C_q), 140.0 (C_q), 139.8 (C_q), 139.4 (C_q), 127.9 (C_q), 127.3, 124.7, 123.9, 122.8, 12.8. **HRMS** (ESI+): calculated *m/z* for $C_{10}H_9O_2S$ [$(M+H)^+$] 193.0318; found 193.0319. Data in accordance with the literature.[33]

5-(Methoxycarbonyl)furan-2-carboxylic acid (**4r**)

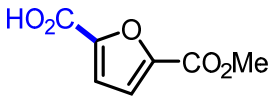

Following GP2a, methyl furan-2-carboxylate (0.4 mmol) gave **4r** (70%) as a pale yellow solid. **^{1}H-NMR** (400 MHz, DMSO-d6) δ 13.72 (bs, 1H), 7.39 (d, *J* = 3.6 Hz, 1H), 7.32 (d, *J* = 3.6 Hz, 1H), 3.85 (s, 3H). **^{13}C-NMR** (101 MHz, DMSO) δ 158.8 (C_q), 157.9 (C_q), 147.4 (C_q), 145.6 (C_q), 119.0, 118.4, 52.3. **HRMS** (ESI+): calculated *m/z* for $C_7H_7O_5$ [$(M+H)^+$] 171.0288; found 171.0289. Data in accordance with the literature.[34]

5-Cyanofuran-2-carboxylic acid (**4s**)

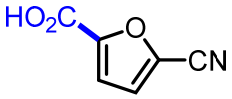

Following GP2a, furan-2-carbonitrile (0.4 mmol) gave **4s** (43%) as a pale yellow solid; **^{1}H-NMR** (400 MHz, DMSO-d_6) δ 13.98 (bs, 1H), 7.72 (d, *J* = 3.8 Hz, 1H), 7.40 (d, *J* = 3.8 Hz, 1H). **^{13}C-NMR** (101 MHz, DMSO) δ 158.0 (C_q), 149.0 (C_q), 126.9 (C_q), 124.6, 117.8, 111.0 (C_q). **HRMS** (EI+): calculated *m/z* for $C_6H_3NO_3$ [$M^{+\bullet}$] 137.01074; found 137.01037.

Benzofuran-2-carboxylic acid (**4t**)

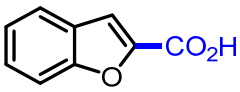

Following GP2a, benzofuran (0.4 mmol) gave **4t** (47%) as a pale yellow solid; **^{1}H-NMR** (400 MHz, DMSO-d_6) δ 13.55 (bs, 1H), 7.78 (d, *J* = 7.8 Hz, 1H), 7.69 (d, *J* = 8.4 Hz, 1H), 7.67 – 7.63 (m, 1H), 7.49 (ddd, *J* = 8.4, 7.1, 1.3 Hz, 1H), 7.38 – 7.32 (m, 1H). **^{13}C-NMR** (101 MHz, DMSO) δ 160.1 (C_q), 155.0 (C_q), 146.3 (C_q), 127.5, 126.9 (C_q), 123.8, 123.1, 113.4, 112.1. **HRMS** (EI+): calculated *m/z* for $C_9H_6O_3$ [$M^{+\bullet}$] 162.03115; found 162.03138. Data in accordance with the literature.[17]

1-(*tert*-butyl) 2-methyl 1*H*-indole-1,2-dicarboxylate (4u)

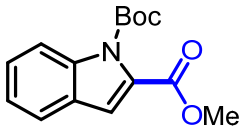

A dry microwave vial (5 mL) equipped with stirring bar, was charged with *tert*-butyl 1*H*-indole-1-carboxylate (0.1 mmol) and 2,3,6,7-tetramethoxyanthracen-9(10*H*)-one (20 mol%). The vial was sealed and transferred to a glovebox after the vial had evacuated and refilled with N_2 (3×) within the antechamber *via* syringe. Cs_2CO_3 (3.0 equiv.) and dry DMSO (1 mL) was added and the vial was sealed with a Supelco aluminium crimp seal with septum (PTFE/butyl). The vial was removed from the glovebox. The reaction mixture then had gaseous CO_2 (22 cm^3) added *via* a gastight Hamilton® syringe, into the head space of the vial. The vial was then irradiated from two sides by two kessil lamps (vials approximately 6 cm away from the light source) with fans placed in front of the vials for cooling (temperatures measured *via* IR ranged between 25-30 °C). After 18 hrs the irradiation was stopped, the pressure was vented *via* syringe and MeI (31 µL, 0.5 mmol) was added. The reaction mixture was left to stir for 4 hrs. The vial was decapped and quenched with aq. HCl (1 mL, 0.3M). The reaction was diluted with brine (10 mL) extracted with EtOAc (3×5 mL). The organic layers were combined and washed with brine (3×10 mL) and then dried *via* phase separator and concentrated *in vacuo*. Purification by column chromatography on silica gel eluting with heptane:EtOAc (9:1) gave the title compound **4u** (40%) as a white waxy solid. R_f 0.51 [Heptane–EtOAc (9:1)]; 8.10 (dq, *J* = 8.5, 0.9 Hz, 1H), 7.60 (ddd, *J* = 7.8, 1.2, 0.8 Hz, 1H), 7.42 (ddd, *J* = 8.5, 7.2, 1.3 Hz, 1H), 7.27 (ddd, *J* = 8.1, 7.2, 1.0 Hz, 1H), 7.11 (d, J = 0.8 Hz, 1H), 3.93 (s, 3H), 1.63 (s, 9H). **^{13}C-NMR** (101 MHz, $CDCl_3$) δ 162.5, 149.4, 137.9, 130.5, 127.6, 126.9, 123.4, 122.3, 115.0, 115.0, 84.7, 52.5, 27.9. Data in accordance with the literature.[35]

1-(*tert*-Butoxycarbonyl)-2-phenyl-1*H*-indole-3-carboxylic acid (4v)

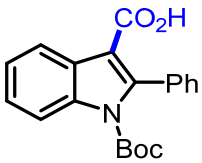

Following GP2a, *tert*-butyl 2-phenyl-1*H*-indole-1-carboxylate (0.4 mmol) gave **4v** (10%) as a white solid; **^{1}H-NMR** (400 MHz, DMSO-d_6) δ 12.40 (bs, 1H), 8.17 – 8.12 (m, 1H), 8.12 – 8.07 (m, 1H), 7.48 – 7.32 (m, 7H), 1.16 (s, 9H). **^{13}C-NMR** (101 MHz, DMSO) δ 164.9 (C_q), 148.9 (C_q), 143.8 (C_q), 135.3 (C_q), 133.1 (C_q), 129.7, 128.1, 127.4, 126.9 (C_q), 124.9, 123.7, 121.6, 114.2, 111.4 (C_q), 84.3 (C_q), 26.8. **HRMS** (ESI+): calculated *m/z* for $C_{20}H_{20}NO_4$ [$(M+H)^+$] 338.1387; found 338.1391.

1-Phenyl-1*H*-pyrazole-5-carboxylic acid (4w)

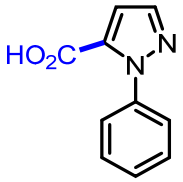

Following GP2a, 1-phenylpyrazole (0.4 mmol) gave **4w** (33%) as a white solid; **^{1}H-NMR** (300 MHz, Methanol-d_4) δ 7.72 (d, J = 2.0 Hz, 1H), 7.52 – 7.39 (m, 5H), 7.05 (d, J = 2.0 Hz, 1H). **^{1}H-NMR** (400 MHz, DMSO-d_6) δ 13.29 (bs, 1H), 7.77 (d, J = 1.9 Hz, 1H), 7.52 – 7.41 (m, 5H), 7.03 (d, J = 1.9 Hz, 1H). **^{13}C-NMR** (101 MHz, DMSO) δ 160.0 (C_q), 140.2 (C_q), 139.7, 134.1 (C_q), 128.5, 128.2, 125.7, 112.5. **HRMS** (ESI+): calculated *m/z* for $C_{10}H_9N_2O_2$ [$(M+H)^+$] 189.0659; found 189.0661. Data in accordance with the literature.[36]

2-cyano-4-methylthiazole-5-carboxylic acid (4x)

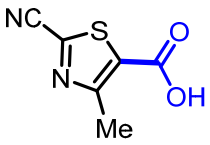

Following GP2c, 4-methylthiazole-2-carbonitrile (0.1 mmol) gave **4x** (53%) as a white soild. **^{1}H-NMR** (500 MHz, $CDCl_3$) δ 2.83 (3H, s); **^{13}C-NMR** (126 MHz, $CDCl_3$) δ 165.4 (Cq), 163.3 (Cq), 139.3 (Cq), 126.6 (Cq), 112.1 (Cq), 17.7; **HRMS** (EI): calculated *m/z* for $C_6H_4N_2O_2S$ [$M^{+\bullet}$] 167.9992; found 168.0003.

4-hydroxybenzo[*b*]thiophene-7-carboxylic acid (6a)

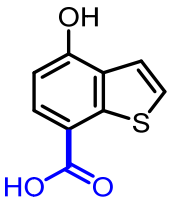

Following GP2c, 4-hydroxybenzo[b]thiophene (0.1 mmol) gave **6a** (99%) as a white solid. **^{1}H-NMR** (500 MHz, DMSO-d_6): δ 7.91 (d, J = 8.2 Hz, 1H), 7.66 (d, J = 5.6 Hz, 1H), 7.51 (d, J = 5.6 Hz, 1H), 6.85 (d, J = 8.2 Hz, 1H); **^{13}C-NMR** (126 MHz, DMSO-d_6) δ 166.9 (C_q), 157.0 (C_q), 141.8 (C_q), 129.8 (C_q), 129.3, 127.7, 119.8, 115.6 (C_q), 108.9; **HRMS** (ESI): calculated *m/z* for $C_9H_5O_3S$ [$(M-H)^+$] 192.9965; found 192.9965.

1-(Tetrahydro-2*H*-pyran-2-yl)-1*H*-indazole-4-carboxylic acid (6b)

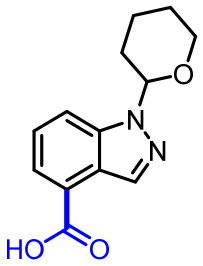

Following GP2c, 1-(tetrahydro-2*H*-pyran-2-yl)-1*H*-indazole (0.1 mmol) gave **6b** (60%) as a white solid. **^{1}H-NMR** (500 MHz, DMSO-d6): δ 12.88 (bs, 1H), 8.42 (s, 1H), 8.03 (d, *J* = 8.4 Hz, 1H), 7.83 (d, *J* = 7.1 Hz, 1H), 7.63-7.43 (m, 1H), 5.92 (dd, *J* = 9.6, 2.1 Hz, 1H), 3.88 (d, *J* = 11.2 Hz, 1H), 3.80-3.71 (m, 1H), 2.42 (qd, *J* = 3.7, 13.0 Hz, 1H), 2.15-1.94 (m, 2H), 1.88-1.67 (m, 1H), 1.65-1.52 (m, 2H); **^{13}C-NMR** (126 MHz, DMSO-d6): δ 167.0, 139.8, 133.6, 125.9, 124.4, 123.3, 122.5, 115.3, 84.0, 66.5, 28.9, 24.7, 22.1; **HRMS** (ESI): calculated *m/z* for $C_{13}H_{15}N_2O_3$ [$(M+H)^+$] 247.1077; found 247.1066.

1-Methyl-1*H*-indazole-4-carboxylic acid (6c)

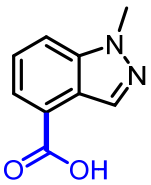

Following GP2c, 1-methyl-1*H*-indazole (0.1 mmol) gave **6c** (58%) as a white solid. **^{1}H-NMR** (500 MHz, $CDCl_3$): δ 8.58 (s, 1H), 8.05 (d, *J* = 6.9 Hz, 1H) 7.69 (d, *J* = 8.8 Hz, 1H), 7.44–7.56 (m, 1H), 4.16 (s, 3H); **^{13}C-NMR** (126 MHz, $CDCl_3$): 171.3, 140.5, 133.9, 125.7, 125.3, 122.8, 122.3, 114.9, 35.9; **HRMS** (ESI): calculated *m/z* for $C_9H_9N_2O_2$ [$(M+H)^+$] 177.0664; found 177.0669.

Pyrazolo[1,5-*a*]pyridine-7-carboxylic acid (6d) & pyrazolo[1,5-*a*]pyridine-4-carboxylic acid (6d')

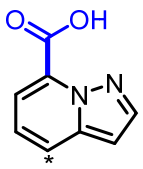

Following GP2c, pyrazolo[1,5-*a*]pyridine (0.1 mmol) gave **6d** (63%) as a white solid & **6d'** (22%) as a white solid. **6d:6d'** = 2.8:1.

Data for 6d: **^{1}H-NMR** (500 MHz, DMSO-d_6) δ 8.20 (d, *J* = 2.3 Hz, 1H), 8.14–7.88 (m, 1H), 7.73–7.58 (m, 1H), 7.38 (dd, *J* = 7.1, 8.8 Hz, 1H), 6.87 (d, *J* = 2.3 Hz, 1H); **^{13}C-NMR** (126 MHz, DMSO-d_6) δ 161.8, 140.8, 140.6, 129.3, 123.6, 122.3, 116.9, 98.5. Data in accordance with the literature.[37]

Data for 6d': **^{1}H-NMR** (500 MHz, DMSO-d_6) δ 13.34 (bs, 1H), 8.94 (d, *J* = 6.8 Hz, 1H), 8.12 (d, *J* = 2.1 Hz, 1H), 7.95 (d, *J* = 6.4 Hz, 1H), 7.03–6.98 (m, 2H); **^{13}C-NMR** (126 MHz, DMSO-d_6) δ 165.5, 142.9, 137.9, 133.0, 128.6, 120.7, 110.9, 98.6. Data in accordance with the literature.[37]

4-(3-((*tert*-butoxycarbonyl)(isopropyl)amino)-2-hydroxypropoxy)benzo[*b*]thiophene-2-carboxylic acid (**6e**)

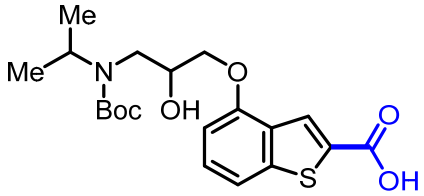

Following GP2c, *tert*-butyl (3-(benzo[*b*]thiophen-4-yloxy)-2-hydroxypropyl)(isopropyl)carbamate (0.1 mmol) gave **6e** (18%) as a yellow oil. **^{1}H-NMR** (500 MHz, $CDCl_3$): δ 8.26 (s, 1H), 7.32–7.49 (m, 2H), 6.77 (d, *J* = 7.5 Hz, 1H), 4.28–4.11 (m, 3H), 4.10–3.99 (m, 1H), 3.47 (s, 2H), 2.05 (s, 1H), 1.50 (s, 9H), 1.18 (dd, *J* = 6.5, 31.4 Hz, 6H); **^{13}C-NMR** (126 MHz, $CDCl_3$) δ ^{13}C NMR (126 MHz, $CDCl_3$) δ 165.6, 154.3, 143.4, 131.0, 129.1, 127.7, 127.3, 114.4, 104.2, 80.0, 71.0, 69.1, 48.0, 46.1, 27.6, 19.7 **HRMS** (ESI): calculated *m/z* for $C_{20}H_{28}NO_6S$ $[(M+H)^+]$ 410.1637; found 410.1655.

Cinnamic acid (**8a**)

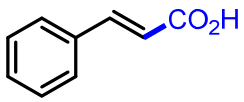

Following GP2a, styrene (0.4 mmol) gave **8a** (54%) as a white solid; **^{1}H-NMR** (400 MHz, DMSO-d_6) δ 12.40 (bs, 1H), 7.72 – 7.64 (m, 2H), 7.59 (d, *J* = 16.0 Hz, 1H), 7.45 – 7.37 (m, 3H), 6.53 (d, *J* = 16.0 Hz, 1H). **^{13}C-NMR** (101 MHz, DMSO) δ 167.6 (C_q), 143.9, 134.2 (C_q), 130.2, 128.9, 128.2, 119.3. **HRMS** (EI+): calculated *m/z* for $C_9H_8O_2$ $[M^{+\bullet}]$ 148.05188; found 148.05161. Data in accordance with the literature.[38]

(*E*)-3-(4-(*tert*-Butyl)phenyl)acrylic acid (8b)

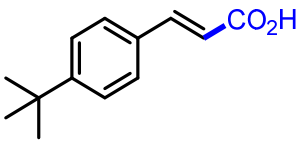

Following GP2a, 1-(*tert*-butyl)-4-vinylbenzene (0.4 mmol) gave **8b** (56%) as a white solid; **^{1}H-NMR** (400 MHz, DMSO-d_6) δ 12.33 (bs, 1H), 7.62 – 7.53 (m, 3H), 7.46 – 7.38 (m, 2H), 6.47 (d, J = 16.0 Hz, 1H), 1.27 (s, 9H). **^{13}C-NMR** (101 MHz, DMSO) δ 167.7 (C_q), 153.1 (C_q), 143.8, 131.5 (C_q), 128.0, 125.7, 118.3, 34.6 (C_q), 30.9. **HRMS** (EI+): calculated *m/z* for $C_{13}H_{16}O_2$ [$M^{+\bullet}$] 204.11448; found 204.11415.

(*E*)-3-(*p*-Tolyl)acrylic acid (8c)

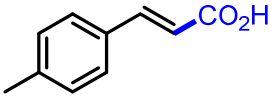

Following GP2a, 4-methylstyrene (0.4 mmol) gave **8c** (53%) as a white solid; **^{1}H-NMR** (400 MHz, DMSO-d_6) δ 12.31 (bs, 1H), 7.60 – 7.51 (m, 3H), 7.22 (d, J = 7.9 Hz, 2H), 6.46 (d, J = 16.0 Hz, 1H), 2.32 (s, 3H). **^{13}C-NMR** (101 MHz, DMSO) δ 167.7 (C_q), 143.9, 140.1 (C_q), 131.5 (C_q), 129.5, 128.2, 118.1, 21.0. **HRMS** (EI+): calculated *m/z* for $C_{10}H_{10}O_2$ [$M^{+\bullet}$] 162.06753; found 162.06783.

(*E*)-3-(4-Methoxyphenyl)acrylic acid (8d)

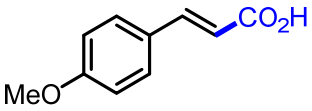

Following GP2a, 4-methoxystyrene (0.4 mmol) gave **8d** (40%) as a pale yellow solid; **^{1}H-NMR** (400 MHz, DMSO-d_6) δ 12.21 (bs, 1H), 7.66 – 7.60 (m, 2H), 7.54 (d, J = 16.0 Hz, 1H), 7.00 – 6.93 (m, 2H), 6.37 (d, J = 15.9 Hz, 1H), 3.79 (s, 3H). **^{13}C-NMR** (101 MHz, DMSO) δ 167.8 (C_q), 160.9 (C_q), 143.7, 129.9, 126.8 (C_q), 116.5, 114.3, 55.3. **HRMS** (EI+): calculated *m/z* for $C_{10}H_{10}O_3$ [$M^{+\bullet}$] 178.06245; found 178.06194.

(*E*)-3-(3-Methoxyphenyl)acrylic acid (8e):

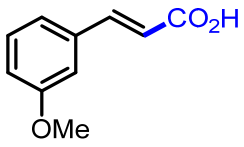

Following GP2a, 3-methoxystyrene (0.4 mmol) gave **8e** (46%) as a white solid; **^{1}H-NMR** (400 MHz, DMSO-d_6) δ 12.40 (bs, 1H), 7.56 (d, J = 16.0 Hz, 1H), 7.36 – 7.20 (m, 3H), 7.03 – 6.92 (m, 1H), 6.55 (d, J = 16.0 Hz, 1H), 3.79 (s, 3H). **^{13}C-NMR** (101 MHz, DMSO) δ 167.6 (C_q), 159.6 (C_q), 143.9, 135.7 (C_q), 129.9, 120.8, 119.6, 116.2, 112.9, 55.2. **HRMS** (EI+): calculated *m/z* for $C_{10}H_{10}O_3$ [$M^{+\bullet}$] 178.06245; found 178.06210.

(*E*)-3-(4-(Trimethylsilyl)phenyl)acrylic acid (8f)

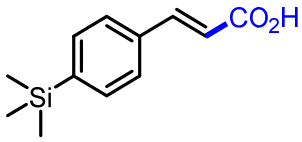

Following GP2a, trimethyl(4-vinylphenyl)silane (0.4 mmol) gave **8f** (53%) as a pale yellow solid; **^{1}H-NMR** (400 MHz, DMSO-d_6) δ 12.38 (bs, 1H), 7.67 – 7.62 (m, 2H), 7.61 – 7.52 (m, 3H), 6.54 (d, J = 16.0 Hz, 1H), 0.24 (s, 9H). **^{13}C-NMR** (101 MHz, DMSO) δ 167.5 (C_q), 143.9, 142.6 (C_q), 134.6 (C_q), 133.7, 127.3, 119.4, −1.3. **HRMS** (EI+): calculated *m/z* for $C_{12}H_{16}O_2Si$ [$M^{+\bullet}$] 220.09141; found 220.09148.

Methyl (*E*)-3-(4-(dimethylamino)phenyl)acrylate (8g)

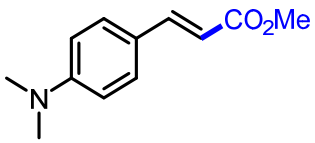

The title compound was prepared according to GP2a with *N*,*N*-dimethyl-4-vinylaniline (0.4 mmol). After irradiating the mixture for 18 hrs the reaction vial was vented and MeI (18.7 µL, 0.3 mmol, 3 equiv.) was added *via* syringe. The resulting mixture was stirred for 2 hrs at 35 °C and was quenched by adding water. The crude mixture was extracted with DCM (3×) and the combined organic layers were dried over Na_2SO_4, filtered and concentrated *in vacuo*. Flash silica gel column chromatography with a mixture of hexanes+NEt_3 (1% v/v) and EtOAc provided the title compound **8g** (14%) as a pale brown solid; **^{1}H-NMR** (400 MHz, Chloroform-*d*) δ 7.63 (d, J = 15.9 Hz, 1H), 7.45 – 7.38 (m, 2H), 6.70 – 6.62 (m, 2H), 6.22 (d, J = 15.8 Hz, 1H), 3.78 (s, 3H), 3.01 (s, 6H). **^{13}C-NMR** (101 MHz, $CDCl_3$) δ

168.5 (C_q), 151.9 (C_q), 145.5, 129.9, 122.3 (C_q), 112.2, 112.0, 51.5, 40.3. **HRMS** (EI+): calculated *m/z* for $C_{12}H_{15}NO_2$ [$M^{+\bullet}$] 205.10973; found 205.10937.

(*E*)-3-(4-(Methylthio)phenyl)acrylic acid (8h)

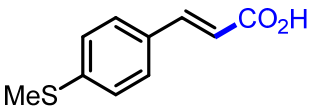

Following GP2a, methyl(4-vinylphenyl)sulfane (0.4 mmol) gave **8h** (38%) as a white solid; **^{1}H-NMR** (400 MHz, DMSO-d_6) δ 12.32 (bs, 1H), 7.65 – 7.60 (m, 2H), 7.55 (d, *J* = 16.0 Hz, 1H), 7.31 – 7.24 (m, 2H), 6.48 (d, *J* = 16.0 Hz, 1H), 2.51 (s, 3H). **^{13}C-NMR** (101 MHz, DMSO) δ 167.7 (C_q), 143.4, 141.3 (C_q), 130.6 (C_q), 128.7, 125.6, 118.0, 14.2. **HRMS** (EI+): calculated *m/z* for $C_{10}H_{10}O_2S$ [$M^{+\bullet}$] 194.03960; found 194.03936.

(*E*)-3-(4-Fluorophenyl)acrylic acid (8i)

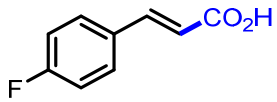

Following GP2a, 4-fluorostyrene (0.4 mmol) gave **8i** (46%) as a white solid; **^{1}H-NMR** (400 MHz, DMSO-d_6) δ 12.39 (bs, 1H), 7.80 – 7.71 (m, 2H), 7.59 (d, *J* = 16.0 Hz, 1H), 7.29 – 7.19 (m, 2H), 6.49 (d, *J* = 16.0 Hz, 1H). **^{13}C-NMR** (101 MHz, DMSO-d_6) δ 167.5 (C_q), 163.1 (d, *J* = 248.3 Hz, C_q), 142.7, 130.9 (d, *J* = 3.2 Hz, C_q), 130.5 (d, *J* = 8.6 Hz), 119.1 (d, *J* = 2.2 Hz), 115.9 (d, *J* = 21.7 Hz). **^{19}F-NMR** (376 MHz, DMSO) δ -110.0. **HRMS** (EI+): calculated *m/z* for $C_9H_7FO_2$ [$M^{+\bullet}$] 166.04246; found 166.04203.

(*E*)-3-(4-(Trifluoromethyl)phenyl)acrylic acid (8j)

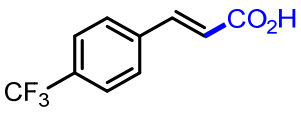

Following GP2a, 1-(trifluoromethyl)-4-vinylbenzene (0.4 mmol) gave **8j** (13%) as a white solid; **^{1}H-NMR** (400 MHz, DMSO-d_6) δ 12.58 (bs, 1H), 7.92 (d, *J* = 8.1 Hz, 2H), 7.76 (d, *J* = 8.1 Hz, 2H), 7.66 (d, *J* = 16.1 Hz, 1H), 6.68 (d, *J* = 16.1 Hz, 1H). **^{13}C-NMR** (101 MHz, DMSO) δ 167.2 (C_q), 142.0, 138.3 (d, *J* = 1.3 Hz, C_q), 129.8 (q, *J* = 31.8 Hz, C_q), 128.8, 125.7 (q, *J* = 3.7 Hz), 124.0 (q, *J* = 272.1 Hz, C_q),

122.3. **^{19}F-NMR** (376 MHz, DMSO) δ -60.8. **HRMS** (ESI+): calculated *m/z* for $C_{10}H_8F_3O_2$ [$(M+H)^+$] 217.0471; found 217.0472. Data in accordance with the literature.[38]

(*E*)-3-(3-Fluorophenyl)acrylic acid (8k)

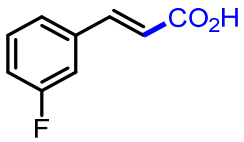

Following GP2a, 3-fluorostyrene (0.4 mmol) gave **8k** (38%) as a white solid; **^{1}H-NMR** (400 MHz, DMSO-d_6) δ 12.49 (bs, 1H), 7.64 – 7.49 (m, 3H), 7.49 – 7.41 (m, 1H), 7.29 – 7.19 (m, 1H), 6.61 (d, J = 16.0 Hz, 1H). **^{13}C-NMR** (101 MHz, DMSO-d_6) δ 167.4 (C_q), 162.42 (d, J = 243.7 Hz, C_q), 142.51 (d, J = 2.6 Hz), 136.82 (d, J = 8.1 Hz, C_q), 130.81 (d, J = 8.4 Hz), 124.63 (d, J = 2.6 Hz), 120.9, 116.86 (d, J = 21.3 Hz), 114.38 (d, J = 22.0 Hz). **^{19}F-NMR** (377 MHz, DMSO) δ -112.4. **HRMS** (ESI+): calculated *m/z* for $C_9H_8FO_2$ [$(M+H)^+$] 167.0503; found 167.0502.

3,4-Dihydronaphthalene-2-carboxylic acid (8l)

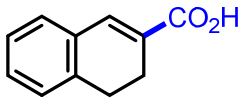

Following GP2a, 1,2-dihydronaphthalene (0.4 mmol) gave **8l** (58%) as a white solid; **^{1}H-NMR** (400 MHz, DMSO-d_6) δ 12.43 (bs, 1H), 7.47 (s, 1H), 7.34 – 7.18 (m, 4H), 2.81 (t, J = 8.3 Hz, 2H), 2.49 – 2.43 (m, 2H). **^{13}C-NMR** (101 MHz, DMSO) δ 168.1 (C_q), 136.5 (C_q), 135.3, 132.3 (C_q), 130.0 (C_q), 129.3, 128.3, 127.5, 126.7, 26.9 (CH_2), 21.9 (CH_2). **HRMS** (EI+): calculated *m/z* for $C_{11}H_{10}O_2$ [$M^{+\bullet}$] 174.06753; found 174.06707. Data in accordance with the literature.[39]

3-(4-Fluorophenyl)but-3-enoic acid (8m) & (*E*)-3-(4-fluorophenyl)but-2-enoic acid (8m')

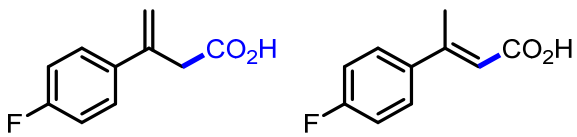

Following GP2a, 4-fluoro-α-methylstyrene (0.4 mmol) gave **8m** (43%) as a white solid and **8m'** (9%) as a pale yellow solid. **8m**:**8m'** = 4.8:1. **HRMS** (EI+): calculated *m/z* for $C_{10}H_9FO_2$ [$M^{+\bullet}$] 180.05811; found 180.05831.

Data for 8m: **^{1}H-NMR** (400 MHz, Chloroform-*d*) δ 9.83 (bs, 1H), 7.45 – 7.35 (m, 2H), 7.06 – 6.97 (m, 2H), 5.52 (s, 1H), 5.24 (s, 1H), 3.52 (s, 2H). **^{13}C-NMR** (101 MHz, Chloroform-*d*) δ 177.5 (C_q), 162.7 (d, *J* = 247.3 Hz, C_q), 139.3 (C_q), 135.7 (d, *J* = 3.3 Hz, C_q), 127.61 (d, *J* = 8.1 Hz), 116.98 (d, *J* = 1.3 Hz, CH_2), 115.49 (d, *J* = 21.5 Hz), 41.1 (CH_2). **^{19}F-NMR** (376 MHz, $CDCl_3$) δ -114.8.

Data for 8m': **^{1}H-NMR** (400 MHz, Chloroform-*d*) δ 7.51 – 7.45 (m, 2H), 7.11 – 7.04 (m, 2H), 6.13 (s, 1H), 2.58 (d, *J* = 0.7 Hz, 3H). **^{19}F-NMR** (376 MHz, $CDCl_3$) δ -112.4. Data in accordance with the literature.[40]

2-(Benzo[*b*]thiophen-2-yl)propan-2-ol (9pa)

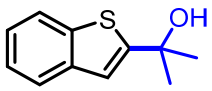

According to GP3 benzo[*b*]thiophene and acetone gave **9pa** (54%) as a white solid; **^{1}H-NMR** (400 MHz, Chloroform-*d*) δ 7.80 (d, *J* = 7.8 Hz, 1H), 7.71 (d, *J* = 7.7 Hz, 1H), 7.31 (dt, *J* = 15.1, 7.4 Hz, 2H), 7.16 (s, 1H), 2.26 (s, 1H), 1.73 (s, 6H). **^{13}C-NMR** (101 MHz, $CDCl_3$) δ 155.1 (C_q), 139.9 (C_q), 139.3 (C_q), 124.3, 124.1, 123.5, 122.4, 118.5, 71.8 (C_q), 32.1. **HRMS** (ESI+): calculated *m/z* for $C_{11}H_{13}O_2S$ [$(M+H)^+$] 175.0576; found 175.0577.

1-(Benzo[*b*]thiophen-2-yl)cyclobutan-1-ol (9pb)

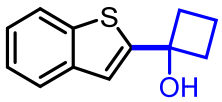

According to GP3 benzo[*b*]thiophene and cyclobutanone gave **9pb** (30%) as a pale yellow oil; **^{1}H-NMR** (300 MHz, Methanol-d_4) δ 7.84 – 7.73 (m, 1H), 7.76 – 7.70 (m, 1H), 7.35 – 7.22 (m, 3H), 2.65 – 2.52 (m, 2H), 2.52 – 2.38 (m, 2H), 2.06 – 1.77 (m, 2H). **^{13}C-NMR** (75 MHz, MeOD) δ 154.1 (C_q), 141.3 (C_q), 141.0 (C_q), 125.1, 125.0, 124.4, 123.2, 119.8, 75.7 (C_q), 39.0 (CH_2), 13.7 (CH_2). **HRMS** (ESI+): calculated *m/z* for $C_{12}H_{13}OS$ [$(M+H)^+$] 187.0576; found 187.0577.

2-(Benzo[*b*]thiophen-2-yl)hex-5-en-2-ol (**9pc**)

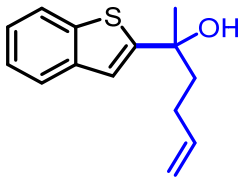

According to GP3 benzo[*b*]thiophene and hex-5-en-2-one gave **9pc** (19%) as a colorless oil; **^{1}H-NMR** (400 MHz, Chloroform-*d*) δ 7.83 – 7.77 (m, 1H), 7.74 – 7.68 (m, 1H), 7.37 – 7.26 (m, 2H), 7.14 (s, 1H), 5.84 (ddt, *J* = 16.8, 10.2, 6.4 Hz, 1H), 5.02 (dq, *J* = 17.1, 1.7 Hz, 1H), 4.96 (dq, *J* = 9.9, 1.3 Hz, 1H), 2.24 – 2.07 (m, 3H), 2.06 – 1.99 (m, 2H), 1.70 (s, 3H). **^{13}C-NMR** (101 MHz, $CDCl_3$) δ 153.9 (C_q), 140.0 (C_q), 139.4 (C_q), 138.4, 124.4, 124.1, 123.4, 122.4, 119.1, 115.1 (CH_2), 74.4 (C_q), 43.5 (CH_2), 30.7, 28.8 (CH_2). **HRMS** (EI+): calculated *m/z* for $C_{14}H_{16}OS$ [$M^{+\bullet}$] 232.09164; found 232.09159.

5 - Spectra

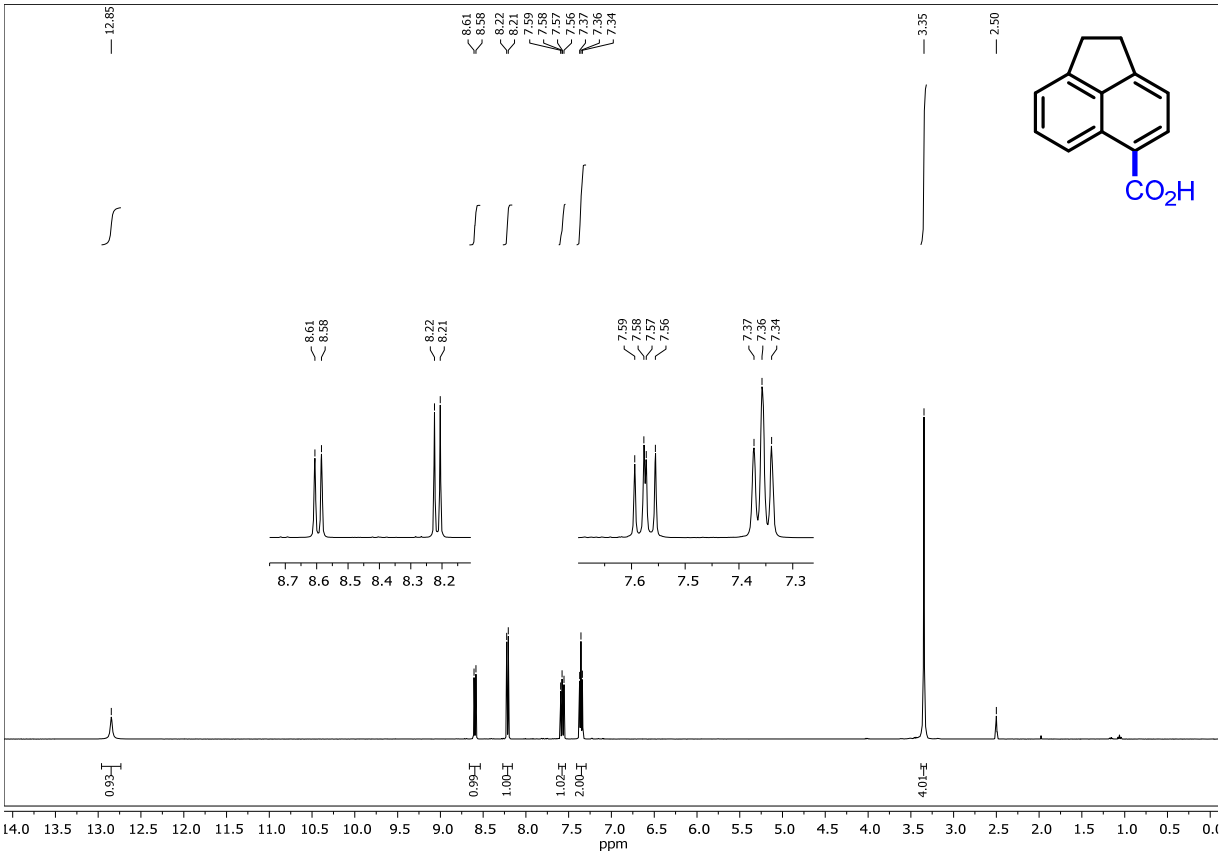
12.85
8.61
8.58
8.22
8.21
7.59
7.58
7.57
7.56
7.37
7.36
7.34
3.35
2.50
CO2H
0.93
0.99
1.00
1.02
2.00
4.01
ppm

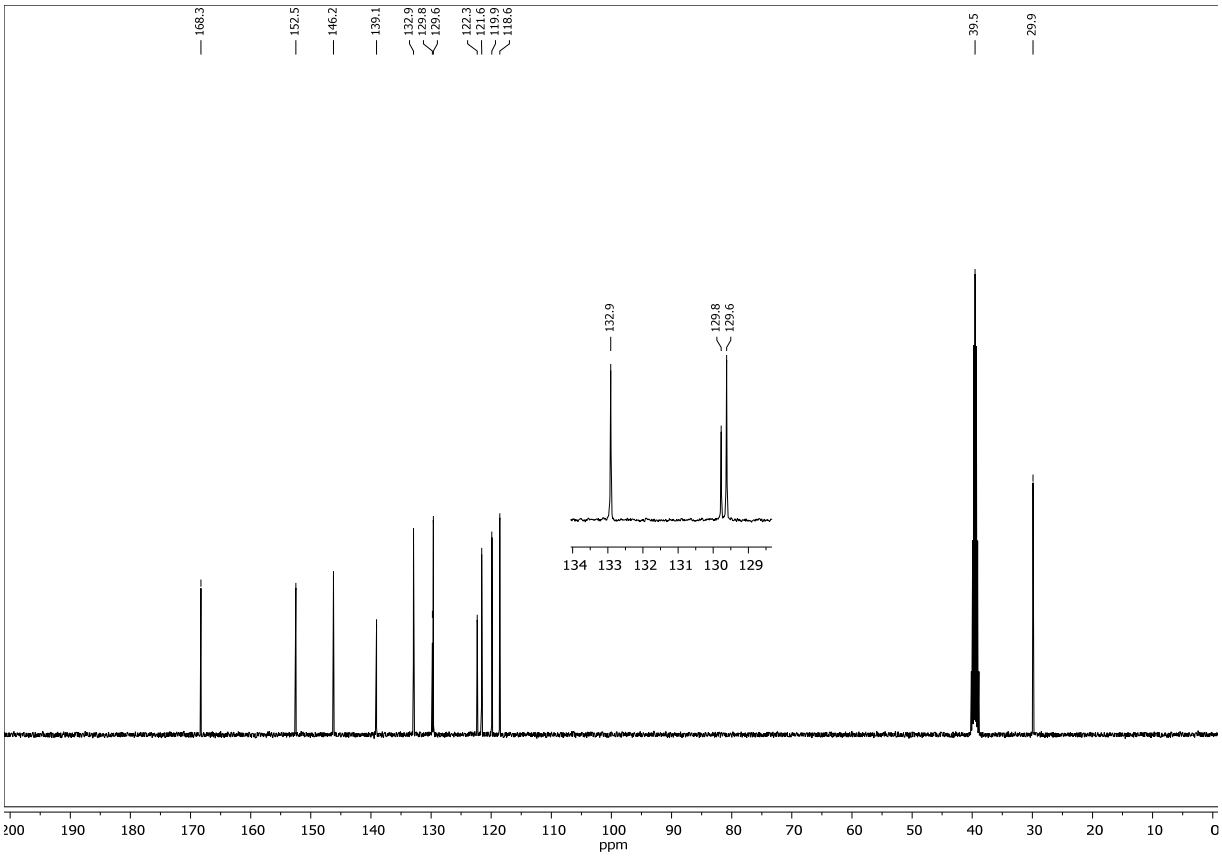
168.3
152.5
146.2
139.1
132.9
129.8
129.6
122.3
121.6
119.9
118.6
39.5
29.9
ppm

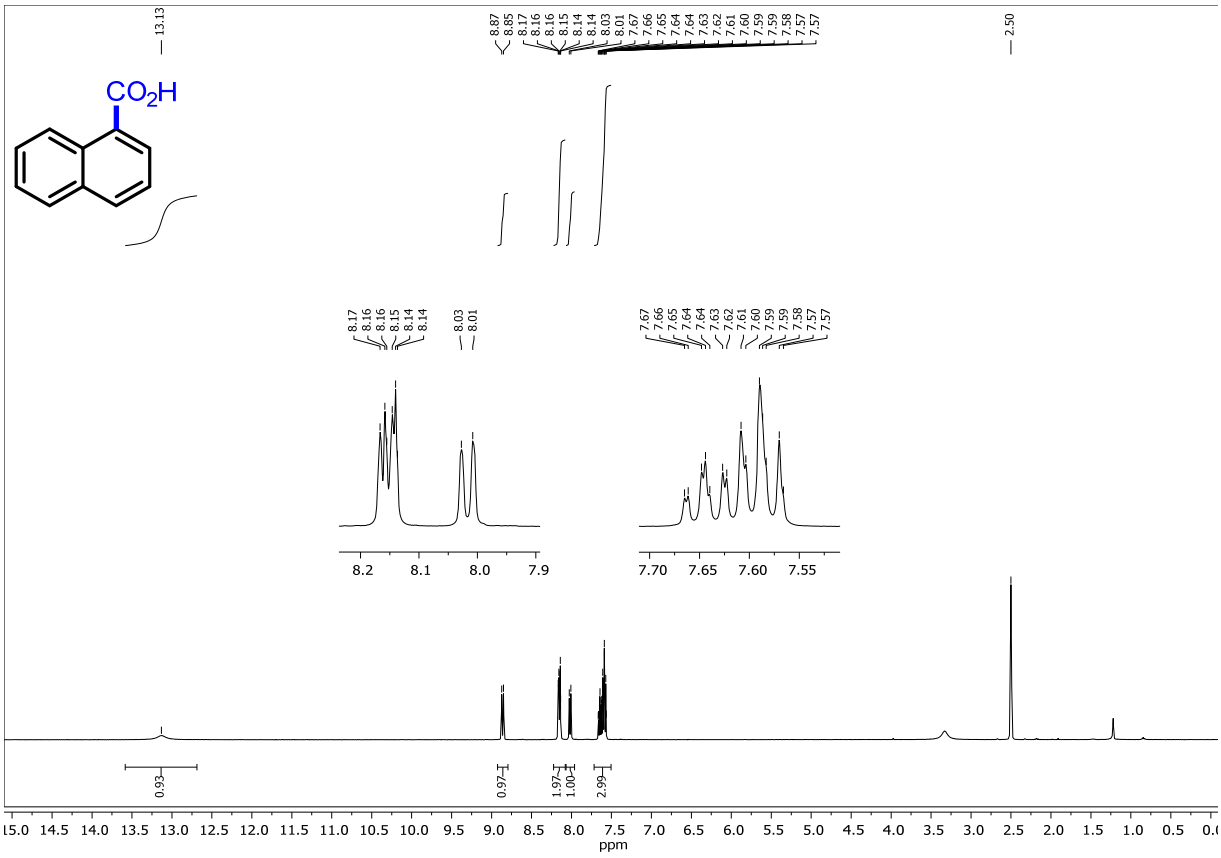
CO2H
13.13
8.87
8.85
8.17
8.16
8.16
8.15
8.14
8.14
8.03
8.01
7.67
7.66
7.65
7.64
7.64
7.63
7.62
7.61
7.60
7.59
7.59
7.58
7.57
7.57
2.50
0.93
0.97
1.97
1.00
2.99
ppm

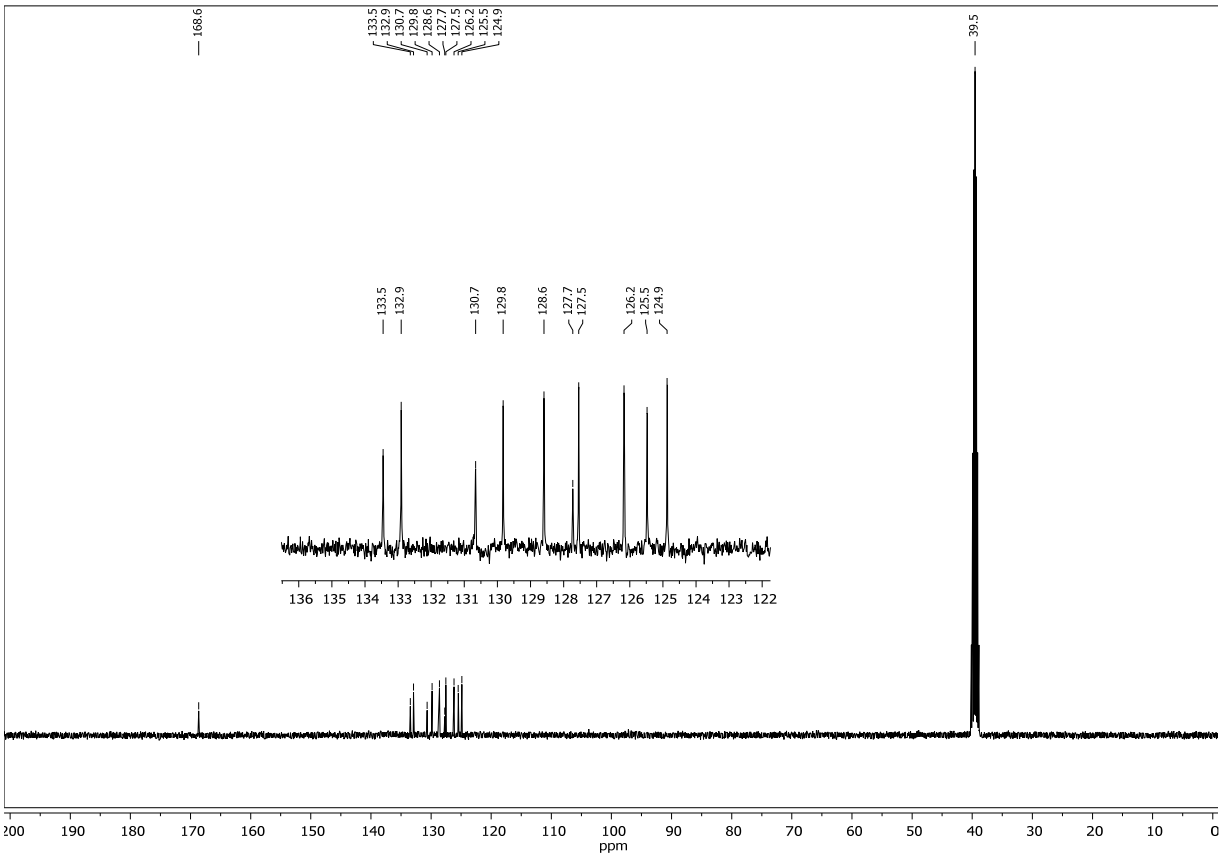
168.6
133.5
132.9
130.7
129.8
128.6
127.7
127.5
126.2
125.5
124.9
39.5
ppm

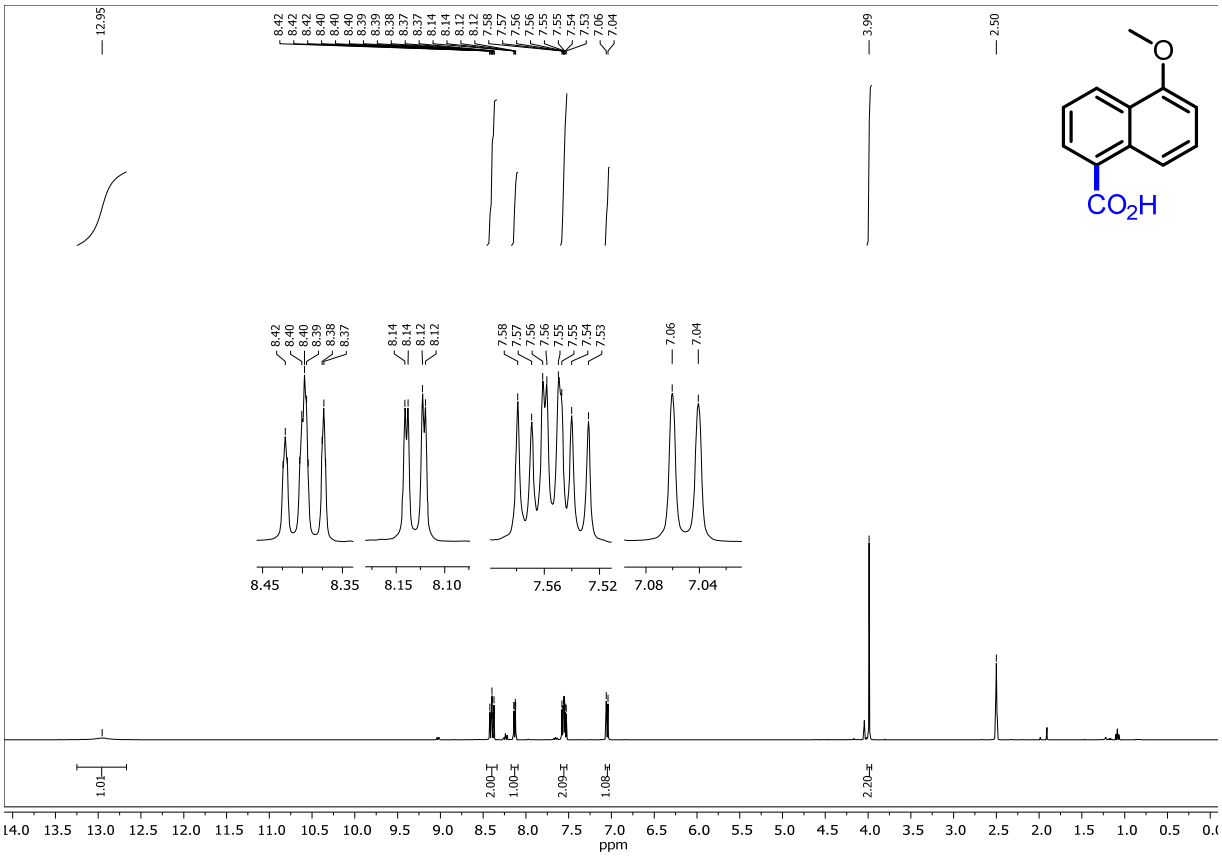
12.95
8.42
8.42
8.42
8.40
8.40
8.40
8.39
8.39
8.38
8.37
8.37
8.14
8.14
8.12
8.12
7.58
7.57
7.56
7.56
7.55
7.55
7.54
7.53
7.06
7.04
3.99
2.50
O
CO2H
8.45
8.35
8.15
8.10
7.56
7.52
7.08
7.04
1.01
2.00
1.00
2.09
1.08
2.20
ppm

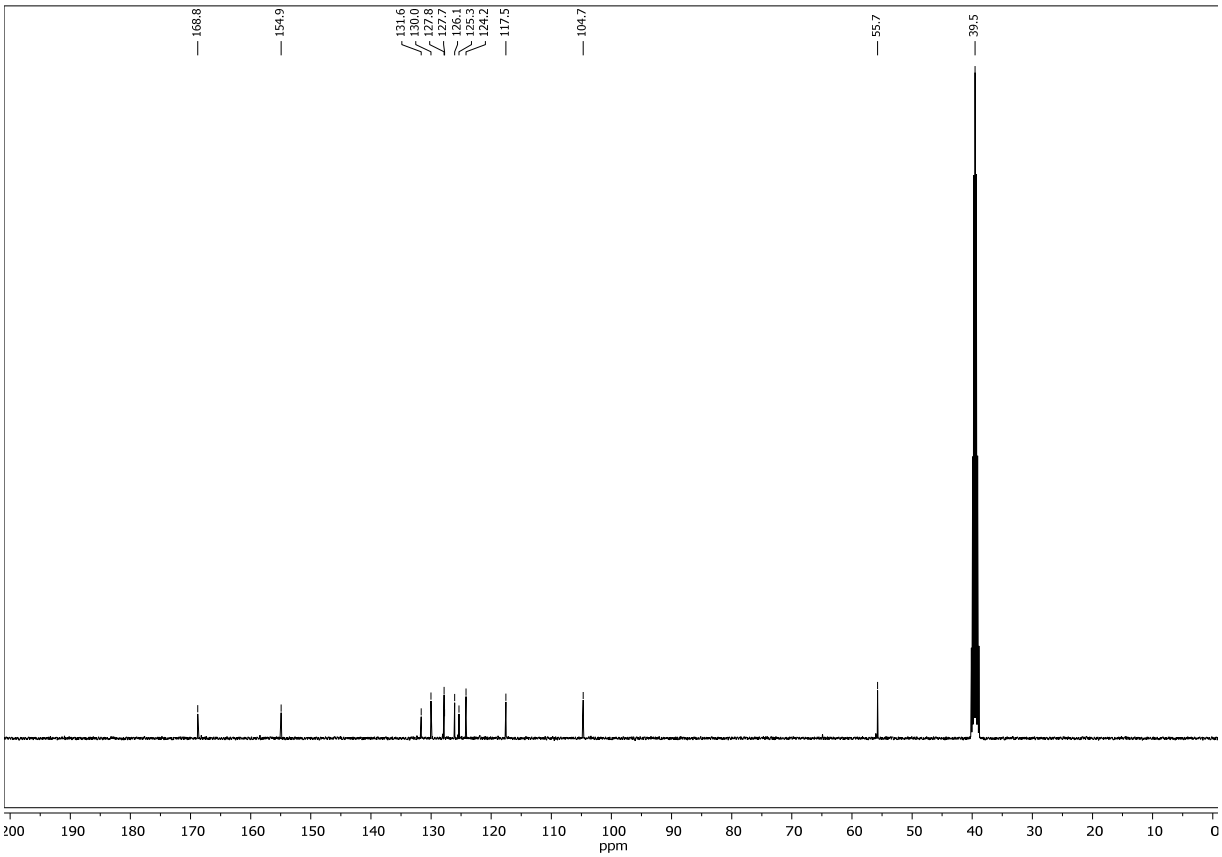
168.8
154.9
131.6
130.0
127.8
127.7
126.1
125.3
124.2
117.5
104.7
55.7
39.5
ppm

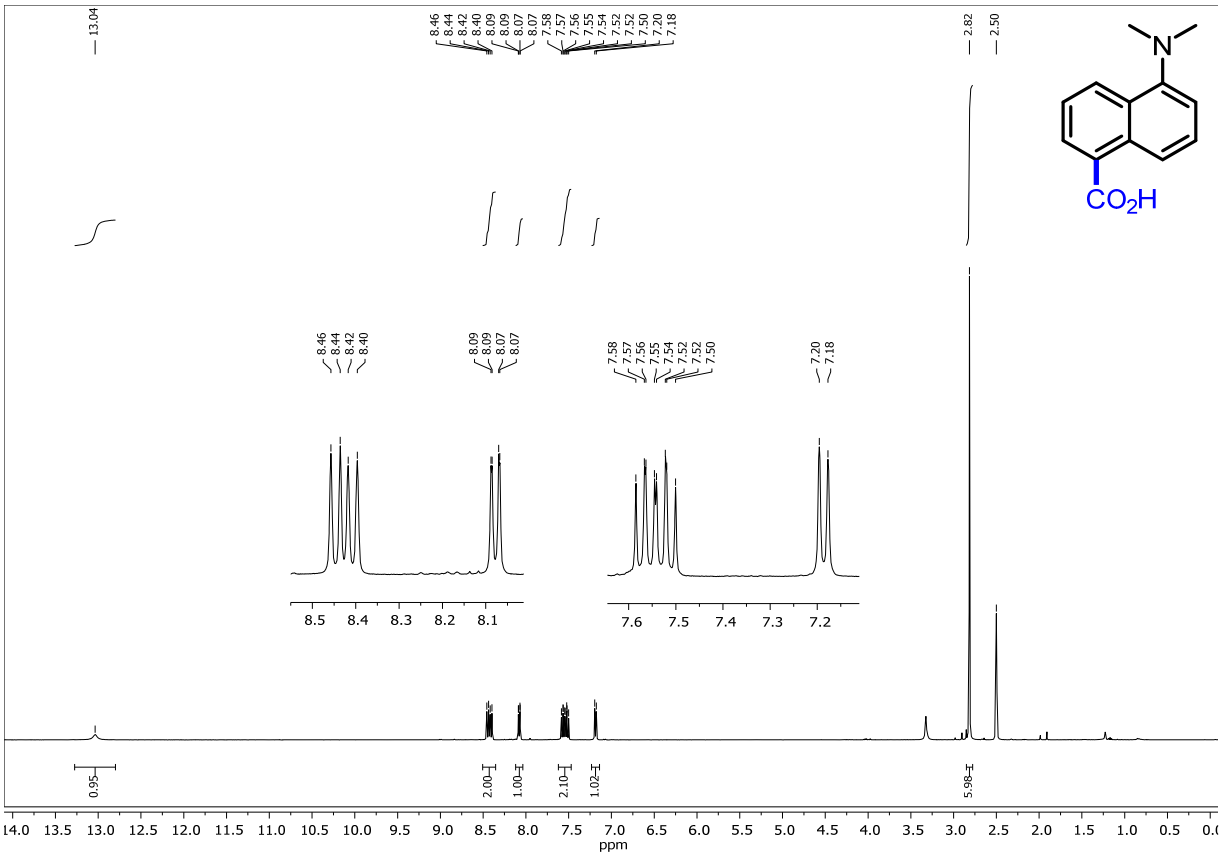
13.04
8.46
8.44
8.42
8.40
8.09
8.09
8.07
8.07
7.58
7.57
7.56
7.55
7.54
7.52
7.52
7.50
7.20
7.18
2.82
2.50
N
CO2H
0.95
2.00
1.00
2.10
1.02
5.98
ppm

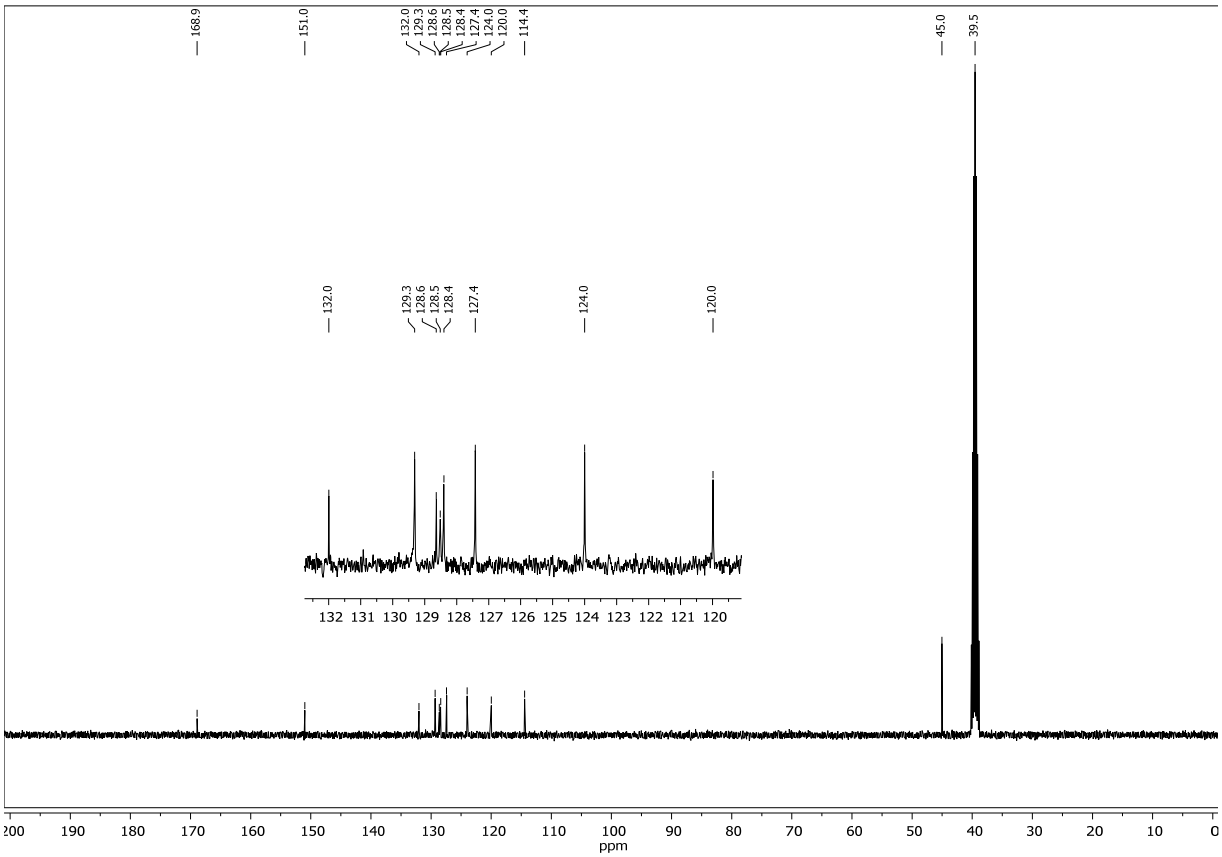
168.9
151.0
132.0
129.3
128.6
128.5
128.4
127.4
124.0
120.0
114.4
45.0
39.5
ppm

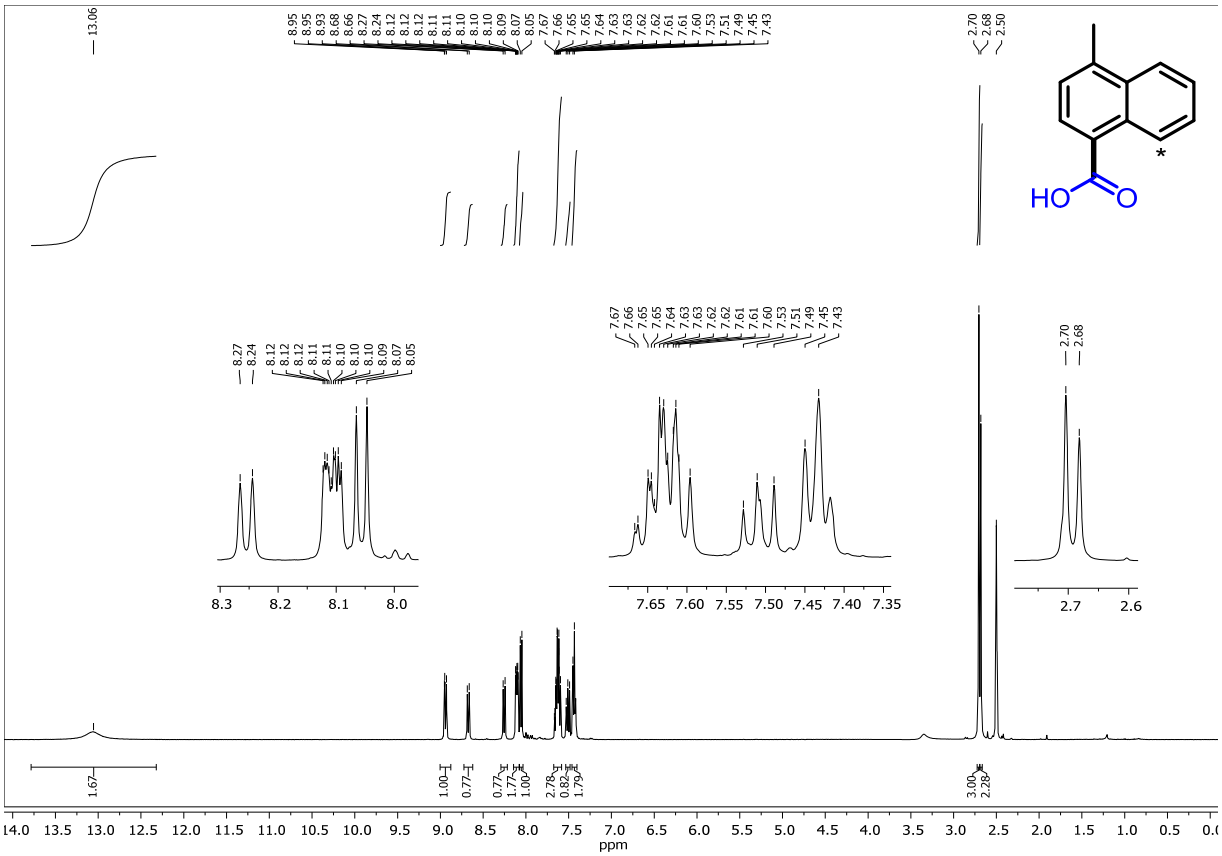
13.06
8.95 8.95 8.93 8.68 8.66 8.27 8.24 8.12 8.12 8.12 8.11 8.11 8.10 8.10 8.10 8.09 8.07 8.05
7.67 7.66 7.65 7.65 7.64 7.63 7.63 7.62 7.62 7.61 7.61 7.60 7.53 7.51 7.49 7.45 7.43
2.70 2.68 2.50
HO
O
*
1.67
1.00 0.77 0.77 1.77 1.00 2.78 0.82 1.79
3.00 2.28
ppm

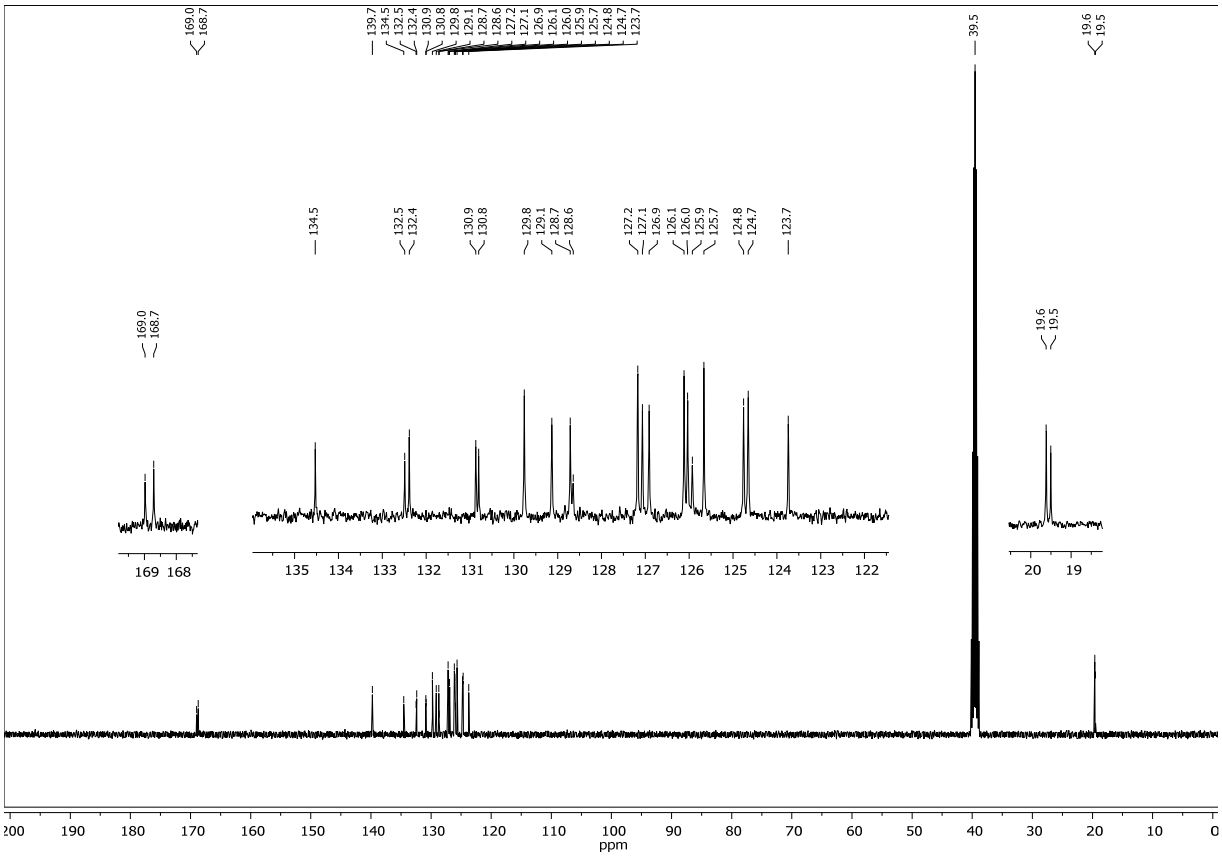
169.0 168.7
139.7 134.5 132.5 132.4 130.9 130.8 129.8 129.1 128.7 128.6 127.2 127.1 126.9 126.1 126.0 125.9 125.7 124.8 124.7 123.7
39.5
19.6 19.5
ppm

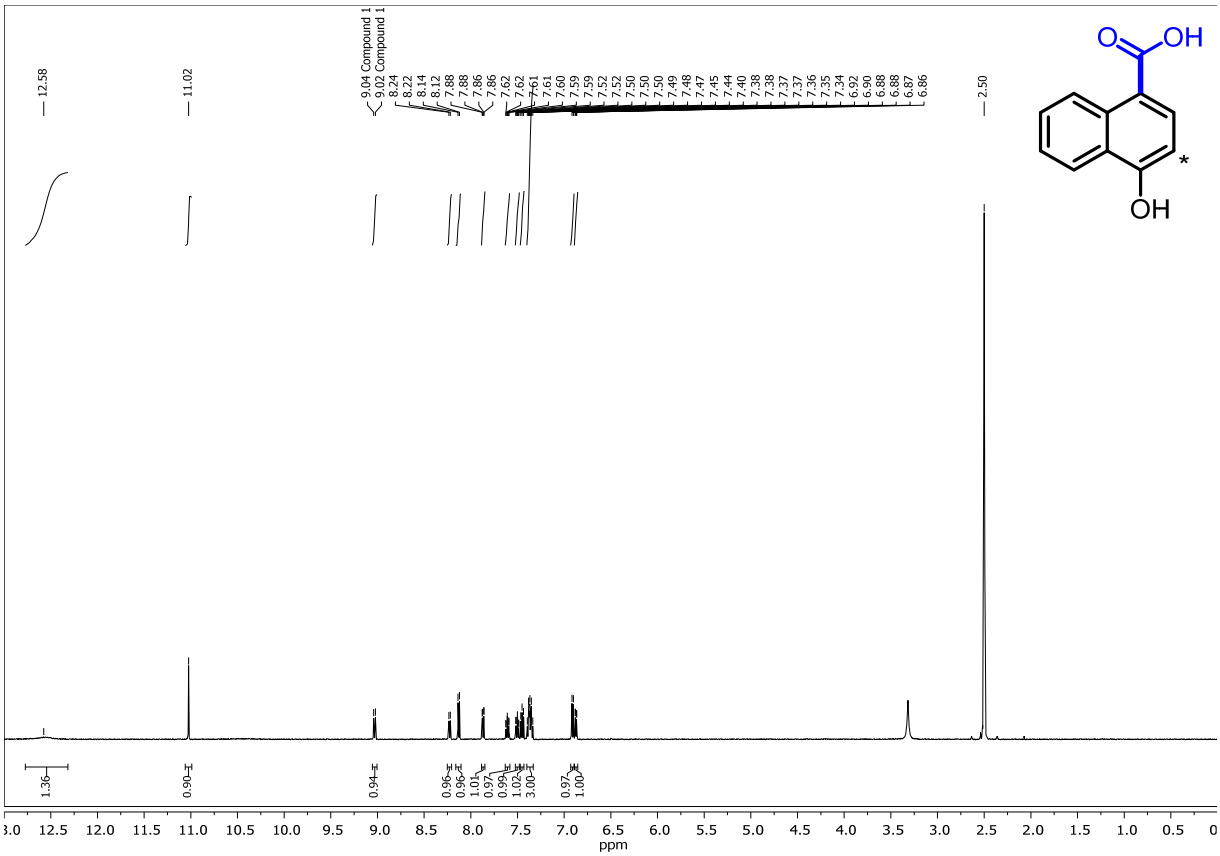
12.58
11.02
9.04 Compound 1
9.02 Compound 1
8.24
8.22
8.14
8.12
7.88
7.88
7.86
7.86
7.62
7.62
7.61
7.61
7.60
7.59
7.59
7.52
7.52
7.50
7.50
7.50
7.49
7.48
7.47
7.45
7.44
7.40
7.38
7.38
7.37
7.37
7.36
7.35
7.34
6.92
6.90
6.88
6.88
6.87
6.86
2.50
OH
OH
*
1.36
0.90
0.94
0.96
0.96
1.01
0.97
0.99
1.02
3.00
0.97
1.00
ppm

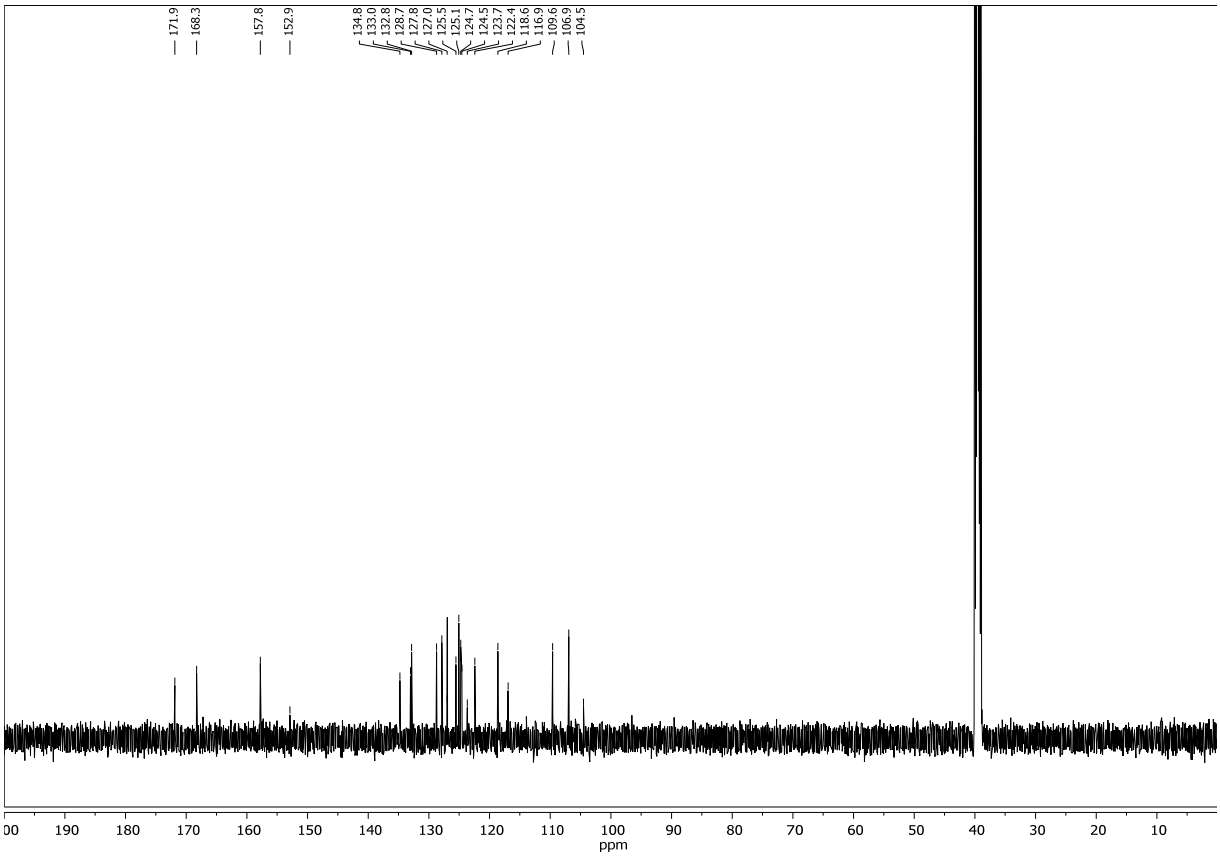
171.9
168.3
157.8
152.9
134.8
133.0
132.8
128.7
127.8
127.0
125.5
125.1
124.7
124.5
123.7
122.4
118.6
116.9
109.6
106.9
104.5
ppm

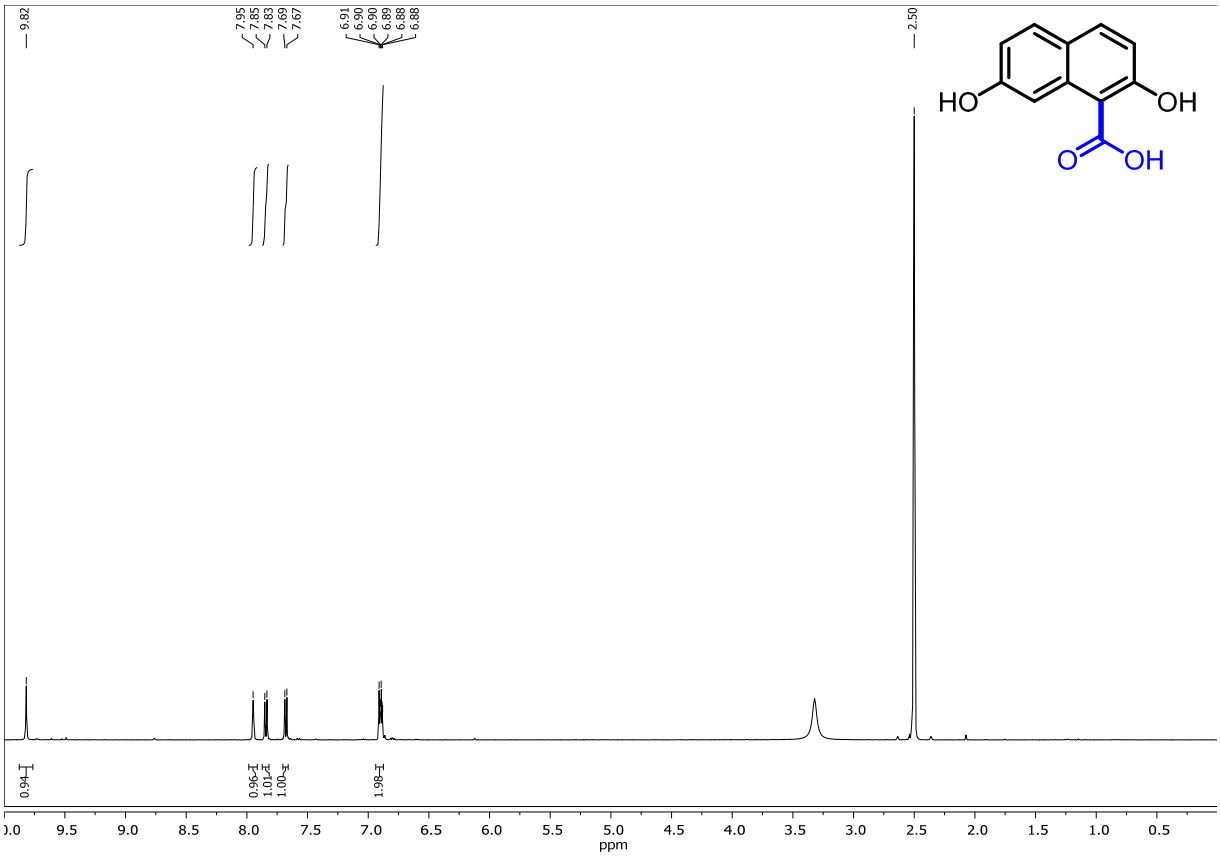
9.82
7.95
7.85
7.83
7.69
7.67
6.91
6.90
6.90
6.89
6.88
6.88
2.50
HO
OH
O
OH
0.94
0.96
1.01
1.00
1.98
ppm

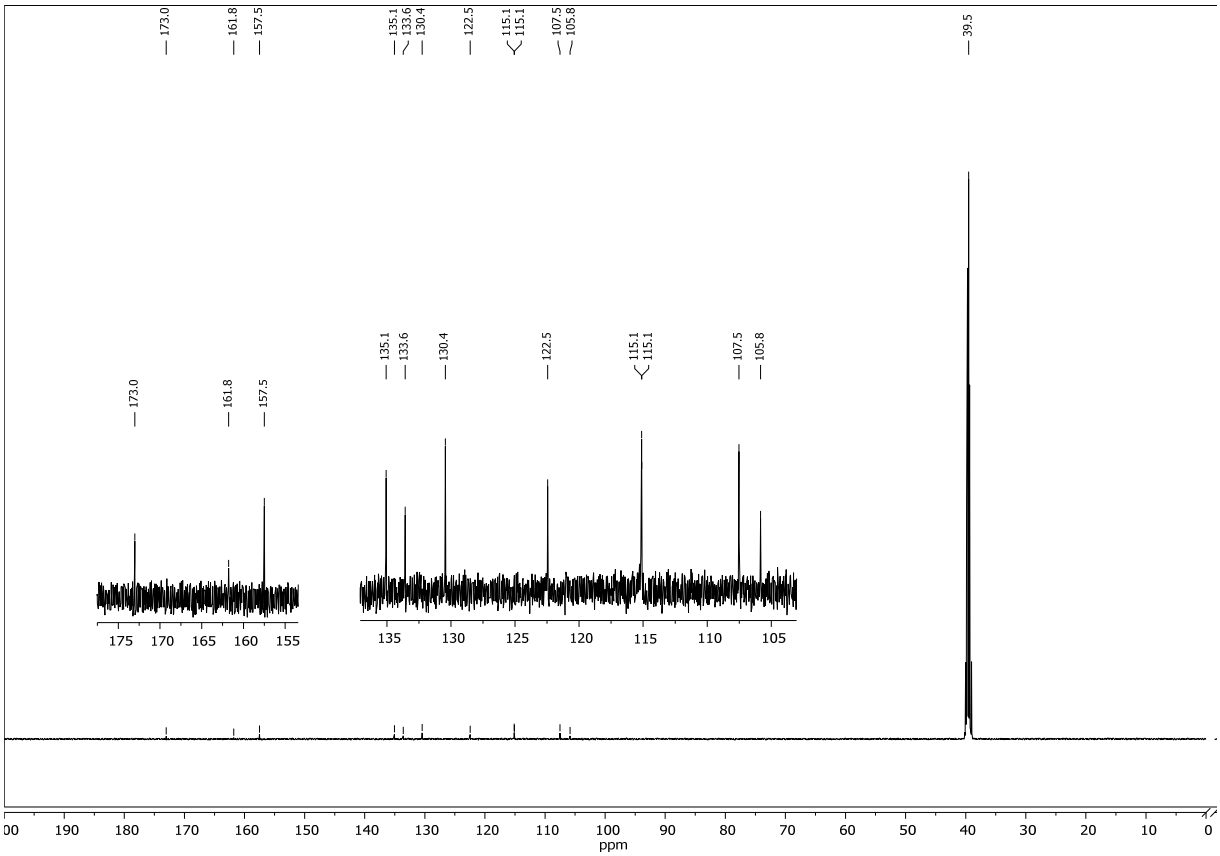
173.0
161.8
157.5
135.1
133.6
130.4
122.5
115.1
115.1
107.5
105.8
39.5
ppm

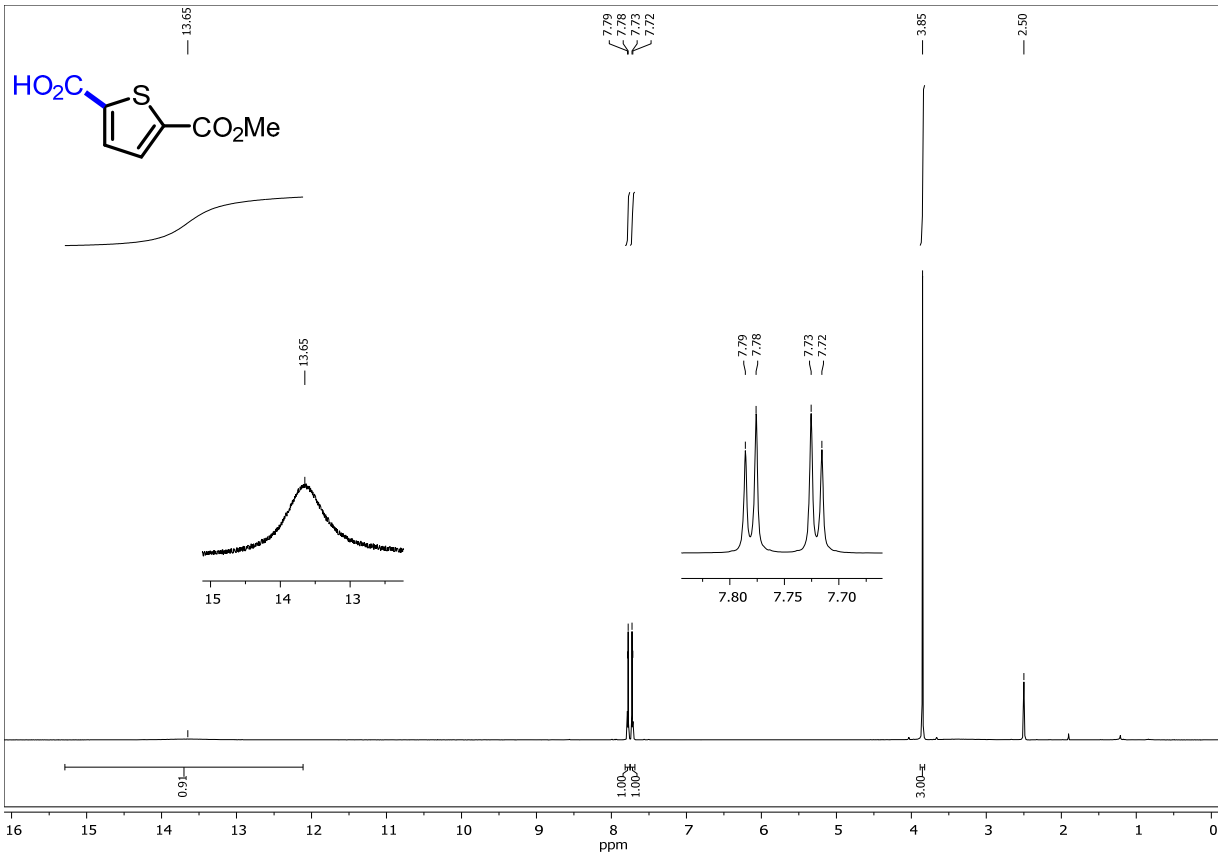
HO2C
S
CO2Me
13.65
7.79
7.78
7.73
7.72
3.85
2.50
0.91
1.00
1.00
3.00
ppm

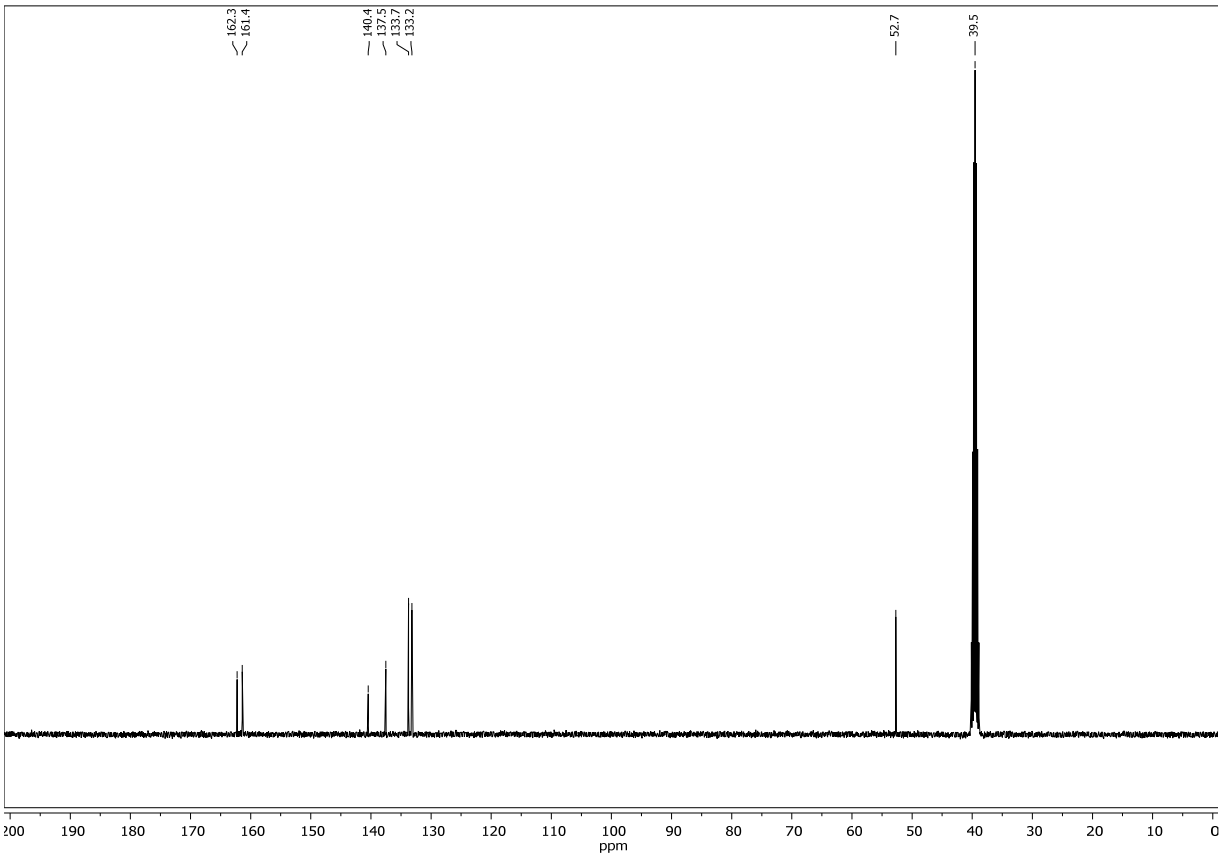
162.3
161.4
140.4
137.5
133.7
133.2
52.7
39.5
ppm

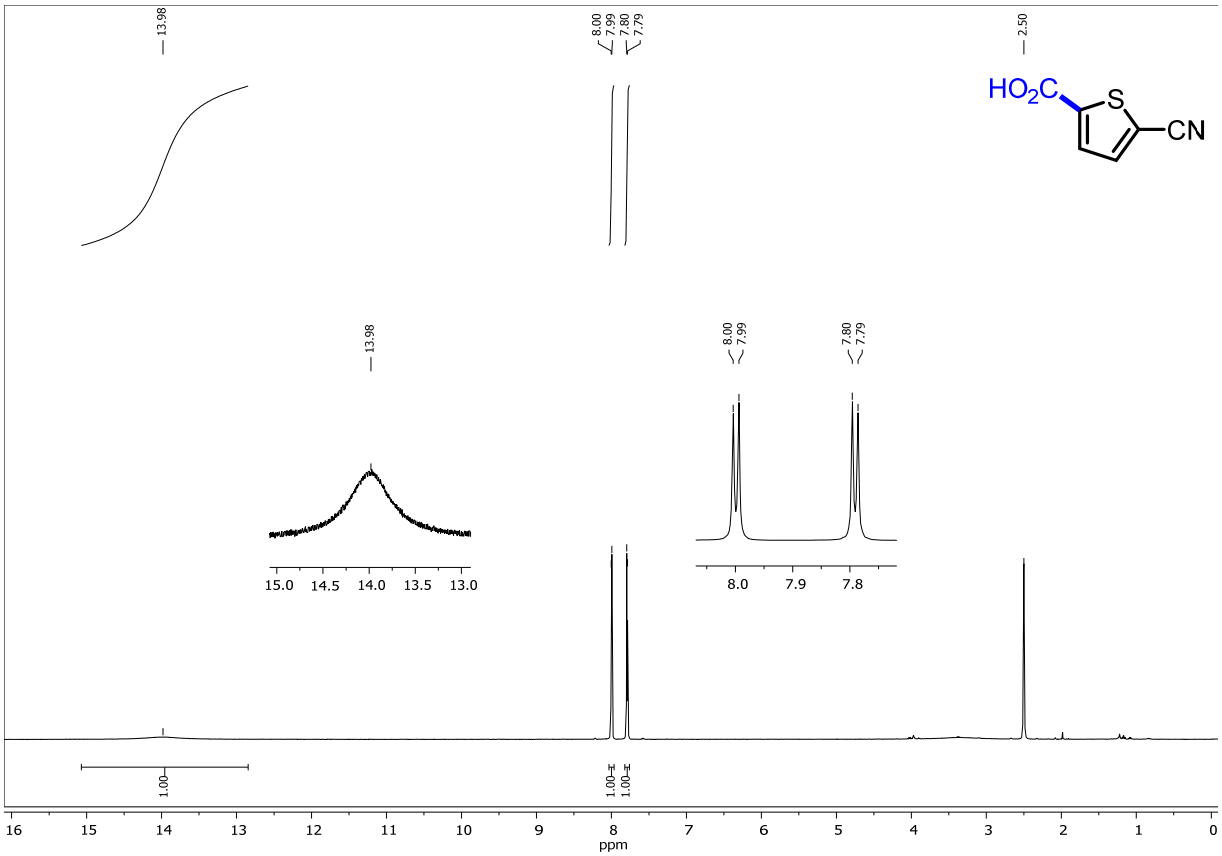
13.98
8.00
7.99
7.80
7.79
2.50
HO2C
S
CN
1.00
1.00
1.00
ppm

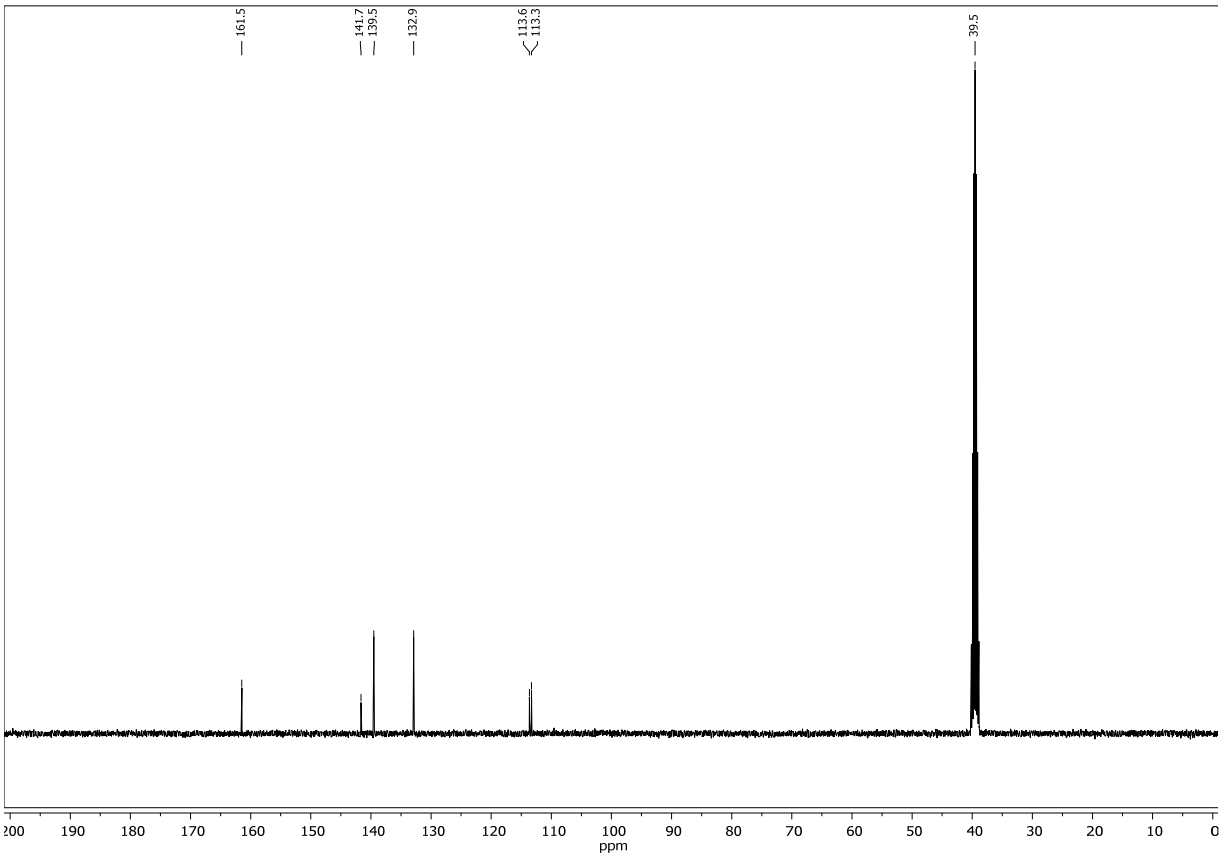
161.5
141.7
139.5
132.9
113.6
113.3
39.5
ppm

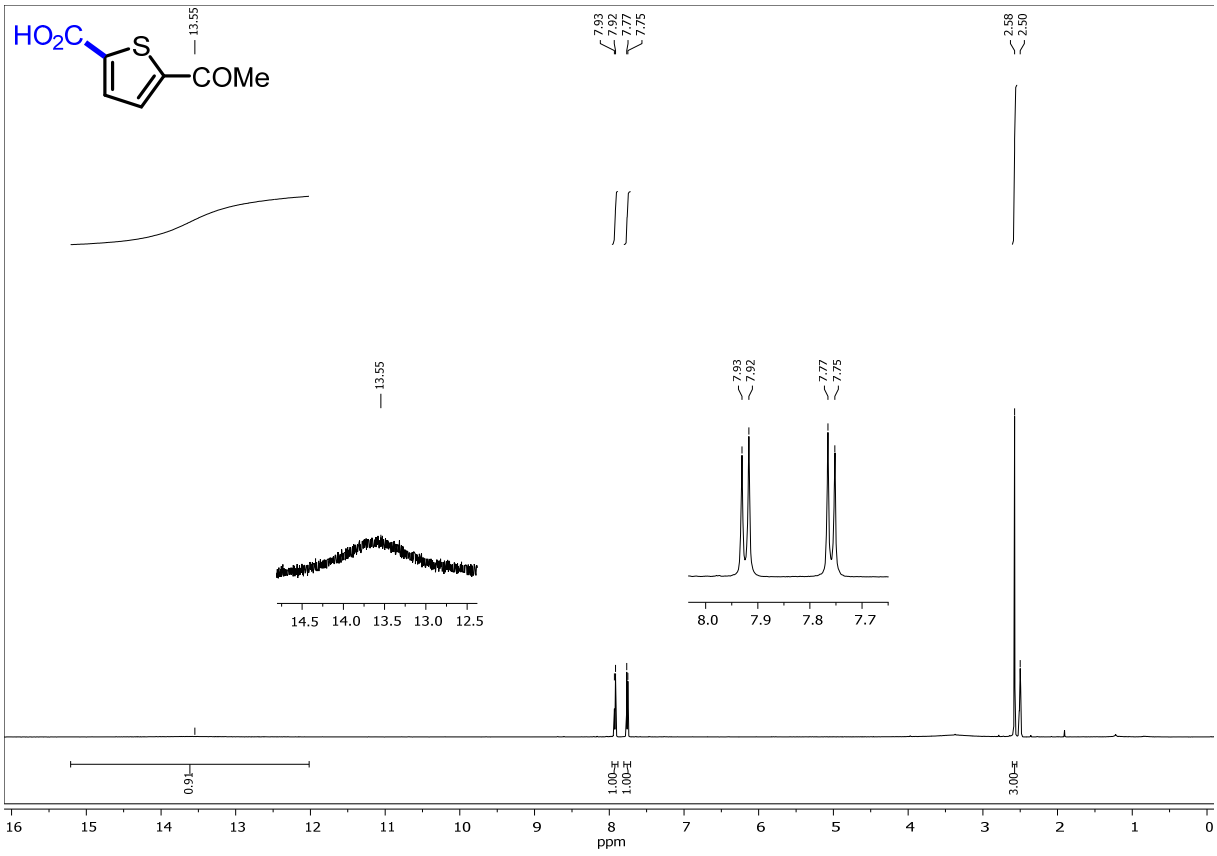
HO2C
S
COMe
13.55
7.93
7.92
7.77
7.75
2.58
2.50
0.91
1.00
1.00
3.00
ppm

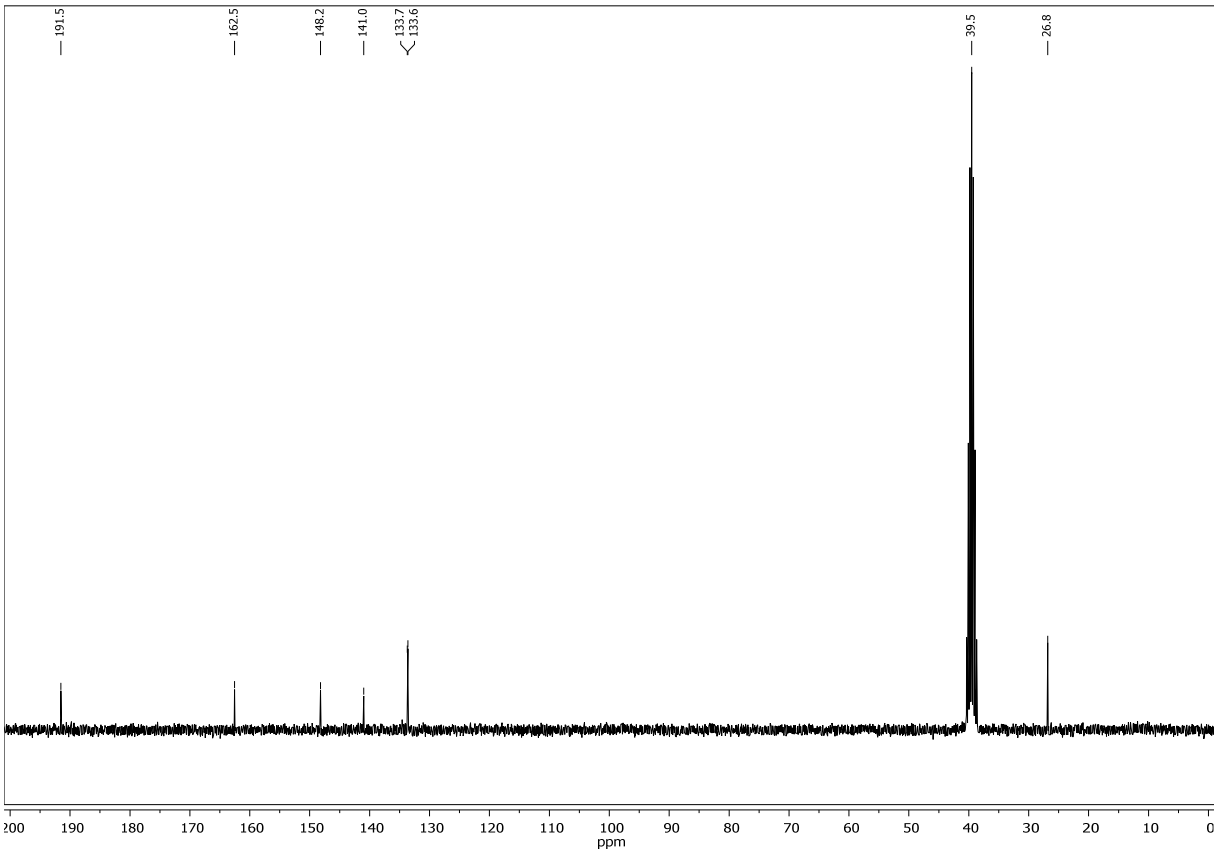
191.5
162.5
148.2
141.0
133.7
133.6
39.5
26.8
ppm

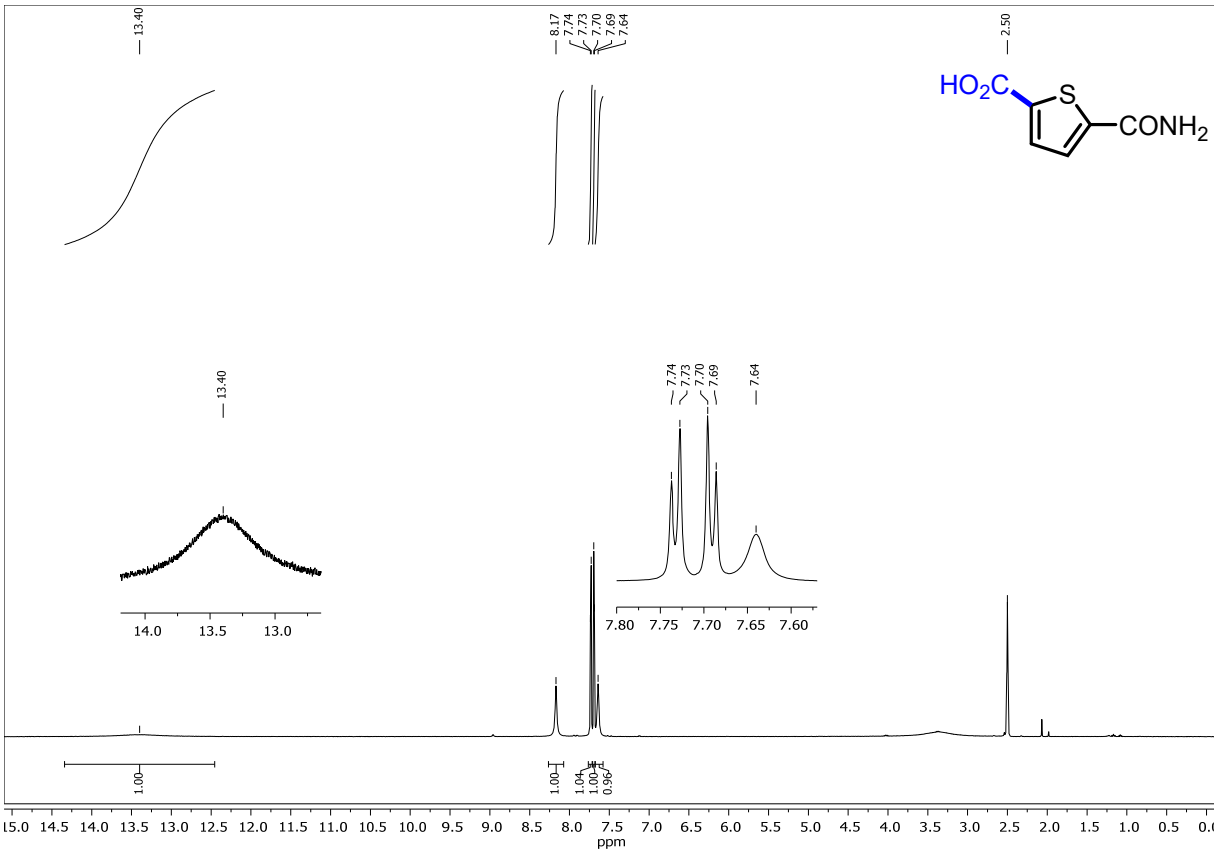
13.40
8.17
7.74
7.73
7.70
7.69
7.64
2.50
HO2C
S
CONH2
14.0
13.5
13.0
7.80
7.75
7.70
7.65
7.60
1.00
1.00
1.04
1.00
0.96
ppm

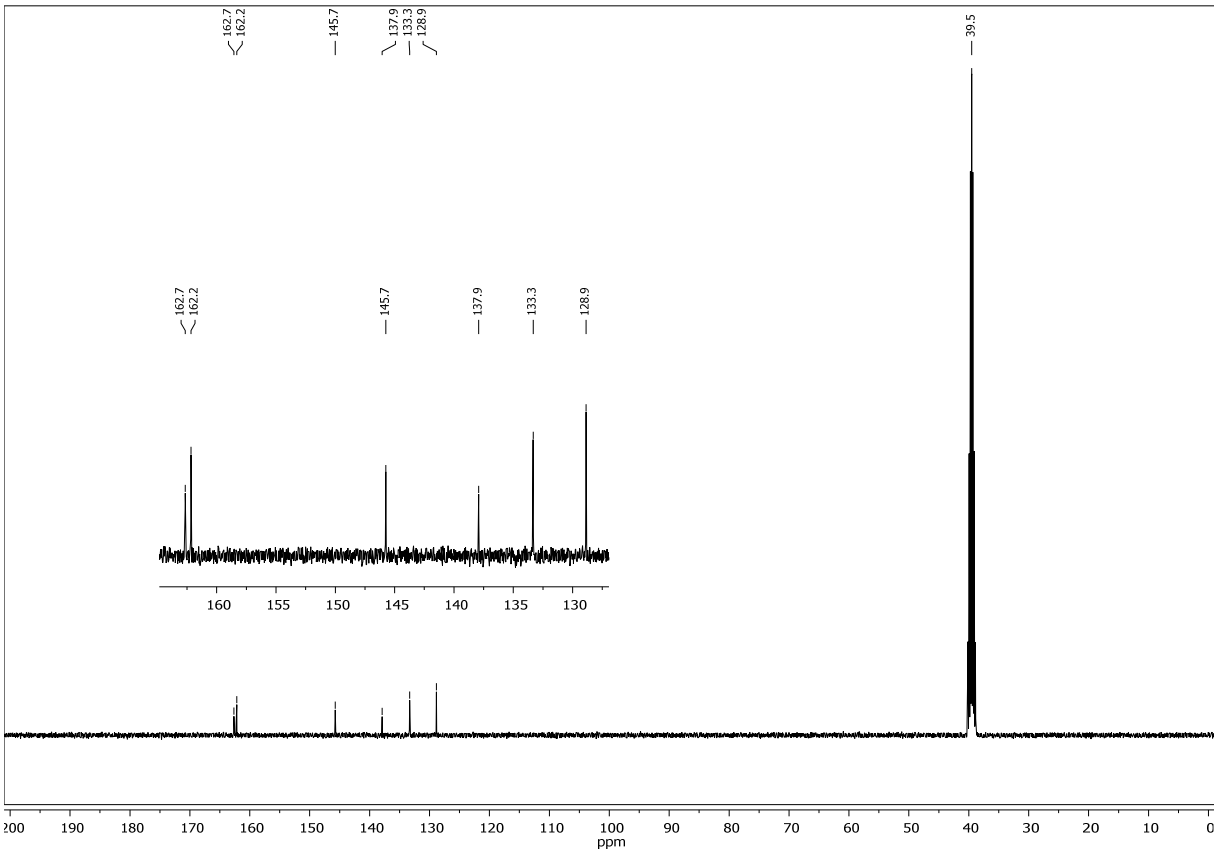
162.7
162.2
145.7
137.9
133.3
128.9
39.5
160
155
150
145
140
135
130
ppm

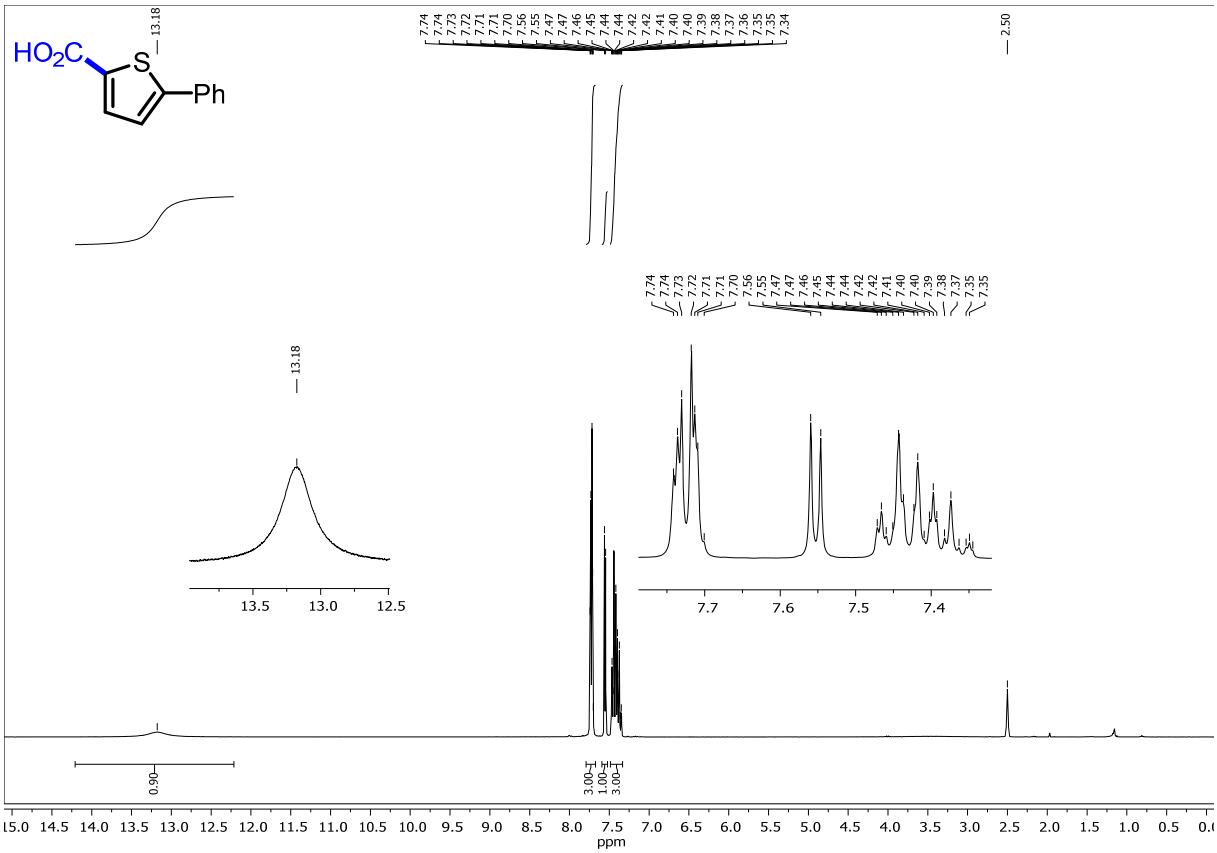
HO2C
S
Ph
13.18
2.50
0.90
3.00
1.00
3.00
ppm

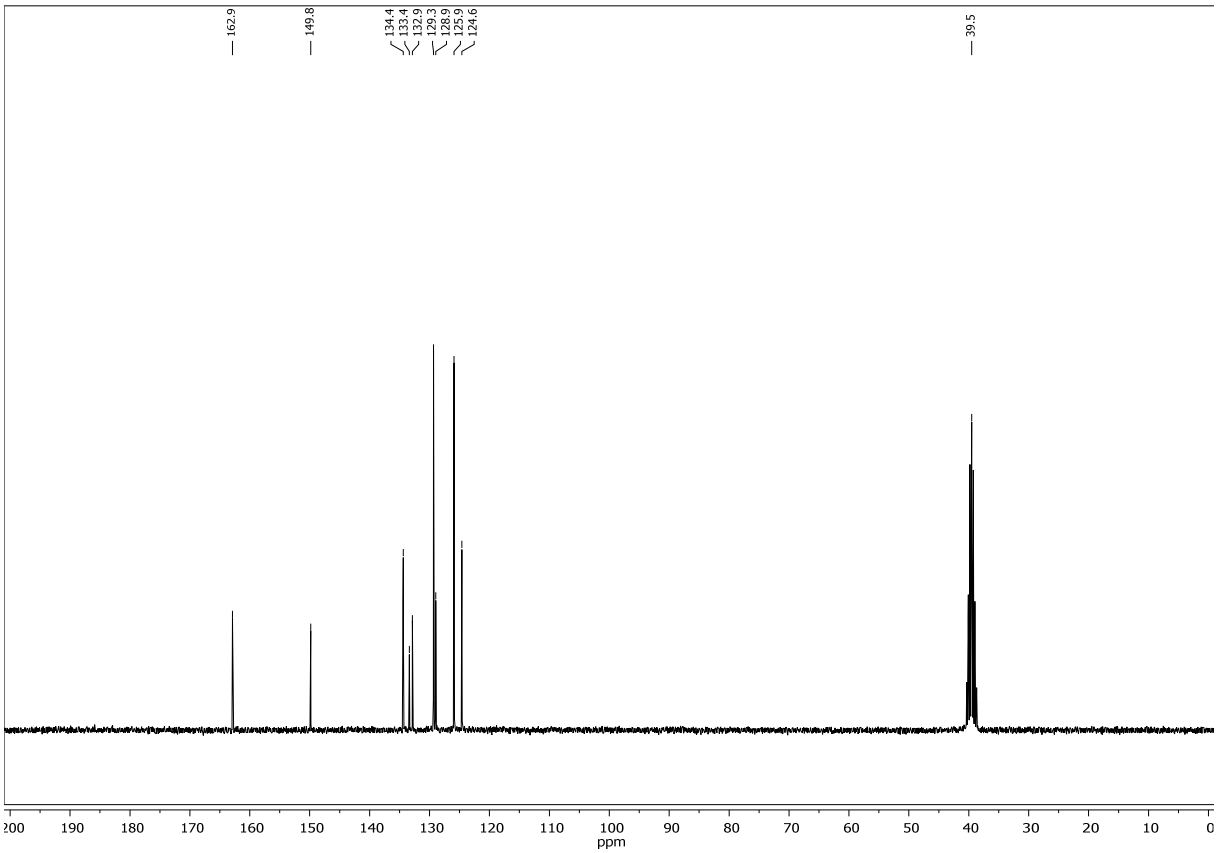
162.9
149.8
134.4
133.4
132.9
129.3
128.9
125.9
124.6
39.5
ppm

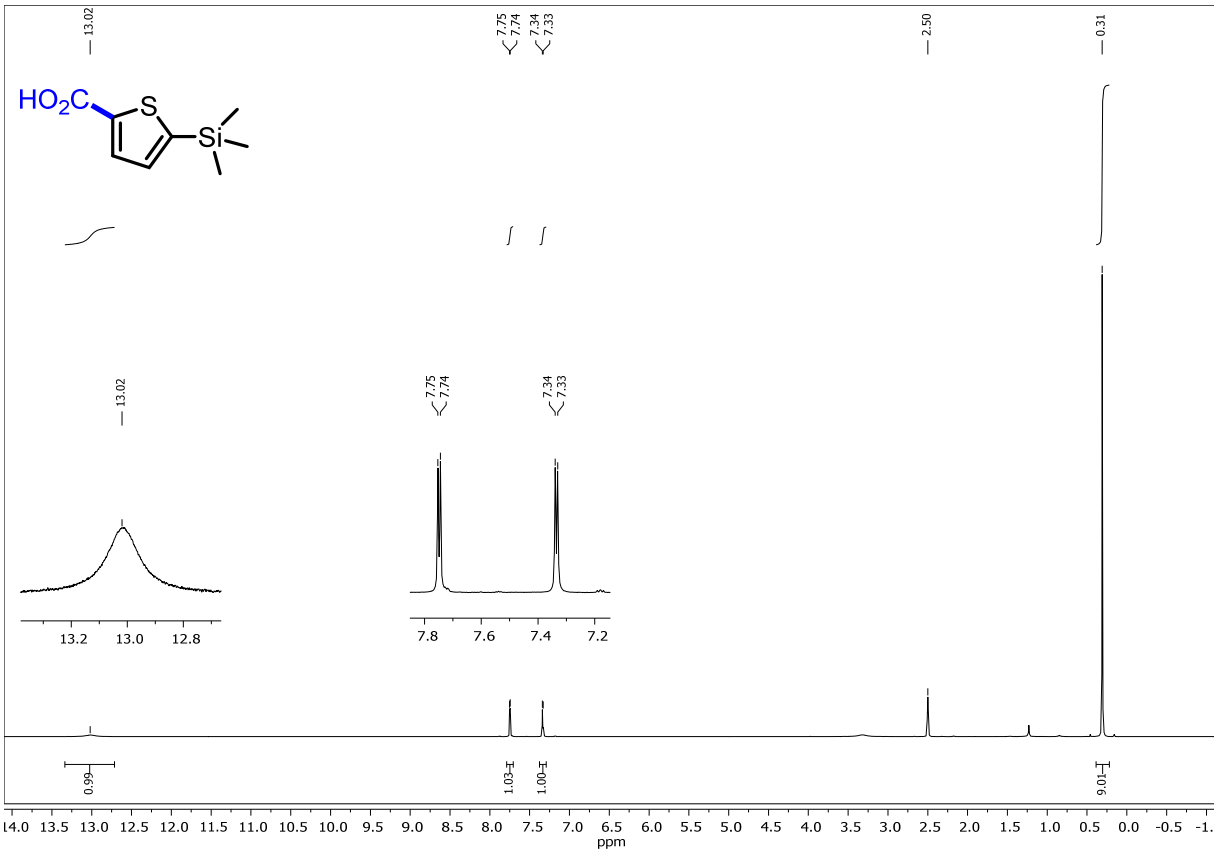
13.02
7.75
7.74
7.34
7.33
2.50
0.31
HO2C
S
Si
0.99
1.03
1.00
9.01
ppm

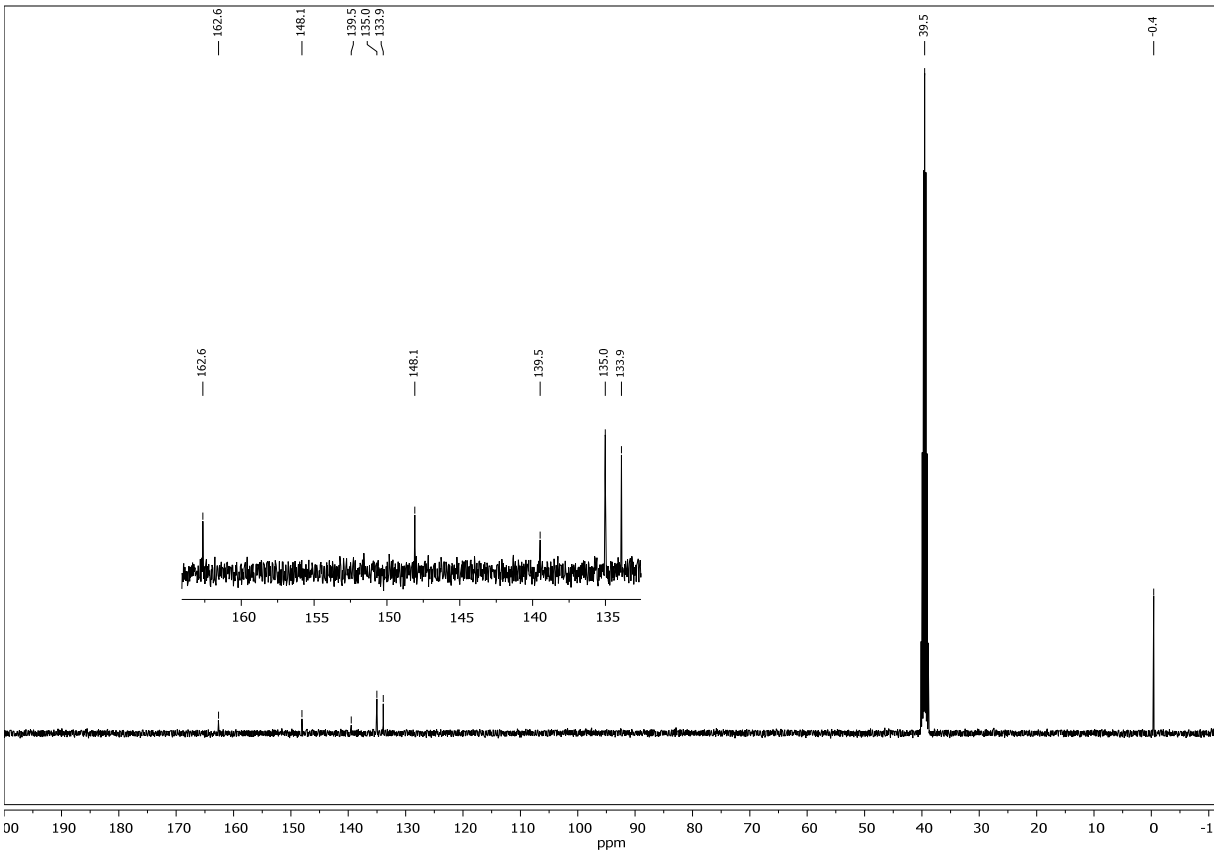
162.6
148.1
139.5
135.0
133.9
39.5
-0.4
ppm

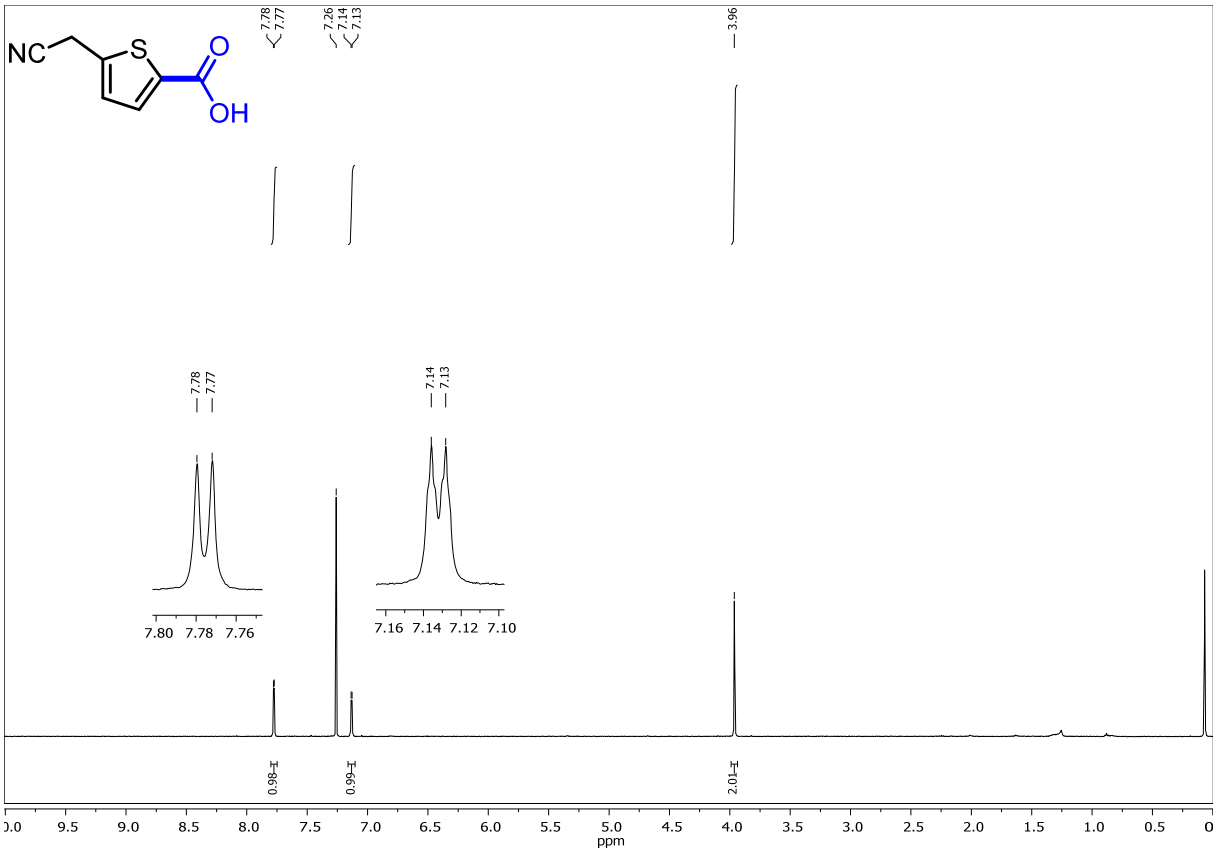
NC
S
O
OH
7.78
7.77
7.26
7.14
7.13
3.96
7.80 7.78 7.76
7.16 7.14 7.12 7.10
0.98
0.99
2.01
ppm

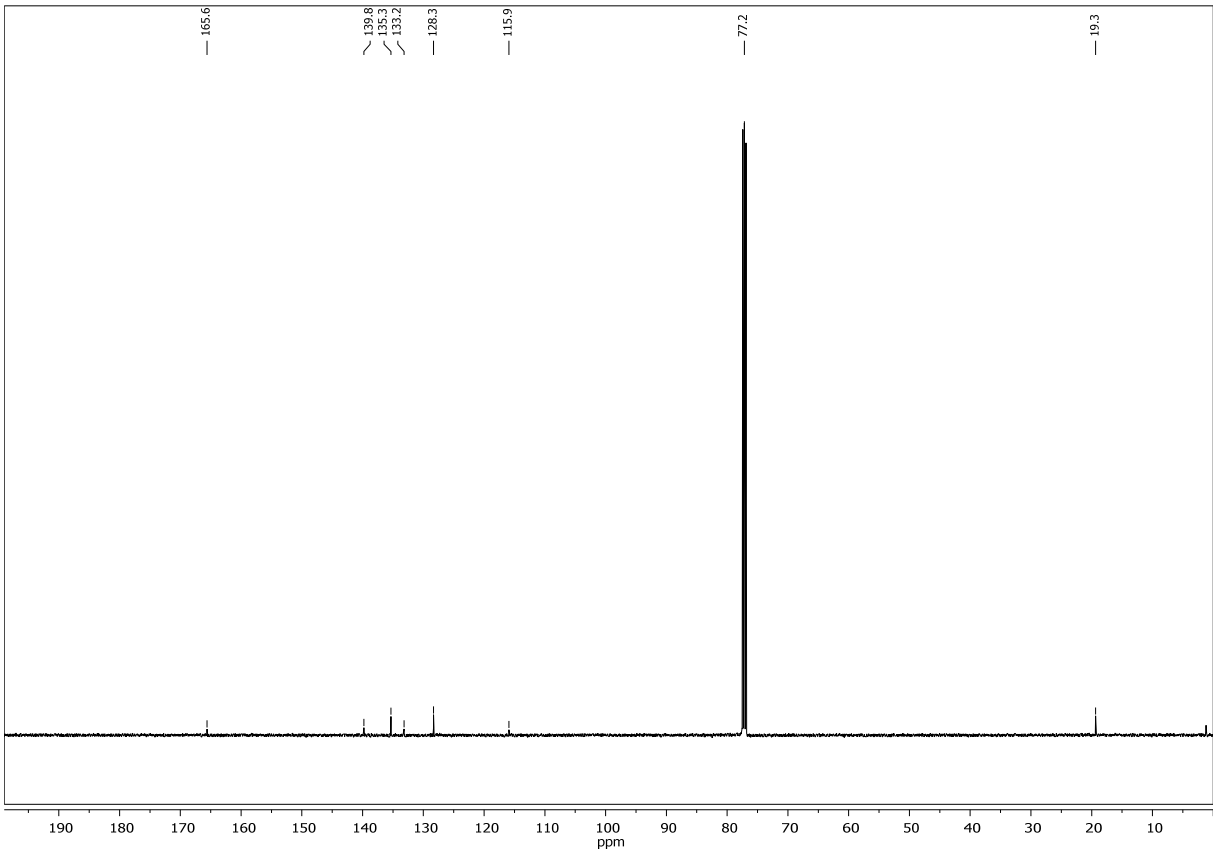
165.6
139.8
135.3
133.2
128.3
115.9
77.2
19.3
ppm

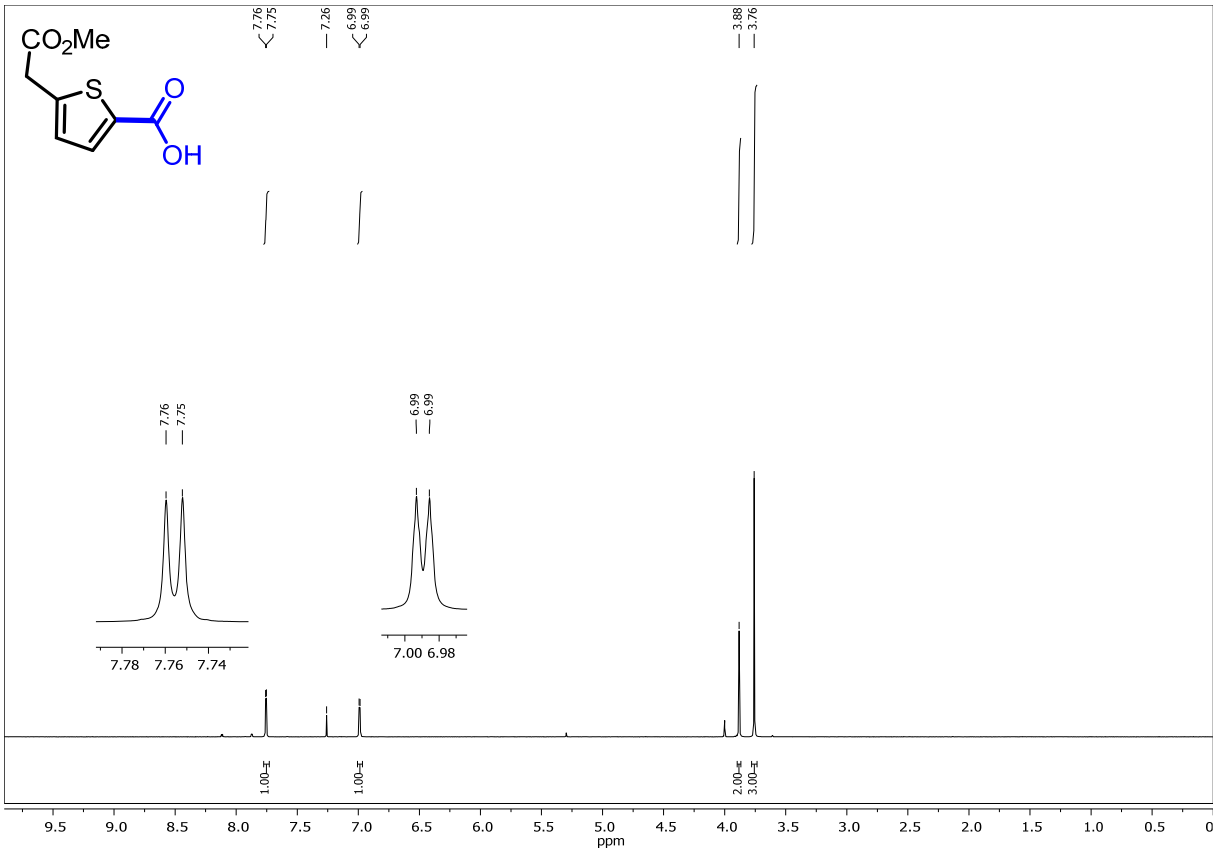
CO2Me
S
O
OH
7.76
7.75
7.26
6.99
6.99
3.88
3.76
7.78 7.76 7.74
7.00 6.98
1.00
1.00
2.00
3.00
ppm

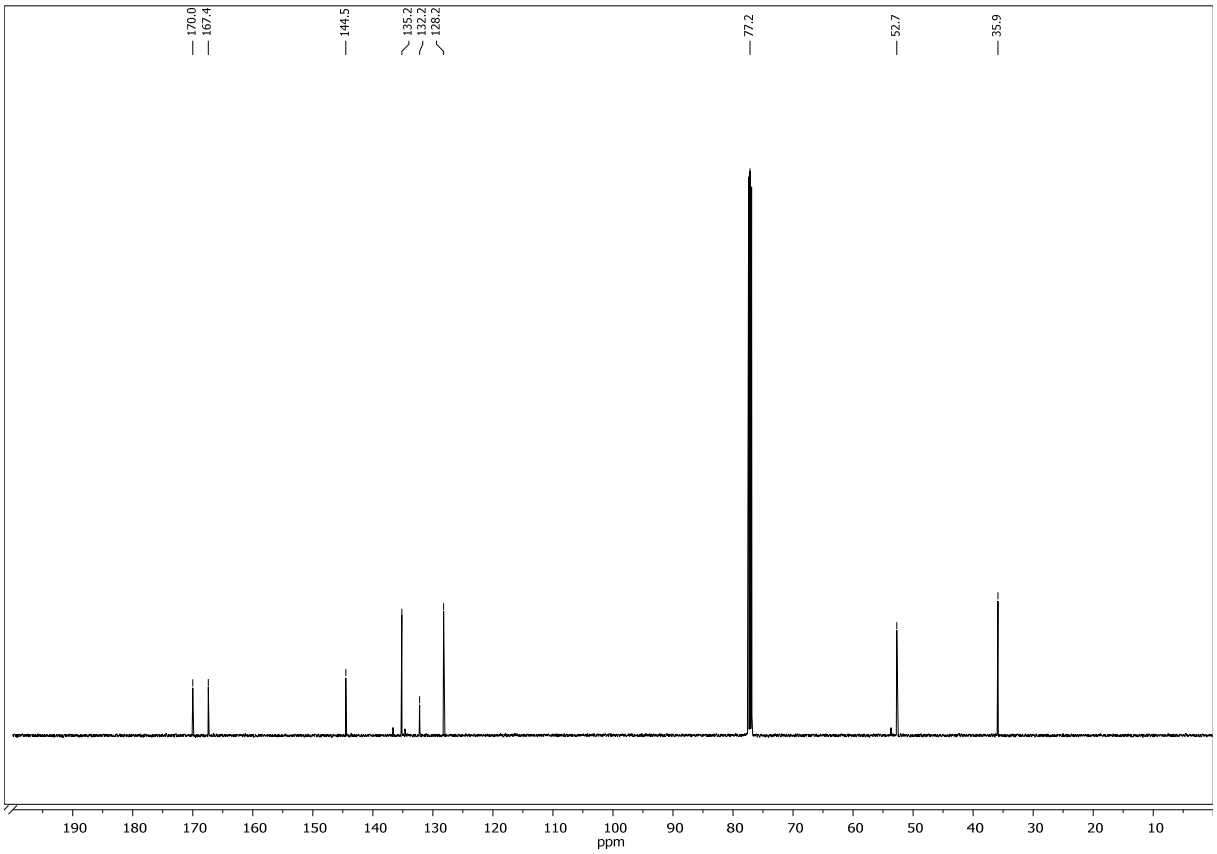
170.0
167.4
144.5
135.2
132.2
128.2
77.2
52.7
35.9
ppm

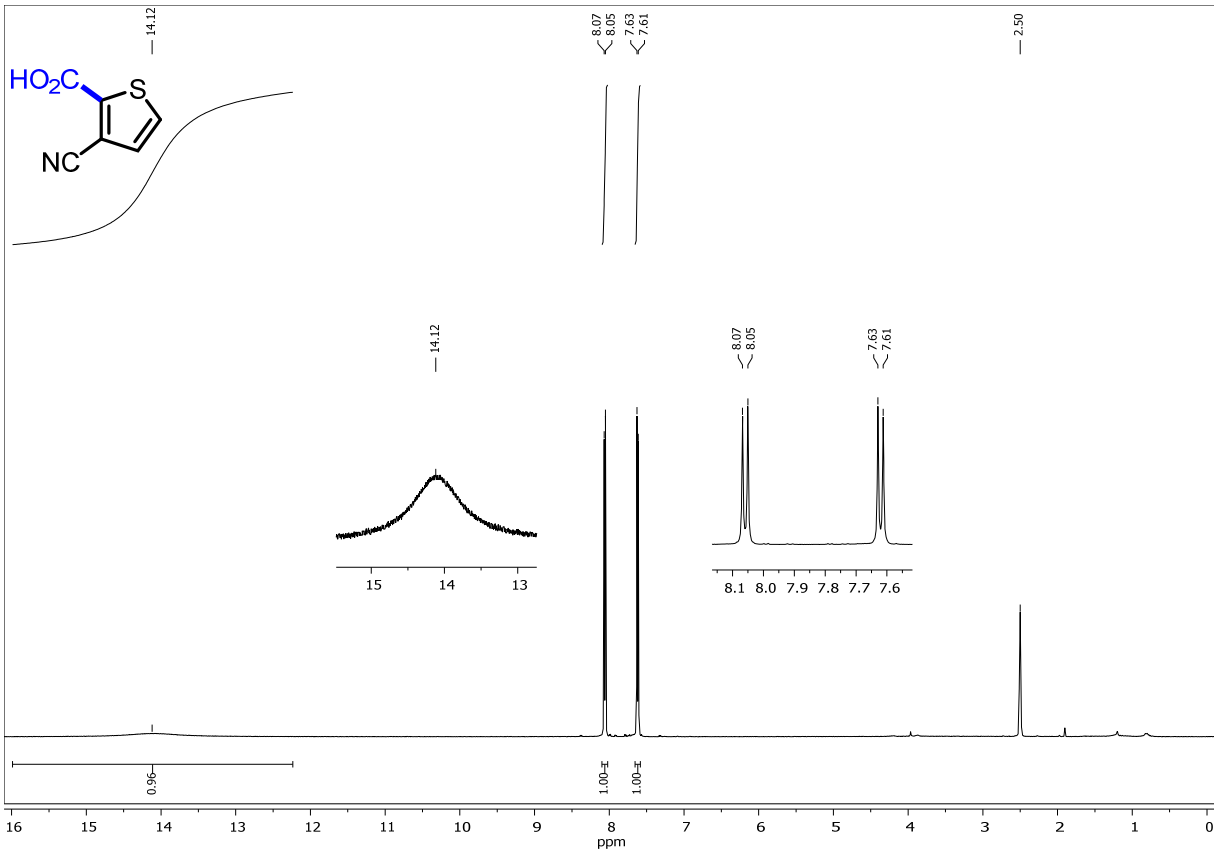
14.12
8.07
8.05
7.63
7.61
2.50
HO2C
S
NC
0.96
1.00
1.00
ppm

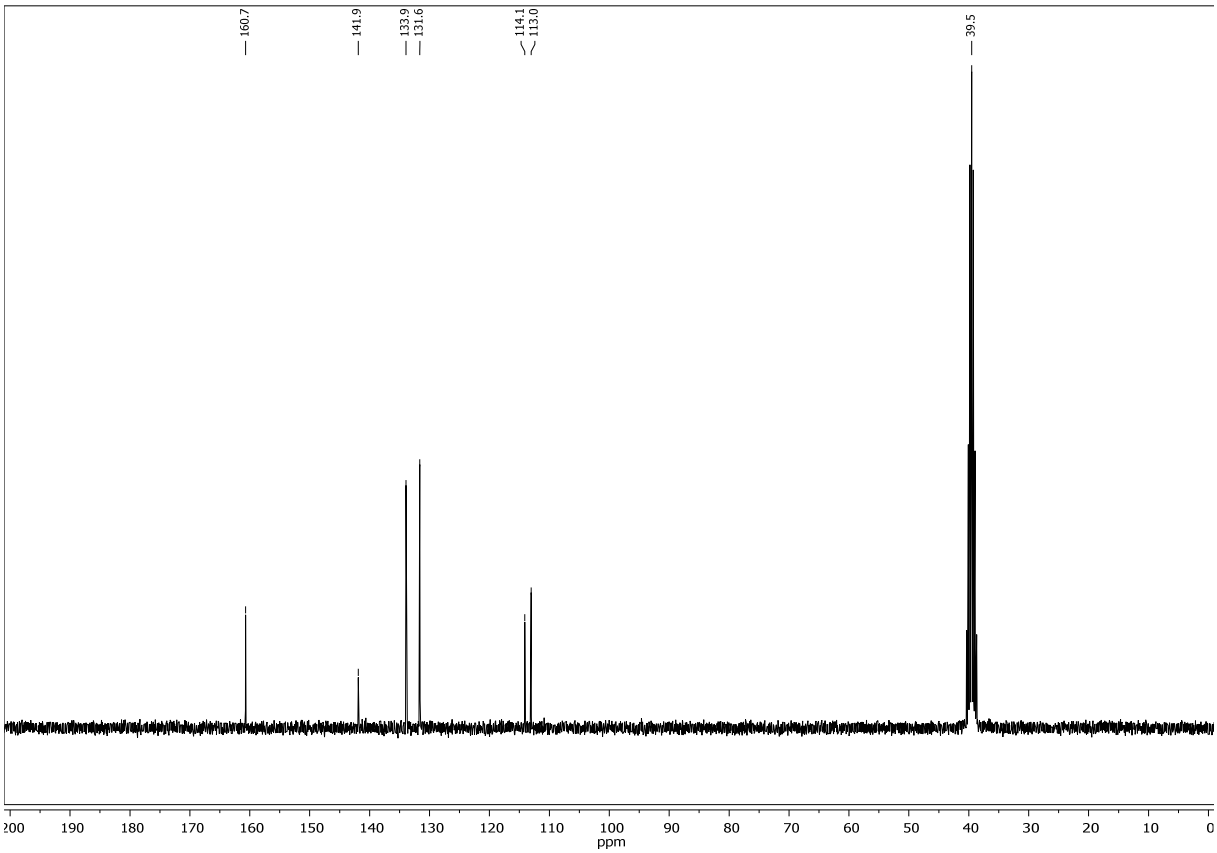
160.7
141.9
133.9
131.6
114.1
113.0
39.5
ppm

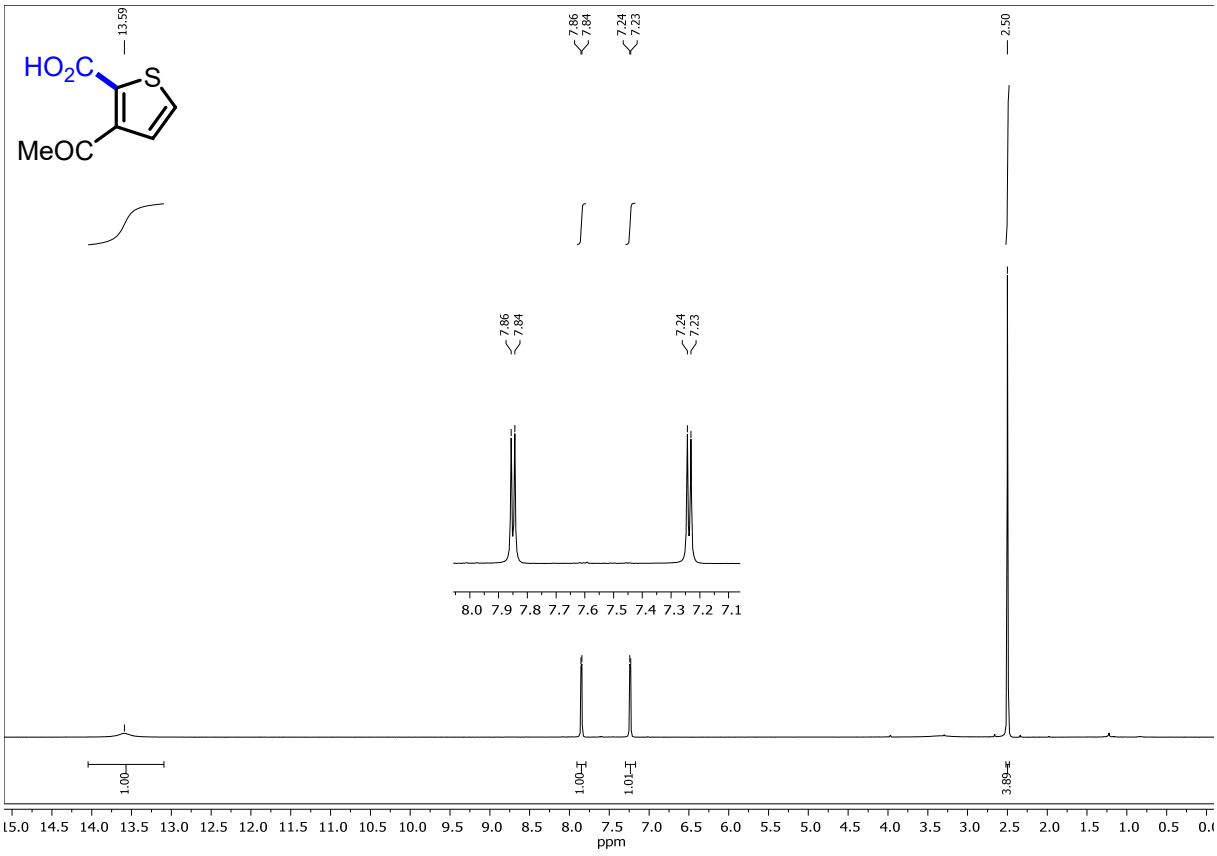
HO2C
S
MeOC
13.59
7.86
7.84
7.24
7.23
2.50
1.00
1.00
1.01
3.89
ppm

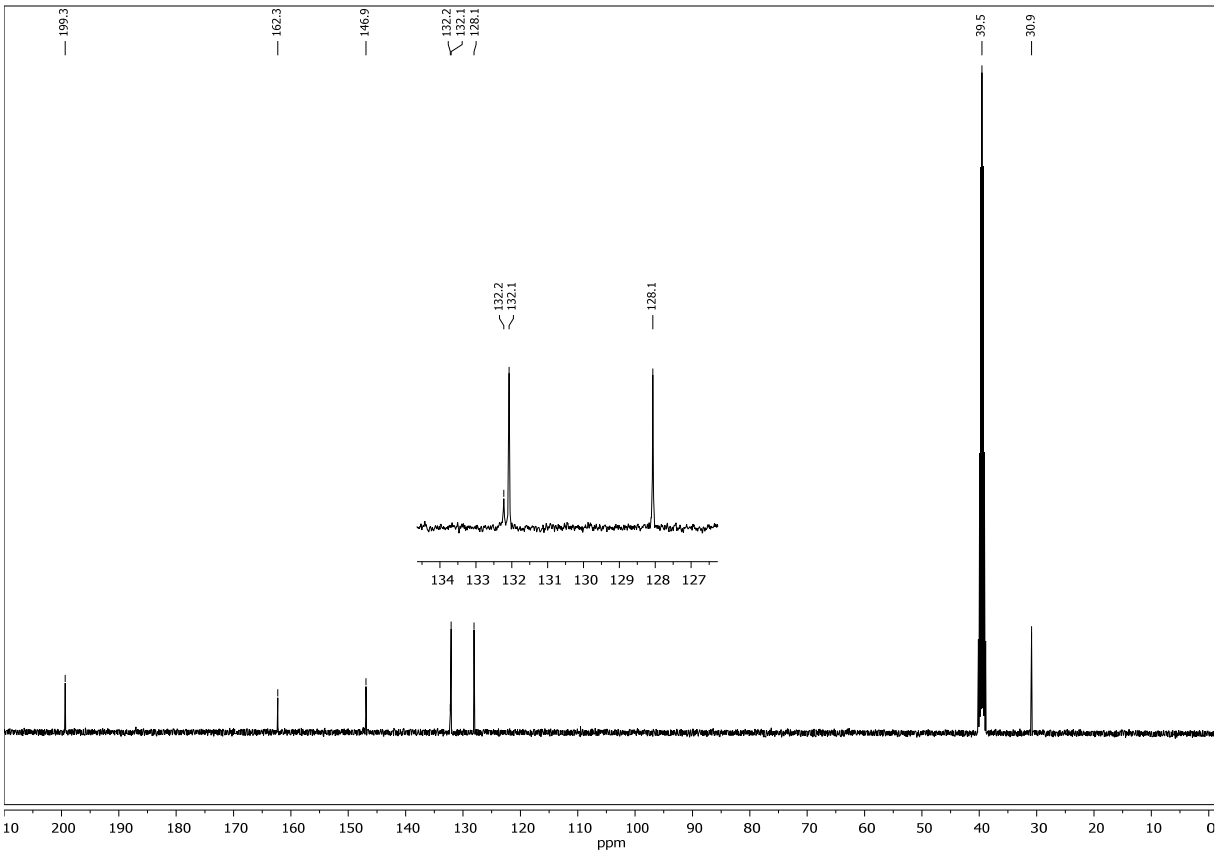
199.3
162.3
146.9
132.2
132.1
128.1
39.5
30.9
ppm

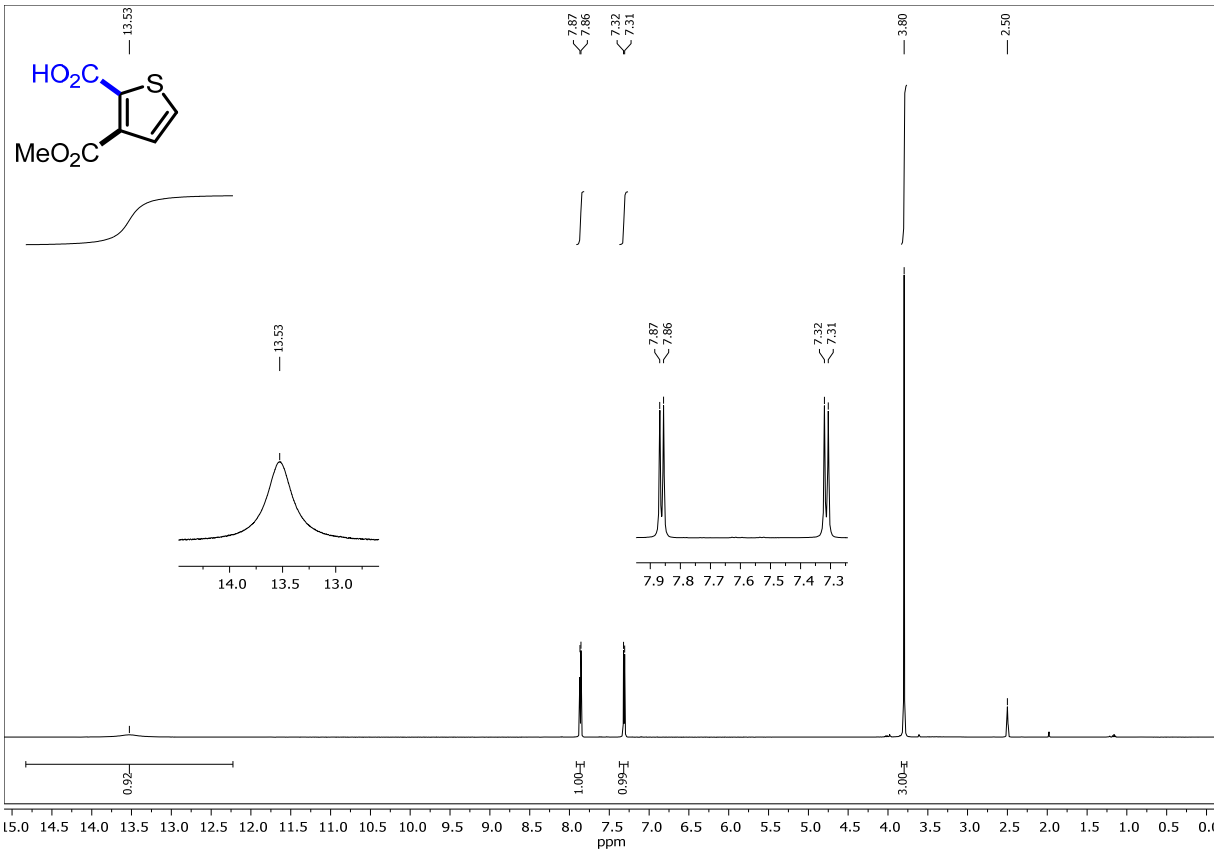
HO2C
S
MeO2C
13.53
7.87
7.86
7.32
7.31
3.80
2.50
0.92
1.00
0.99
3.00
ppm

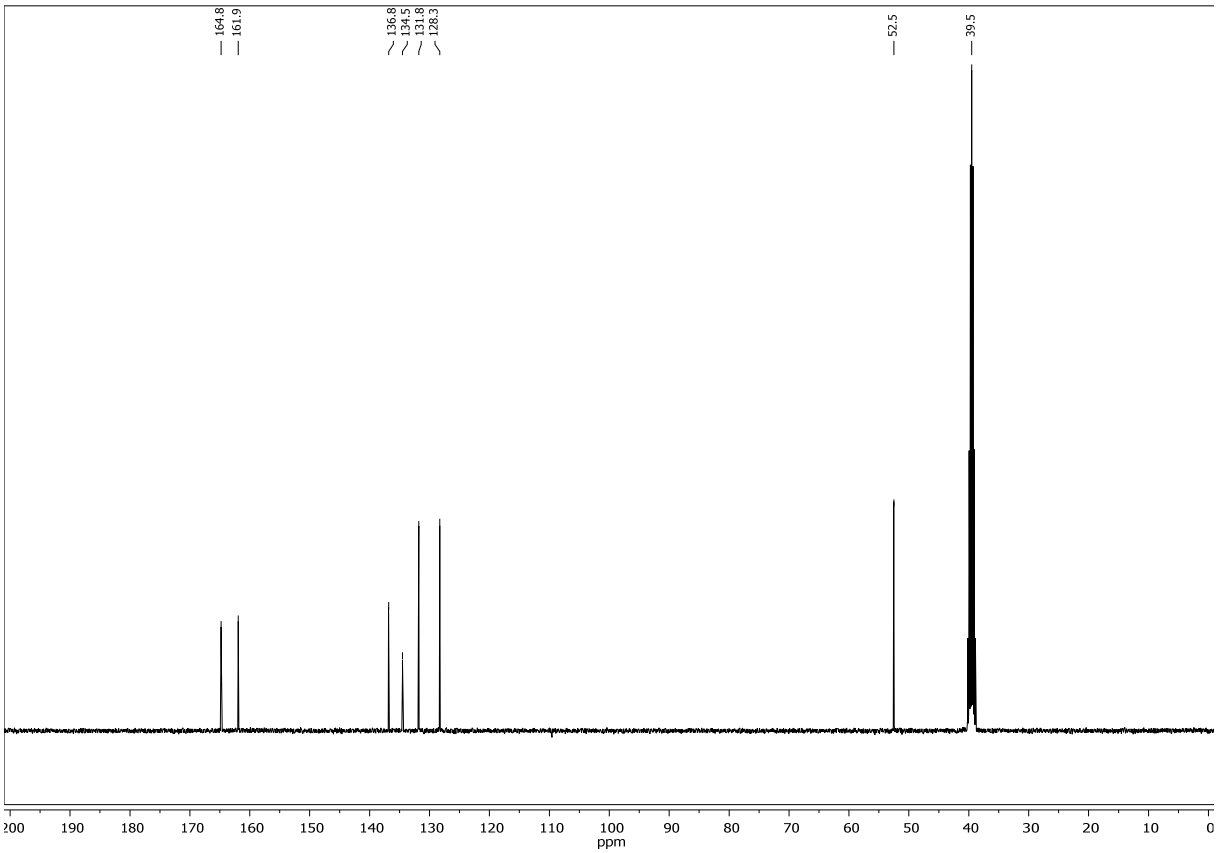
164.8
161.9
136.8
134.5
131.8
128.3
52.5
39.5
ppm

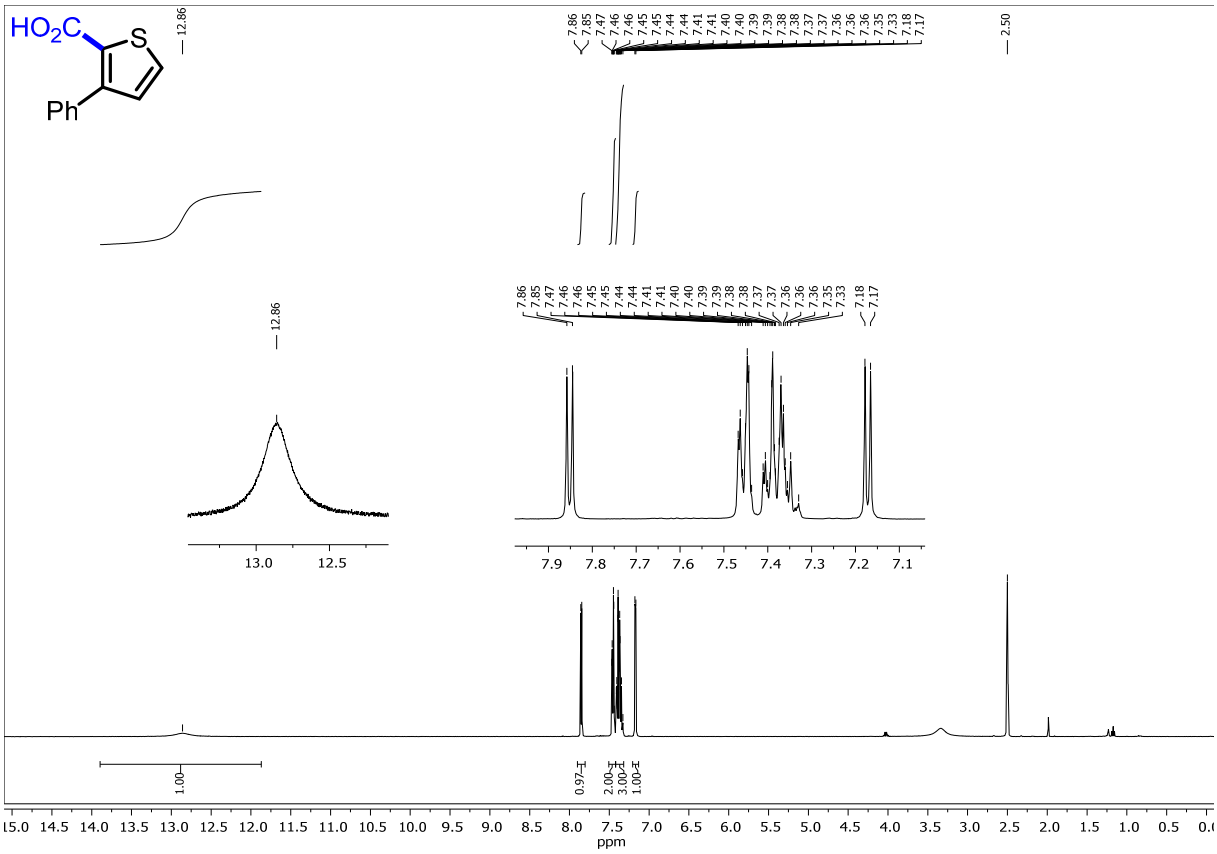
HO2C
S
Ph
12.86
7.86
7.85
7.47
7.46
7.46
7.45
7.45
7.44
7.44
7.41
7.41
7.40
7.40
7.39
7.39
7.38
7.38
7.37
7.37
7.36
7.36
7.35
7.33
7.18
7.17
2.50
13.0
12.5
7.9
7.8
7.7
7.6
7.5
7.4
7.3
7.2
7.1
1.00
0.97
2.00
3.00
1.00
ppm

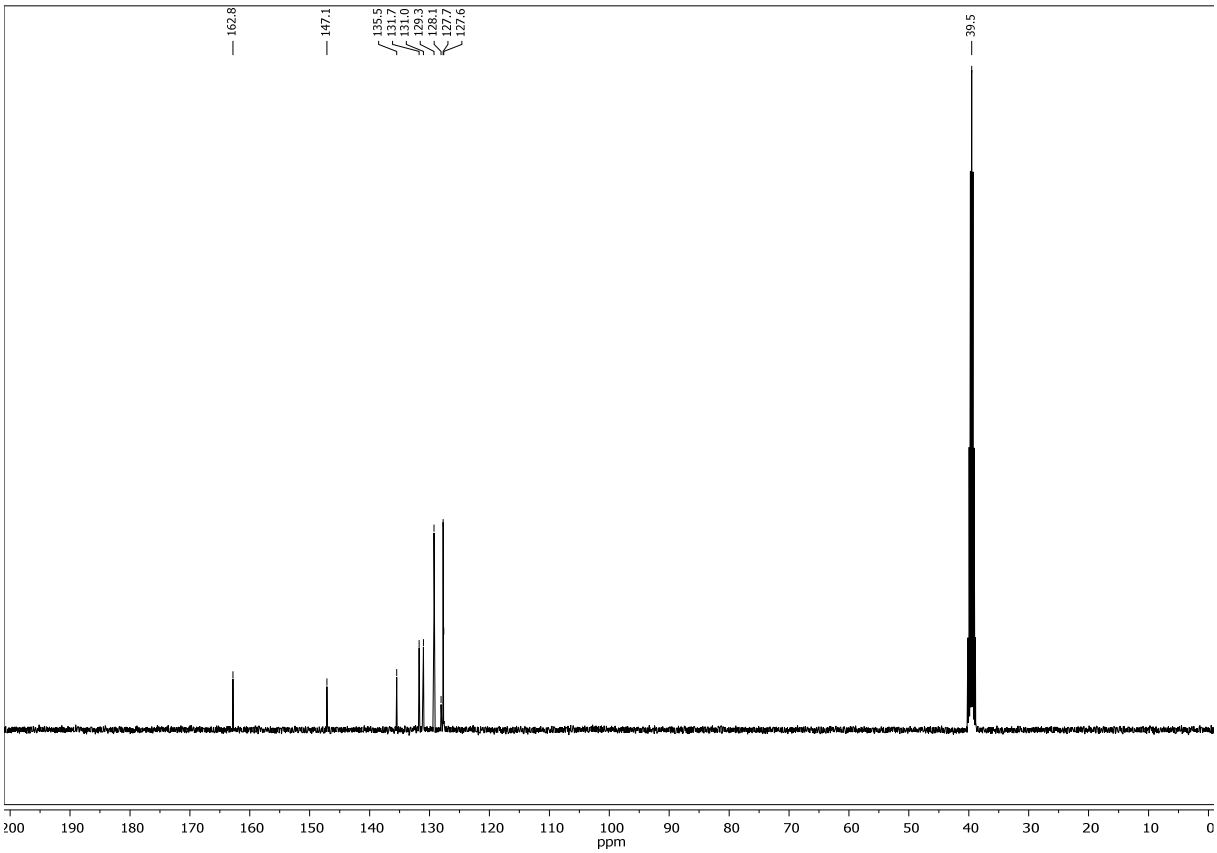
162.8
147.1
135.5
131.7
131.0
129.3
128.1
127.7
127.6
39.5
ppm

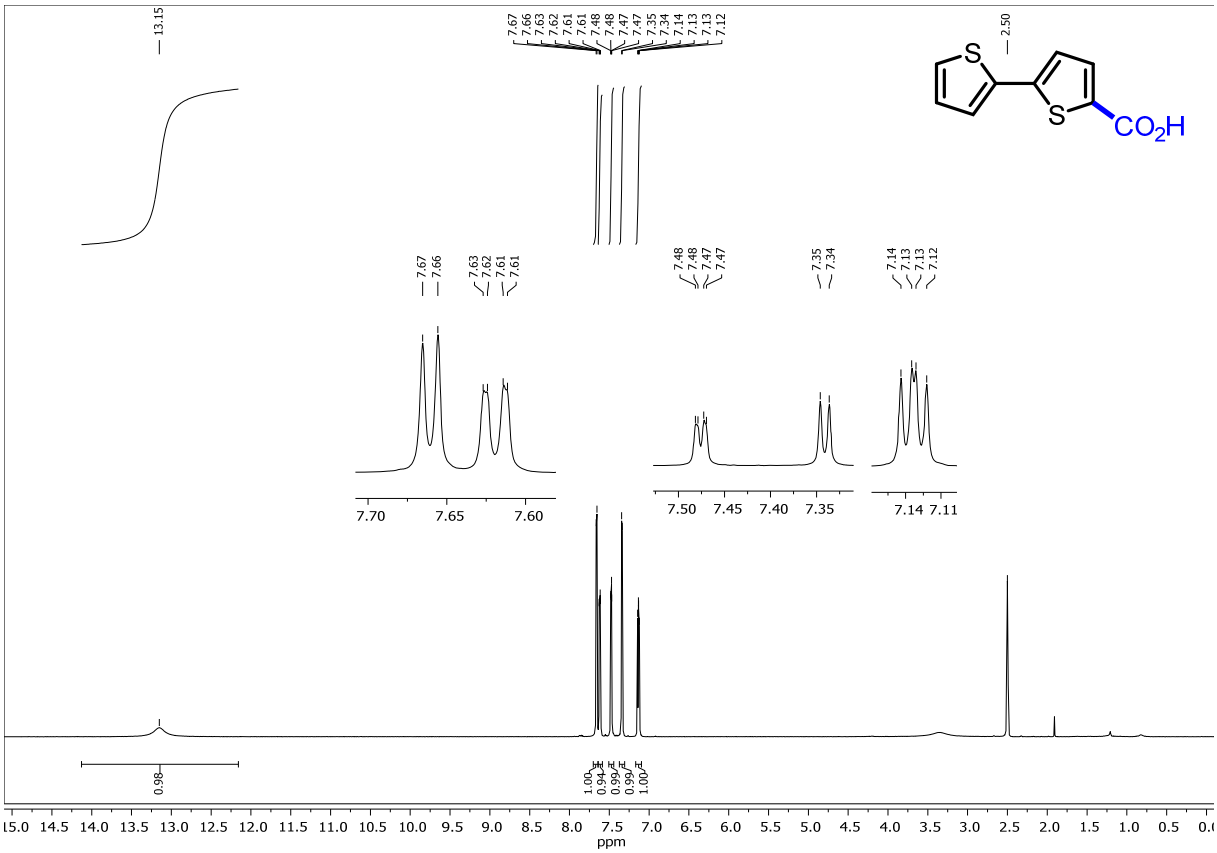
13.15
7.67
7.66
7.63
7.62
7.61
7.61
7.48
7.47
7.47
7.35
7.34
7.14
7.13
7.13
7.12
2.50
S
S
CO2H
7.70
7.65
7.60
7.50
7.45
7.40
7.35
7.14
7.11
0.98
1.00
0.94
0.99
0.99
1.00
ppm

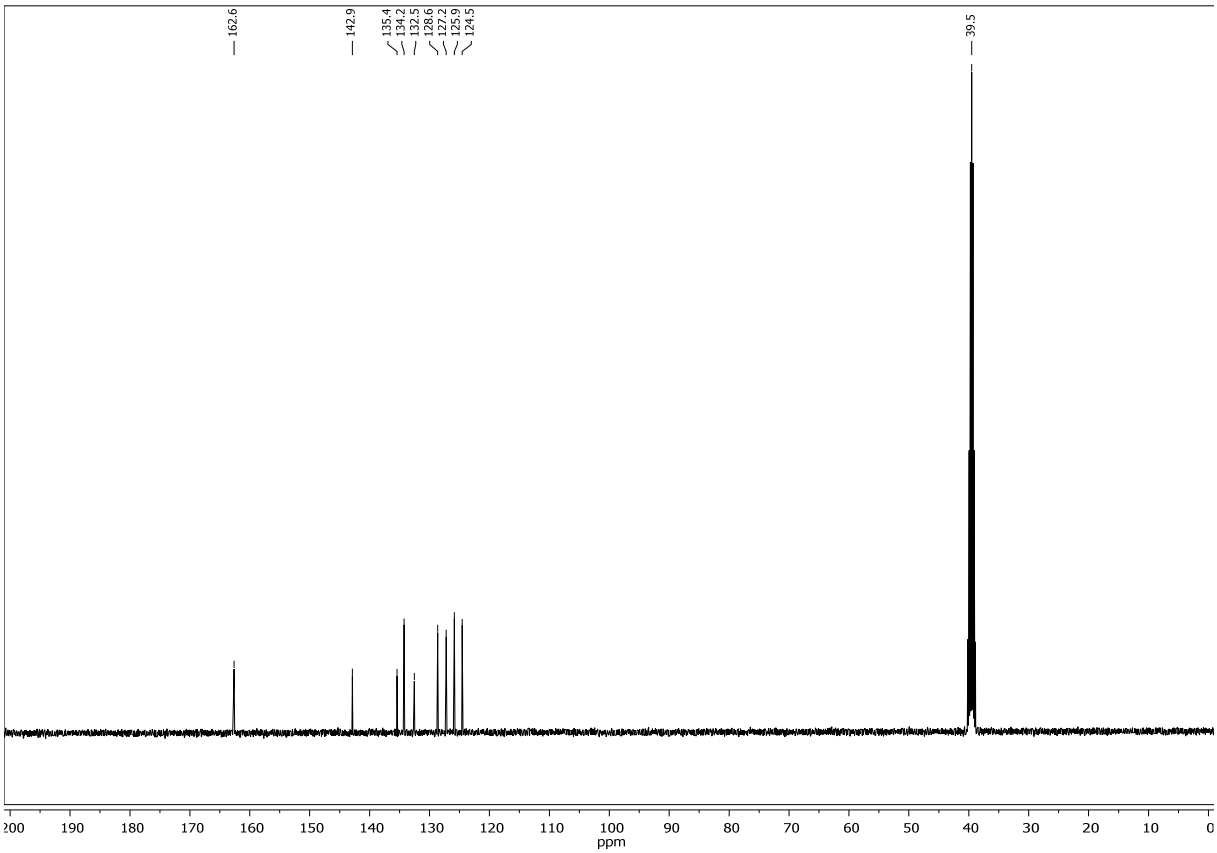
162.6
142.9
135.4
134.2
132.5
128.6
127.2
125.9
124.5
39.5
ppm

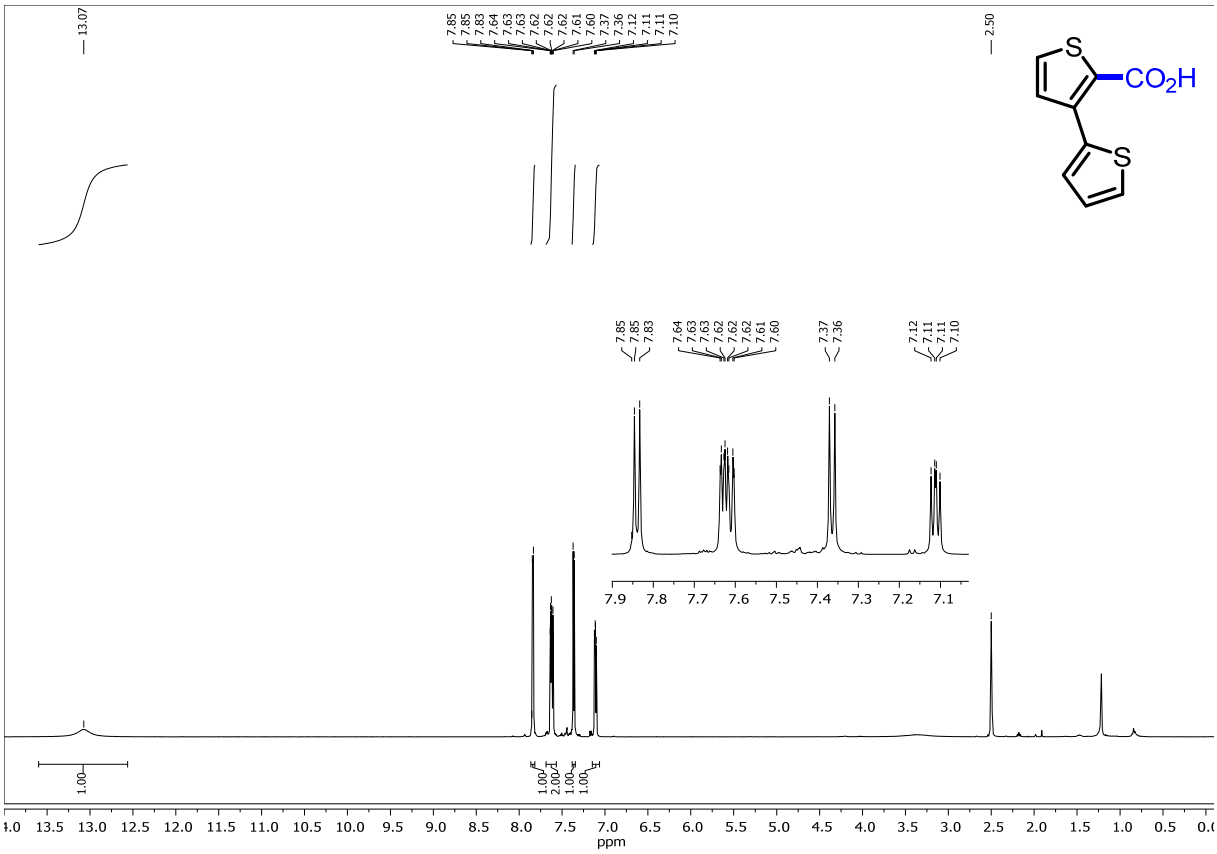
13.07
7.85
7.85
7.83
7.64
7.63
7.63
7.62
7.62
7.62
7.61
7.60
7.37
7.36
7.12
7.11
7.11
7.10
2.50
S
CO2H
S
1.00
2.00
1.00
1.00
ppm

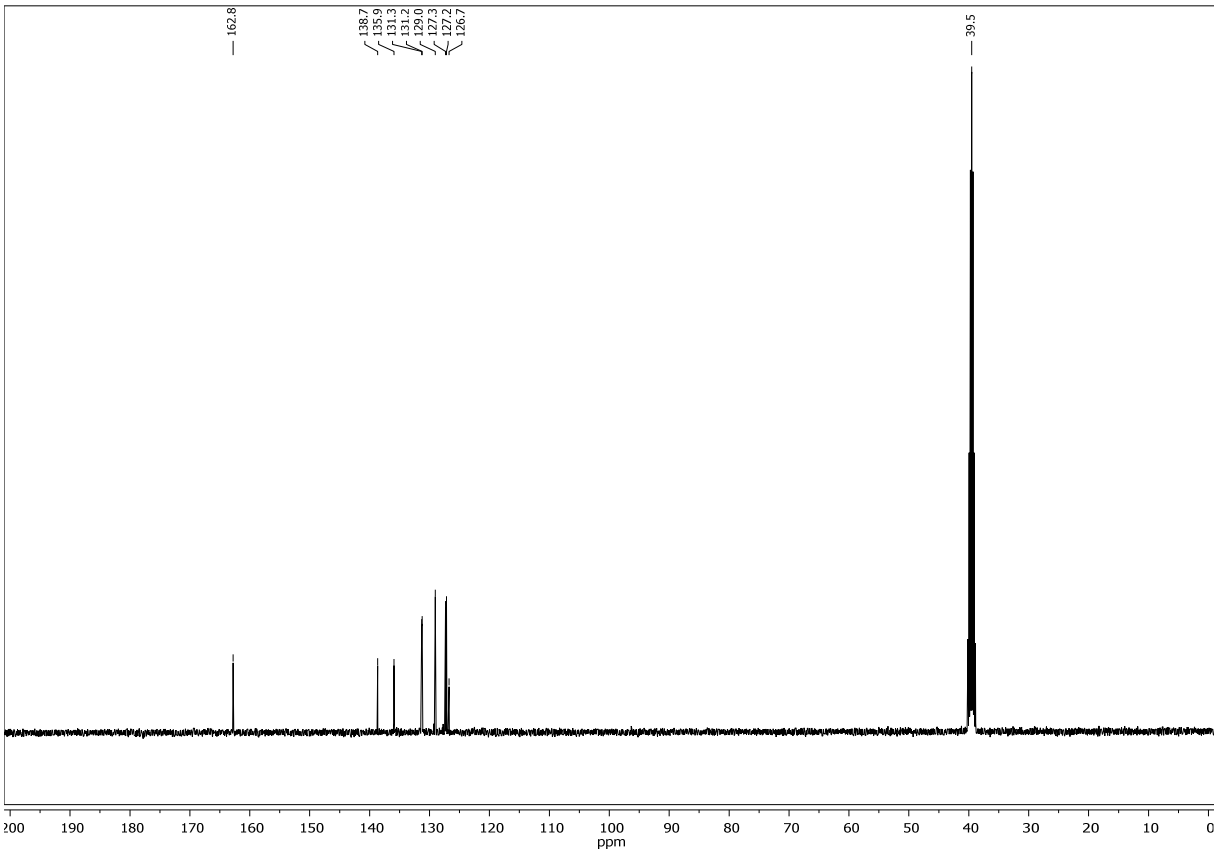
162.8
138.7
135.9
131.3
131.2
129.0
127.3
127.2
126.7
39.5
ppm

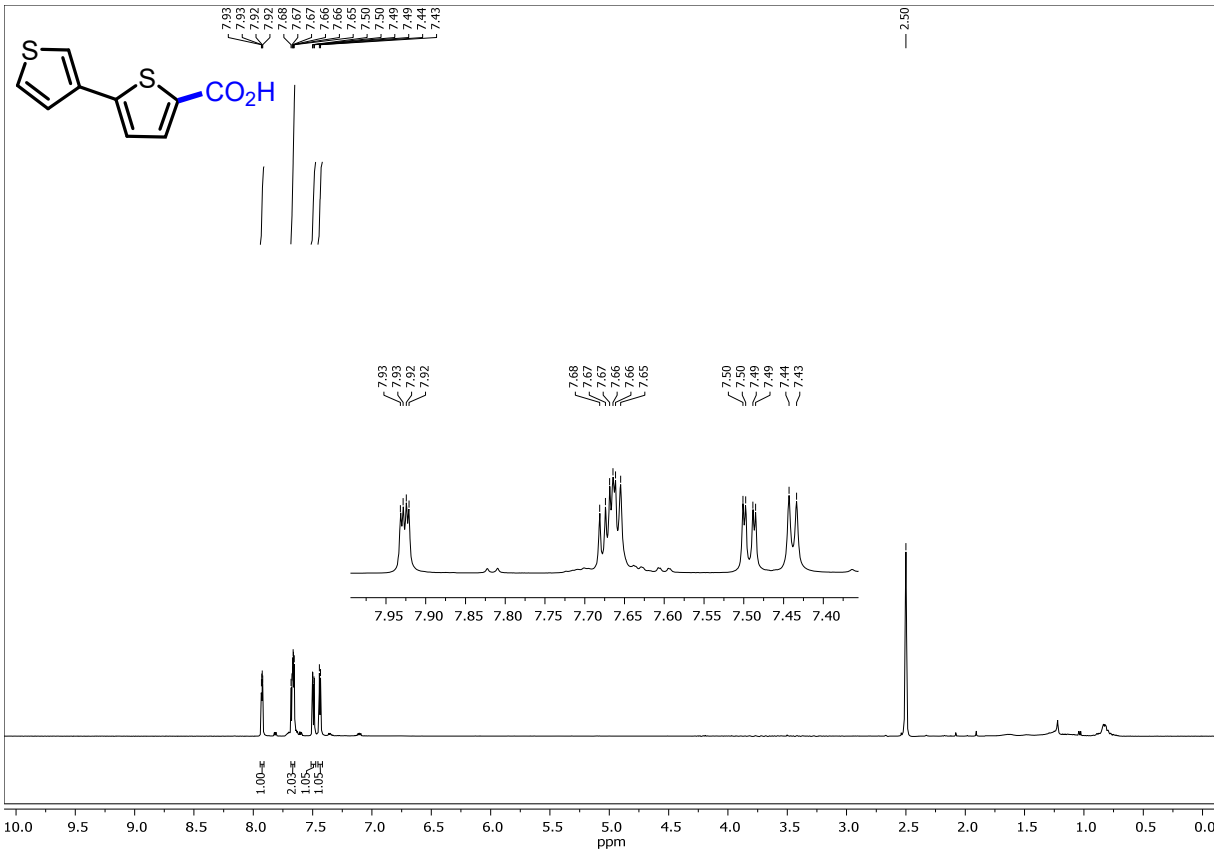
S
S
CO2H
7.93
7.93
7.92
7.92
7.68
7.67
7.67
7.66
7.66
7.65
7.50
7.50
7.49
7.49
7.44
7.43
2.50
1.00
2.03
1.05
1.05
10.0 9.5 9.0 8.5 8.0 7.5 7.0 6.5 6.0 5.5 5.0 4.5 4.0 3.5 3.0 2.5 2.0 1.5 1.0 0.5 0.0
ppm

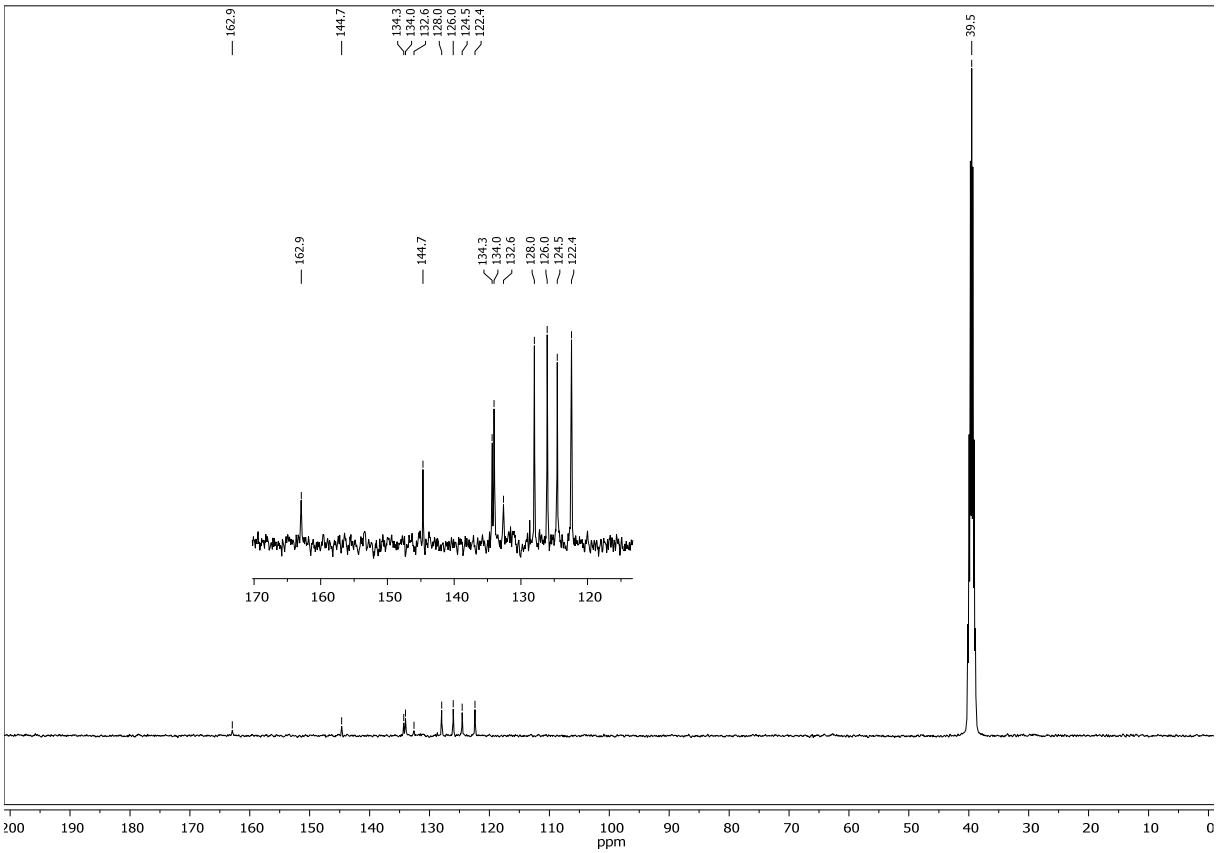
162.9
144.7
134.3
134.0
132.6
128.0
126.0
124.5
122.4
39.5
170 160 150 140 130 120
200 190 180 170 160 150 140 130 120 110 100 90 80 70 60 50 40 30 20 10 0
ppm

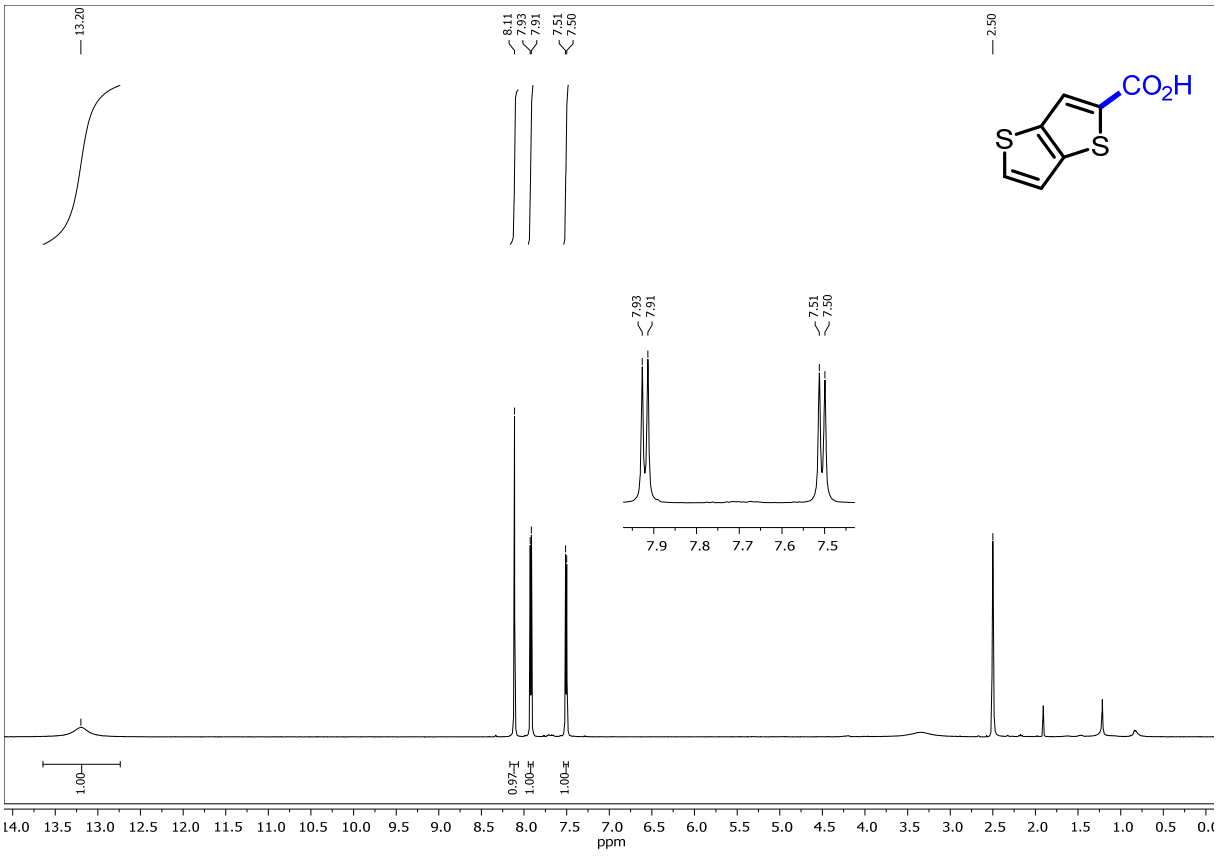
13.20
8.11
7.93
7.91
7.51
7.50
2.50
CO2H
S
S
7.93
7.91
7.51
7.50
7.9
7.8
7.7
7.6
7.5
1.00
0.97
1.00
1.00
14.0 13.5 13.0 12.5 12.0 11.5 11.0 10.5 10.0 9.5 9.0 8.5 8.0 7.5 7.0 6.5 6.0 5.5 5.0 4.5 4.0 3.5 3.0 2.5 2.0 1.5 1.0 0.5
ppm

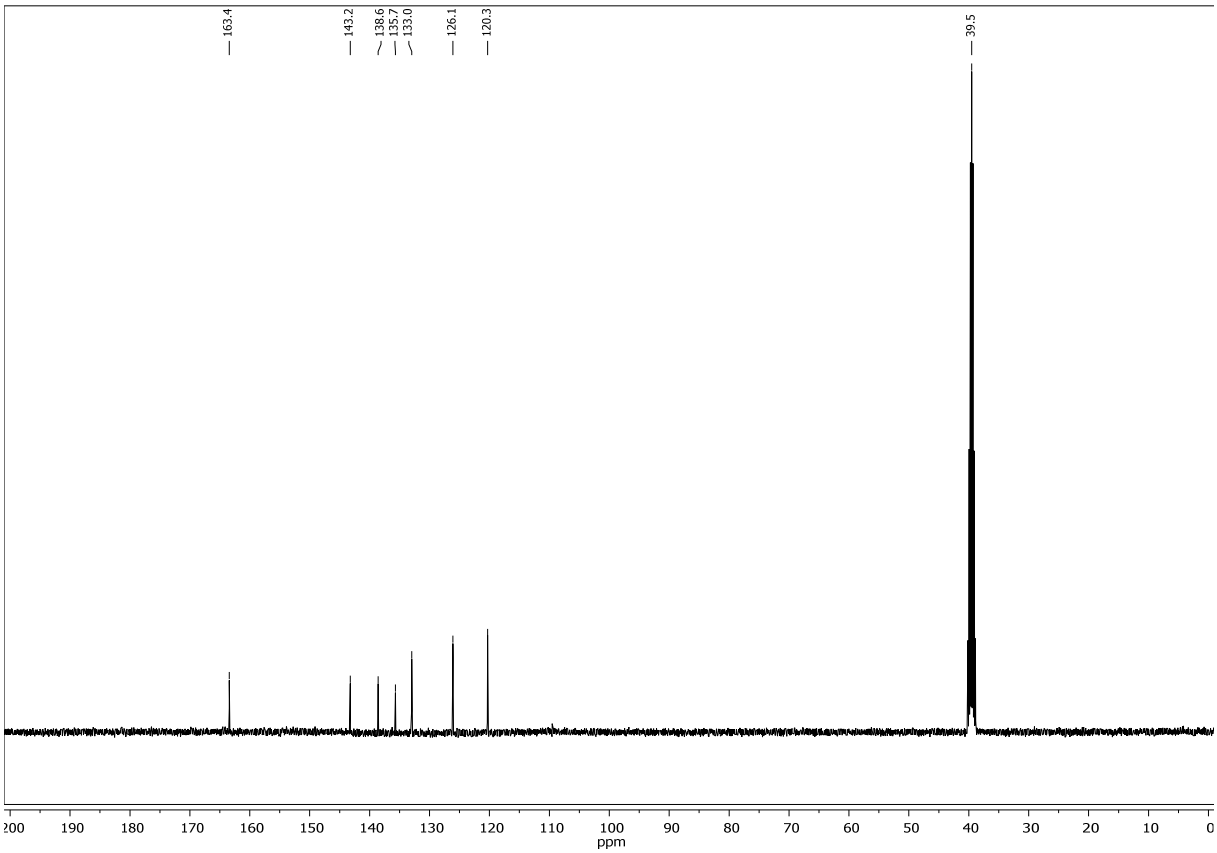
163.4
143.2
138.6
135.7
133.0
126.1
120.3
39.5
200 190 180 170 160 150 140 130 120 110 100 90 80 70 60 50 40 30 20 10 0
ppm

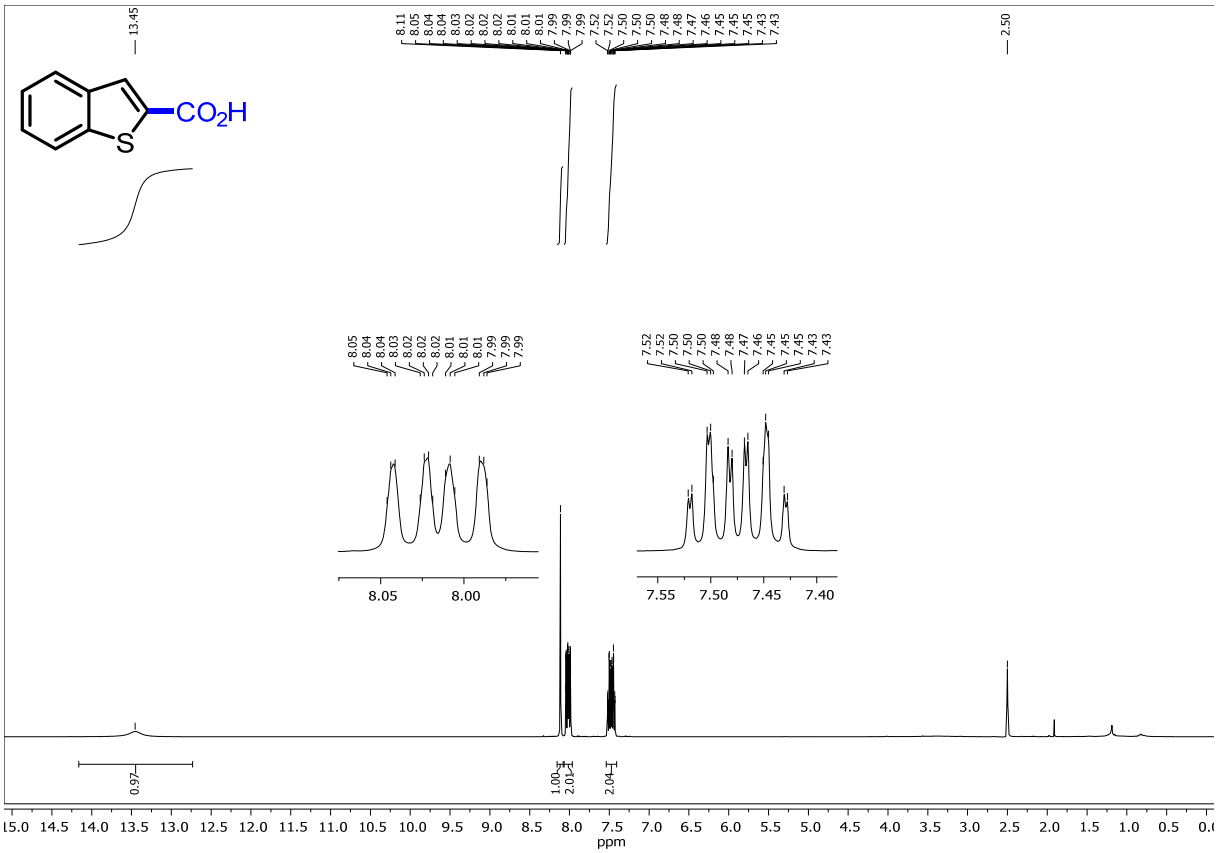
13.45
2.50
CO2H
S
8.11
8.05
8.04
8.04
8.03
8.02
8.02
8.02
8.01
8.01
8.01
7.99
7.99
7.99
7.52
7.52
7.50
7.50
7.50
7.48
7.48
7.47
7.46
7.45
7.45
7.45
7.43
7.43
8.05
8.04
8.04
8.03
8.02
8.02
8.02
8.01
8.01
8.01
7.99
7.99
7.99
7.52
7.52
7.50
7.50
7.50
7.48
7.48
7.47
7.46
7.45
7.45
7.45
7.43
7.43
8.05
8.00
7.55
7.50
7.45
7.40
0.97
1.00
2.01
2.04
15.0 14.5 14.0 13.5 13.0 12.5 12.0 11.5 11.0 10.5 10.0 9.5 9.0 8.5 8.0 7.5 7.0 6.5 6.0 5.5 5.0 4.5 4.0 3.5 3.0 2.5 2.0 1.5 1.0 0.5
ppm

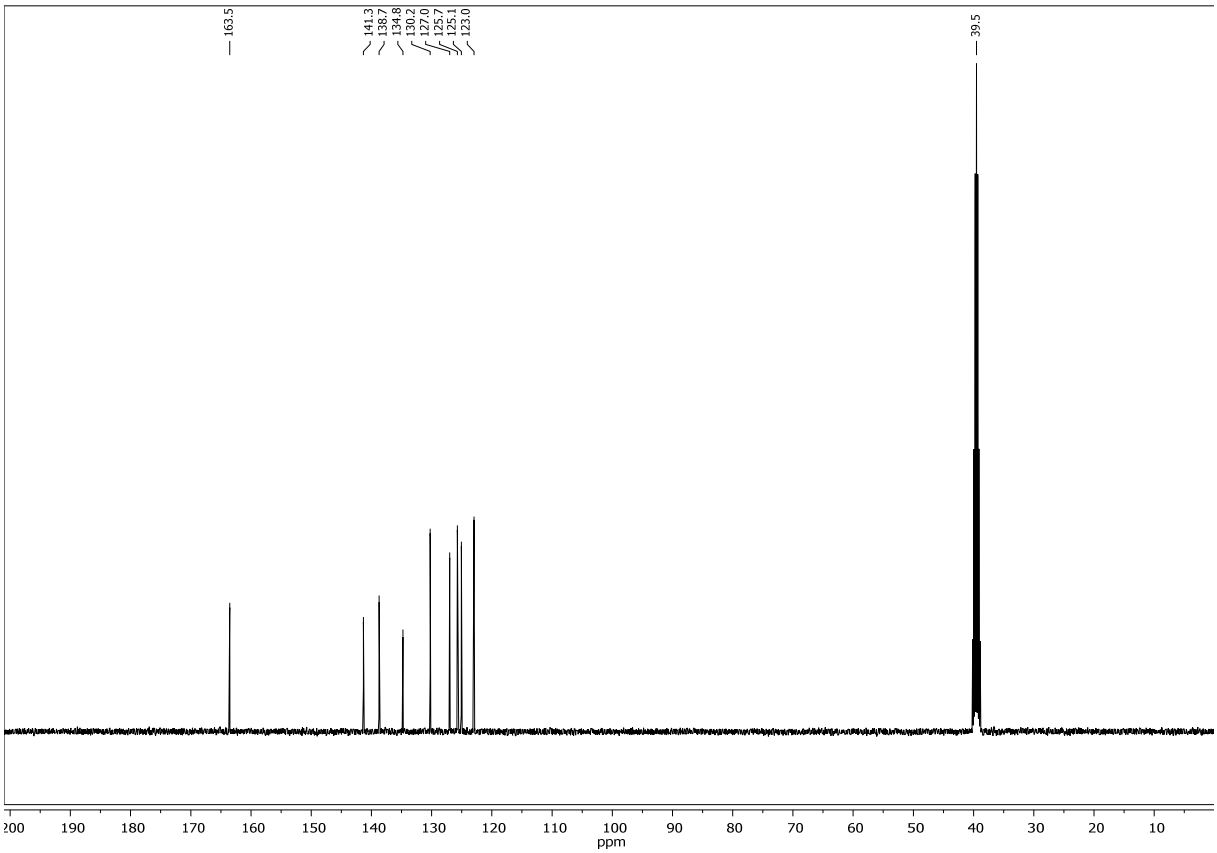
163.5
141.3
138.7
134.8
130.2
127.0
125.7
125.1
123.0
39.5
200 190 180 170 160 150 140 130 120 110 100 90 80 70 60 50 40 30 20 10
ppm

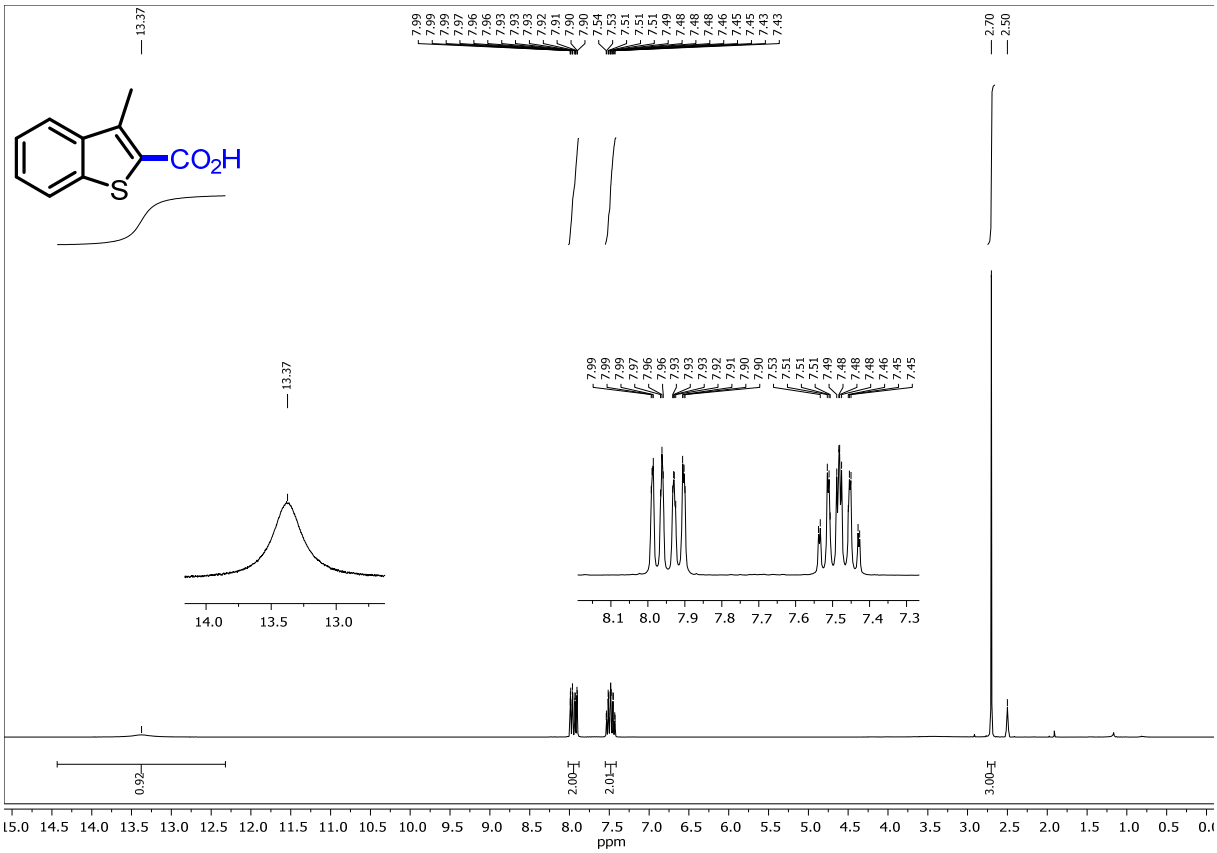
13.37
7.99
7.99
7.99
7.97
7.96
7.96
7.93
7.93
7.92
7.91
7.90
7.90
7.54
7.53
7.51
7.51
7.51
7.49
7.48
7.48
7.48
7.46
7.45
7.45
7.43
7.43
2.70
2.50
CO2H
S
0.92
2.00
2.01
3.00
ppm

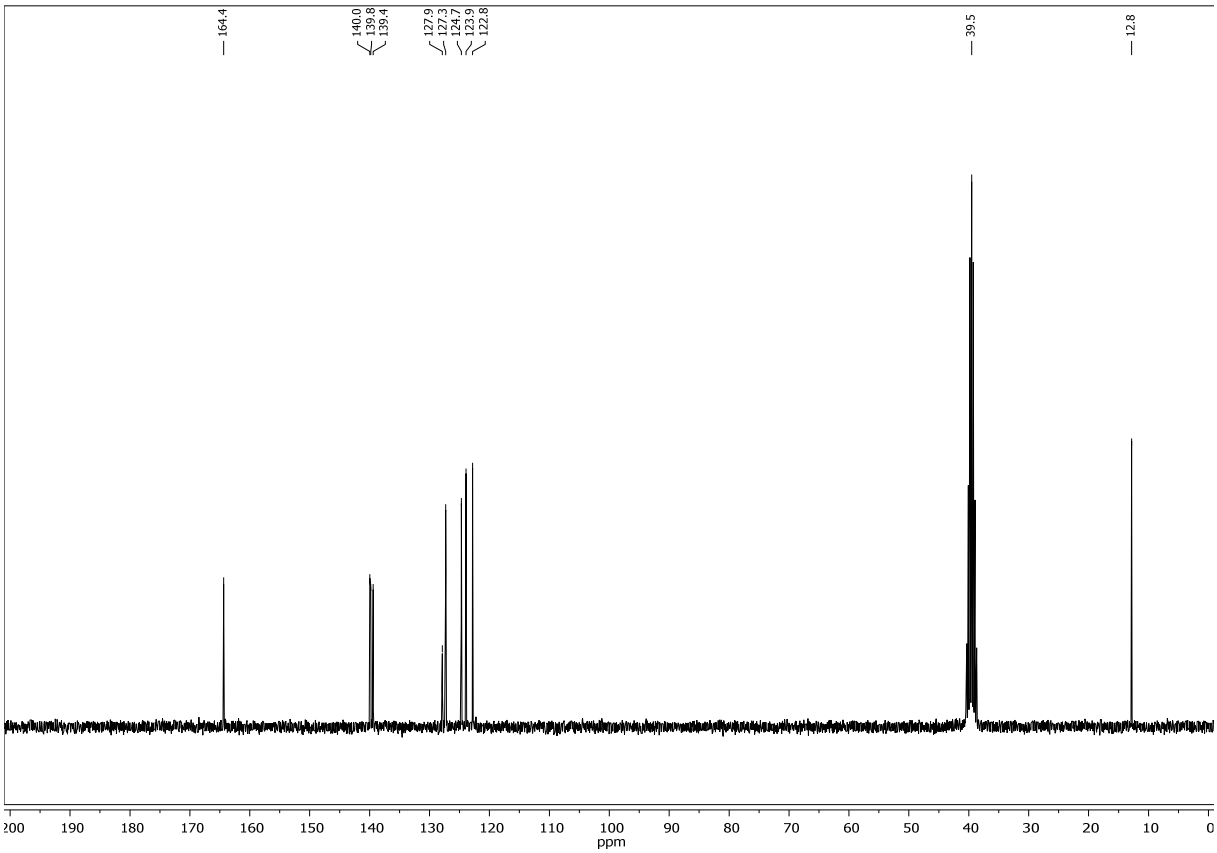
164.4
140.0
139.8
139.4
127.9
127.3
124.7
123.9
122.8
39.5
12.8
ppm

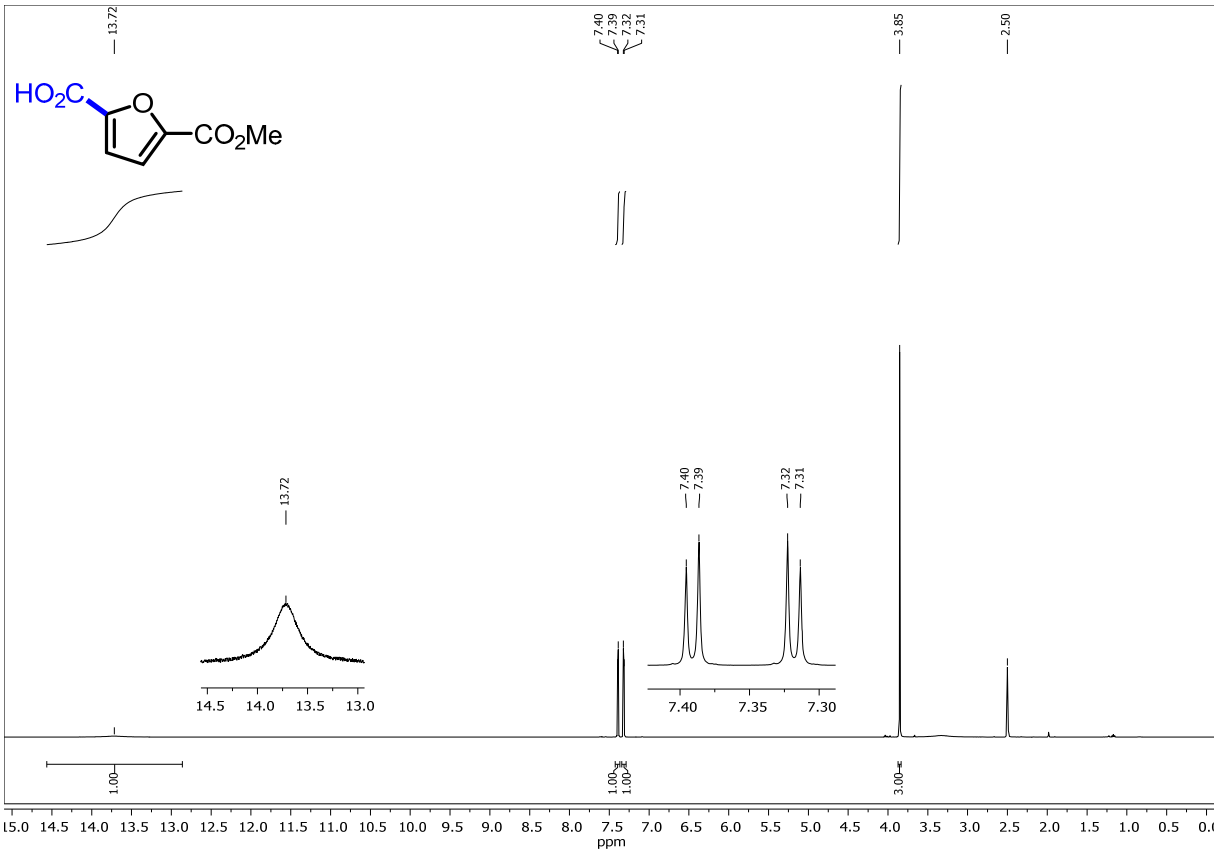
13.72
7.40
7.39
7.32
7.31
3.85
2.50
HO2C
CO2Me
1.00
1.00
1.00
3.00
ppm

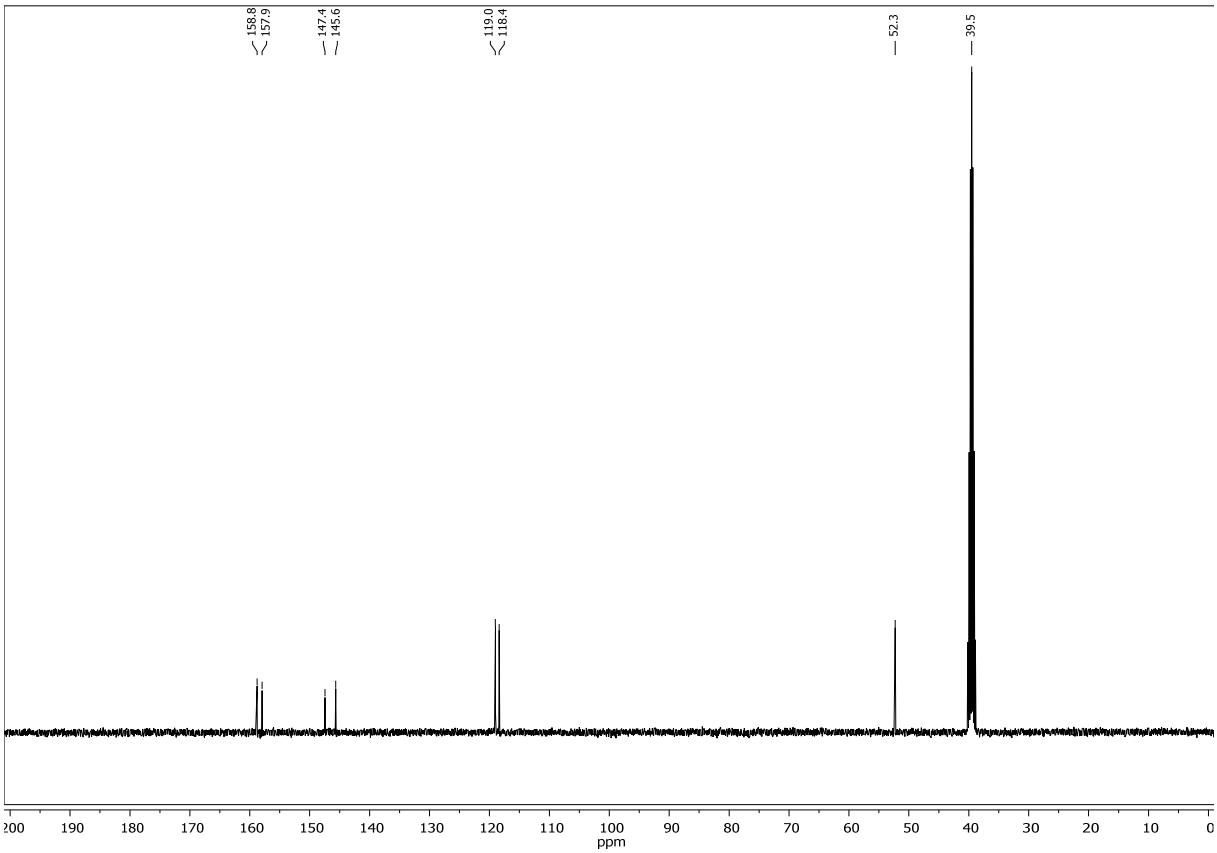
158.8
157.9
147.4
145.6
119.0
118.4
52.3
39.5
ppm

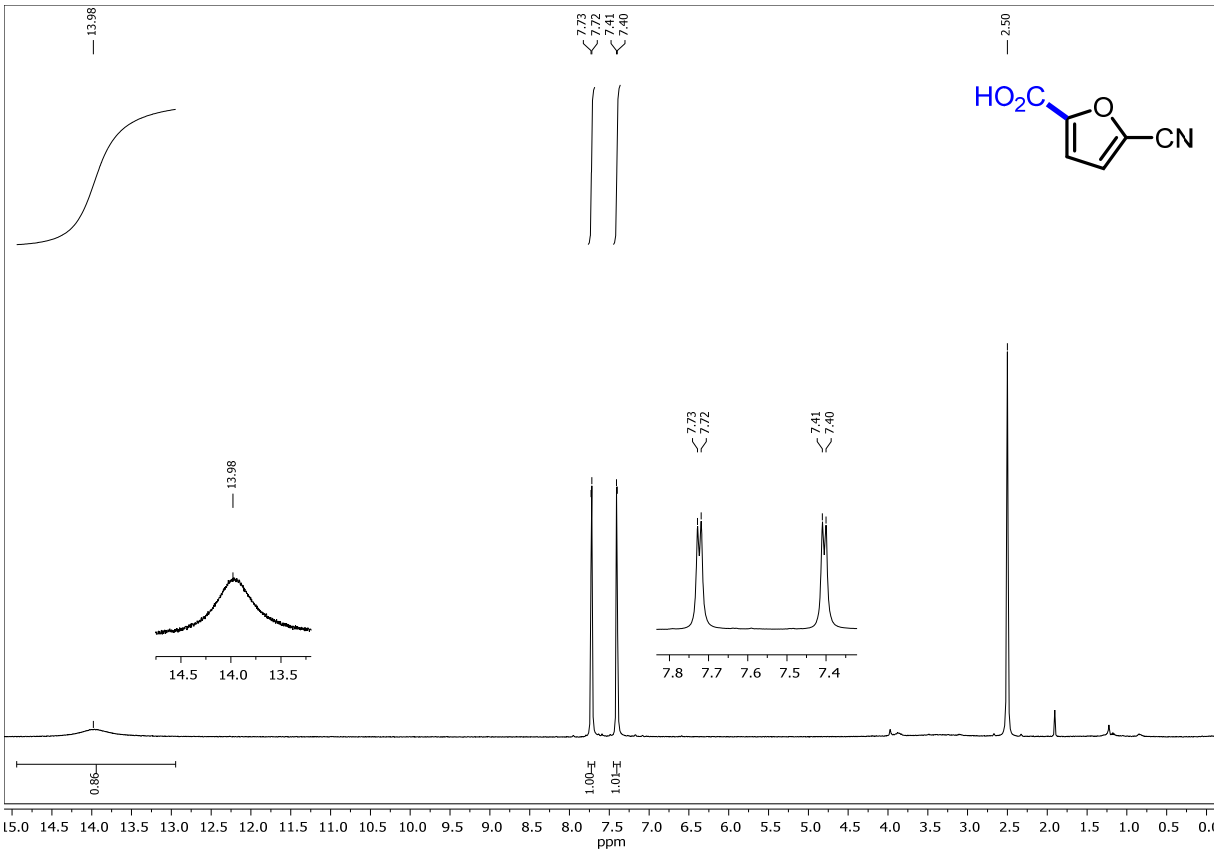
13.98
7.73
7.72
7.41
7.40
2.50
HO2C
O
CN
14.5 14.0 13.5
7.8 7.7 7.6 7.5 7.4
0.86
1.00
1.01
ppm

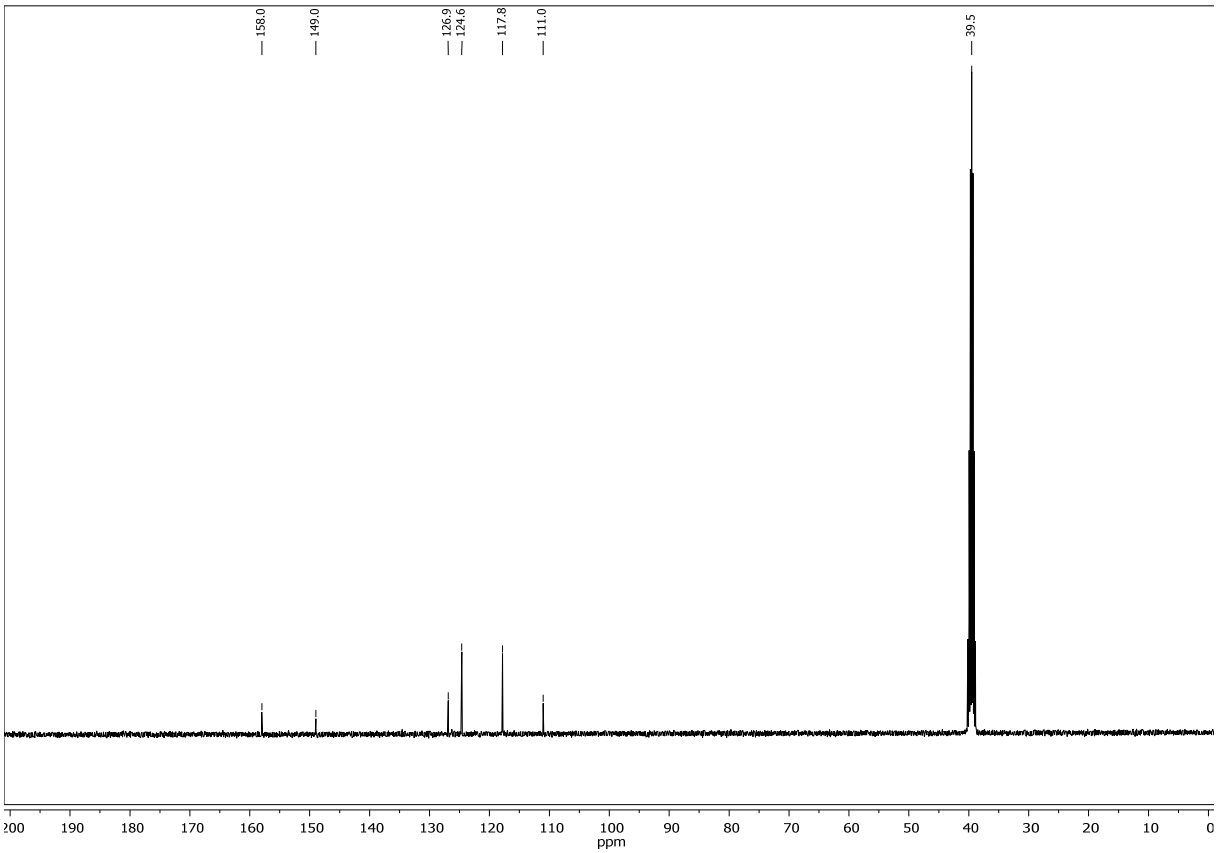
158.0
149.0
126.9
124.6
117.8
111.0
39.5
ppm

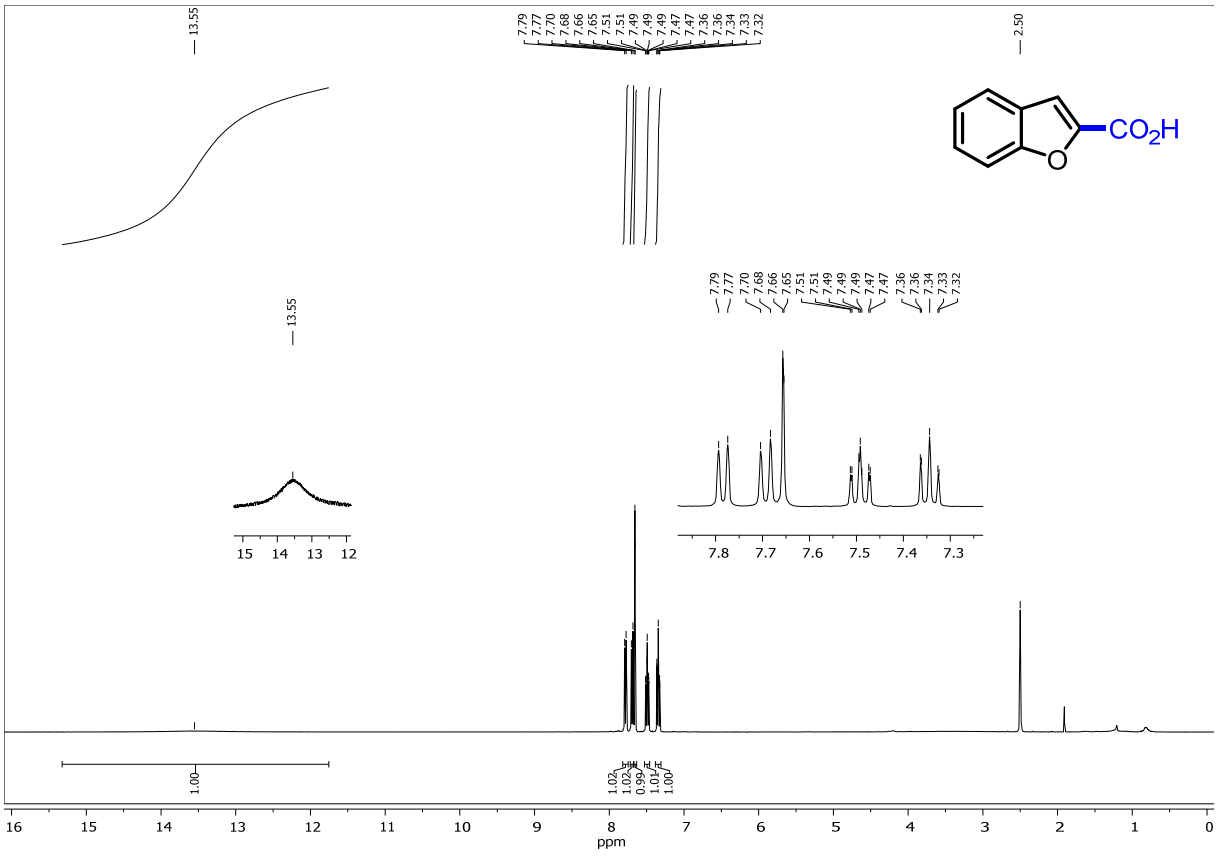
13.55
7.79
7.77
7.70
7.68
7.66
7.65
7.51
7.49
7.49
7.47
7.47
7.36
7.36
7.34
7.33
7.32
2.50
CO2H
O
15 14 13 12
7.8 7.7 7.6 7.5 7.4 7.3
1.00
1.03
1.02
0.99
1.01
1.00
16 15 14 13 12 11 10 9 8 7 6 5 4 3 2 1 0
ppm

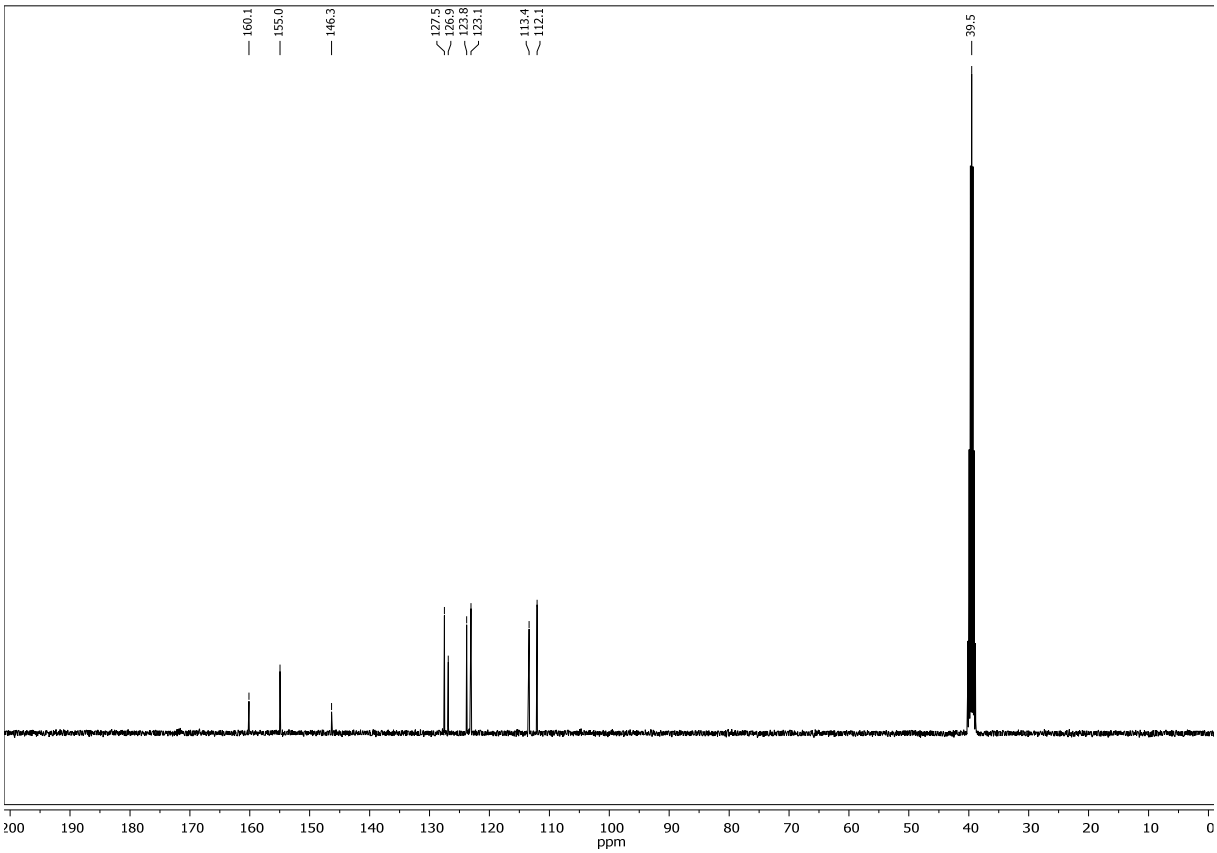
160.1
155.0
146.3
127.5
126.9
123.8
123.1
113.4
112.1
39.5
200 190 180 170 160 150 140 130 120 110 100 90 80 70 60 50 40 30 20 10 0
ppm

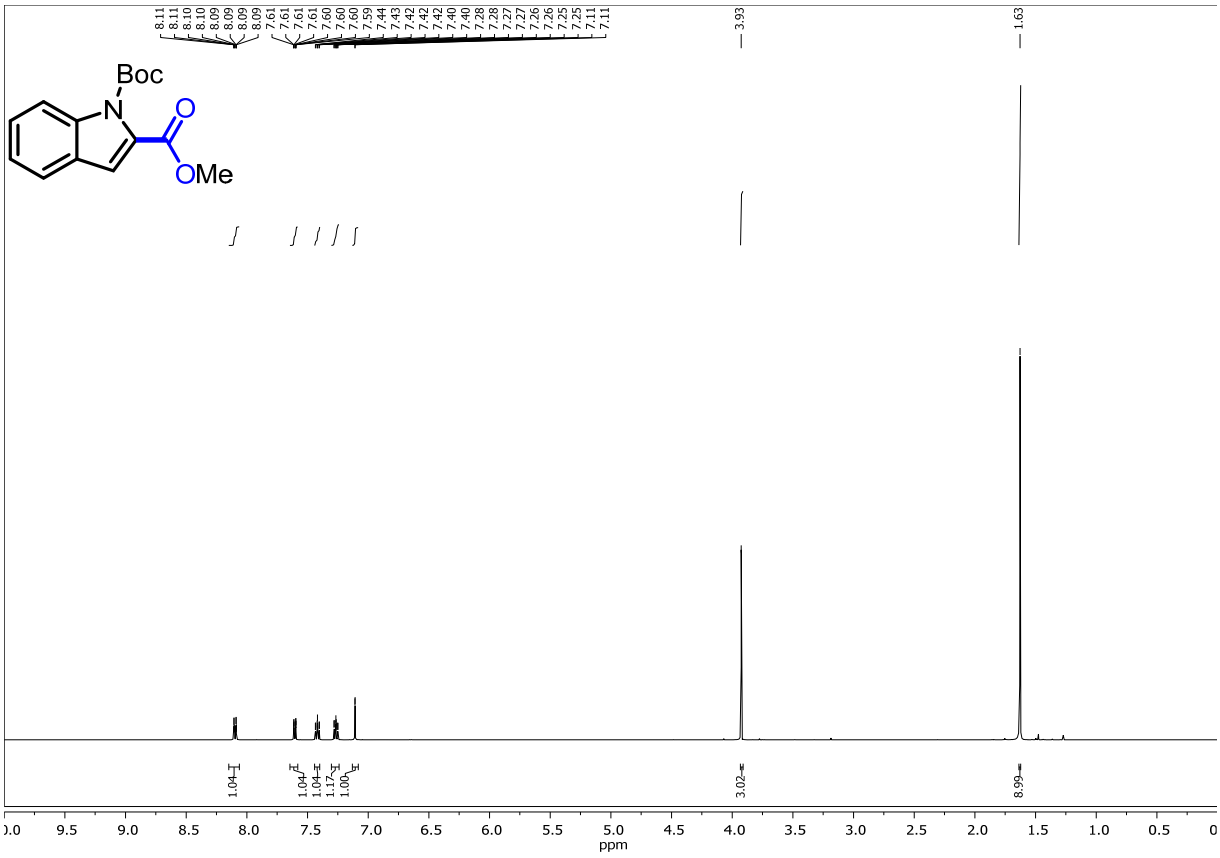
Boc
N
O
OMe
8.11
8.11
8.10
8.09
8.09
8.09
8.09
7.61
7.61
7.61
7.61
7.60
7.60
7.60
7.59
7.44
7.43
7.42
7.42
7.42
7.40
7.28
7.28
7.27
7.26
7.26
7.25
7.25
7.11
7.11
3.93
1.63
1.04
1.04
1.04
1.17
1.06
3.02
8.99
ppm

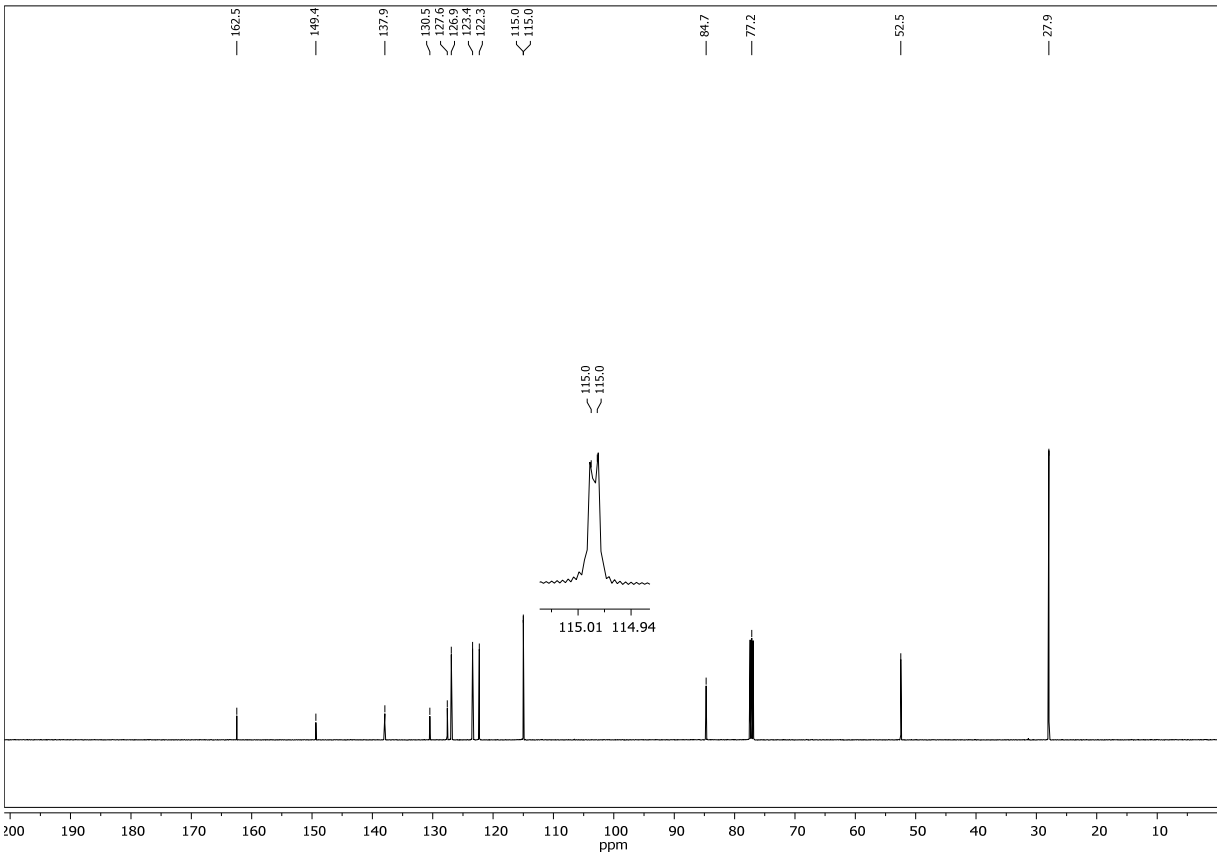
162.5
149.4
137.9
130.5
127.6
126.9
123.4
122.3
115.0
115.0
84.7
77.2
52.5
27.9
115.0
115.0
115.01
114.94
ppm

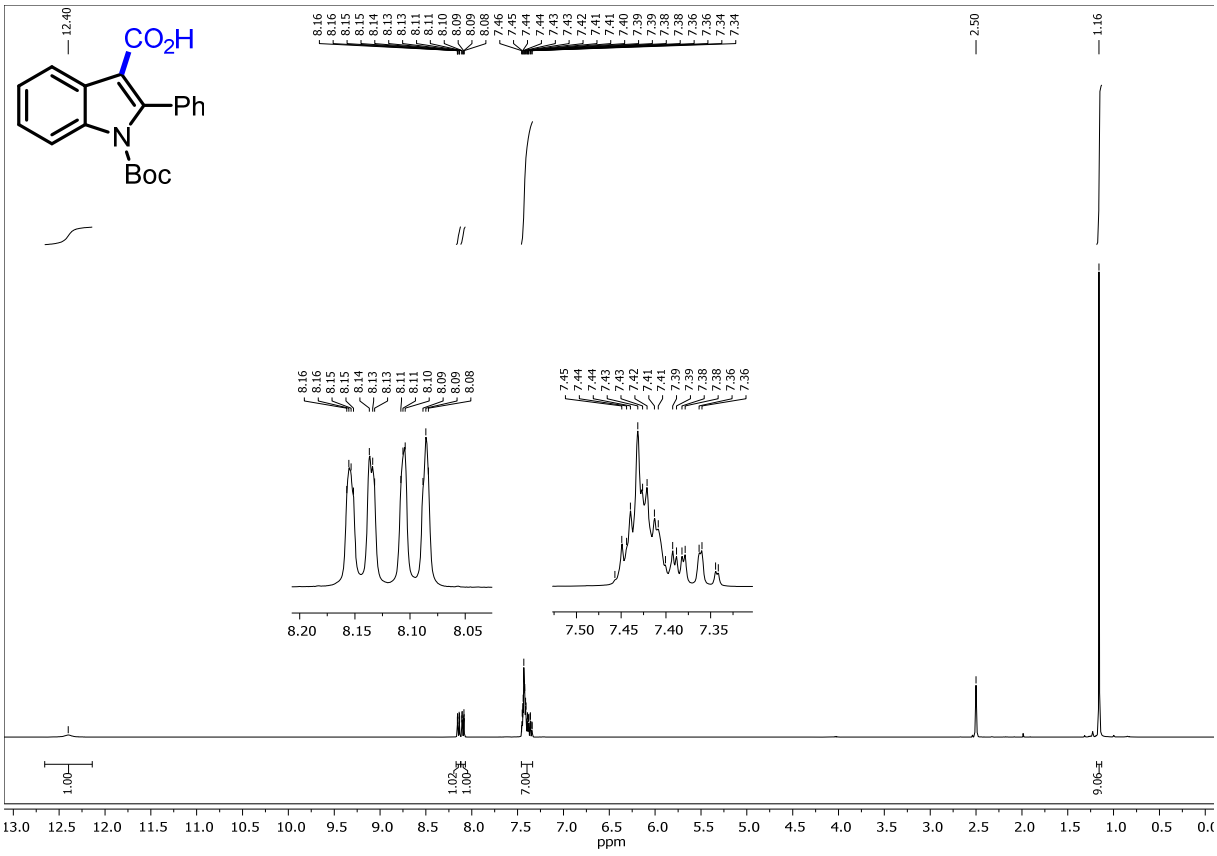
CO2H
Ph
N
Boc
ppm

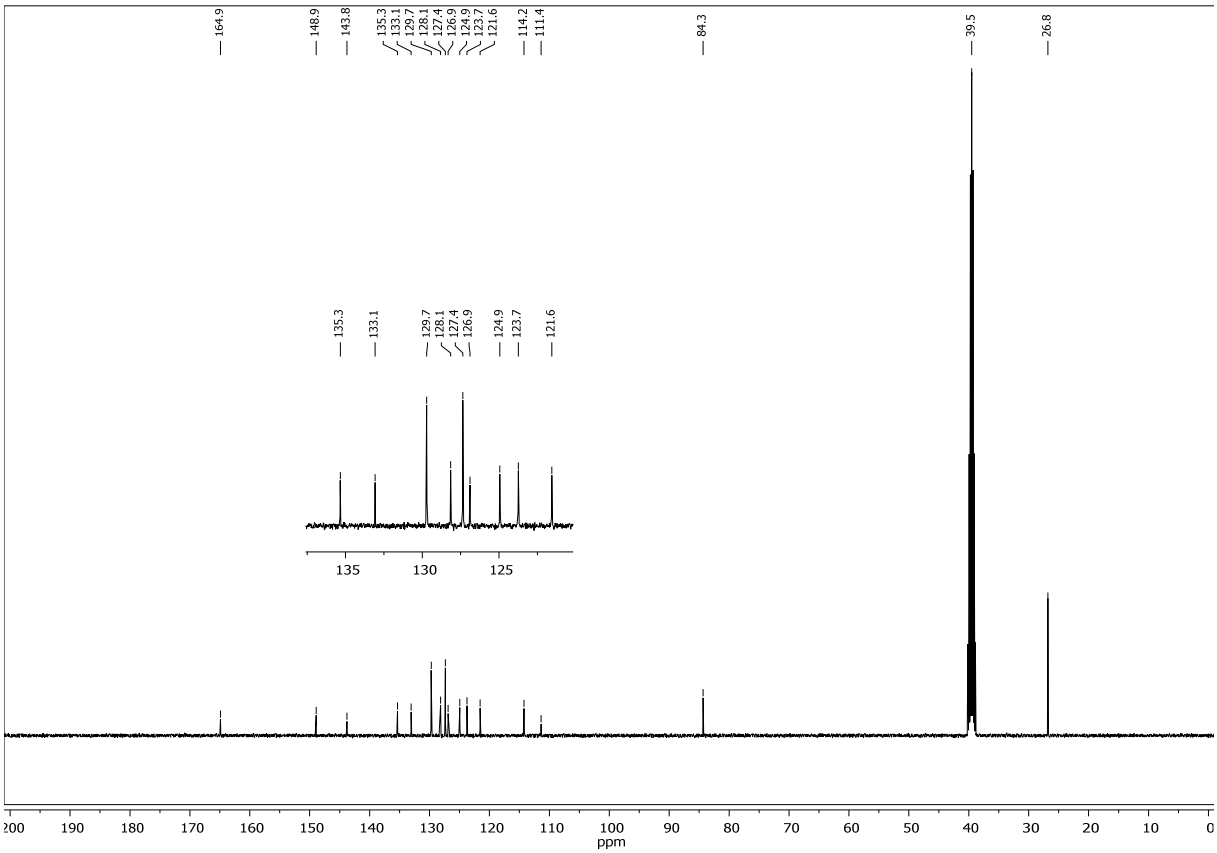
ppm

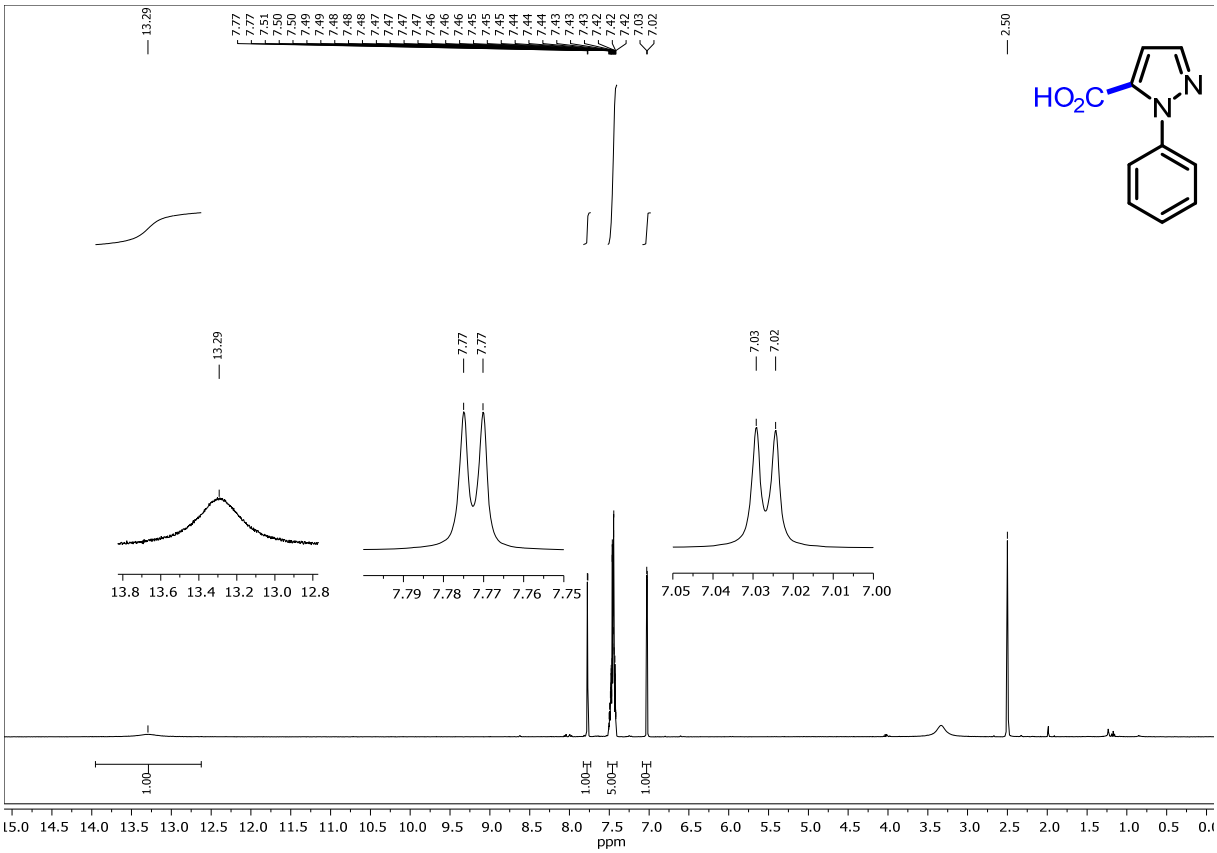
13.29
7.77
7.77
7.51
7.50
7.50
7.49
7.49
7.48
7.48
7.48
7.47
7.47
7.47
7.46
7.46
7.46
7.45
7.45
7.44
7.44
7.44
7.43
7.43
7.42
7.42
7.42
7.03
7.02
2.50
HO2C
N
N
13.29
7.77
7.77
7.03
7.02
13.8 13.6 13.4 13.2 13.0 12.8
7.79 7.78 7.77 7.76 7.75
7.05 7.04 7.03 7.02 7.01 7.00
1.00
1.00
5.00
1.00
15.0 14.5 14.0 13.5 13.0 12.5 12.0 11.5 11.0 10.5 10.0 9.5 9.0 8.5 8.0 7.5 7.0 6.5 6.0 5.5 5.0 4.5 4.0 3.5 3.0 2.5 2.0 1.5 1.0 0.5
ppm

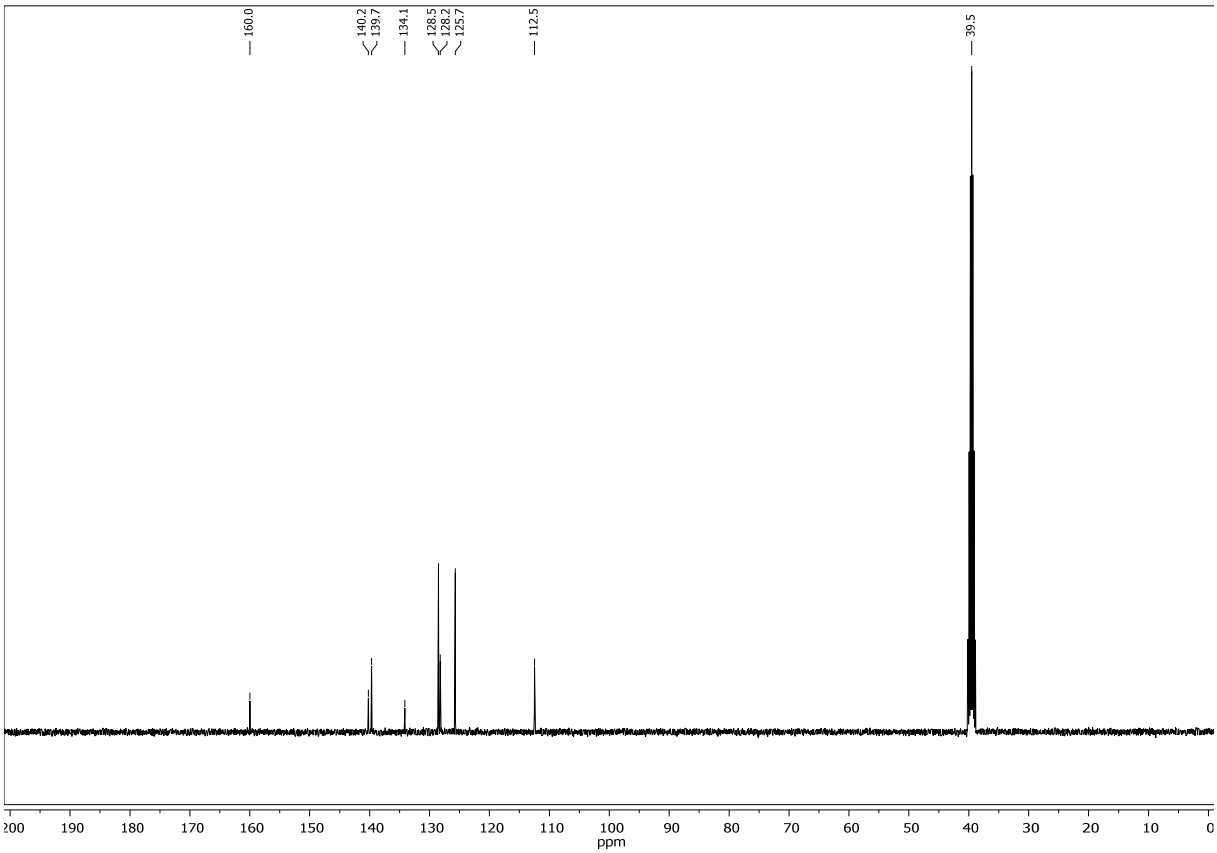
160.0
140.2
139.7
134.1
128.5
128.2
125.7
112.5
39.5
200 190 180 170 160 150 140 130 120 110 100 90 80 70 60 50 40 30 20 10 0
ppm

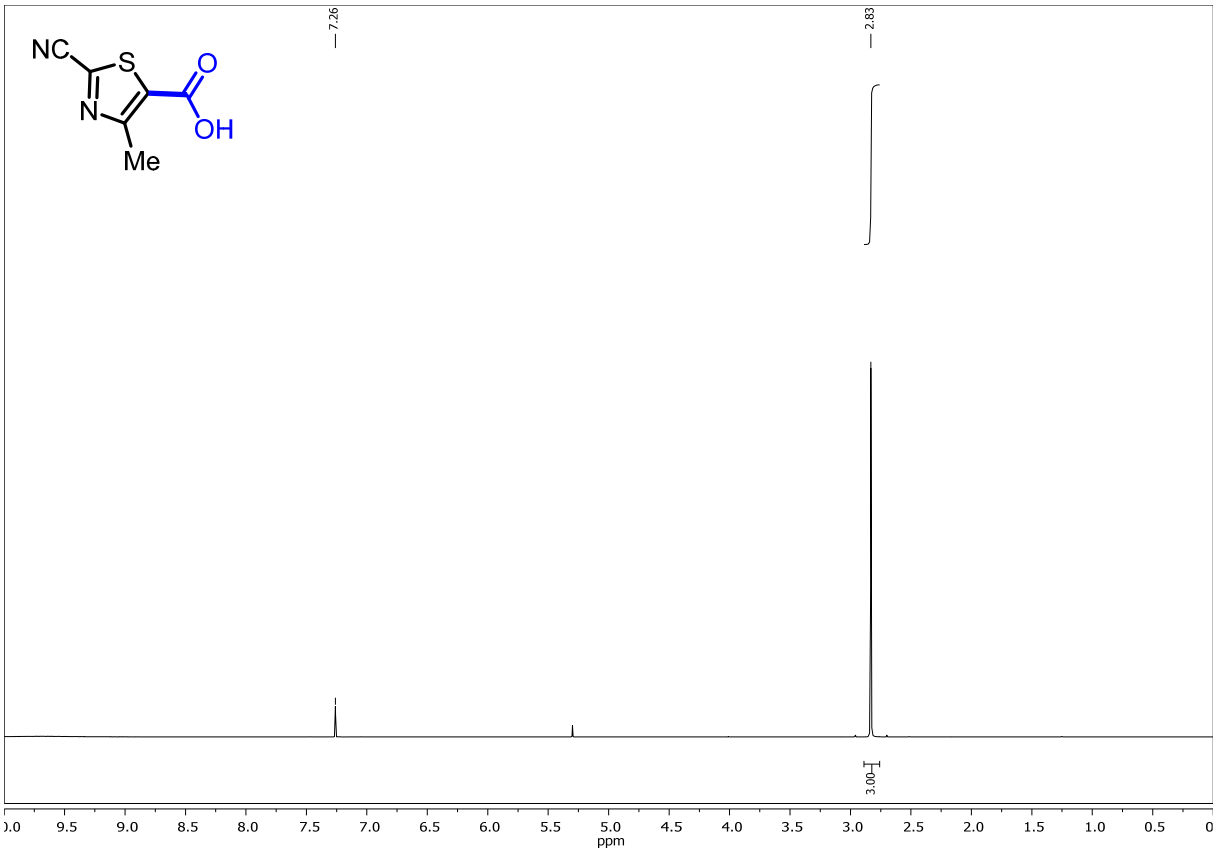
NC
S
N
O
OH
Me
7.26
2.83
3.00
ppm

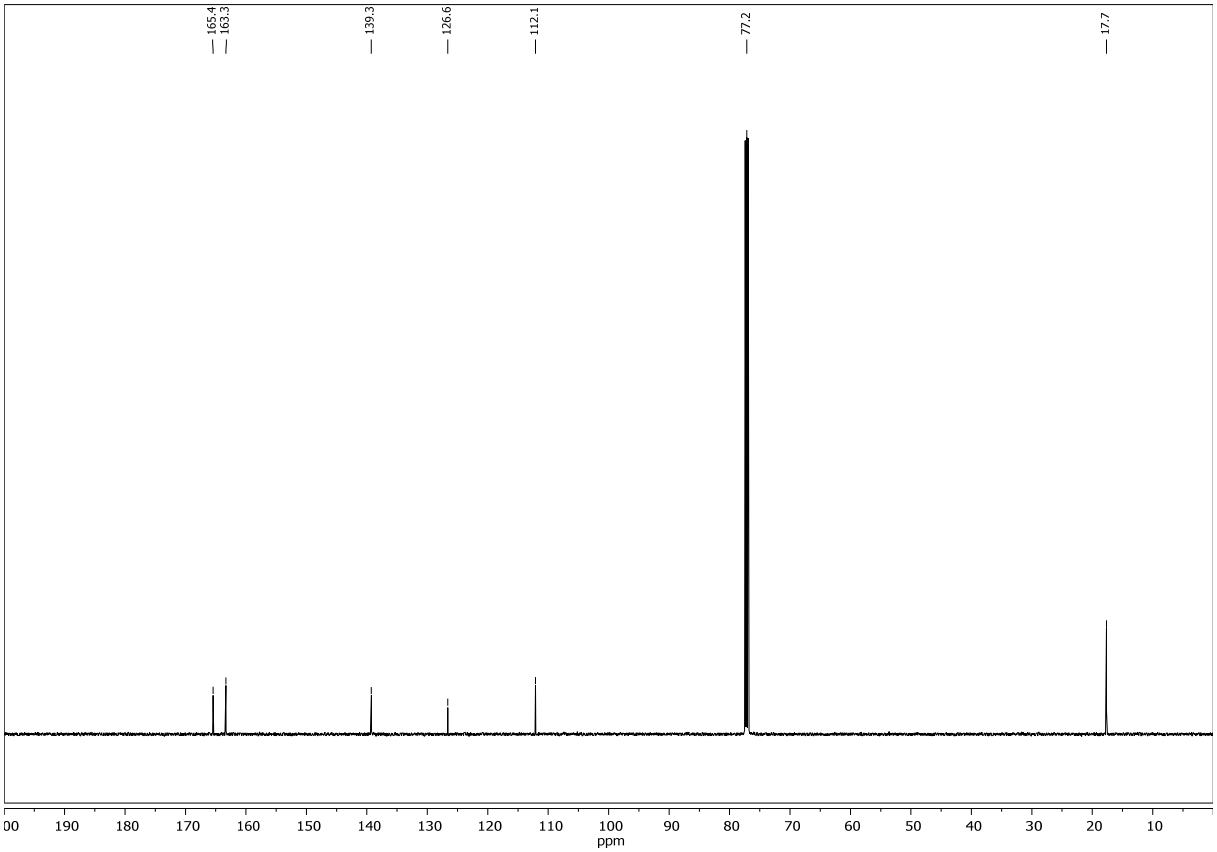
165.4
163.3
139.3
126.6
112.1
77.2
17.7
ppm

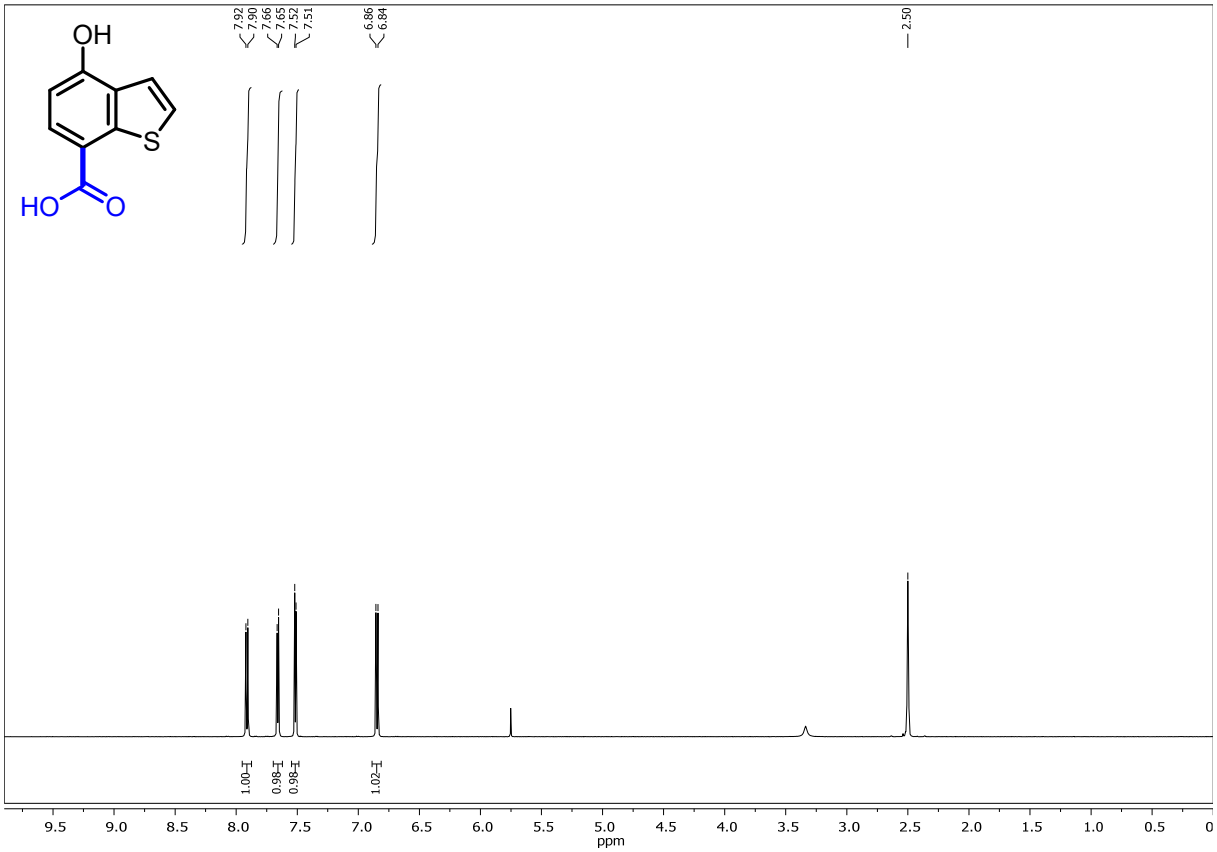
OH
S
HO
O
7.92
7.90
7.66
7.65
7.52
7.51
6.86
6.84
2.50
1.00
0.98
0.98
1.02
9.5
9.0
8.5
8.0
7.5
7.0
6.5
6.0
5.5
5.0
4.5
4.0
3.5
3.0
2.5
2.0
1.5
1.0
0.5
0
ppm

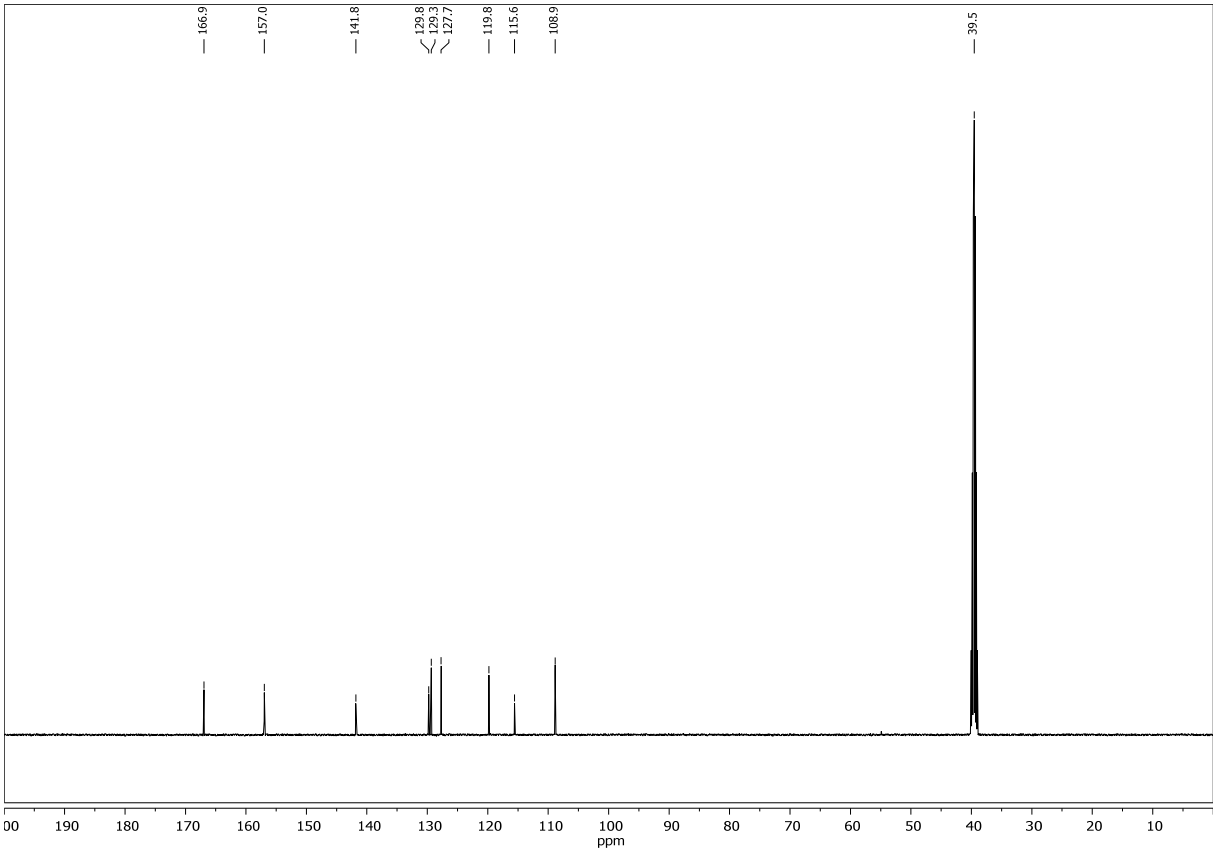
166.9
157.0
141.8
129.8
129.3
127.7
119.8
115.6
108.9
39.5
00
190
180
170
160
150
140
130
120
110
100
90
80
70
60
50
40
30
20
10
ppm

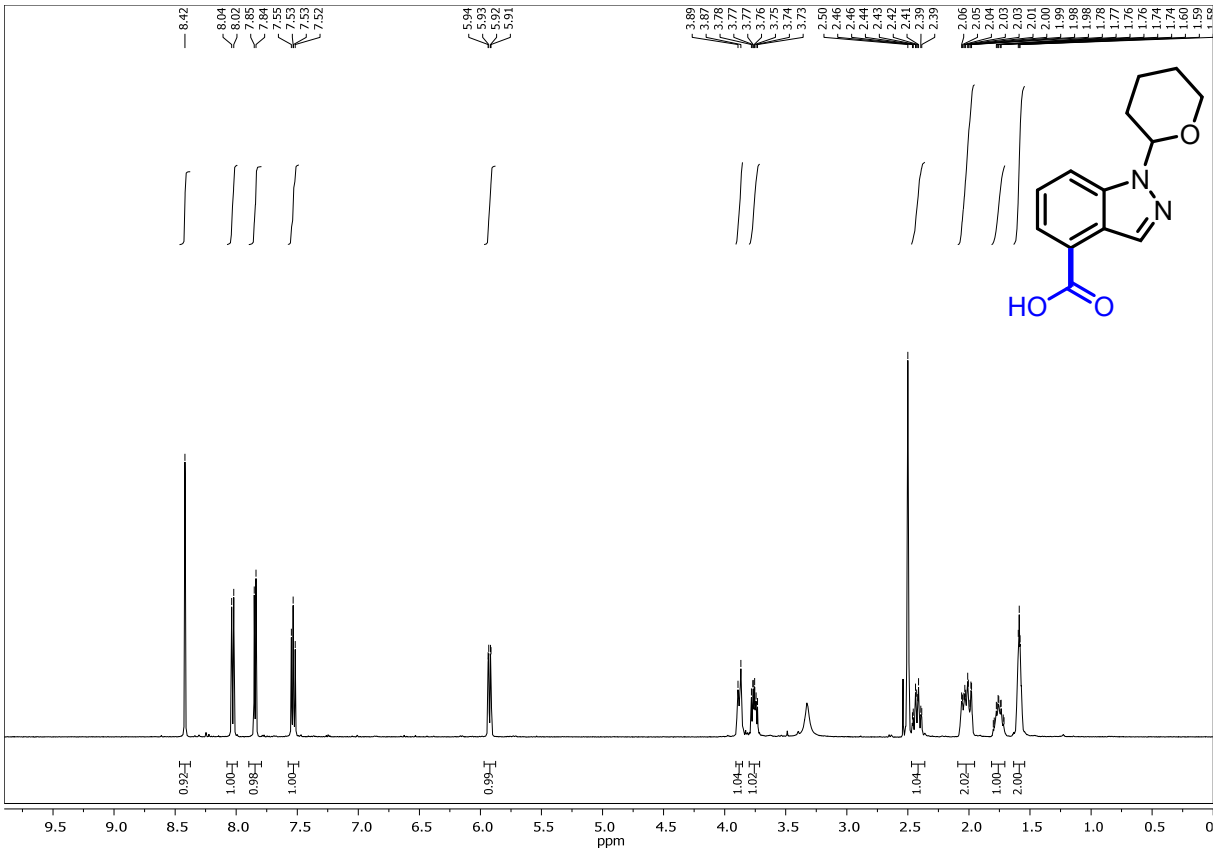
8.42
8.04
8.02
7.85
7.84
7.55
7.53
7.52
5.94
5.93
5.92
5.91
3.89
3.87
3.78
3.77
3.77
3.76
3.75
3.74
3.73
2.50
2.46
2.46
2.44
2.43
2.42
2.41
2.39
2.39
2.06
2.05
2.04
2.03
2.01
2.00
1.99
1.98
1.98
1.78
1.77
1.76
1.76
1.74
1.74
1.60
1.59
O
N
N
HO
O
0.92
1.00
0.98
1.00
0.99
1.04
1.02
1.04
2.02
1.00
2.00
9.5
9.0
8.5
8.0
7.5
7.0
6.5
6.0
5.5
5.0
4.5
4.0
3.5
3.0
2.5
2.0
1.5
1.0
0.5
0
ppm

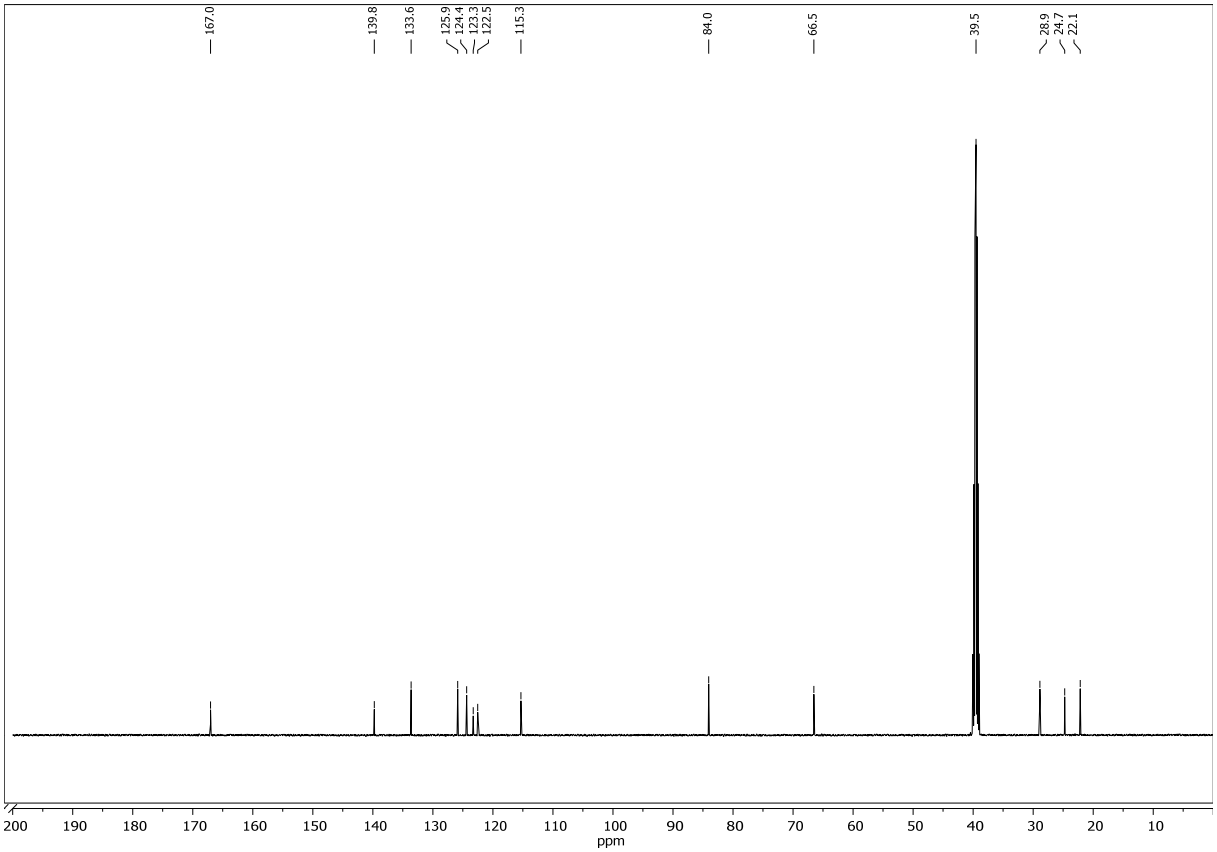
167.0
139.8
133.6
125.9
124.4
123.3
122.5
115.3
84.0
66.5
39.5
28.9
24.7
22.1
200
190
180
170
160
150
140
130
120
110
100
90
80
70
60
50
40
30
20
10
ppm

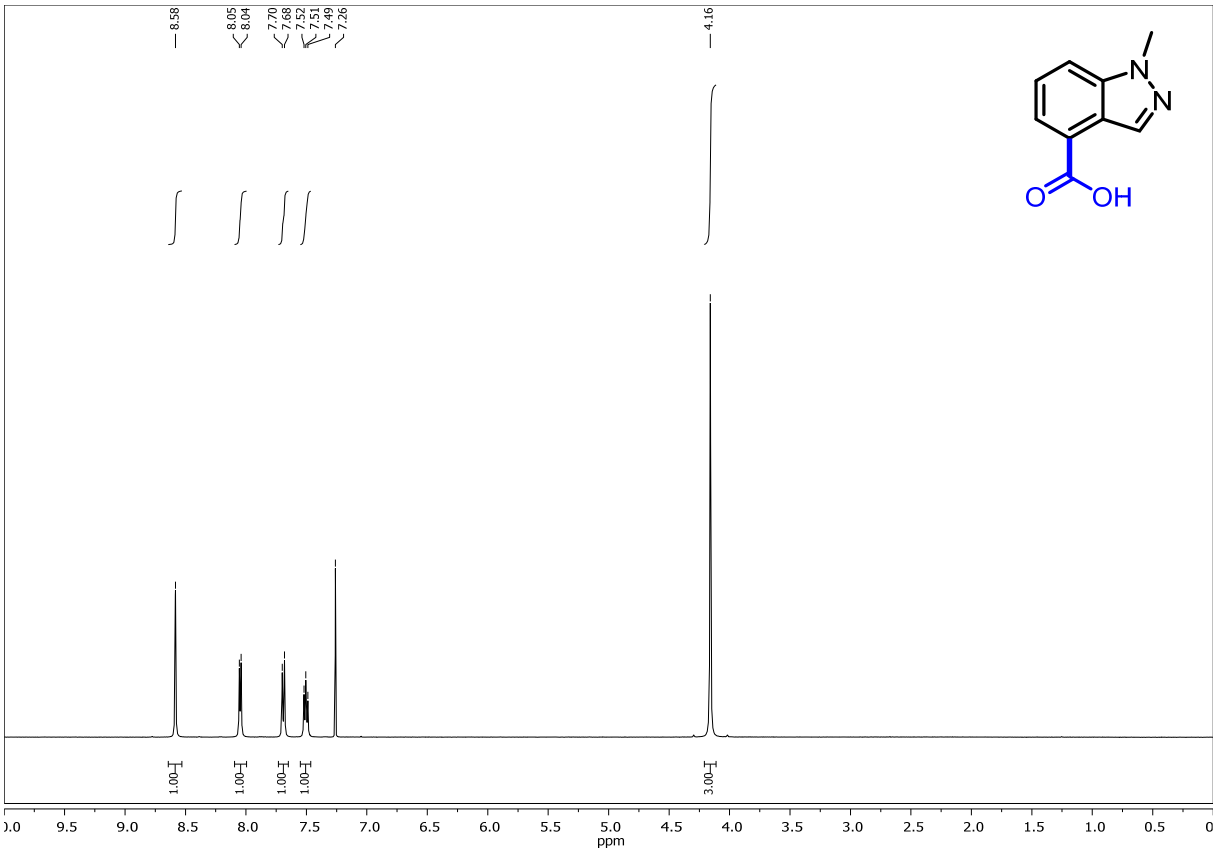
8.58
8.05
8.04
7.70
7.68
7.52
7.51
7.49
7.26
4.16
1.00
1.00
1.00
1.00
3.00
N
N
O
OH
ppm

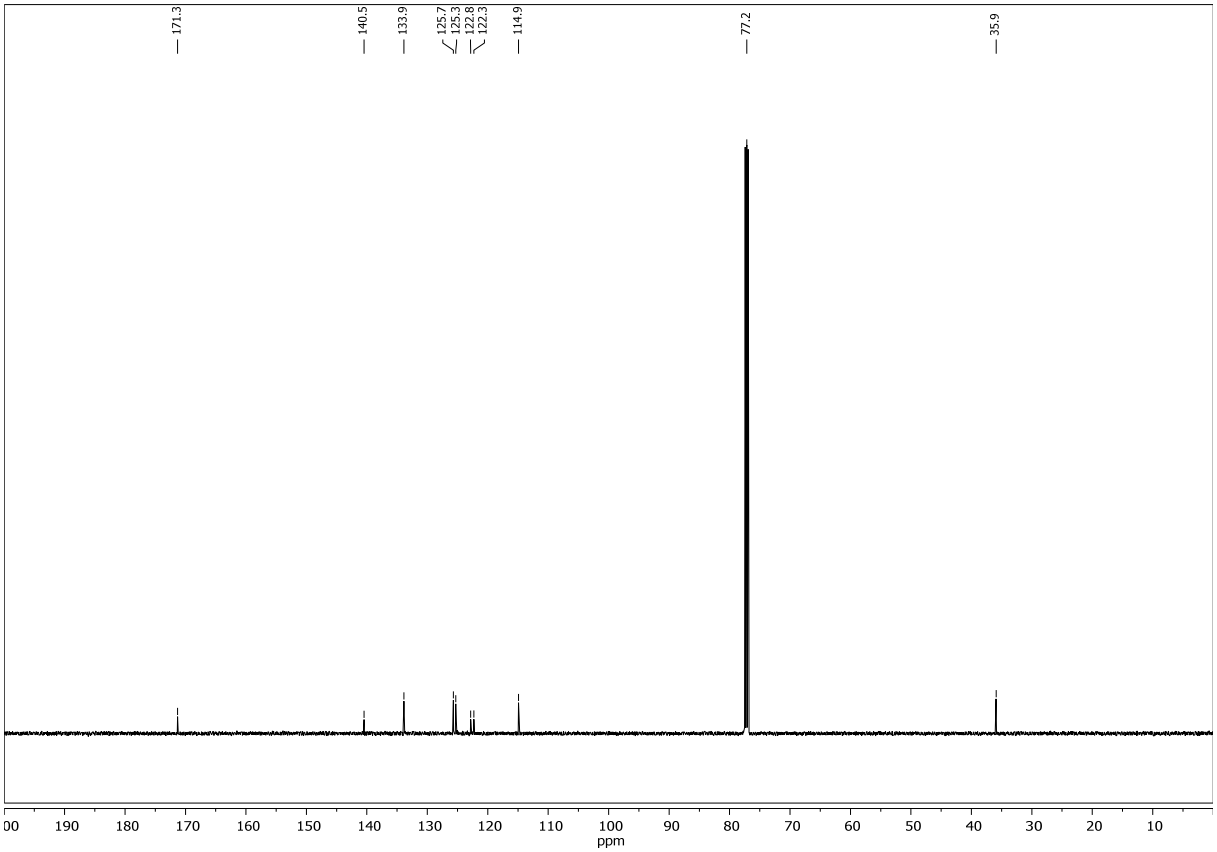
171.3
140.5
133.9
125.7
125.3
122.8
122.3
114.9
77.2
35.9
ppm

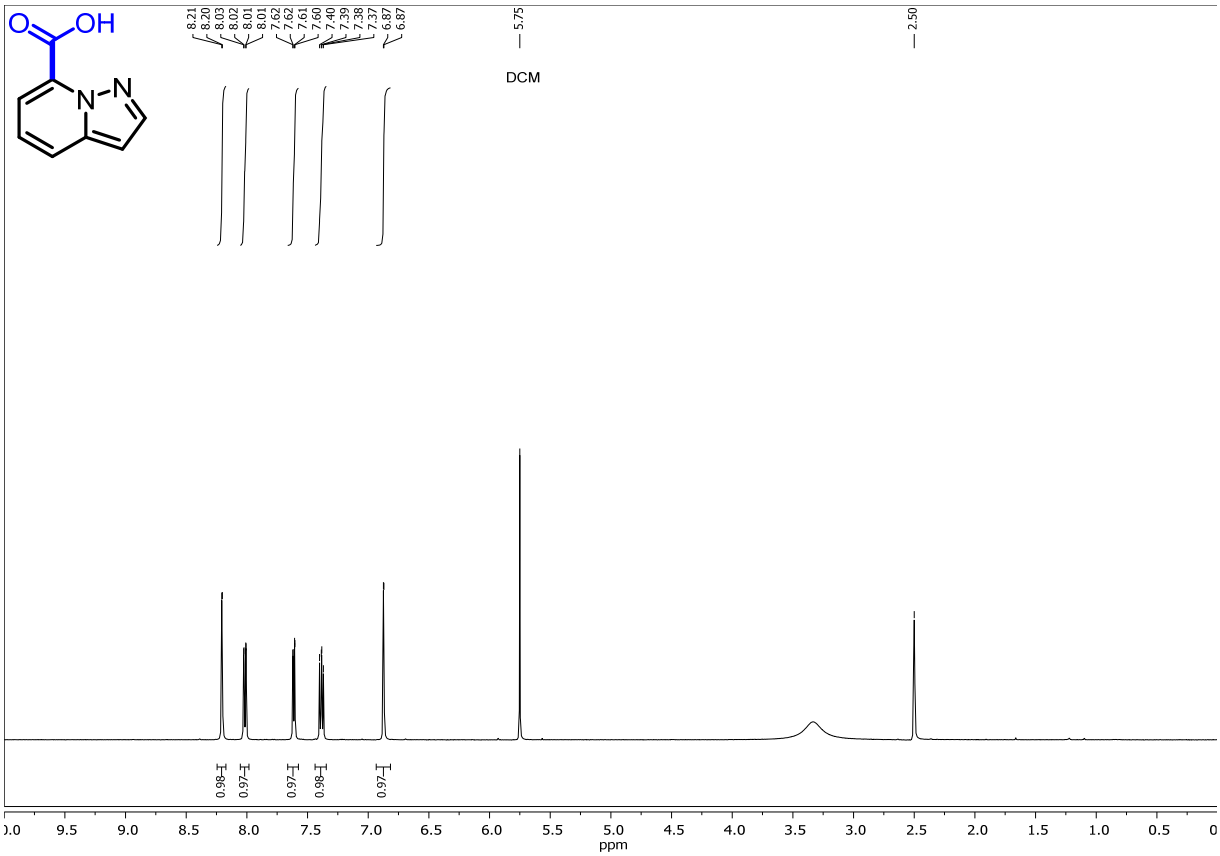
O
OH
N
N
8.21
8.20
8.03
8.02
8.01
8.01
7.62
7.62
7.61
7.60
7.40
7.39
7.38
7.37
6.87
6.87
5.75
DCM
2.50
0.98
0.97
0.97
0.98
0.97
ppm

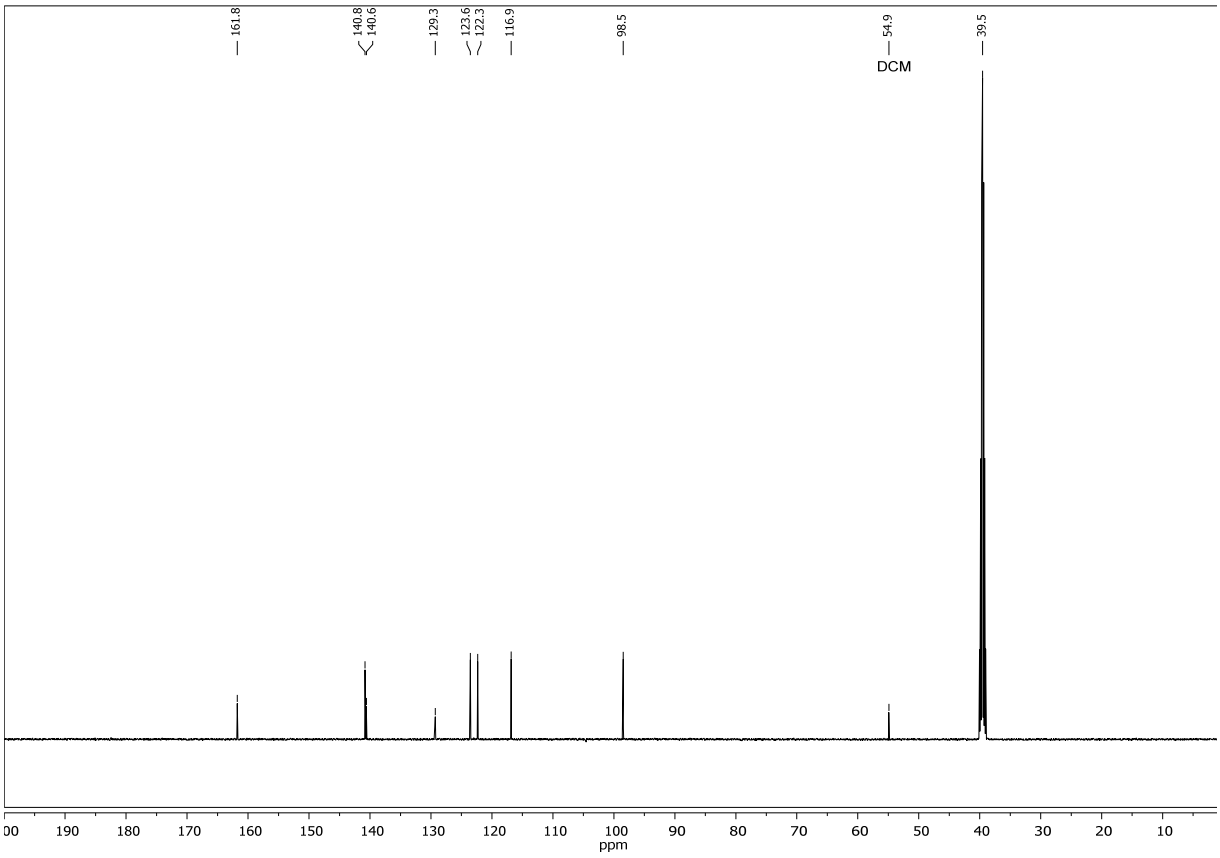
161.8
140.8
140.6
129.3
123.6
122.3
116.9
98.5
54.9
DCM
39.5
ppm

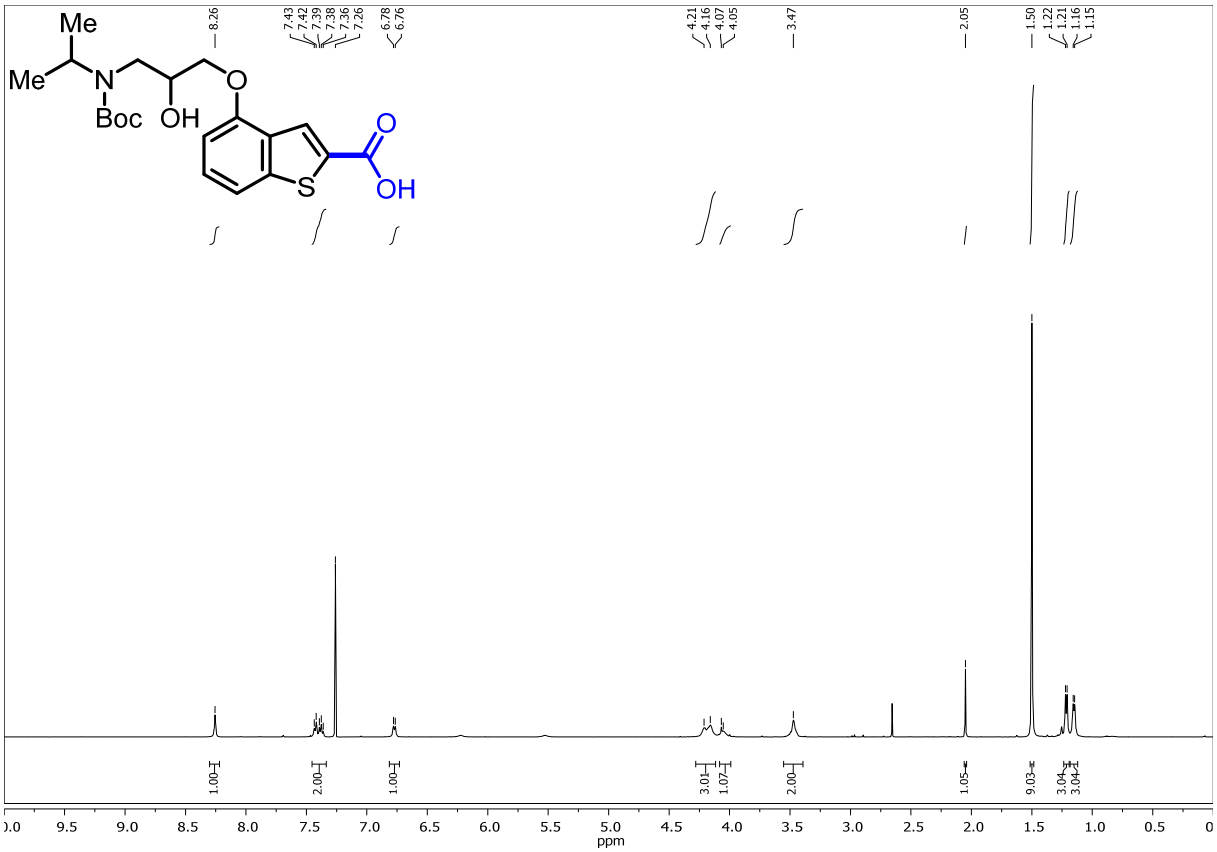
Me
Me
N
Boc
OH
O
O
OH
S
8.26
7.43
7.42
7.39
7.38
7.36
7.26
6.78
6.76
4.21
4.16
4.07
4.05
3.47
2.05
1.50
1.22
1.21
1.16
1.15
1.00
2.00
1.00
3.01
1.07
2.00
1.05
9.03
3.04
3.04
ppm

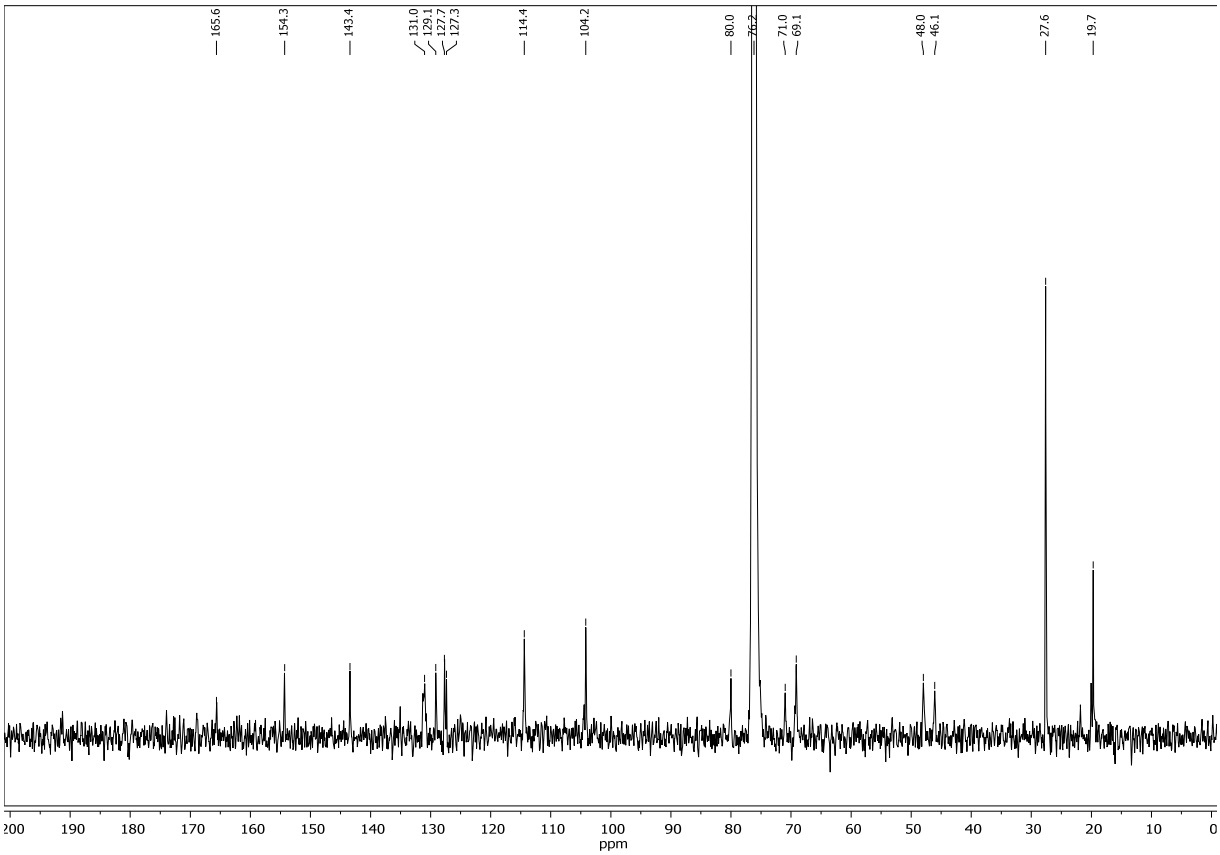
165.6
154.3
143.4
131.0
129.1
127.7
127.3
114.4
104.2
80.0
76.2
71.0
69.1
48.0
46.1
27.6
19.7
ppm

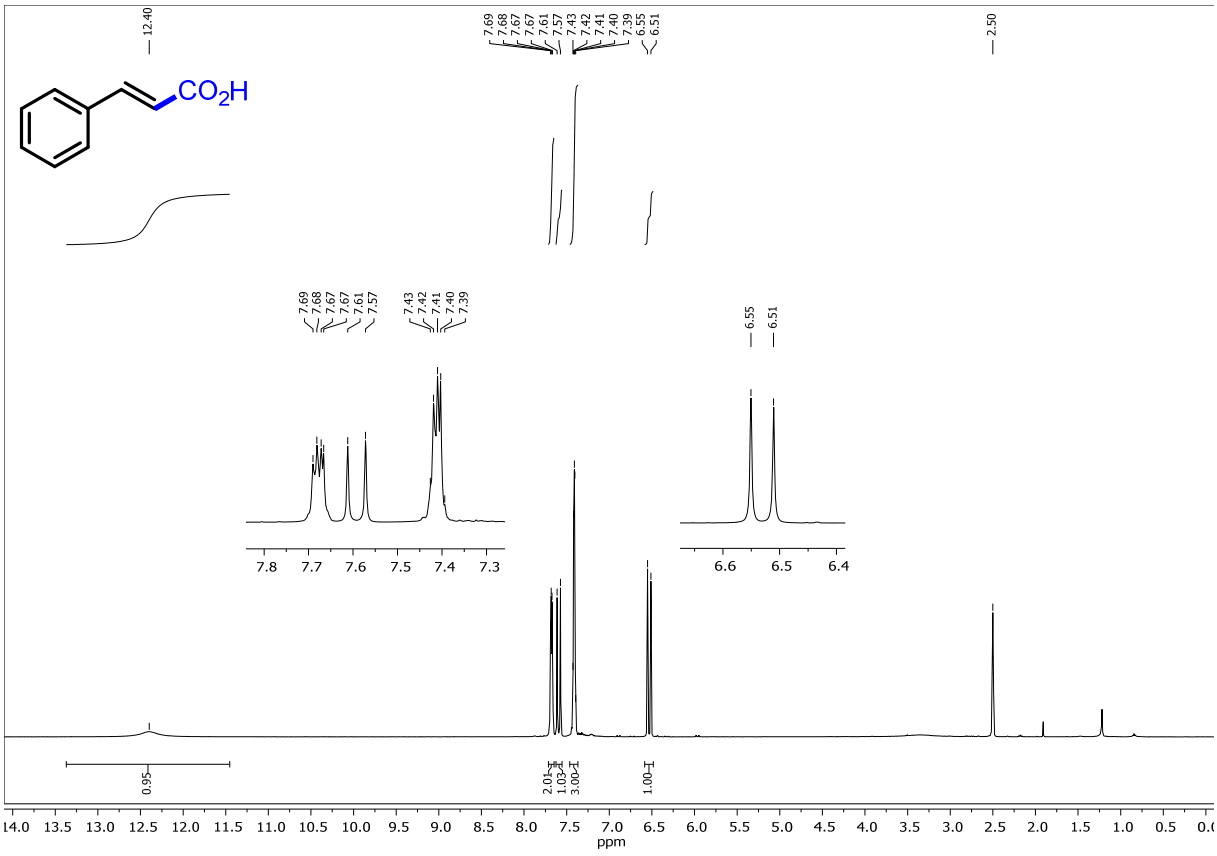
12.40
7.69
7.68
7.67
7.67
7.61
7.57
7.43
7.42
7.41
7.40
7.39
6.55
6.51
2.50
CO2H
0.95
2.01
1.03
3.00
1.00
ppm

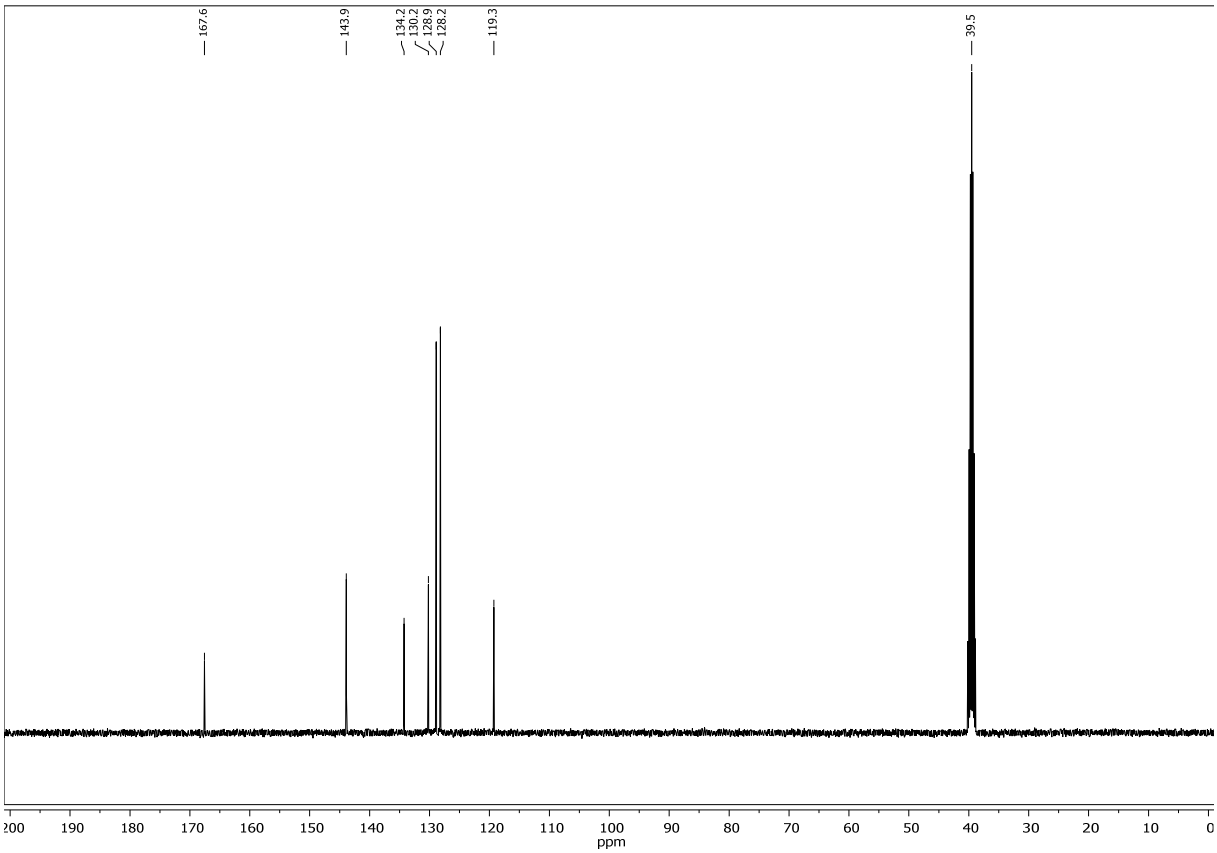
167.6
143.9
134.2
130.2
128.9
128.2
119.3
39.5
ppm

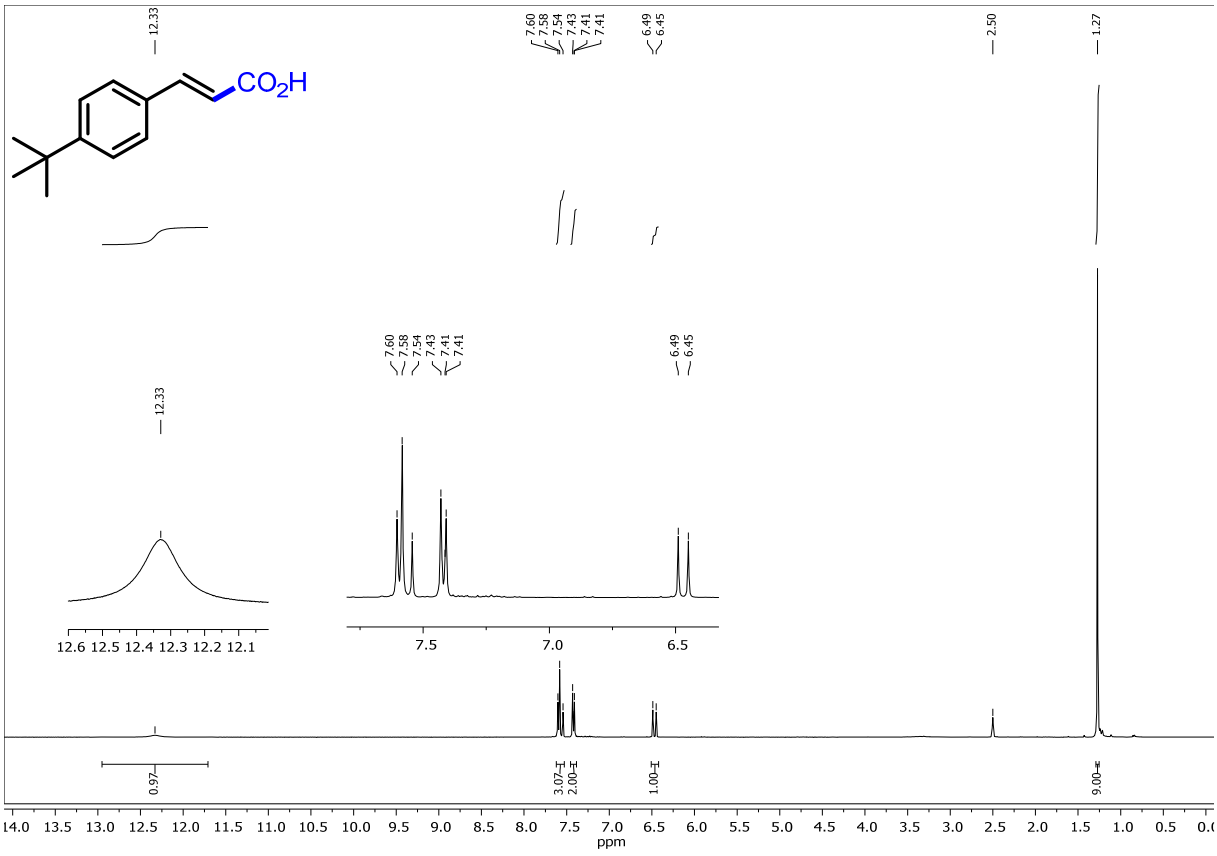
12.33
7.60
7.58
7.54
7.43
7.41
7.41
6.49
6.45
2.50
1.27
CO2H
12.6 12.5 12.4 12.3 12.2 12.1
7.5
7.0
6.5
0.97
3.07
2.00
1.00
9.00
ppm

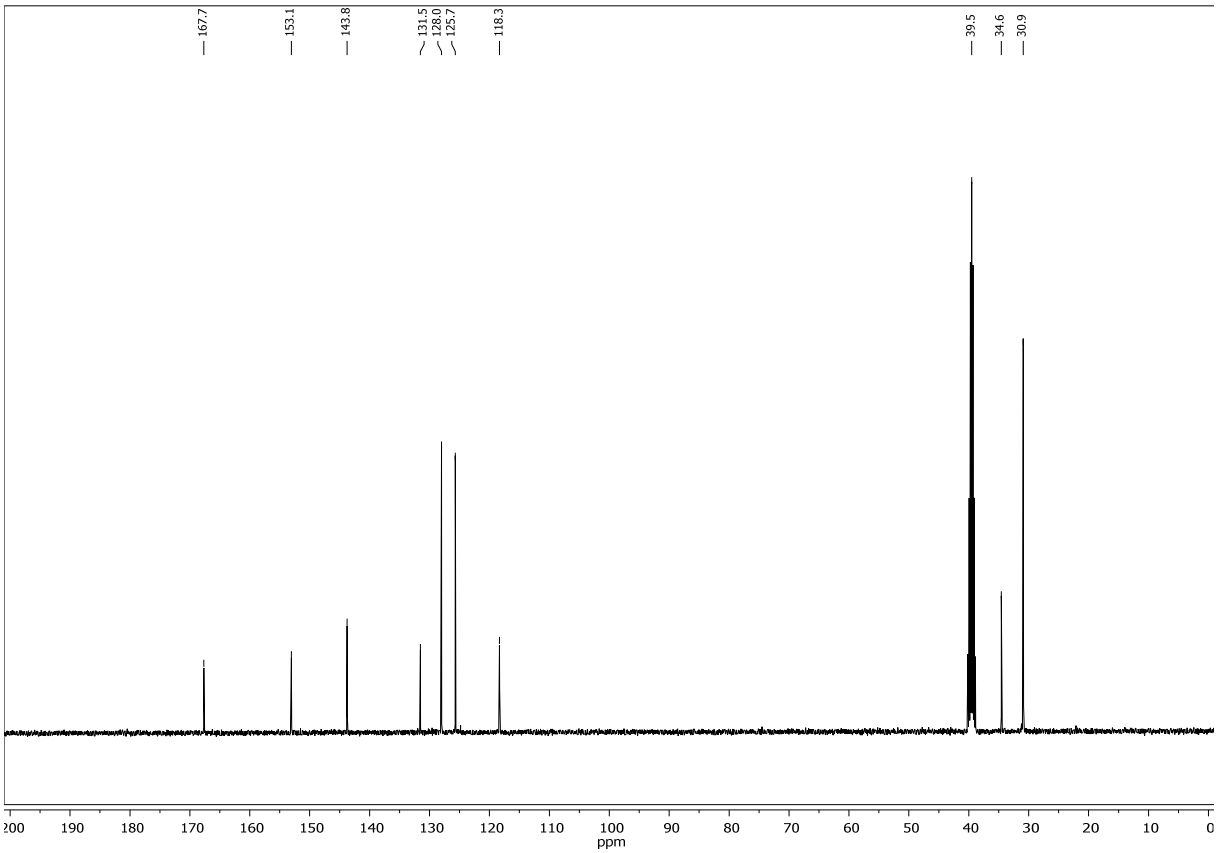
167.7
153.1
143.8
131.5
128.0
125.7
118.3
39.5
34.6
30.9
ppm

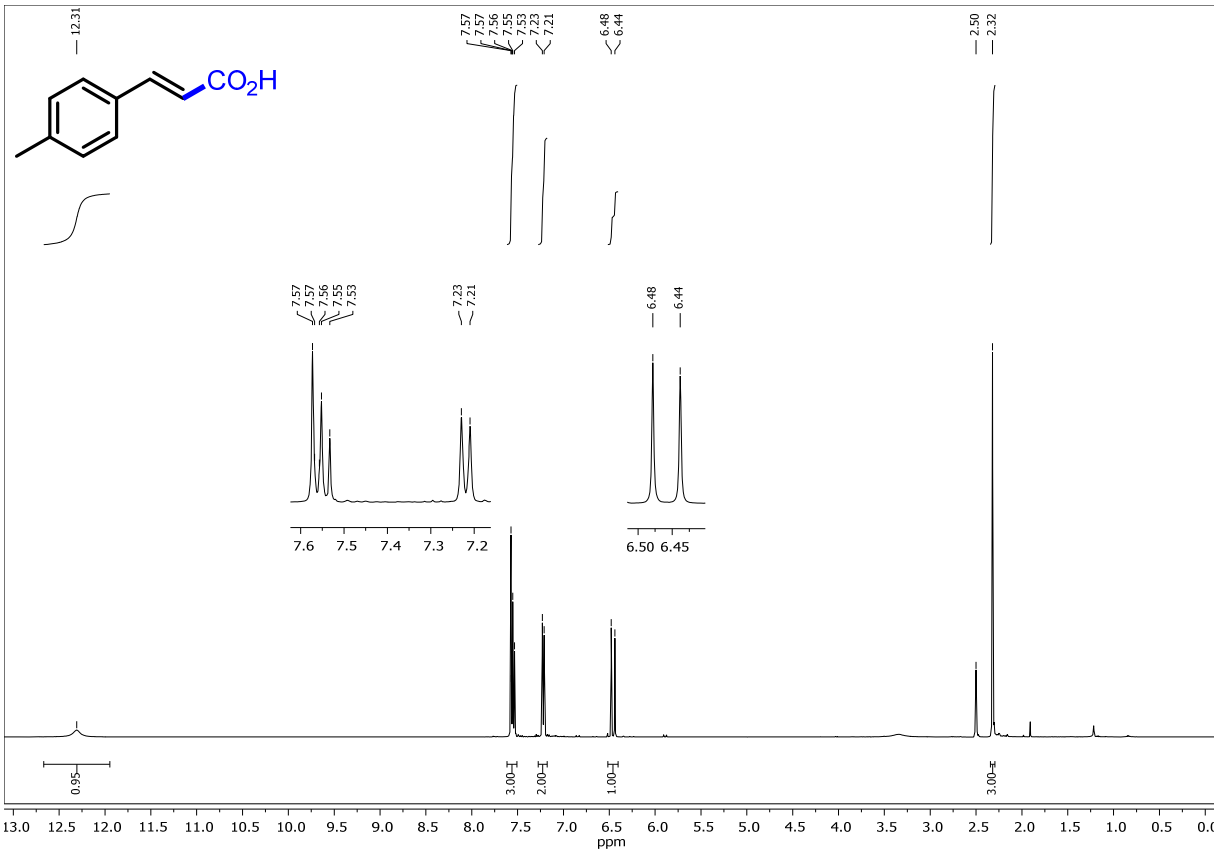
12.31
7.57
7.57
7.56
7.55
7.53
7.23
7.21
6.48
6.44
2.50
2.32
CO2H
0.95
3.00
2.00
1.00
3.00
ppm

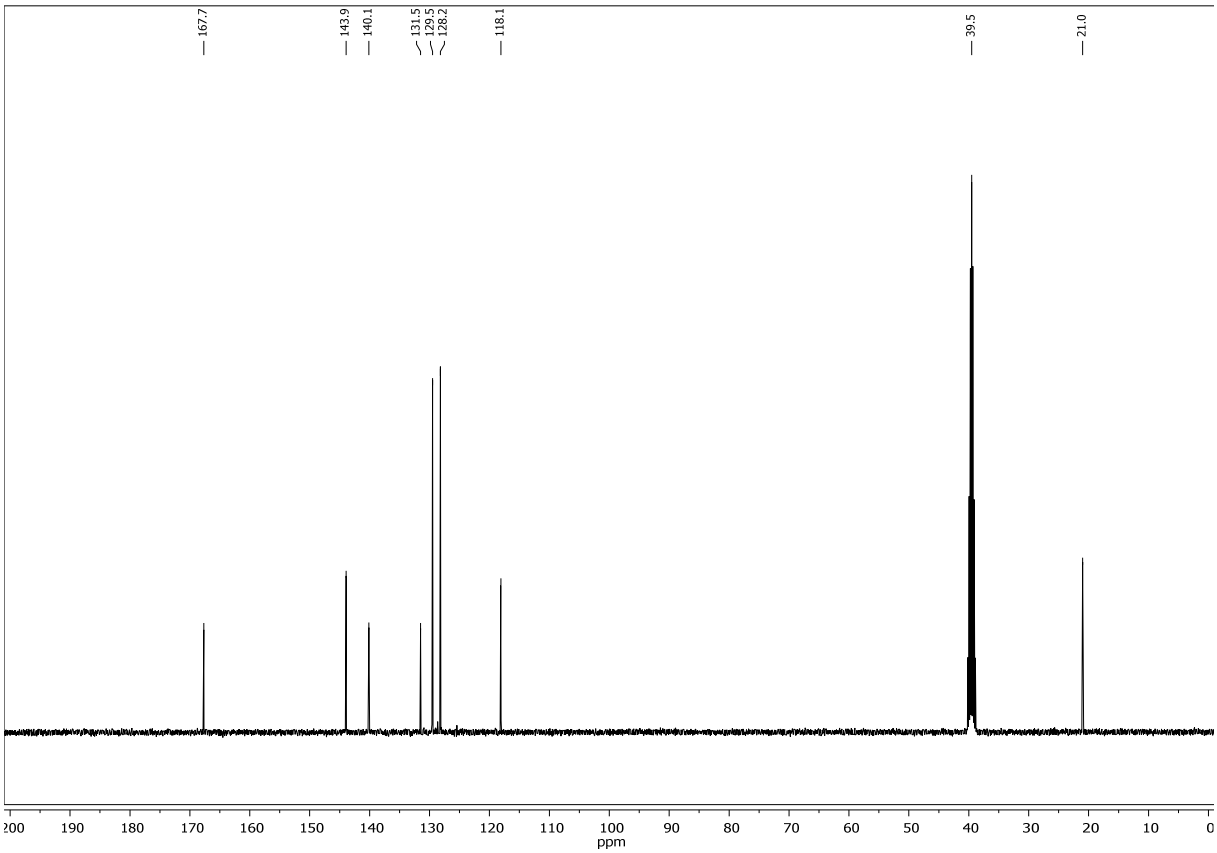
167.7
143.9
140.1
131.5
129.5
128.2
118.1
39.5
21.0
ppm

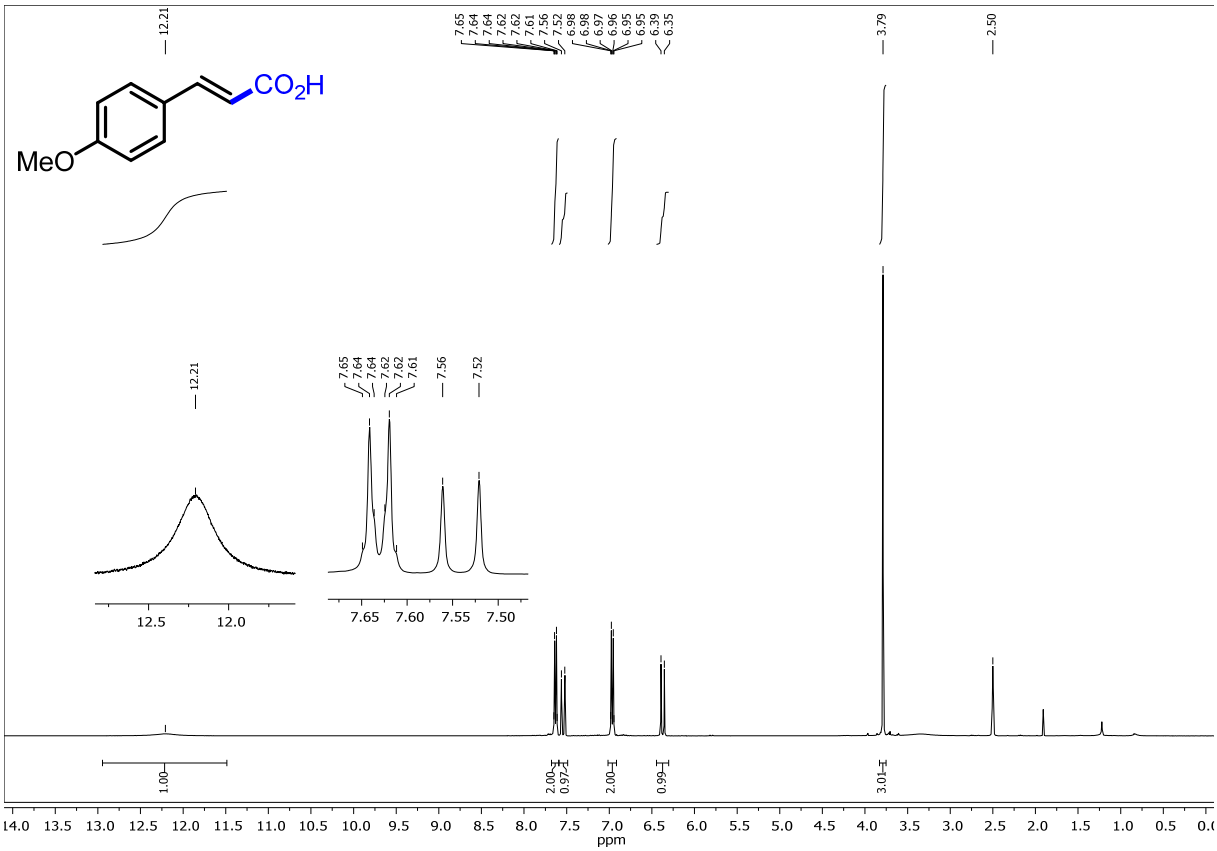
12.21
7.65
7.64
7.64
7.62
7.62
7.61
7.56
7.52
6.98
6.97
6.96
6.95
6.39
6.35
3.79
2.50
CO2H
MeO
12.5
12.0
7.65
7.60
7.55
7.50
1.00
2.00
0.97
2.00
0.99
3.01
ppm

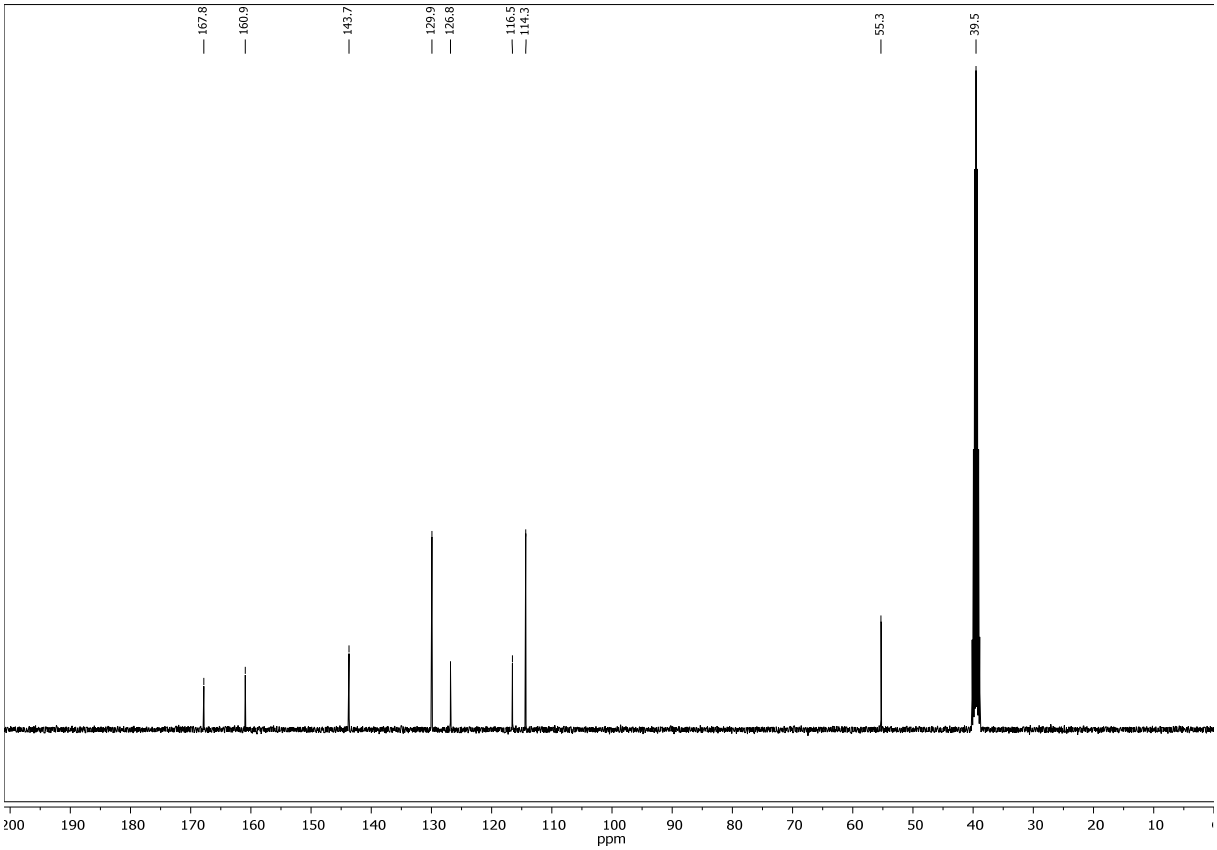
167.8
160.9
143.7
129.9
126.8
116.5
114.3
55.3
39.5
ppm

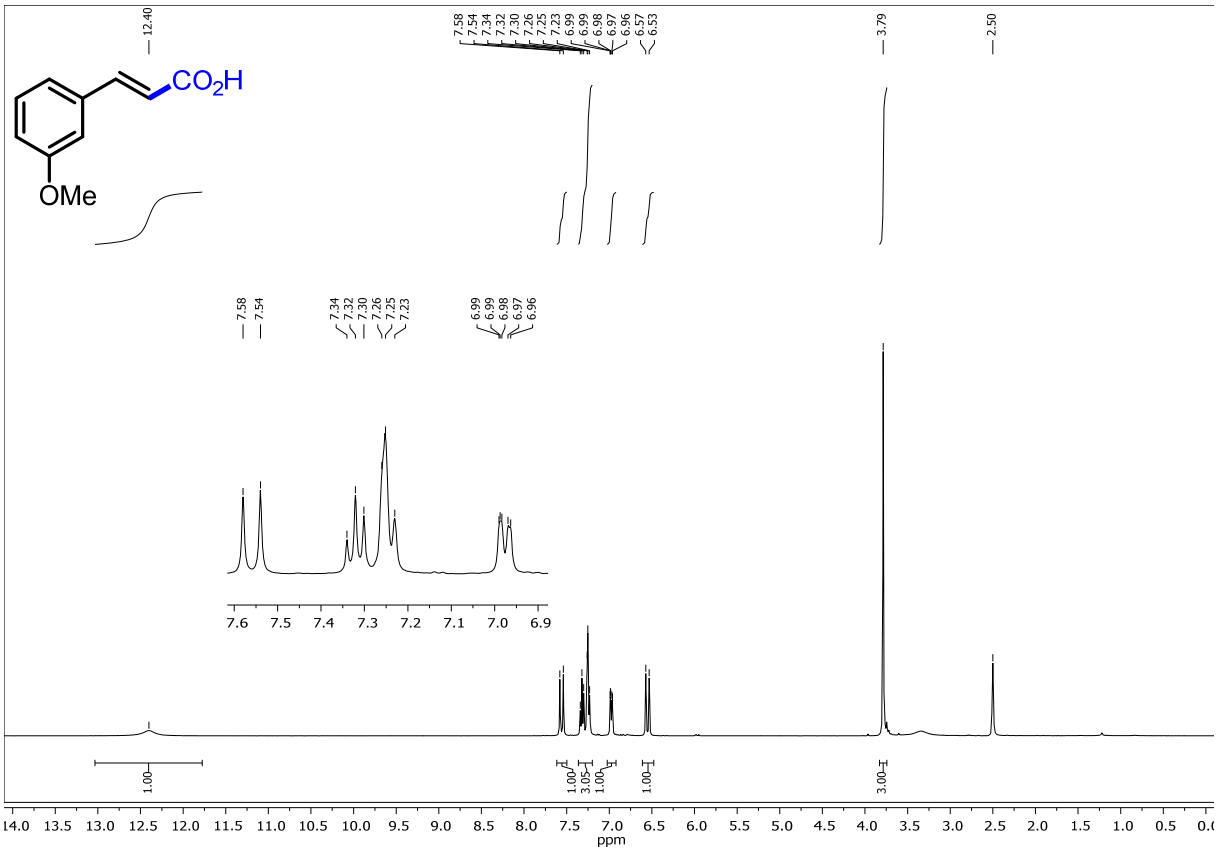
CO2H
OMe
12.40
7.58
7.54
7.34
7.32
7.30
7.26
7.25
7.23
6.99
6.98
6.97
6.96
6.57
6.53
3.79
2.50
1.00
1.00
3.05
1.00
1.00
3.00
ppm

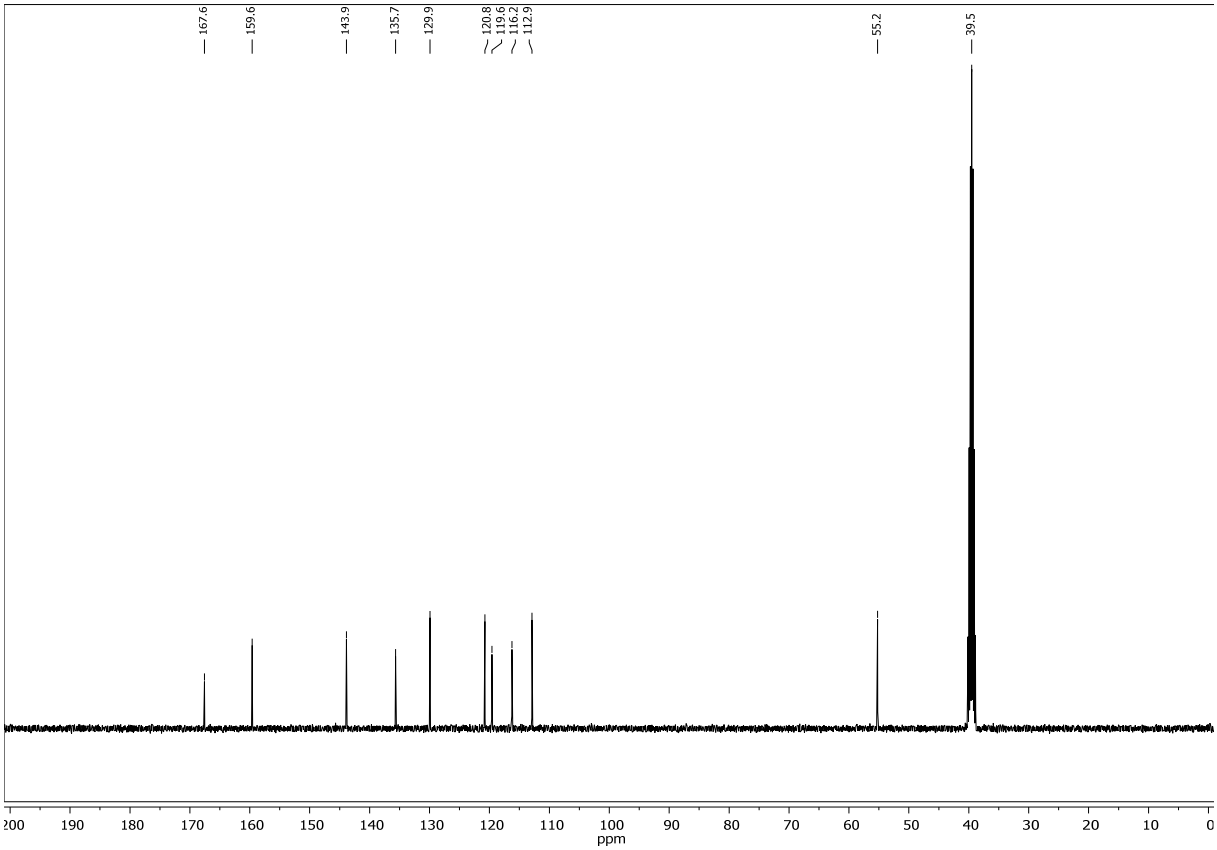
167.6
159.6
143.9
135.7
129.9
120.8
119.6
116.2
112.9
55.2
39.5
ppm

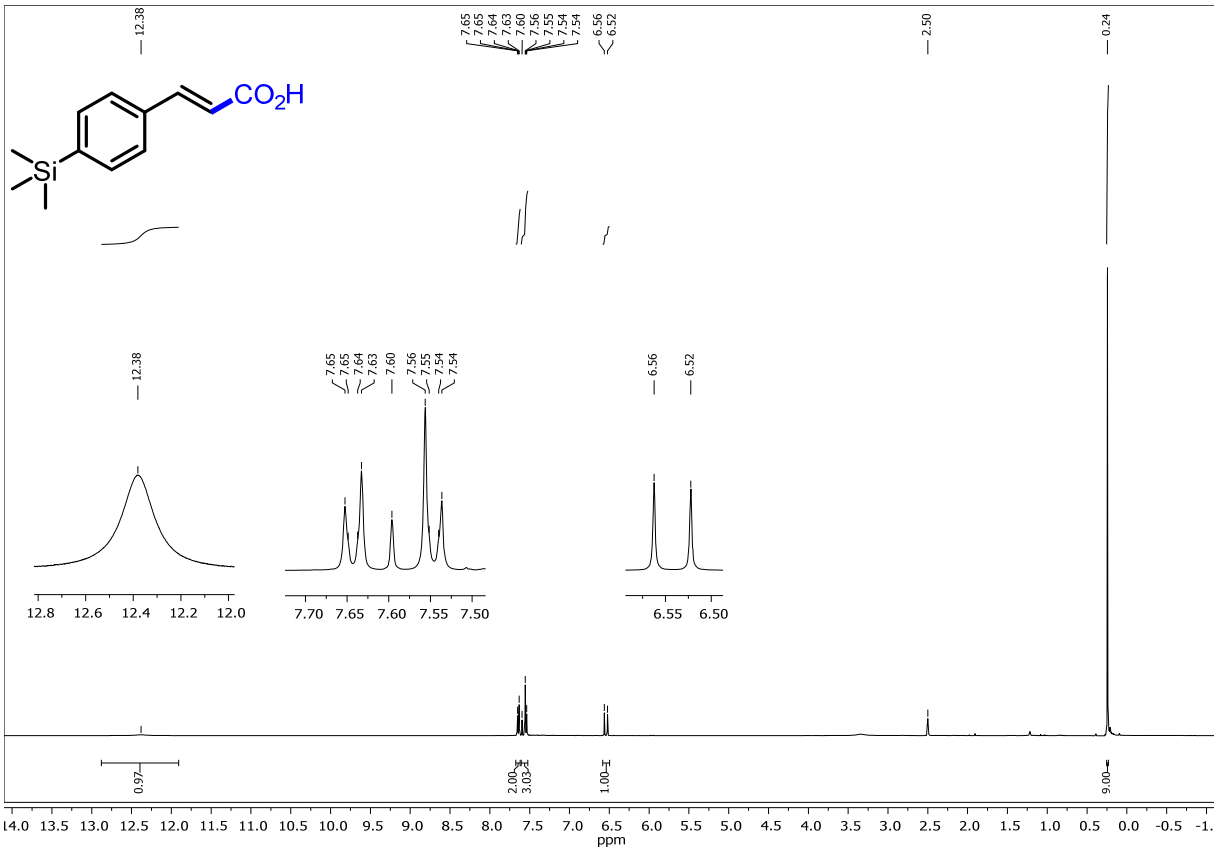
12.38
7.65
7.65
7.64
7.63
7.60
7.56
7.55
7.54
7.54
6.56
6.52
2.50
0.24
CO2H
Si
12.8 12.6 12.4 12.2 12.0
7.70 7.65 7.60 7.55 7.50
6.55 6.50
0.97
2.00
3.03
1.00
9.00
ppm

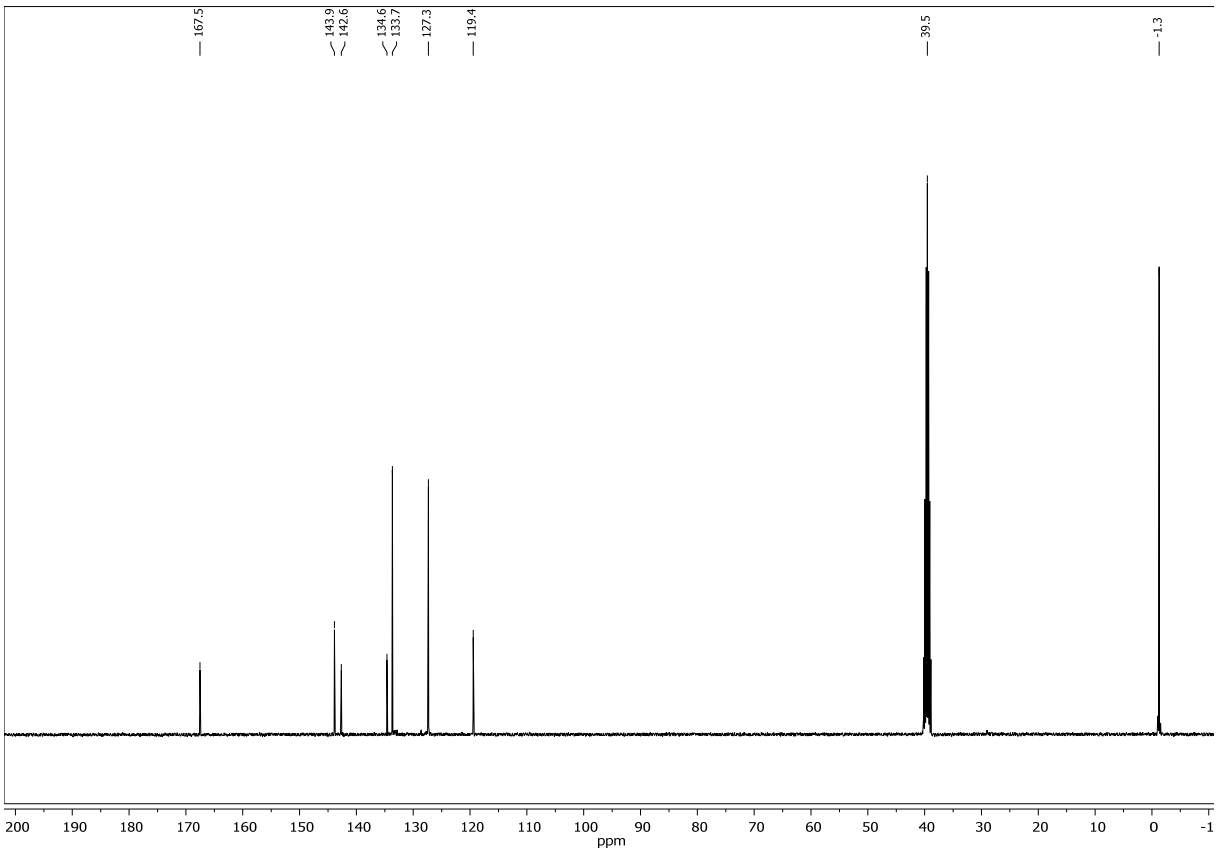
167.5
143.9
142.6
134.6
133.7
127.3
119.4
39.5
-1.3
ppm

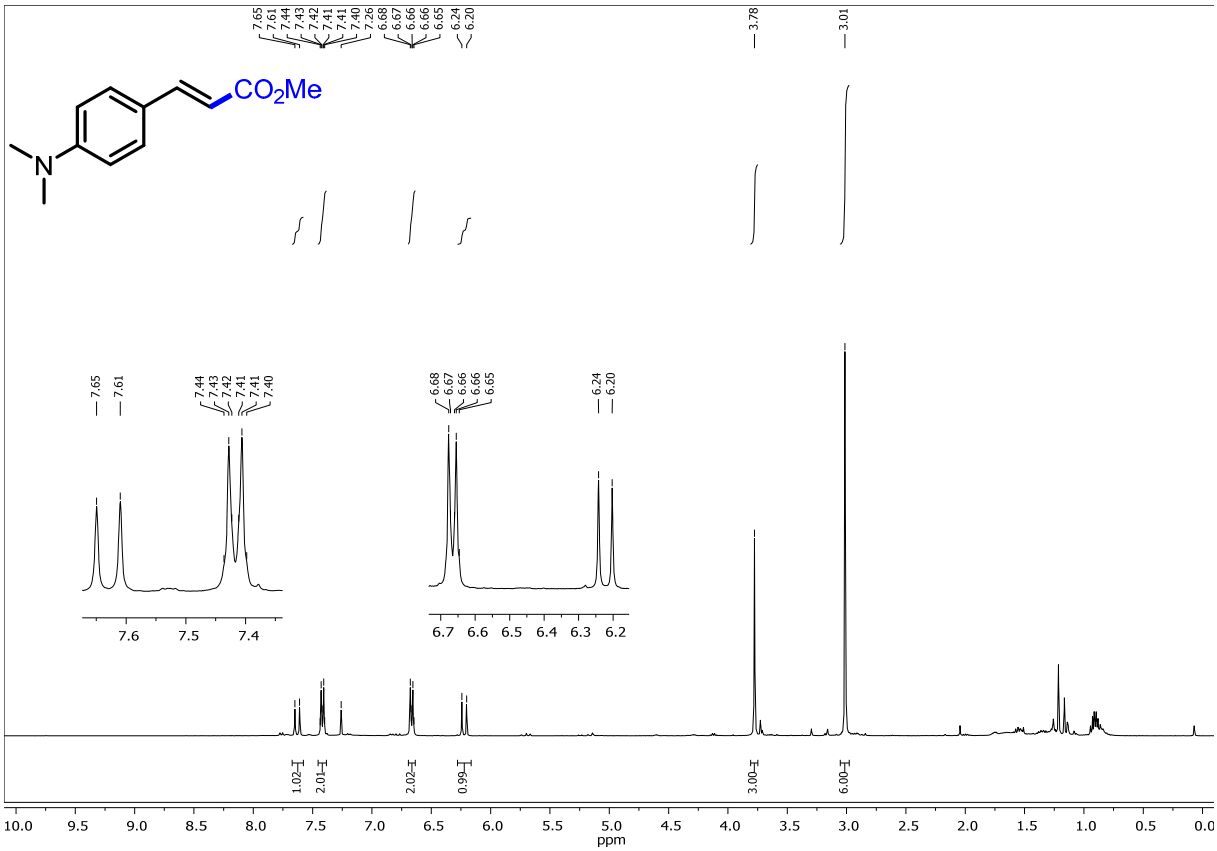
7.65
7.61
7.44
7.43
7.42
7.41
7.41
7.40
7.26
6.68
6.67
6.66
6.66
6.65
6.24
6.20
3.78
3.01
CO2Me
N
1.02
2.01
2.02
0.99
3.00
6.00
ppm

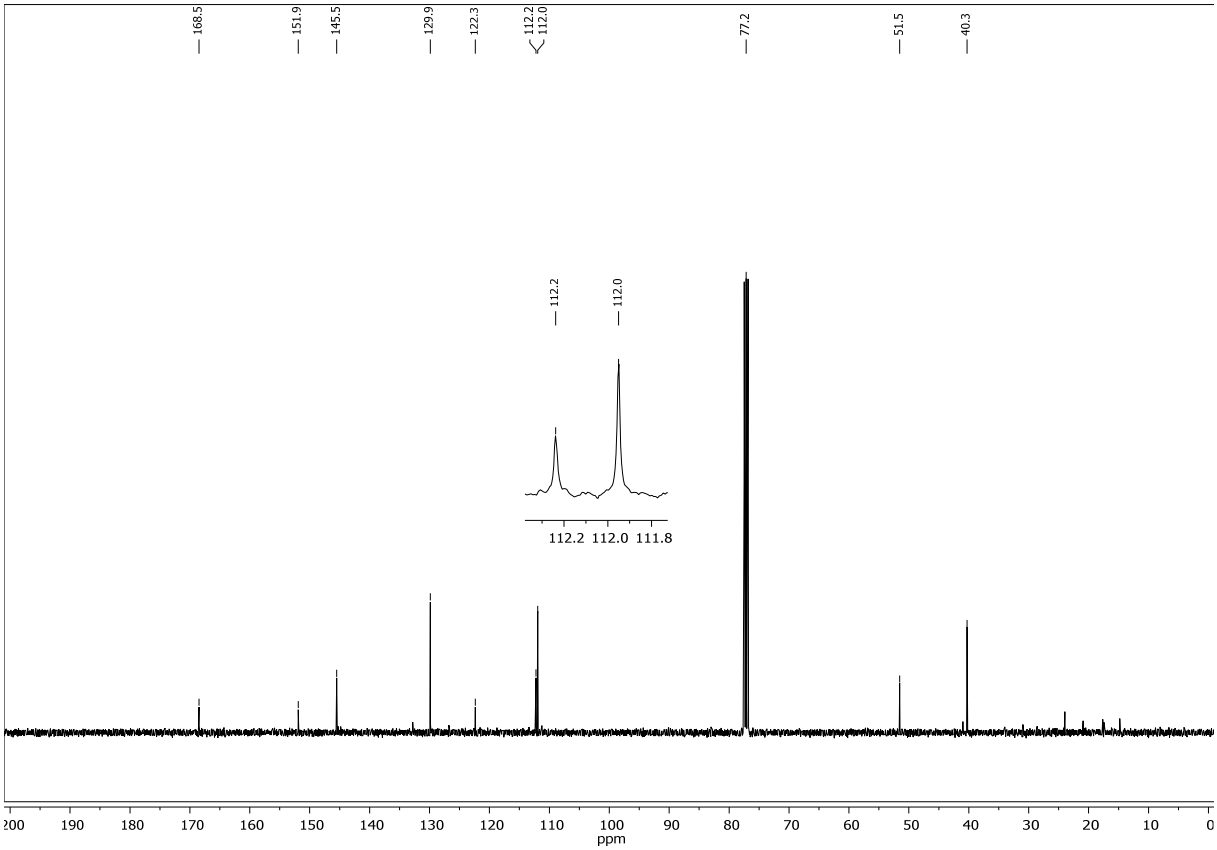
168.5
151.9
145.5
129.9
122.3
112.2
112.0
77.2
51.5
40.3
ppm

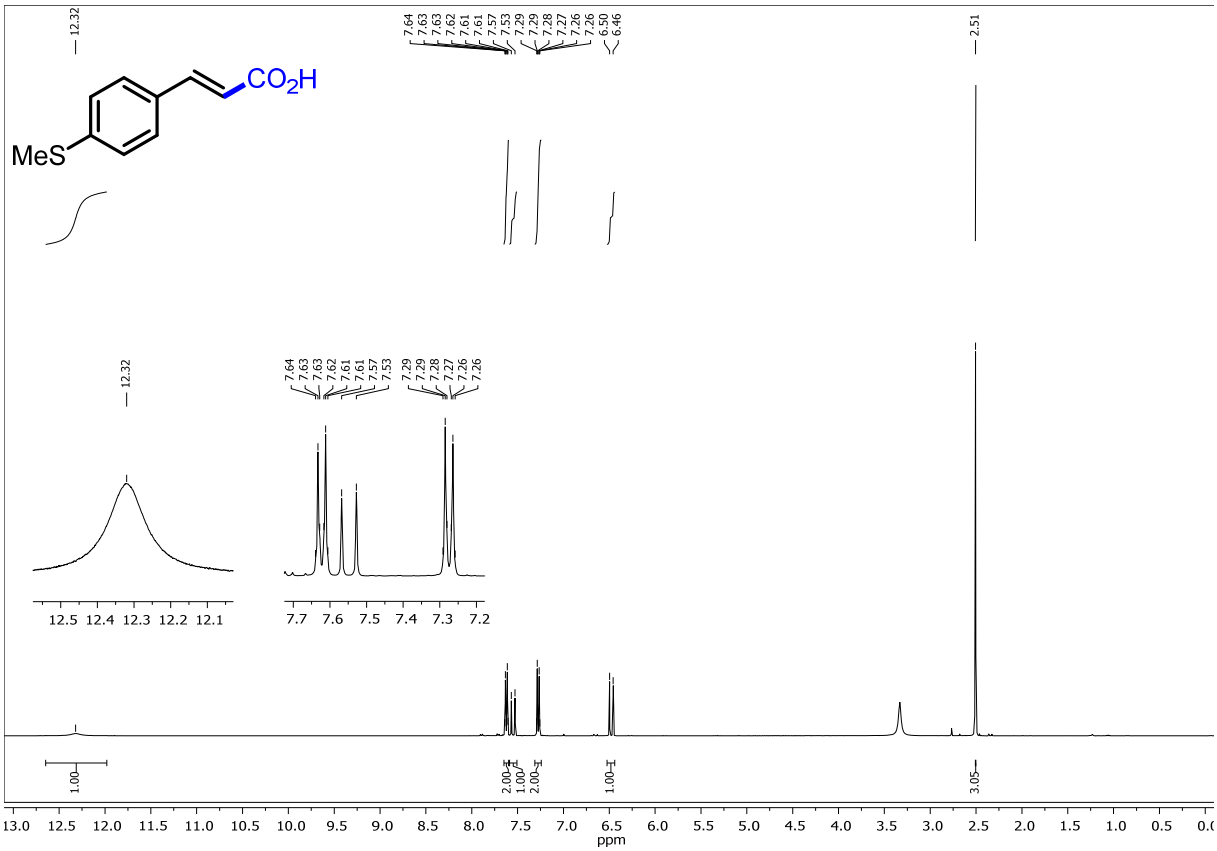
12.32
7.64
7.63
7.63
7.62
7.61
7.61
7.57
7.53
7.29
7.29
7.28
7.27
7.26
7.26
6.50
6.46
2.51
CO2H
MeS
12.5 12.4 12.3 12.2 12.1
7.7 7.6 7.5 7.4 7.3 7.2
1.00
2.00
1.00
2.00
1.00
3.05
ppm

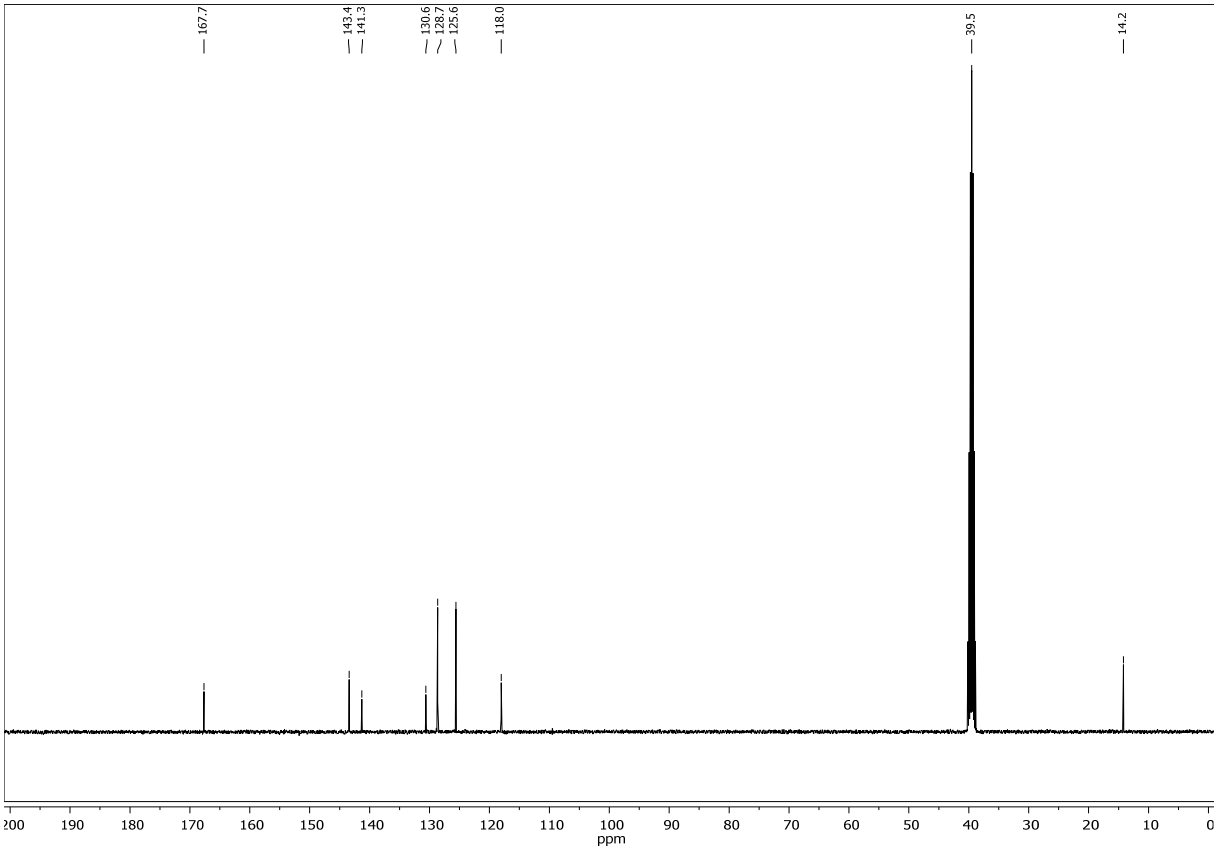
167.7
143.4
141.3
130.6
128.7
125.6
118.0
39.5
14.2
ppm

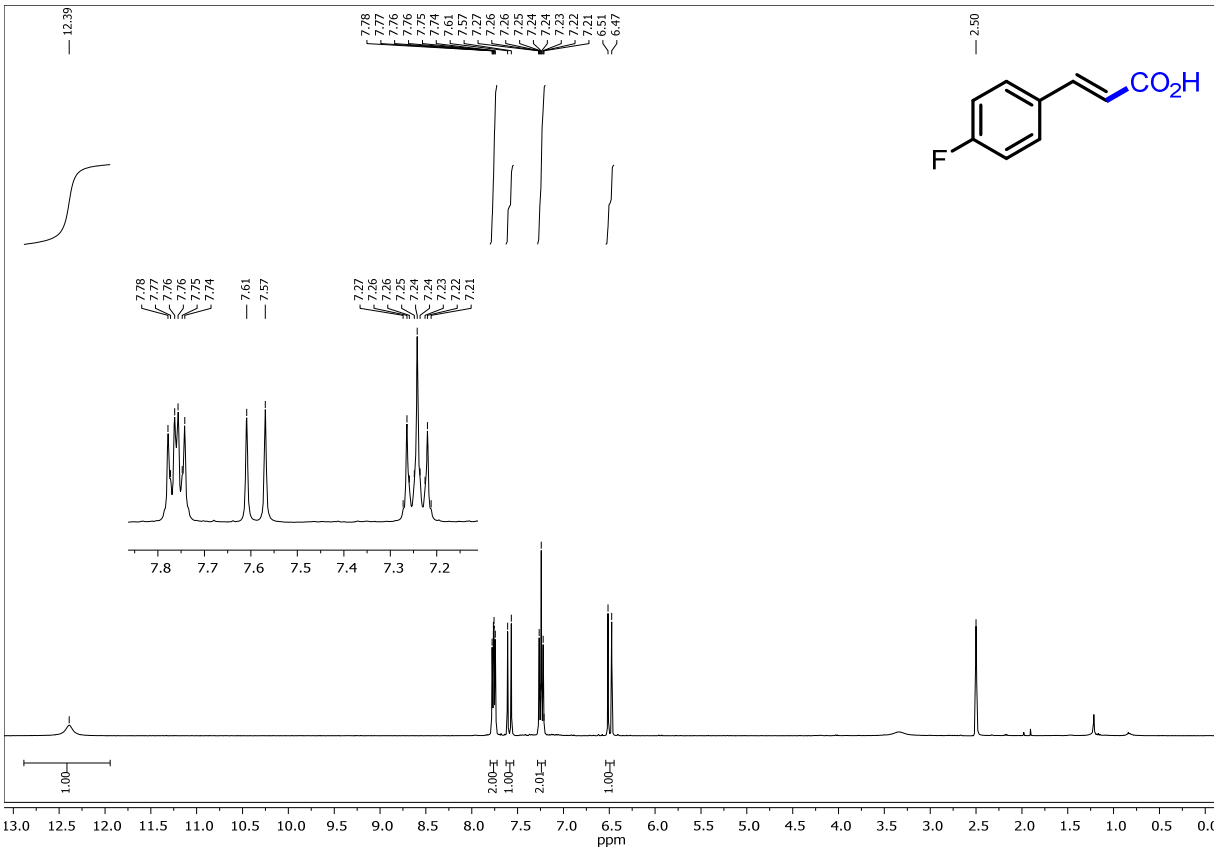
12.39
7.78
7.77
7.76
7.75
7.74
7.61
7.57
7.27
7.26
7.25
7.24
7.23
7.22
7.21
6.51
6.47
2.50
CO2H
F
1.00
2.00
1.00
2.01
1.00
ppm

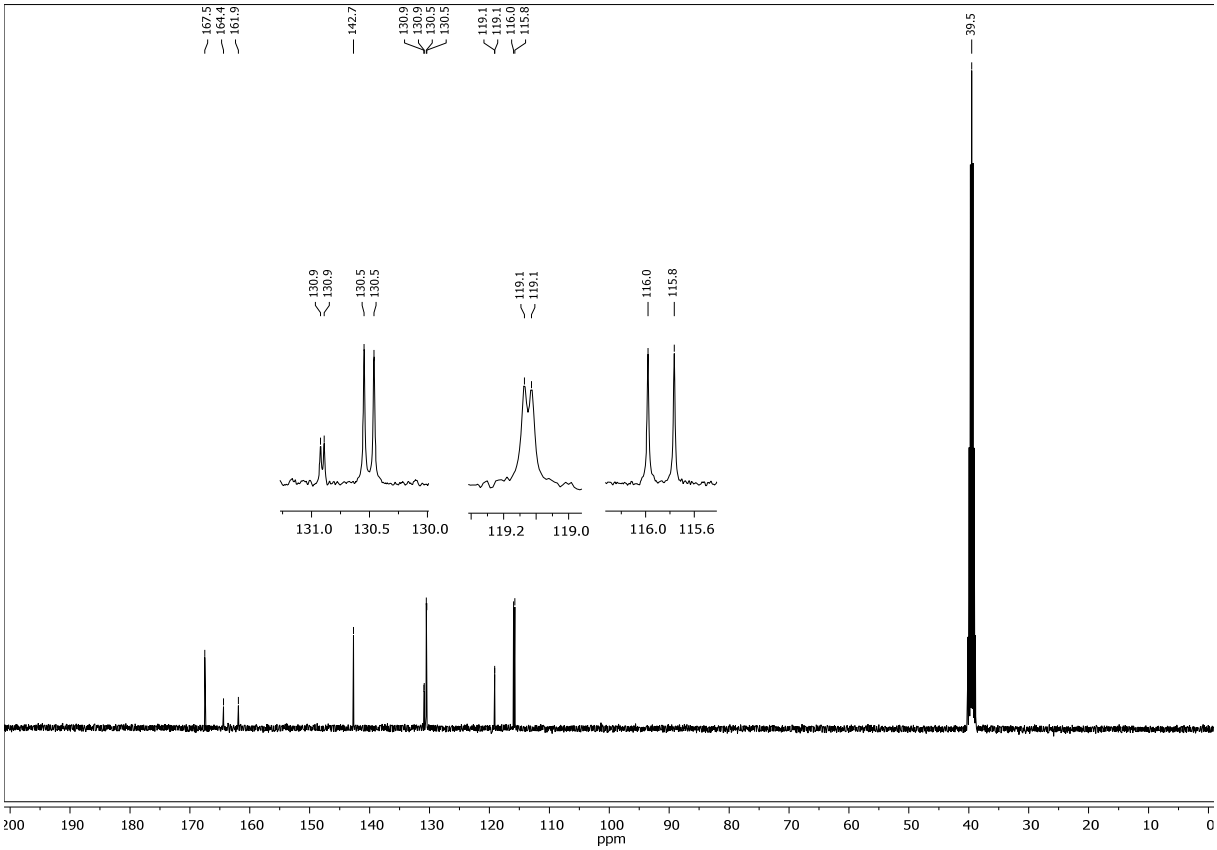
167.5
164.4
161.9
142.7
130.9
130.9
130.5
130.5
119.1
119.1
116.0
115.8
39.5
ppm

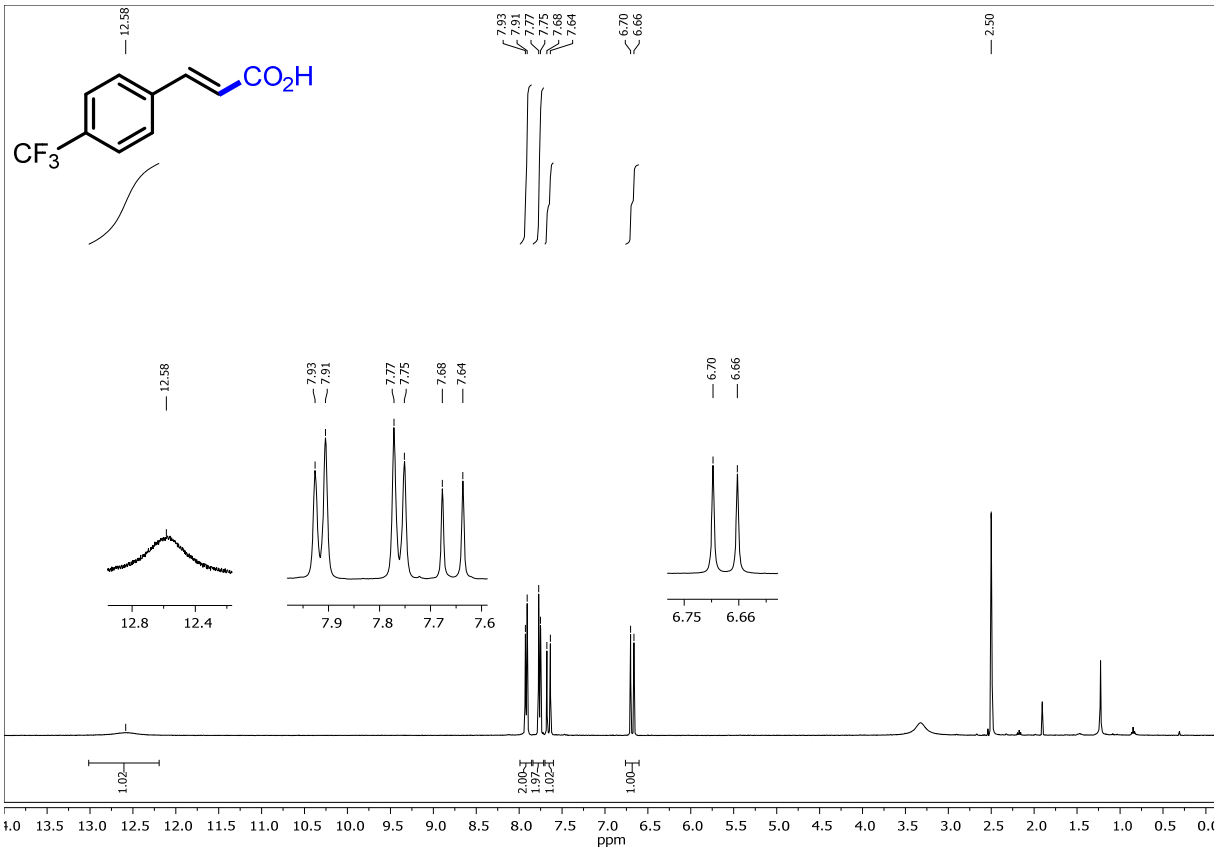
12.58
7.93
7.91
7.77
7.75
7.68
7.64
6.70
6.66
2.50
CO2H
CF3
1.02
2.00
1.97
1.02
1.00
ppm

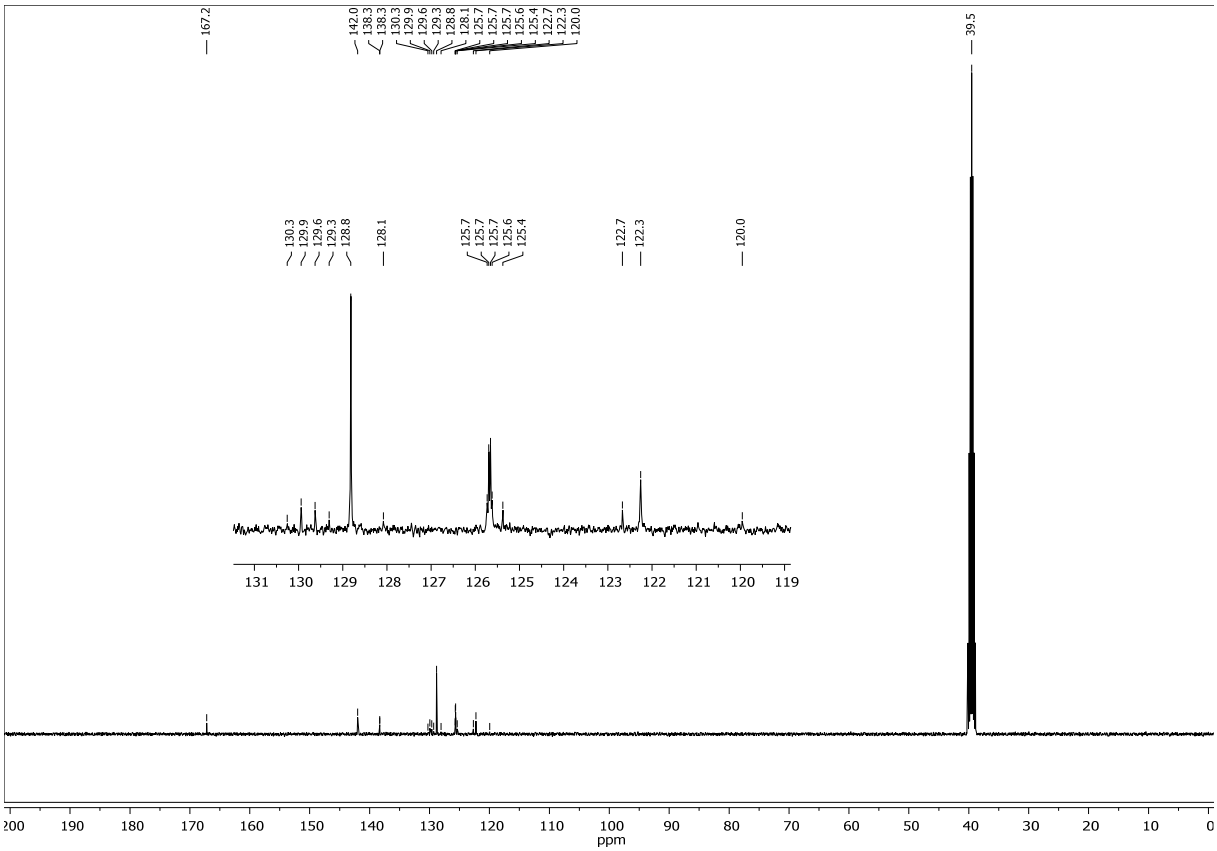
167.2
142.0
138.3
138.3
130.3
129.9
129.6
129.3
128.8
128.1
125.7
125.7
125.7
125.6
125.4
122.7
122.3
120.0
39.5
ppm

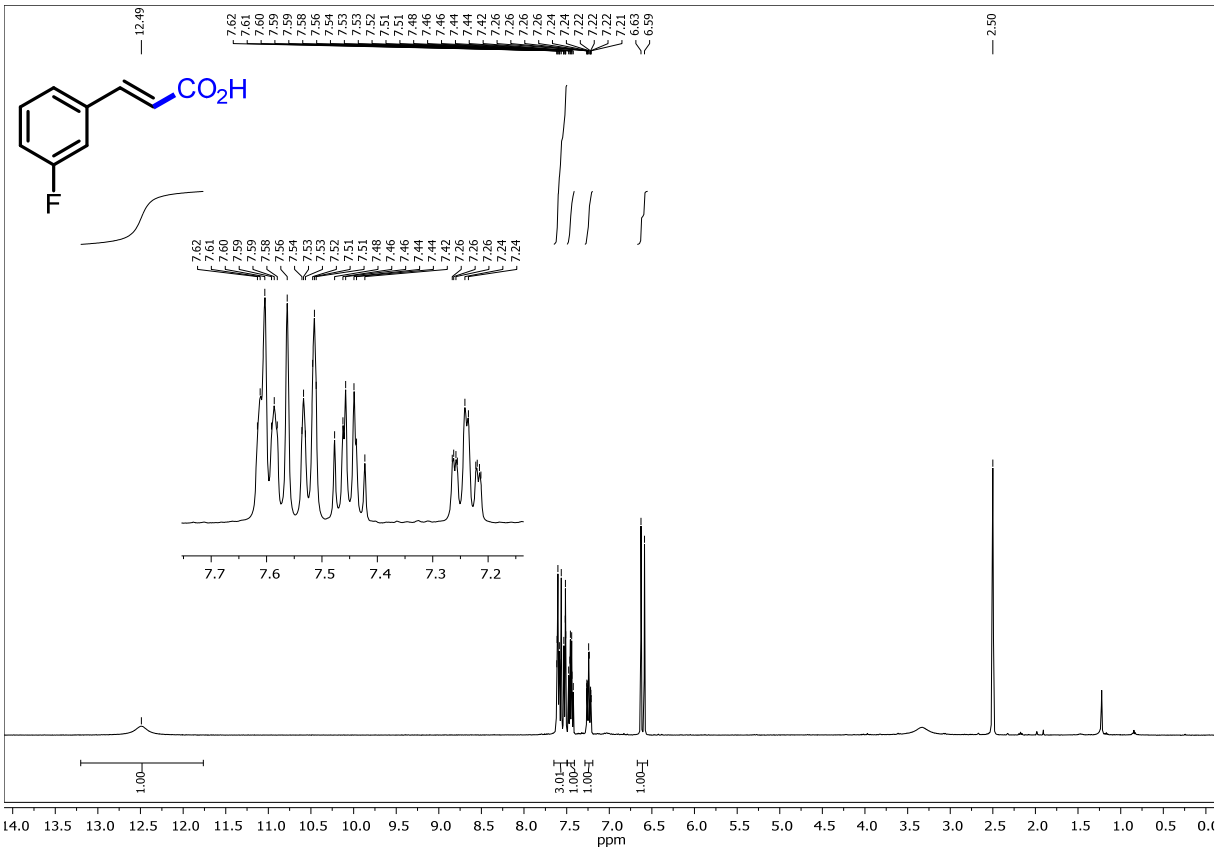
12.49
7.62
7.61
7.60
7.59
7.59
7.59
7.58
7.56
7.54
7.53
7.53
7.52
7.51
7.51
7.51
7.48
7.46
7.46
7.44
7.44
7.42
7.26
7.26
7.26
7.26
7.24
7.24
7.22
7.22
7.22
7.21
6.63
6.59
2.50
CO2H
F
1.00
3.01
1.00
1.00
1.00
ppm

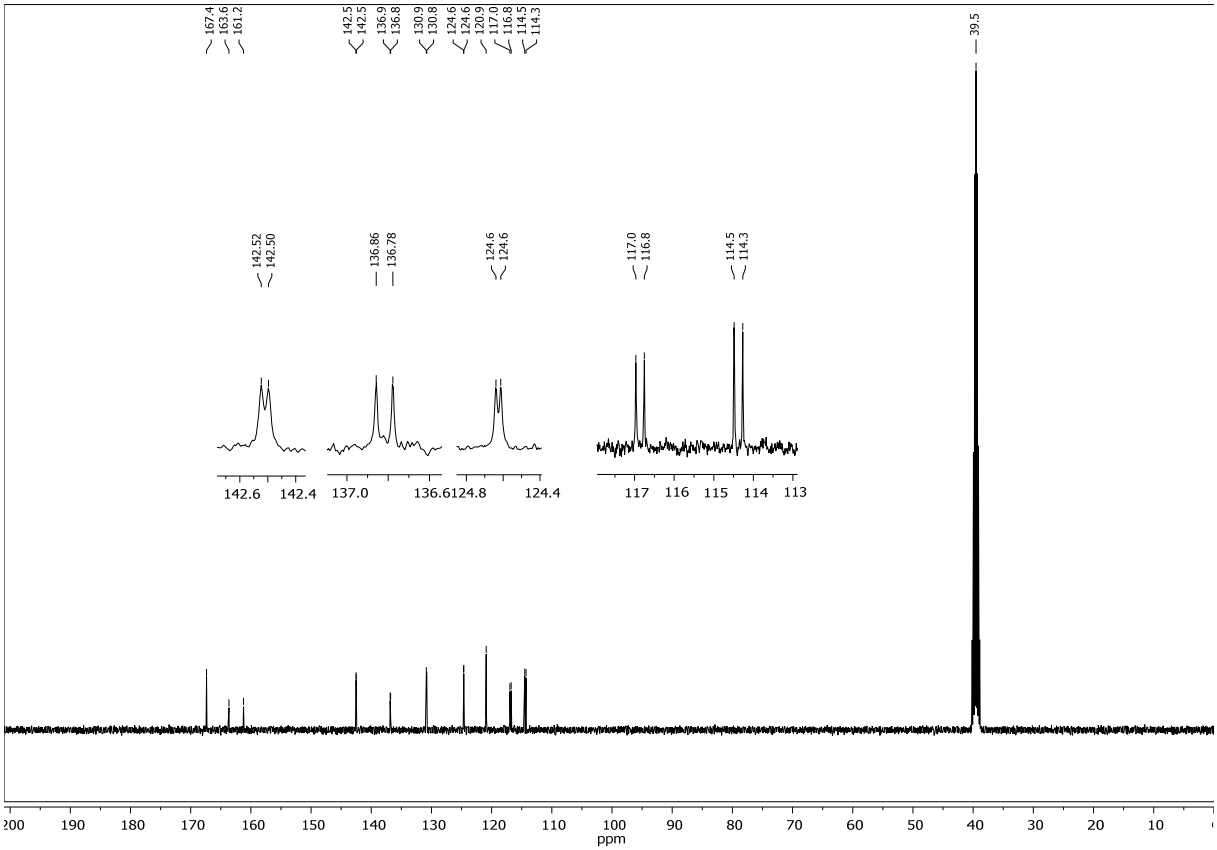
167.4
163.6
161.2
142.5
142.5
136.9
136.8
130.9
130.8
124.6
124.6
120.9
117.0
116.8
114.5
114.3
39.5
142.52
142.50
136.86
136.78
124.6
124.6
117.0
116.8
114.5
114.3
ppm

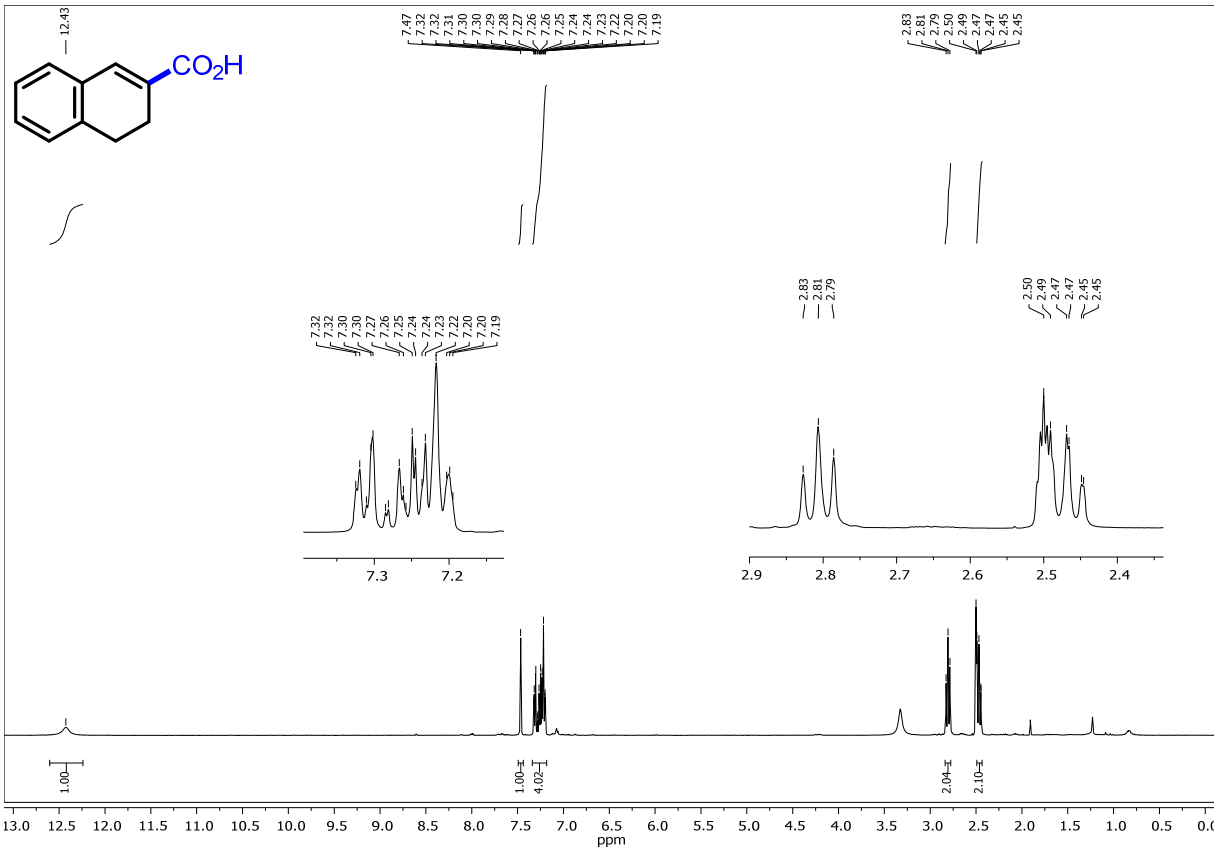
12.43
CO2H
7.47
7.32
7.32
7.31
7.30
7.30
7.29
7.28
7.27
7.27
7.26
7.26
7.25
7.24
7.24
7.23
7.22
7.20
7.20
7.19
2.83
2.81
2.79
2.50
2.49
2.47
2.47
2.45
2.45
1.00
1.00
4.02
2.04
2.10
ppm

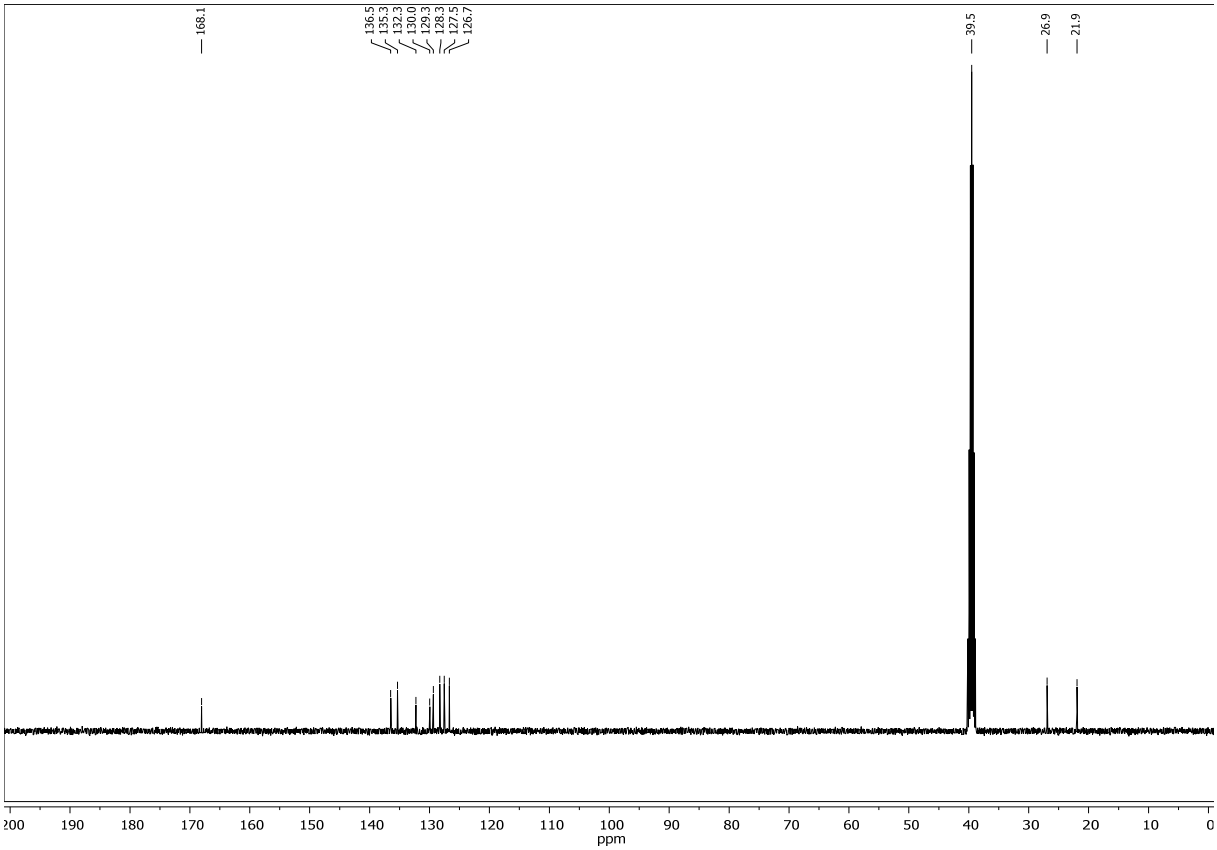
168.1
136.5
135.3
132.3
130.0
129.3
128.3
127.5
126.7
39.5
26.9
21.9
ppm

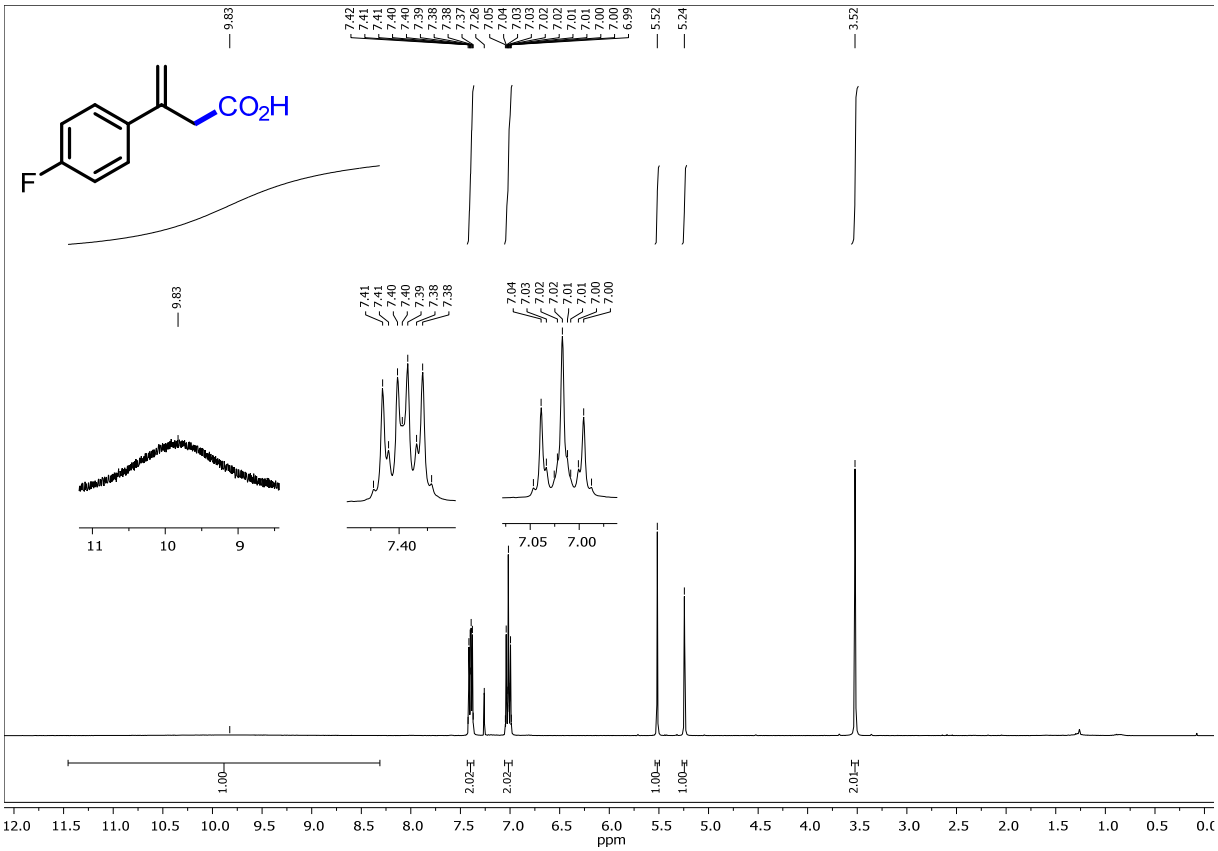
CO2H
F
ppm

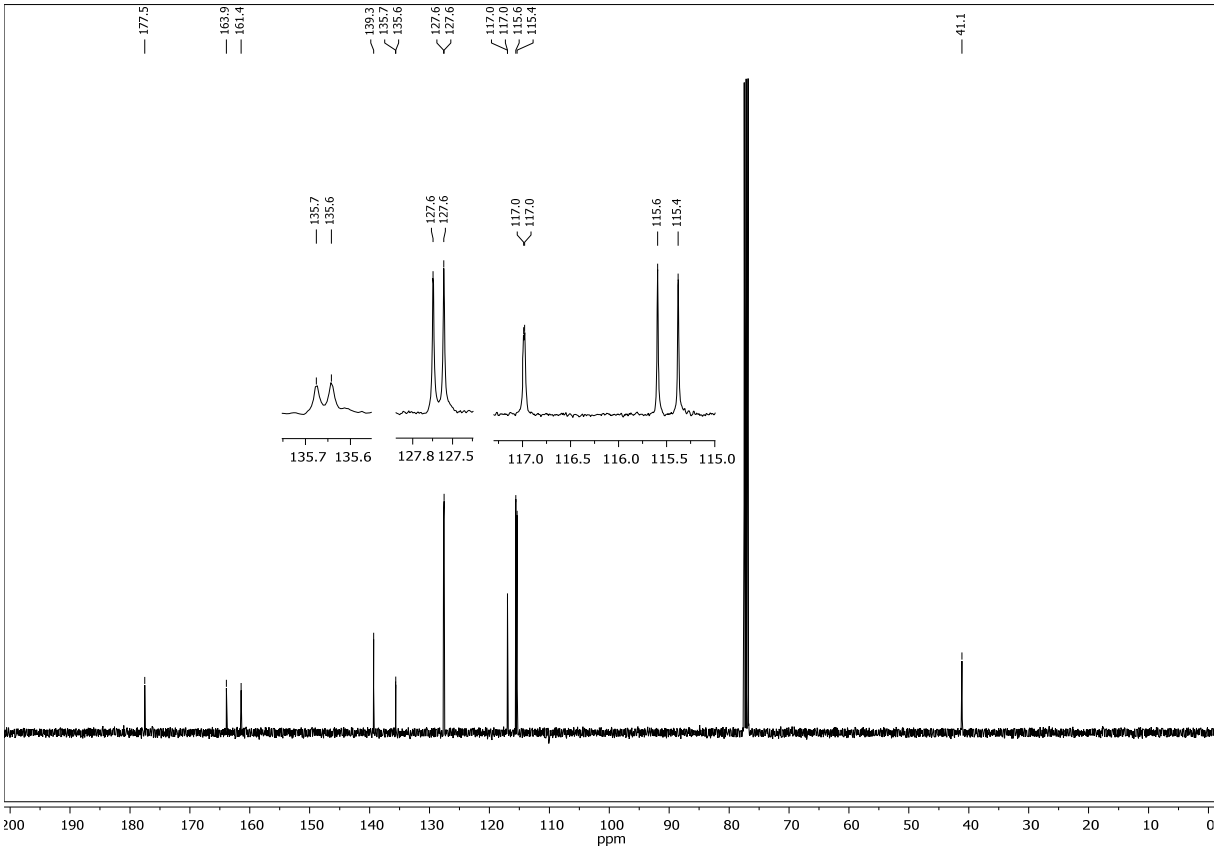
ppm

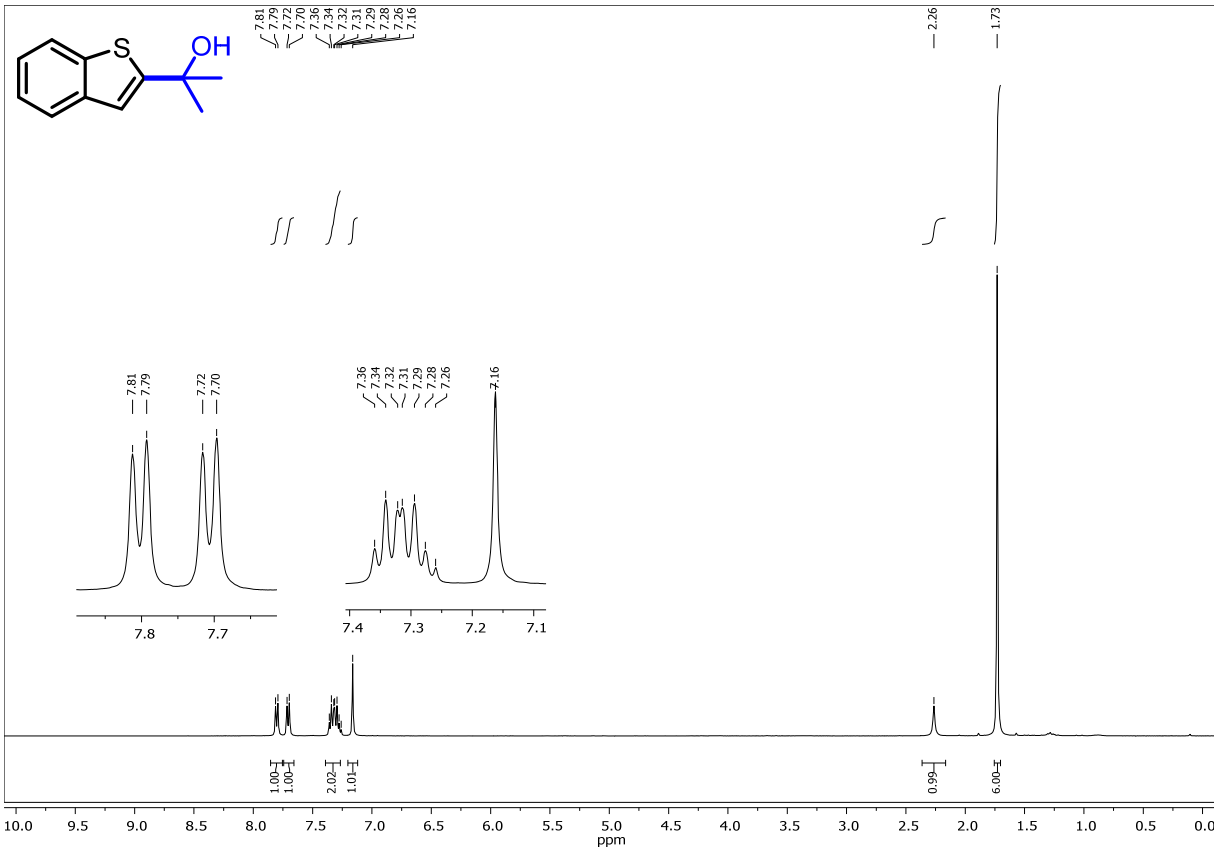
S
OH
7.81
7.79
7.72
7.70
7.36
7.34
7.32
7.31
7.29
7.28
7.26
7.16
2.26
1.73
1.00
1.00
2.02
1.01
0.99
6.00
ppm

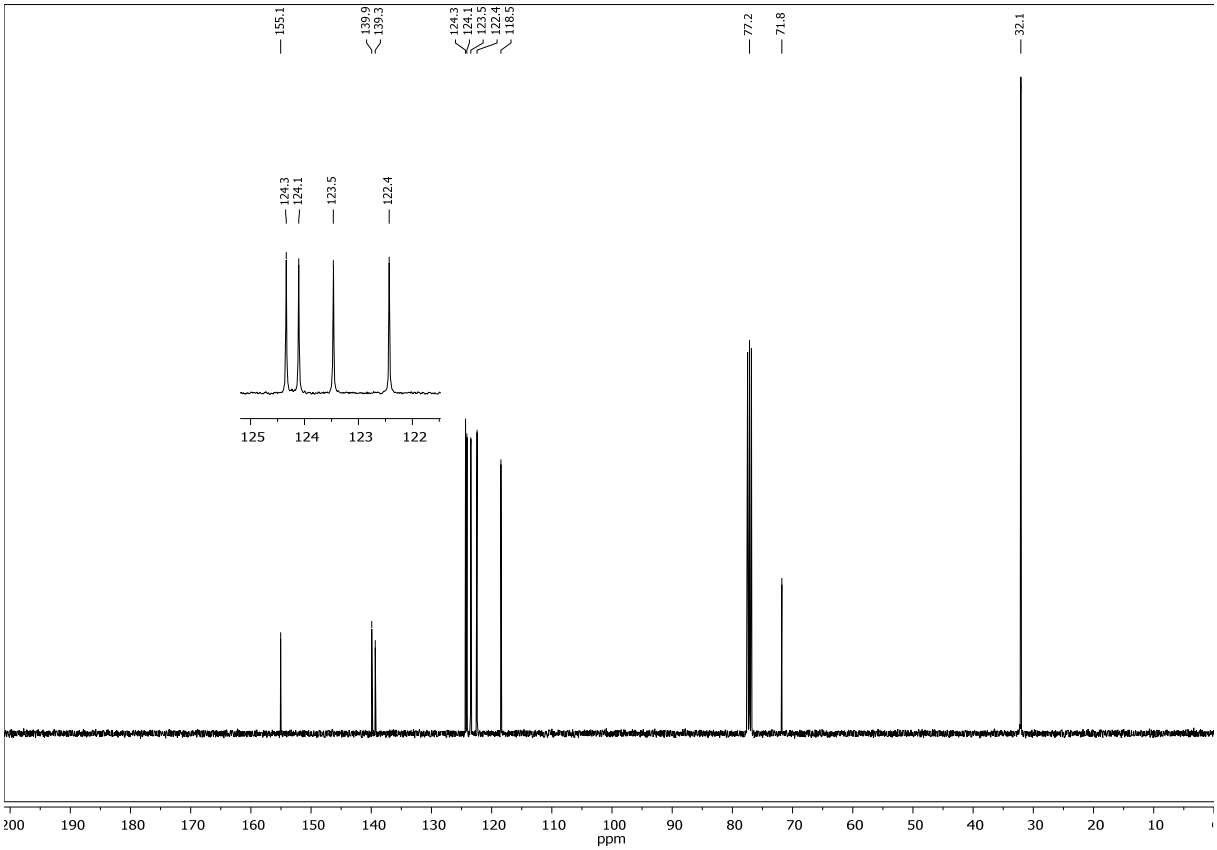
155.1
139.9
139.3
124.3
124.1
123.5
122.4
118.5
77.2
71.8
32.1
ppm

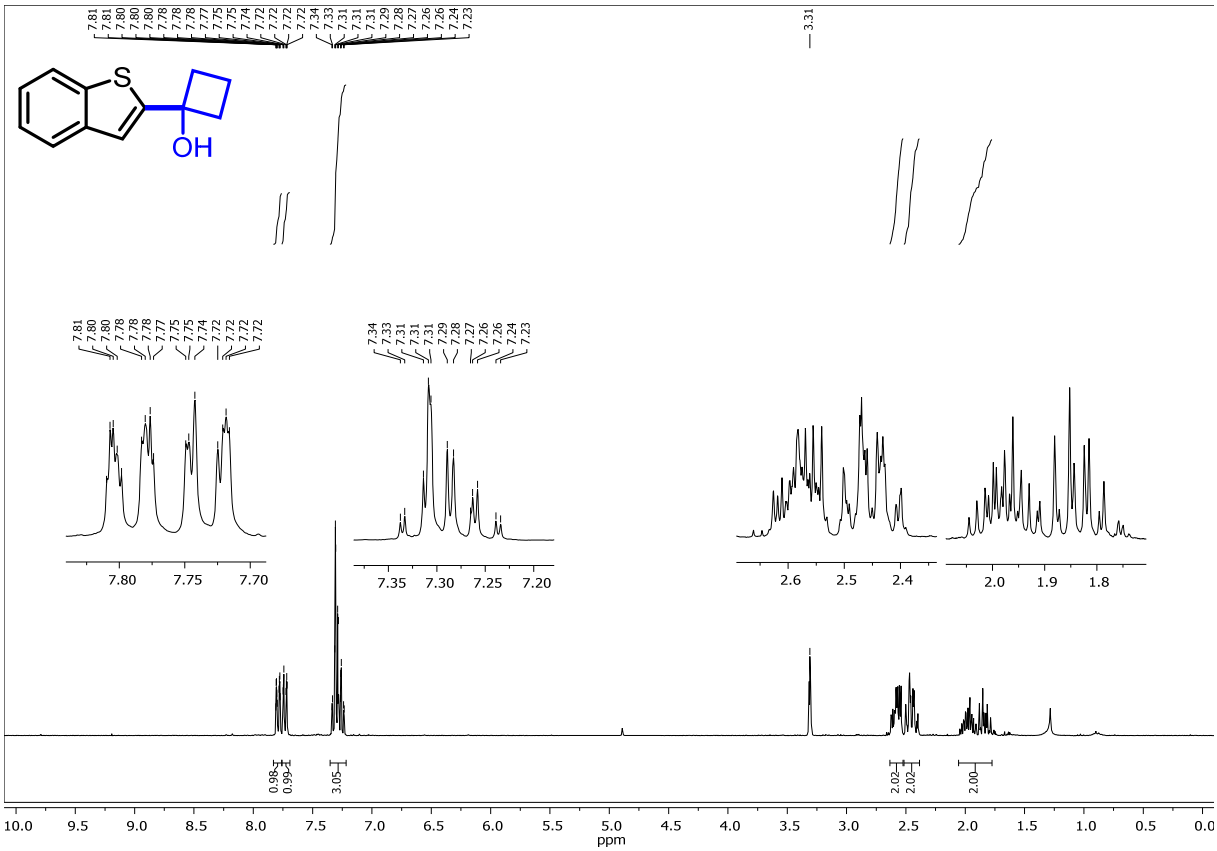
S
OH
7.81 7.81 7.80 7.80 7.80 7.78 7.78 7.77 7.75 7.75 7.74 7.72 7.72 7.72 7.34 7.33 7.31 7.31 7.31 7.29 7.28 7.27 7.26 7.26 7.24 7.23
3.31
7.80 7.75 7.70
7.35 7.30 7.25 7.20
2.6 2.5 2.4
2.0 1.9 1.8
0.98 0.99 3.05 2.02 2.02 2.00
ppm

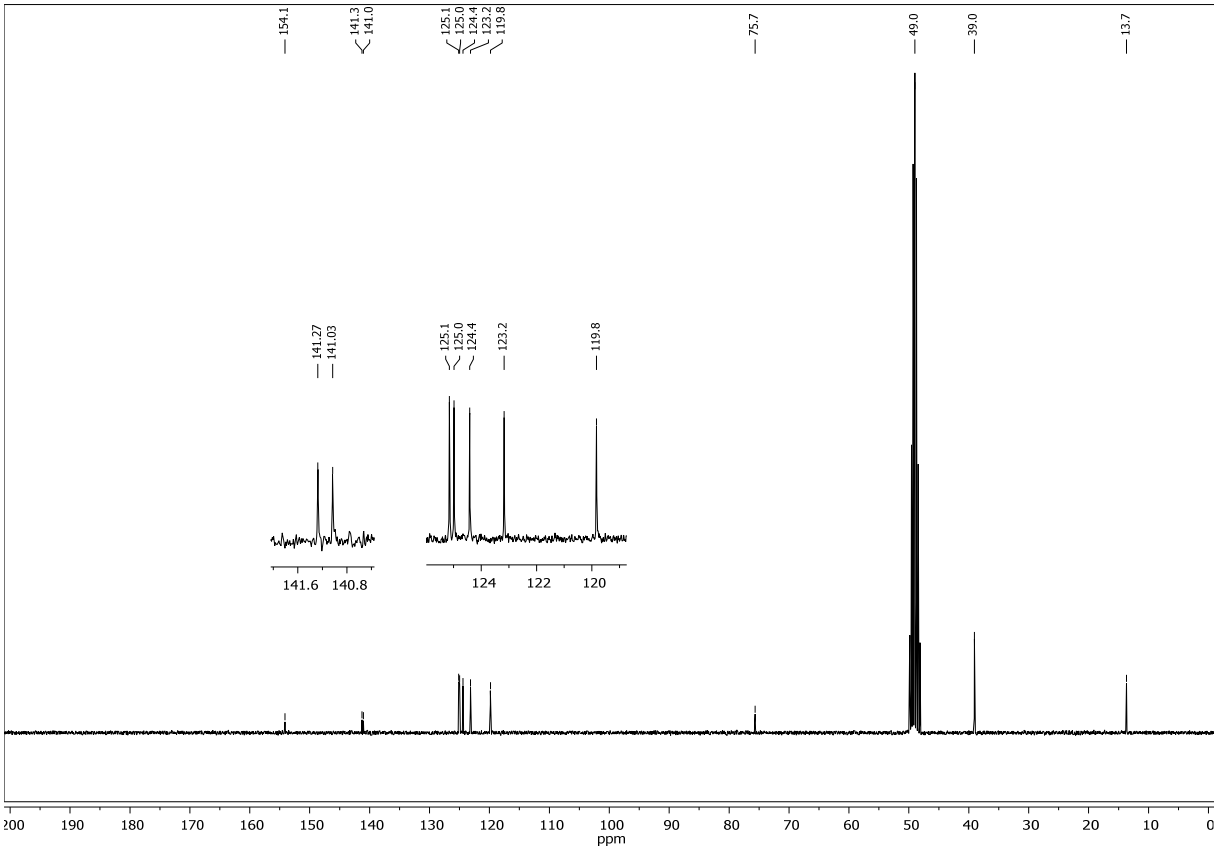
154.1
141.3 141.0
125.1 125.0 124.4 123.2 119.8
75.7
49.0
39.0
13.7
141.27 141.03
141.6 140.8
124 122 120
ppm

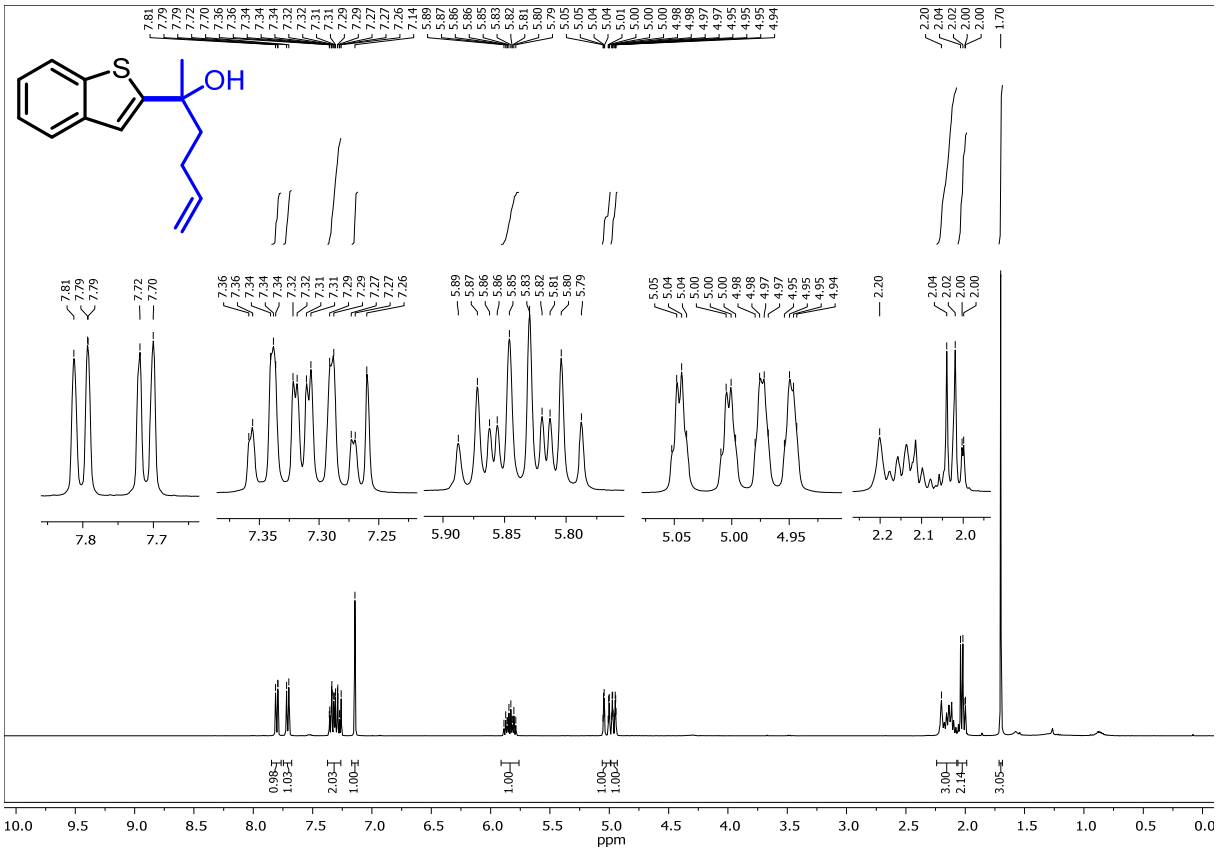
S
OH
ppm

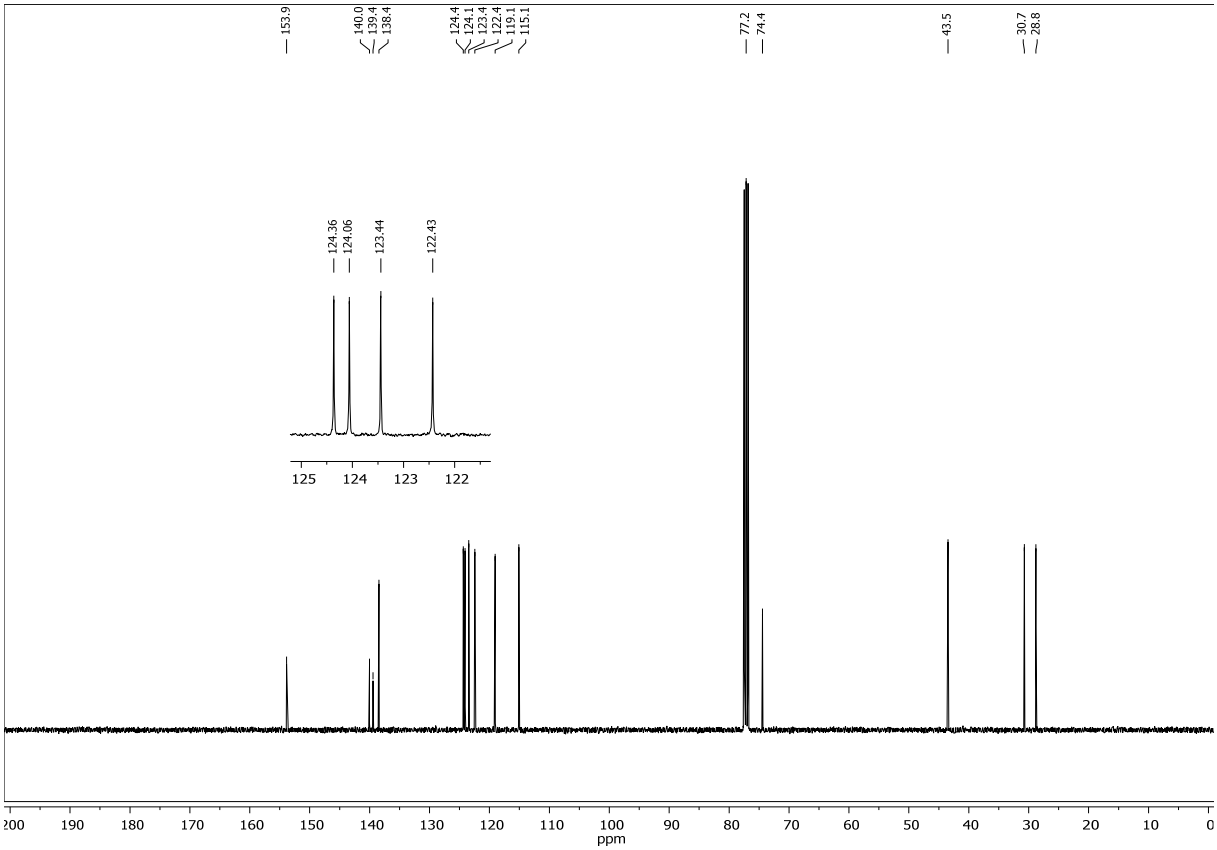
ppm

6 - Mechanistic Studies

6.1 - General Procedure for High-throughput Screening of Arenes

To a paradox 96-well plate fitted with 0.5 mL glass vials containing magnetic stirrer bars was added the arene (0.03 mmol) and 2,3,6,7-tetramethoxyanthracen-9(10*H*)-one (2.0 mg, 20 mol%). The vials were partially-sealed and transferred to a glovebox antechamber after the vial had evacuated and refilled with N_2 (3×) within the antechamber. DMSO (0.3 mL) was dispensed to each of the vials followed by 1,1,3,3-tetramethylguanidine (11 μL, 0.09 mmol) and the plate was sealed with the plate lid, two rubber mats and a Teflon TFA film. The plate was then removed and transferred to a glove-bag filled with an over-pressure of CO_2. The plate was then unsealed and placed on a stirrer plate with 3×456 nm Kessil lamps clamped overhead. The vial was then irradiated from above by two kessil lamps (vials approximately 10 cm away from the light source). After 18 hrs the irradiation was stopped and the plate was removed from the glove bag and quenched with aq. HCl (0.2 mL, 0.5M) and samples were taken and filtered before being placed on a plastic 96 well plate for HPLC analysis.

Figure S9. a) photo showing the removal of the plate lid within the CO_2 glove-bag for mass screening of substrates. **b)** 96 well plate reactions running in the CO_2 glove-bag set up.

6.2 - Deuterium Labeling Experiments

Upon formation of an arene radical anion **3q**-I we envisioned a H/**D** exchange reaction giving rise to **3q-II** in presence of a deuterium source. After reoxidation and deprotonation **3q**-**D** would be formed (Scheme S3).

To a dry flat-bottomed crimp vial (5 mL) equipped with stirring bar, was added **3q** (0.1 mmol) and 2,3,6,7-tetramethoxyanthracen-9(10*H*)-one (6.3 mg, 0.02 mmol, 20 mol%, only for entry 1-3 Table S3). Cs_2CO_3 (98 mg, 3 equiv.) was quickly added and the vial was sealed with a Supelco aluminium crimp

seal with septum (PTFE/butyl). The vial was then evacuated and refilled with N_2 (5×) *via* syringe needle. The reaction mixture was dissolved in DMSO-d6 (1 mL, dry and degassed by bubbling with N_2) and the deuterium source was added *via* syringe. The vial was then irradiated from the bottom side with blue LED light and a constant reaction temperature (25°C) was maintained by employing a water-cooling circuit connected to a thermostat. After 18 hrs of reaction time the reaction was quenched by the addition of water and the crude mixture was extracted with Et_2O (3×). The combined organic layers were dried over Na_2SO_4, concentrated and purified *via* flash silica column chromatography using a mixture of hexanes and DCM (95:5) as eluent. The obtained product was dried in vacuo and analyzed by ^{1}H-NMR (Table S3 and Figures S10a-b) and GC-MS (Figure S10c).

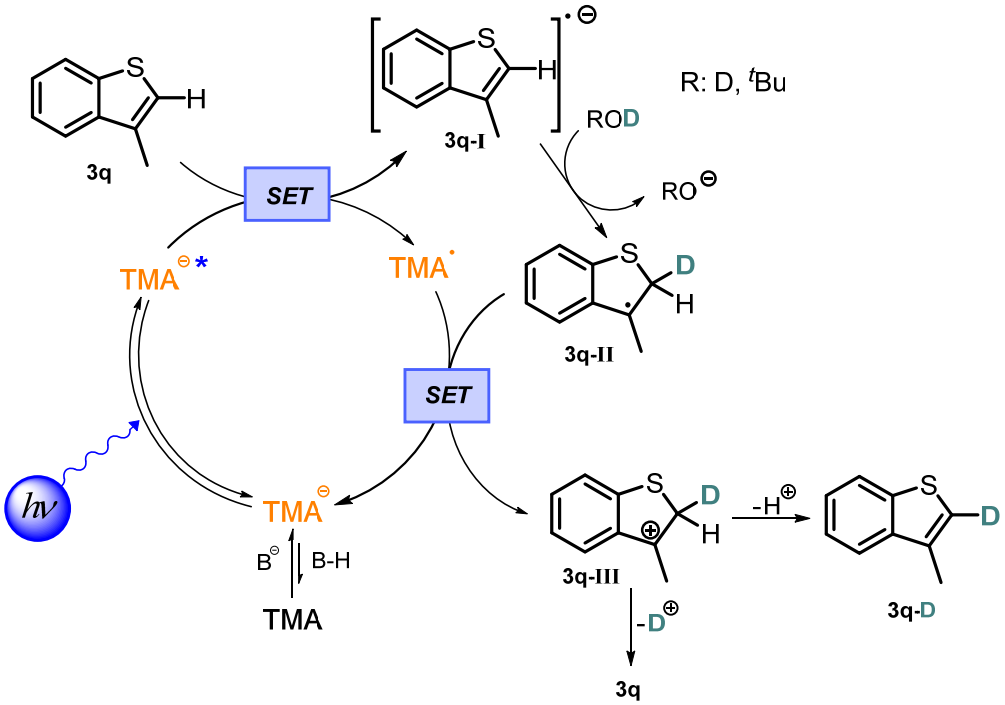

Scheme S3. Proposed mechanism for the deuterium labeling experiments using **3q** as substrate.

Table S3. Deuterium labeling experiments

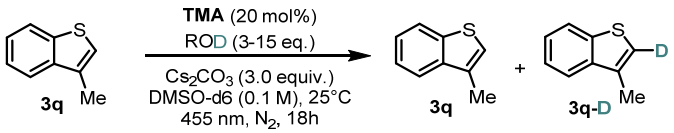

entry	catalyst	λ [nm]	D-source (eq.)	D-incorporation [%][a]
1	**TMAH**	455	D_2O (3)	10
2	**TMAH**	455	D_2O (15)	14
3	**TMAH**	455	^{t}BuOD (10)	15
4[b]	-	dark	D_2O (15)	<1

[a] determined by ^{1}H-NMR integration upon isolation and purification of the reaction mixture; [b] reaction was stirred in the dark.

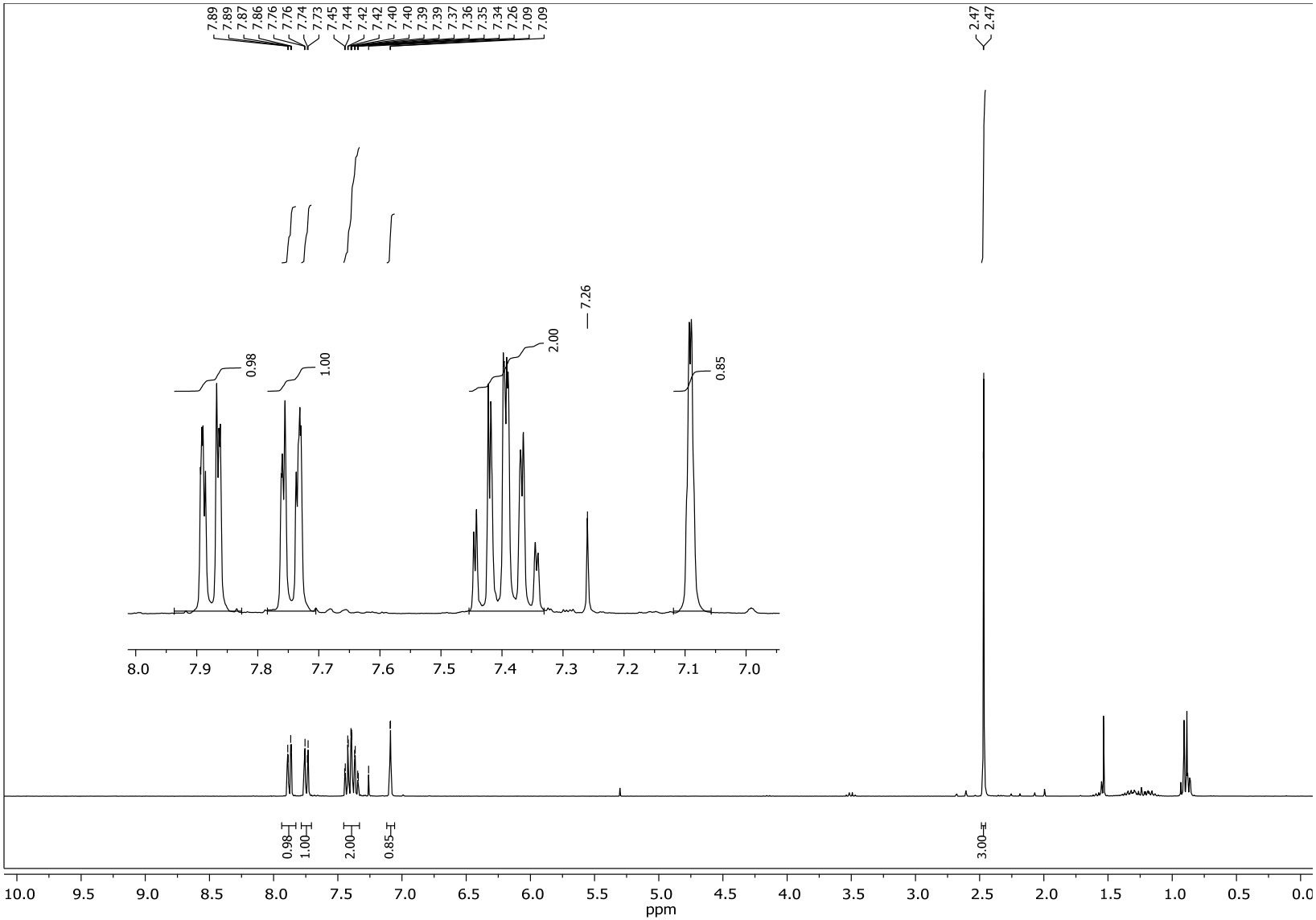

Figure S10a. [1]H-NMR recorded after reaction work-up and column chromatography according to entry 3, Table S3. The signal at 7.1 ppm corresponds to the proton in position 2 of **3q**. Peak integration revealed a slightly reduced value of 0.85. The signal at 7.75 ppm served as reference and was set to integral 1.00.

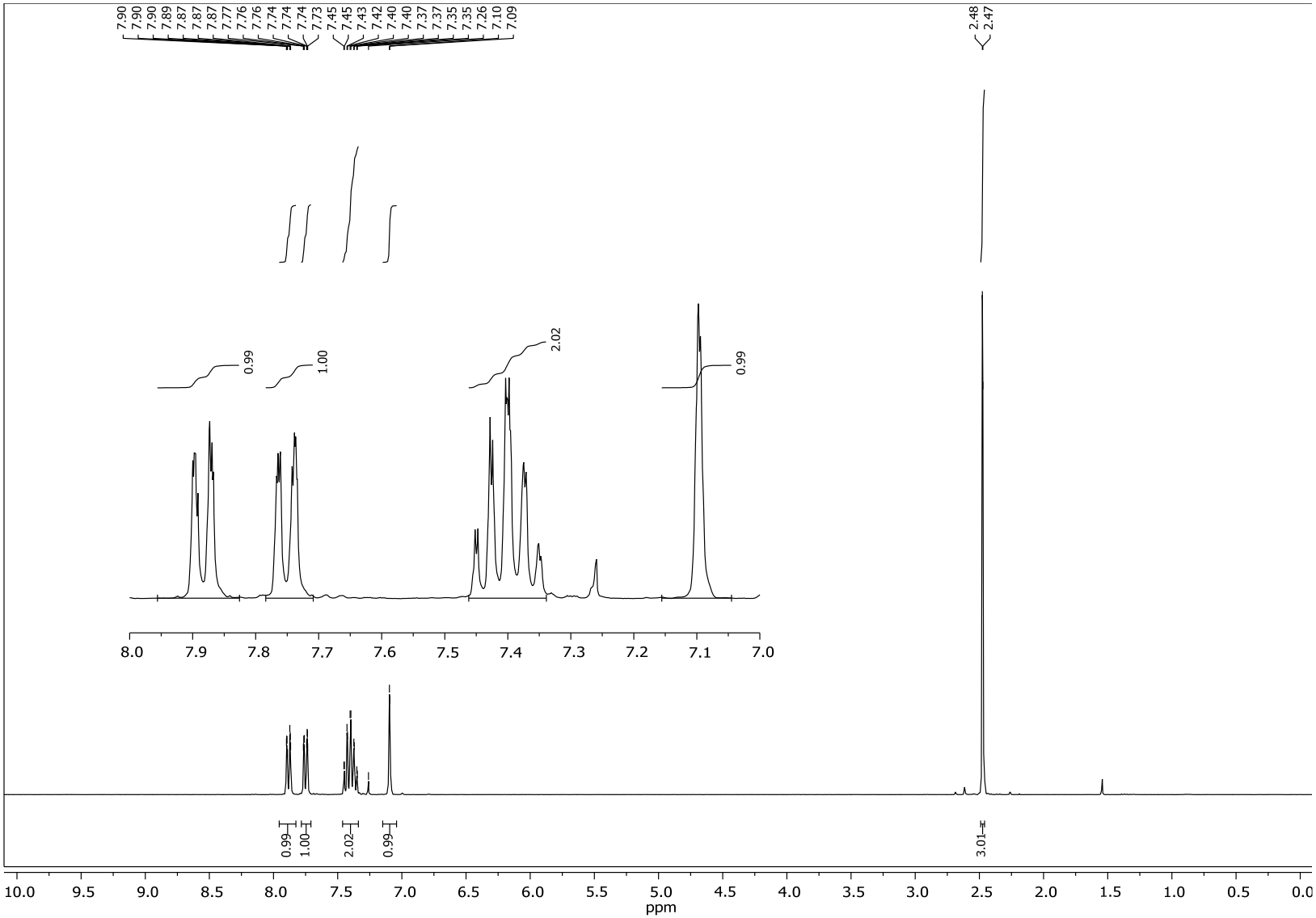

Figure S10b. [1]H-NMR recorded after reaction work up and column chromatography according to entry 4, Table S3. The signal at 7.1 ppm corresponds to the proton in position 2 of **3q**. Peak integration revealed a value of 0.99. The signal at 7.75 ppm served as reference and was set to integral 1.00.

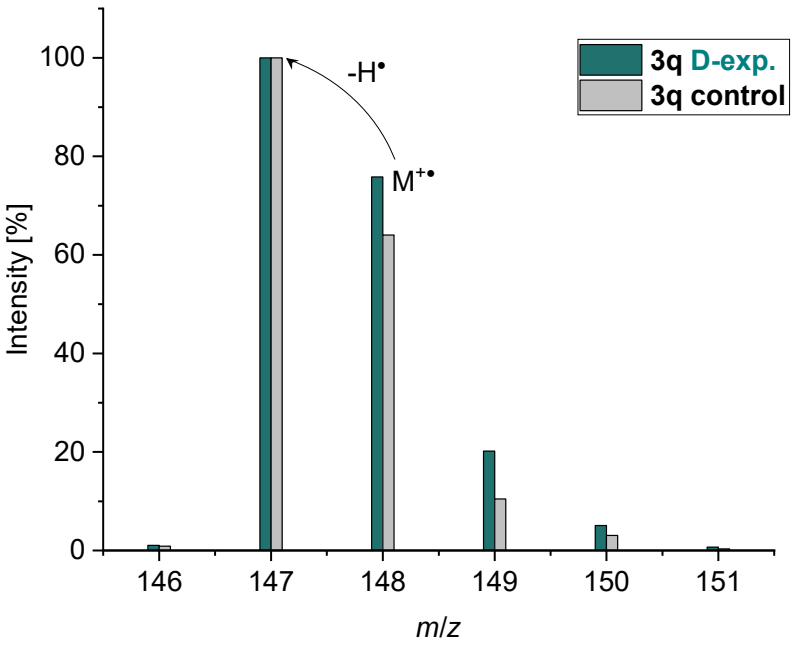

Figure S10c. GC-MS analysis after reaction work up and column chromatography according to entry 3 from Table S3 (green) and purchased **3q** (grey). Mass spectra was recorded upon electron impact ionization (70 eV). The ionized **3q** is prone to lose a hydrogen atom causing the most intense peak at *m*/*z* 147.

Figure S10a shows the ^{1}H-NMR spectrum from the isolated product of the deuterium labeling experiment in presence of ^{t}BuOD (entry 3, Table S3). Integration over the signal at 7.1 ppm, which corresponds to the proton in position 2 of benzothiophene **3q**, revealed a slightly decreased value (0.85 instead of 1.00). This deviance can be explained by the partial exchange of hydrogen by deuterium.

Figure S10b shows the ^{1}H-NMR spectrum from the isolated product of the control reaction (entry 4, Table S3). Integration over the signal at 7.1 ppm gave a value close to unity and suggests no or only traces of incorporated deuterium.

In addition to ^{1}H-NMR analysis, the incorporation of deuterium was verified by GC mass. Compared to the set of peaks caused by the purchased starting material **3q** (Figure S10c, grey), the different ratios in the isotope pattern suggest the partial incorporation of deuterium into the product isolated upon deuterium labeling reaction (entry 3, Table S3).

6.3 - Time-resolved Luminescence Quenching studies

A first prediction regarding possibly working substrates was made by time-resolved luminescence quenching of the photoexcited catalyst. If there is an interaction between the excited PC and the substrate (electron transfer is proposed), the luminescence lifetime is shortened. Such processes can be easily followed by luminescence lifetime analysis and from the data obtained a Stern-Volmer plot of the time-resolved experiment was developed (Figure S11a-d and S13). A linear correlation between concentration of quencher [Q] and $\tau_0 \times \tau^{-1}$ indicates a dynamic luminescence quenching. The luminescence lifetime was recorded in dry, degassed DMSO in presence of cesium carbonate by using a quartz cuvette (1×1 cm) with septum screw cap. The cuvette was degassed *in vacuo* and backfilled with N_2 (5×) before the stock solution of quencher and the catalyst solution were added *via* syringe. A **TMAH** concentration of c(TMAH) = 40 µM in the cuvette was used for all experiments. For excitation of the sample, a 452 nm laser diode was used and an optical longpass filter (cut-on wavelength 500 nm) was installed before the detection unit. The time range for the measurement was set to 400 ns. The experimental data were fitted with a mono-exponential function. The quenching experiment using CO_2 as quencher was recorded as described above using a CO_2-saturated DMSO solution. The approximated concentration of dissolved CO_2 was calculated from literature data.[41]

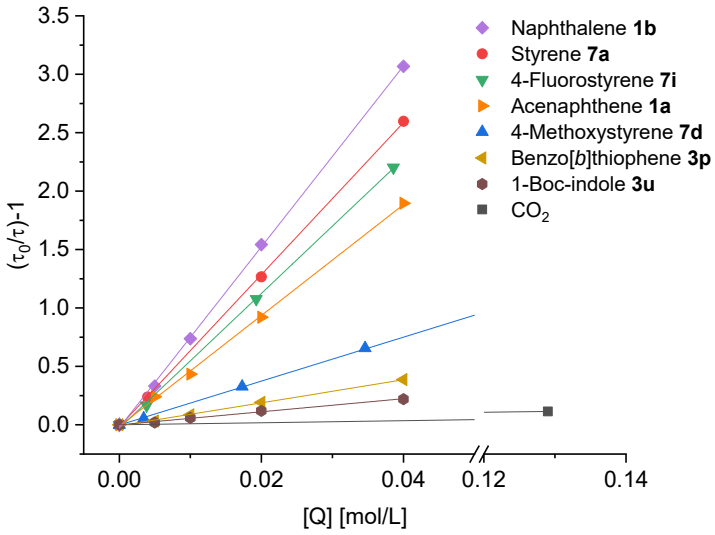

Figure S8a. Stern-Volmer plot developed with data obtained from time-resolved quenching experiments of **TMAH** in presence of Cs_2CO_3 with tolerated substrates and a CO_2-saturated solution of DMSO.

Thiophene derivatives **3c**, **e**, **j** are excellent quenchers and are tolerated in the carboxylation reaction whereas benzo[*b*]thiophene (**3p**) was found to quench the excited state of $\mathbf{TMA}^{-}$, however less efficiently. No quenching was observed in presence of thiophene and no carboxylation occurred when thiophene was used as substrate under the optimized reaction conditions (Figure S11b). The tested N-heteroarenes containing at least one nitrogen are quenching the excited photocatalyst. However, carboxylation products were only obtained using **3u** (Figure S11a) or **3w** (Figure S11c). Using acetone

9a as electrophile instead of CO_2 gave rise to the respective tertiary alcohol **9pa**. Quenching studies revealed that adding acetone (up to 2000 eq. regarding to catalyst concentration) does not quench the photoexcited **TMA**$^-$ (Figure S11d), supporting the hypothesis of a nucleophilic arene radical anion which attacks the electrophile.

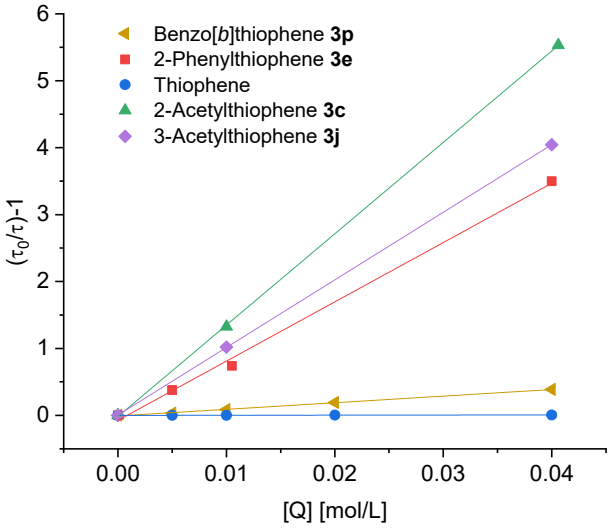

Figure S9b. Stern-Volmer plot developed with data obtained from time-resolved quenching experiments of **TMAH** in presence of Cs_2CO_3 with thiophene derivatives. In case of thiophene, no quenching was observed. No carboxylation occurred using thiophene as substrate under the optimized reaction conditions.

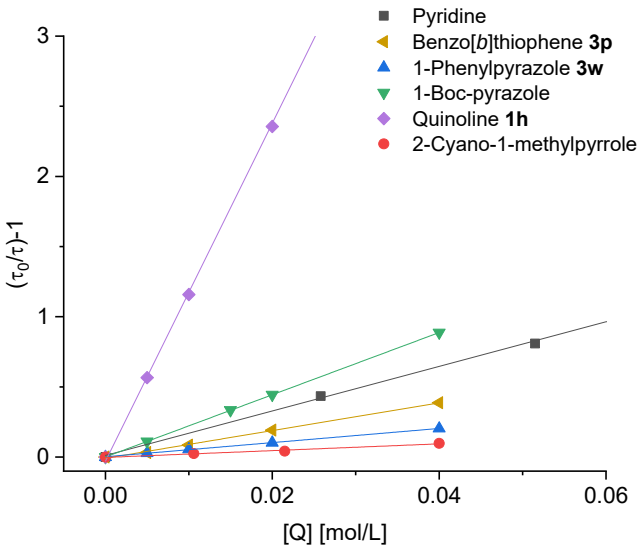

Figure S10c. Stern-Volmer plot developed with data obtained from time-resolved quenching experiments of **TMAH** in presence of Cs_2CO_3 with *N*-heteroarenes and benzo[*b*]thiophene as reference.

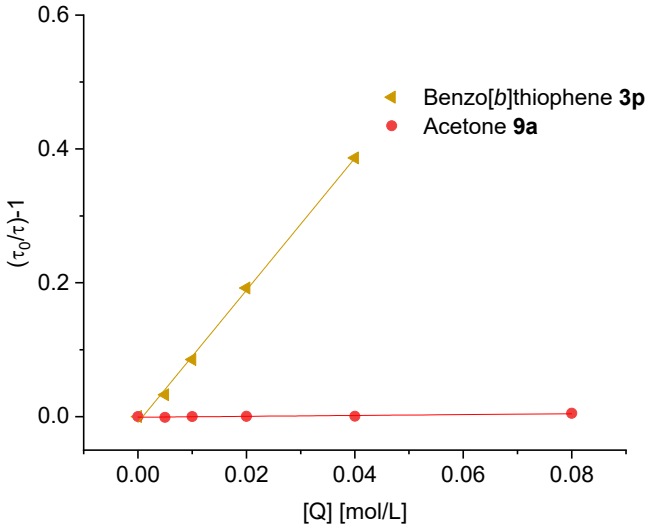

Figure S11d: Stern-Volmer plot developed with data obtained from time-resolved quenching experiments of **TMAH** in presence of Cs_2CO_3 with acetone and benzo[*b*]thiophene as reference.

6.4 - Computational Analysis

Screening density functional theory (DFT) calculations were performed on substrates and radical anions to derive molecular and atomic properties that could rationalize the reaction outcomes. Geometries were optimized using the B3LYP-D3[42] *a posteriori*-corrected hybrid functional[43] with the LACVP**+ basis set, and final energies and atomic properties were calculated using B3LYP-D3/LACV3P**+ together with the PBF solvation model[44] for DMSO. The calculations were performed within the Schrödinger Small-Molecule Drug Discovery Suite 2019-2 using Jaguar version 10.4.[45] To facilitate convergence to a minimum, any apparent symmetry in the starting geometry was ignored in the optimizations (isymm=0). To facilitate SCF convergence for some radical anions the use of the pseudospectral method was turned off during all calculations (nops=1; ***J*** and ***K*** operators constructed from analytic two-electron integrals; no grid used). For each substrate and radical anion, Atomic Fukui indices, Mulliken charges and the spin population were calculated. The electron affinity for each substrate was roughly estimated by the direct DFT energy difference between the radical anion and the substrate and are given in kcal mol^{-1}.

As seen in Figures S10-13, there is a strong correlation with reactivity and a positive outcome and calculated atomic descriptors and estimated electron affinities. However, there are also substrates that seem to fall within the acceptable range of estimated electron affinity, atomic charge, spin distribution and nucleophilicity that does not yield the desired products. This could be due to subsequent spontaneous decarboxylation as for **3u** (requiring trapping the carboxyl acid as an ester) or the presence of non-tolerated functional groups. According to the calculations, the regioselectivity is most strongly correlated to the Mulliken spin population.

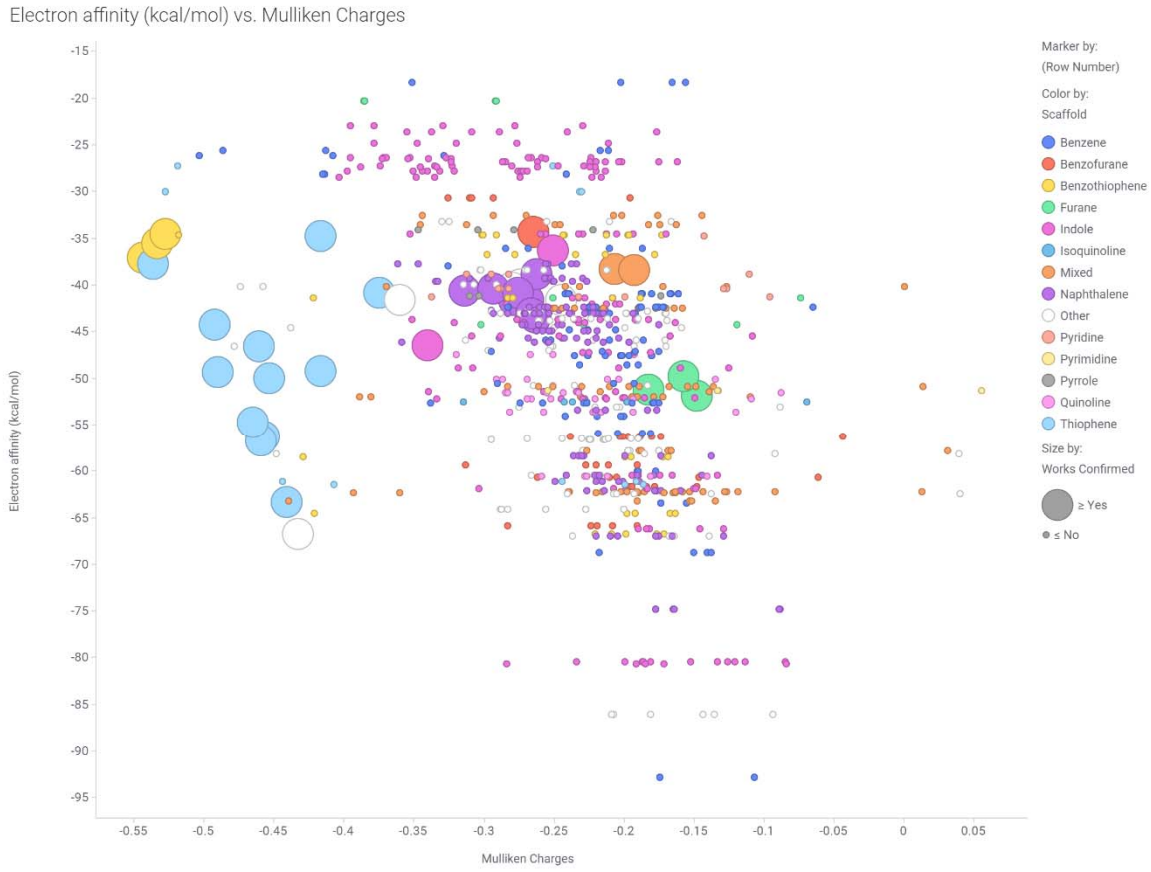

Figure S12a. A plot of the DFT estimated electron affinities (kcal mol^{-1}) *vs*. Mulliken charges of the radical anions for the carbons reacting with CO_2 and for all CH carbons in the aromatic rings of non-reacting substrates, highlighting that most of the reactive substrates are located within a triangle. Three reacting furanes coloured in green are outliers.

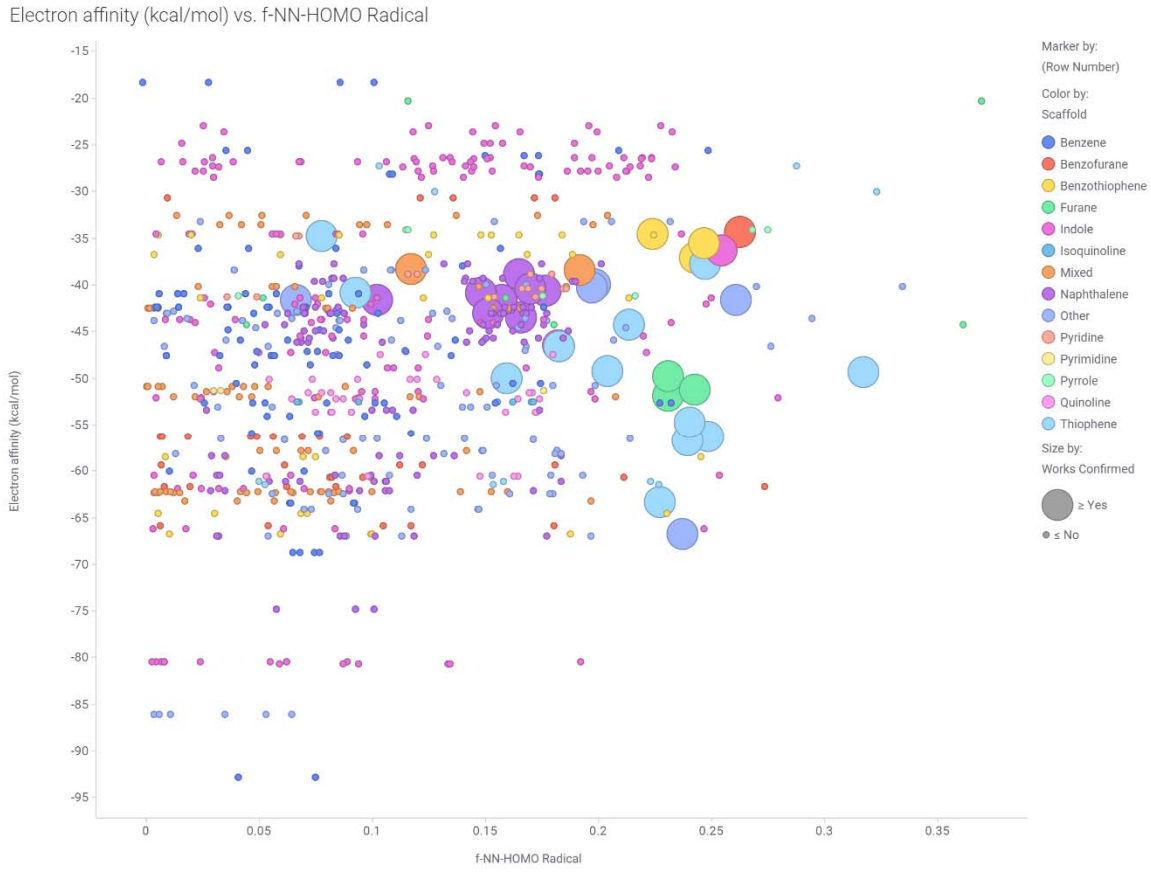

Figure S12b. A plot of the DFT estimated electron affinities (kcal mol^{-1}) *vs*. the Fukui f-NN-index (describing nucleophilicity) of the radical anions for the carbons reacting with CO_2 and all CH carbons in the aromatic rings of non-reacting substrates illustrating that most of the reactive substrates have more nucleophilic radical anions.

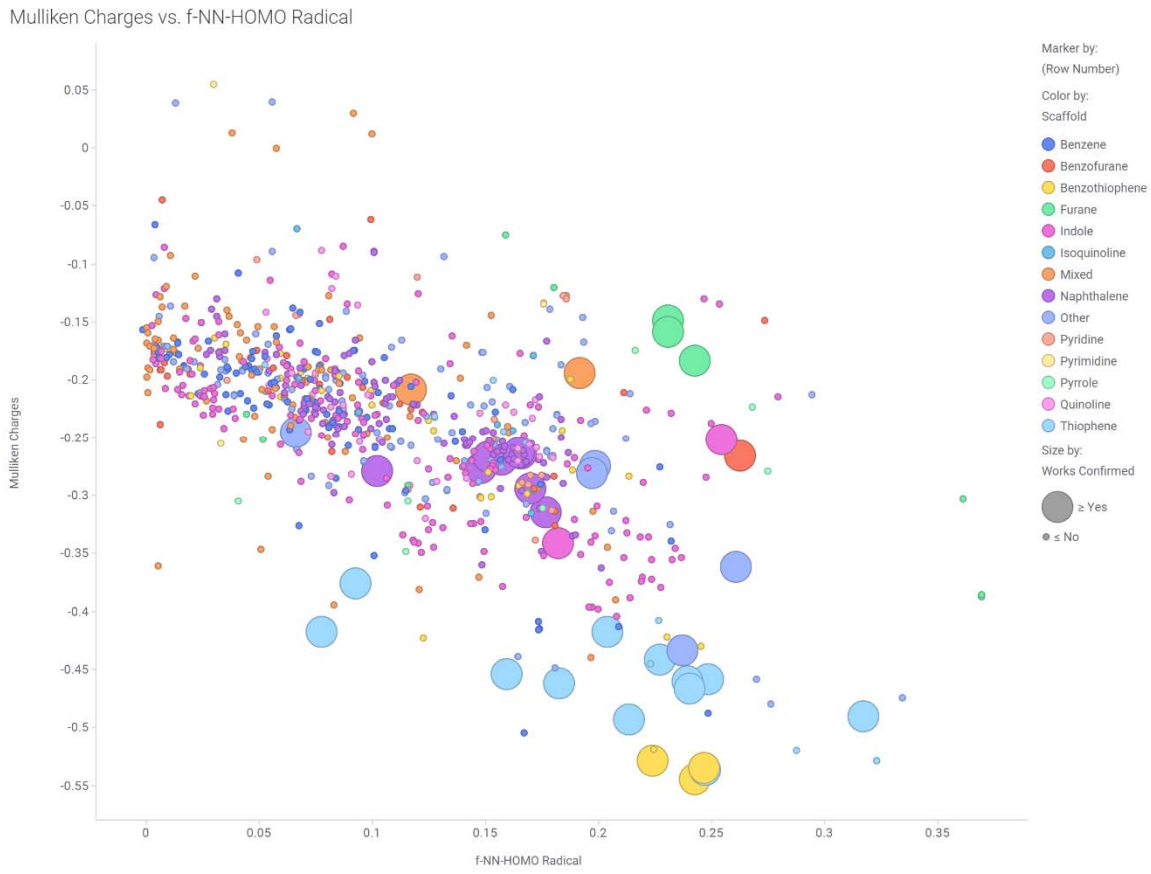

Figure S12c. A plot of the DFT Mulliken charges of the radical anions *vs*. Fukui f-NN-index of the radical anions for the carbons reacting with CO_2 and all CH carbons in the aromatic rings of non-reacting substrates illustrating that most of the non-reactive carbons are less negatively charged and have lower predicted nucleophilicity.

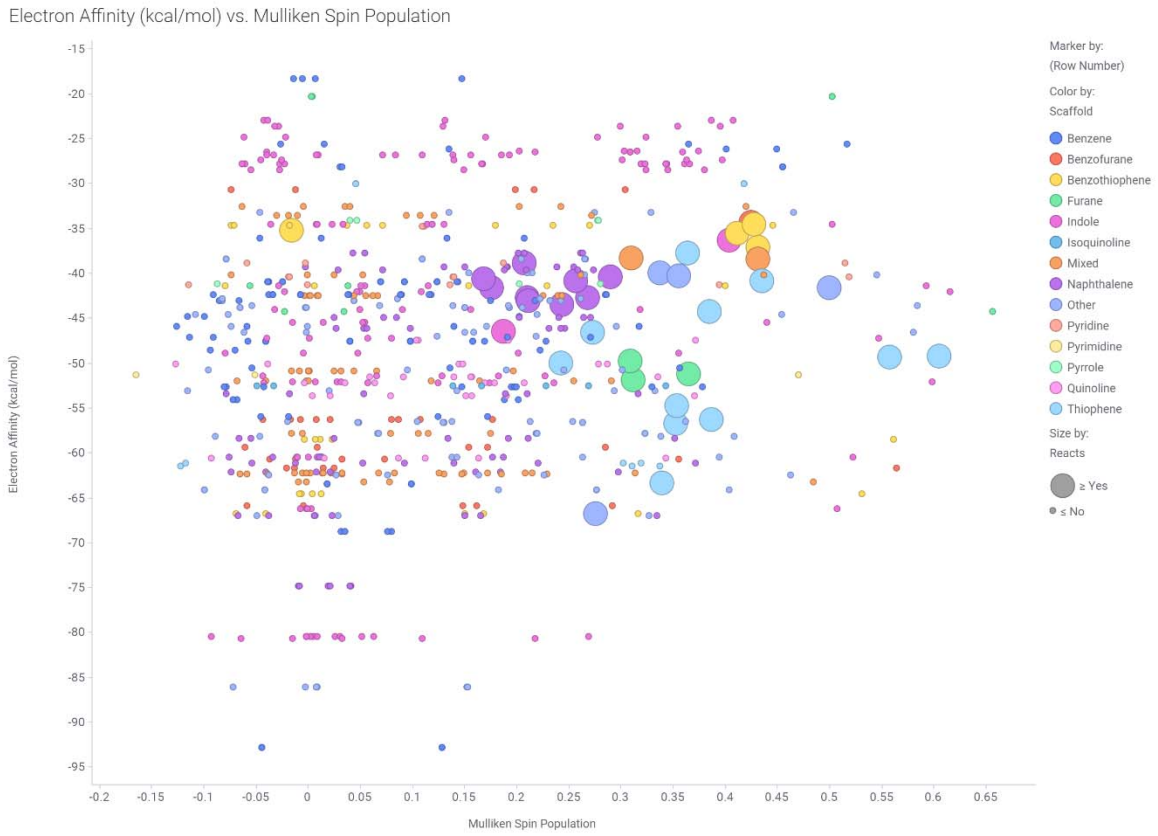

Figure S12d. A zoom in plot of the DFT Mulliken charges of the radical anions *vs.* Fukui f-NN-index of the radical anions for the carbons reacting with CO_2 and all CH carbons in the aromatic rings of non-reacting substrates including only compounds with DFT estimated electron affinities within the values among the substrates that react. Highlighted are substrates with required electron affinities and nucleophilicity but not reacting due to non-compatible functional groups.

7 - Miscellaneous

7.1 - Synthetic route towards FDCA and DMFDC

Modifying the conditions during reaction work-up allows for the direct transformation of the crude reaction mixture of **4r** to either 2,5-furandicarboxylic acid (FDCA) or dimethyl 2,5-furandicarboxylate (DMFDC). Both are important monomers for the manufacture of polyesters derived from biomass (Scheme S4). The reaction work-up with conc. HCl would cause the hydrolysis of the ester giving rise to the dicarboxylic acid FDCA. In contrast, the addition of MeI after releasing the CO_2 overpressure allows for the formation of dimethyl dicarboxylate DMFDC.

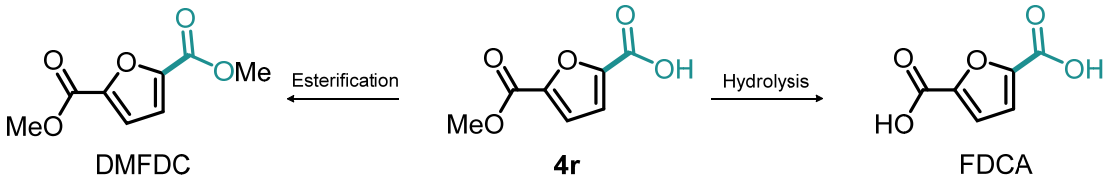

Scheme S4: Synthetic route towards FDCA and DMFDC starting from crude reaction mixture of **4r**.

7.2 - Carboxylation of biphenyl

Biphenyl acts as a good quencher but the resulting carboxylation product [1,1'-biphenyl]-4-carboxylic acid was only obtained in low yield (6%). Nevertheless, this result shows that also benzene derivatives can be activated towards a C–H carboxylation with our method. The thermodynamic driving force for this transformation with CO_2 however seems to be low.

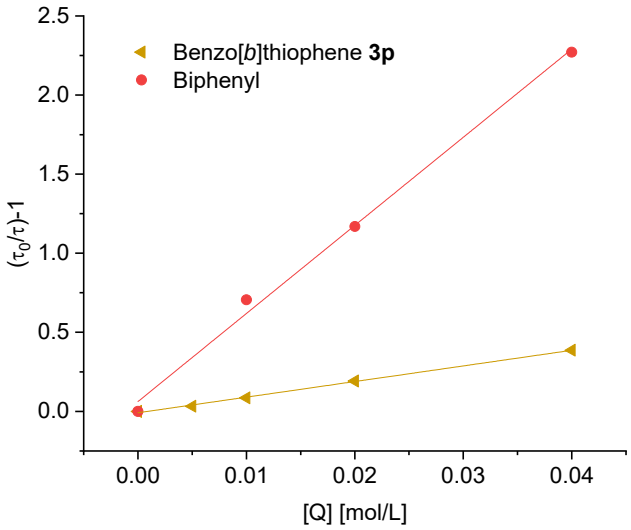

Figure S13. Stern-Volmer plot developed with data obtained from time-resolved quenching experiments of **TMAH** in presence of Cs_2CO_3 with biphenyl and benzo[*b*]thiophene **3p** as reference.

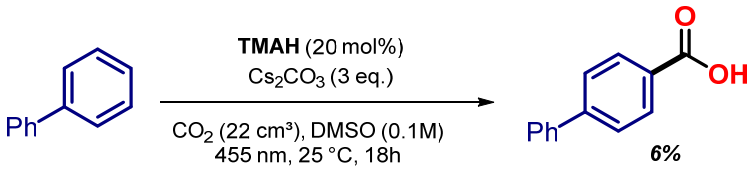

Scheme S5. TMAH-catalyzed carboxylation reaction of biphenyl.

^{1}H-NMR (400 MHz, DMSO-d_6) δ 12.93 (s, 1H), 8.02 (d, J = 8.4 Hz, 2H), 7.80 (d, J = 8.4 Hz, 2H), 7.76 – 7.70 (m, 2H), 7.54 – 7.47 (m, 2H), 7.45 – 7.40 (m, 1H). **HRMS** (ESI+): calculated *m/z* for $C_{13}H_{11}O_2$ $[(M+H)^+]$ 199.0754; found 199.0751.

7.3 - Unsuccessful Substrates

The following substrates (excerpt of examined scope) were found to be not successful under the reported reaction conditions (Figure S14a-c). Structures marked in red do not quench the excited photocatalyst, structures marked in blue were found to quench the excited photocatalyst and structures in black were not tested regarding luminescence quenching.

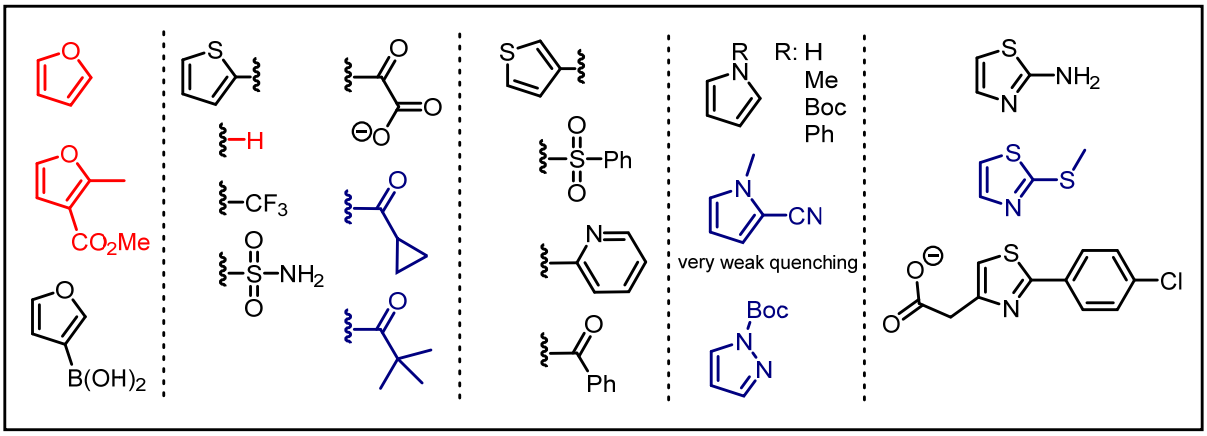

Figure S14a. Non-tolerated examined furans, thiophenes, pyrroles and thiazoles.

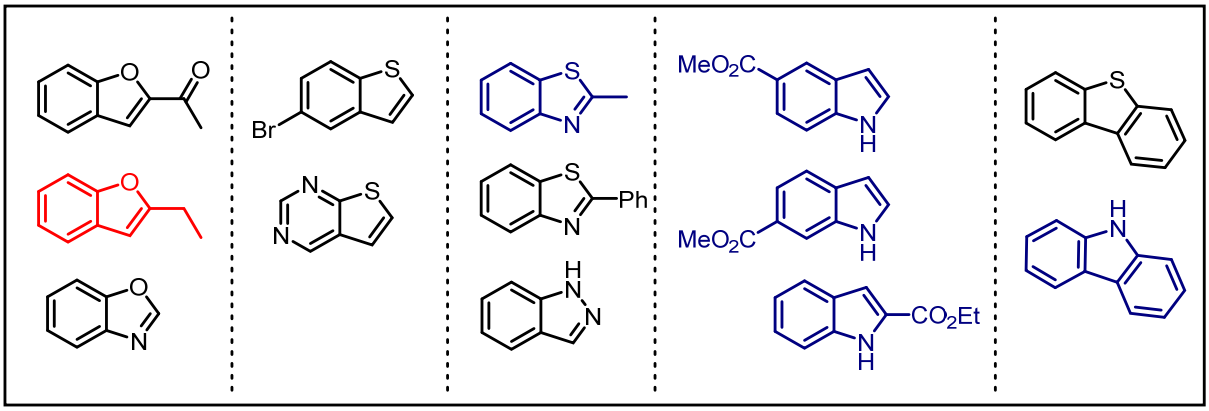

Figure S14b. Non-tolerated examined benzofurans, benzothiophenes, indoles, carbazoles and related heterocycles.

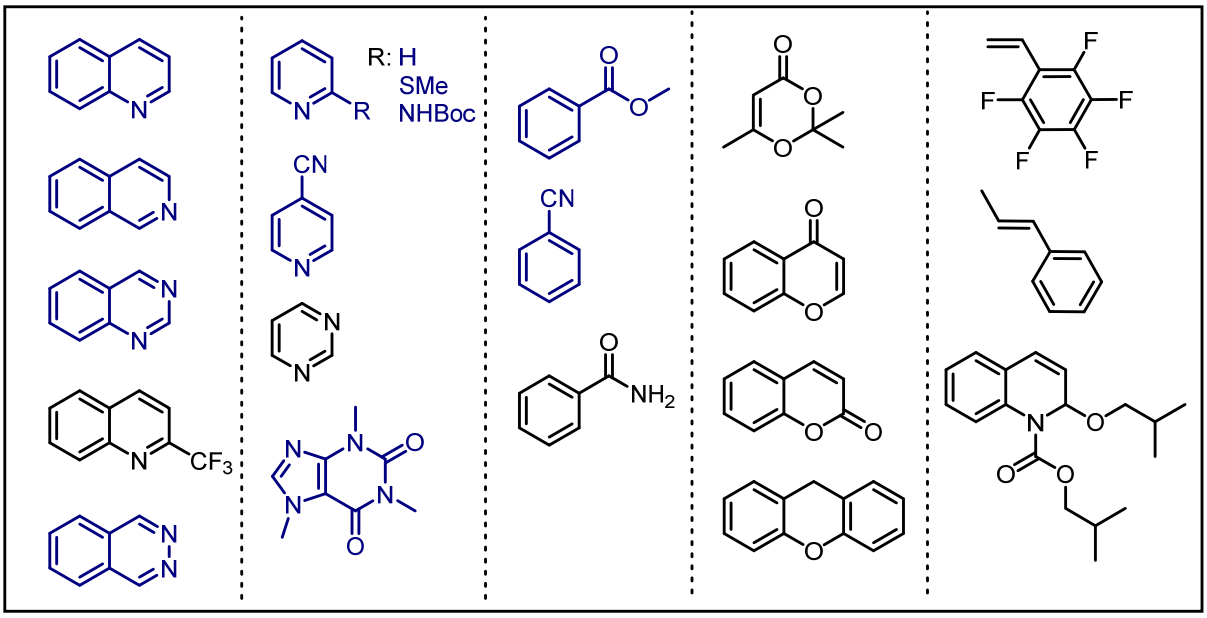

Figure S14c. Non-tolerated quinolines, pyridines, benzenes, benzopyrans, styrenes and related compounds.

8 - References

1. Müller, A., Raltschewa, M., and Papp, M. (1942). Über die Dimerisation des Isoeugenolmethyläthers (Harzphenole I). Ber. Dtsch. Chem. Ges. A *75*, 692–703.
2. Stewart, P., Renney, C.M., Mooibroek, T.J., Ferheen, S., and Davis, A.P. (2018). Maltodextrin recognition by a macrocyclic synthetic lectin. Chem. Commun. *54*, 8649–8652.
3. Miao, Q., Nguyen, T.-Q., Someya, T., Blanchet, G.B., and Nuckolls, C. (2003). Synthesis, Assembly, and Thin Film Transistors of Dihydrodiazapentacene: An Isostructural Motif for Pentacene. J. Am. Chem. Soc. *125*, 10284–10287.
4. Keller, F., and Rüchardt, C. (1998). Bimolecular formation of radicals by hydrogen transfer. 14: The uncatalyzed transfer hydrogenation of α-methylstyrene by 2,6-disubstituted 9,10-dihydroanthracenes. J. prakt. Chem. *340*, 642–648.
5. Pavlishchuk, V. V., and Addison, A.W. (2000). Conversion constants for redox potentials measured versus different reference electrodes in acetonitrile solutions at 25°C. Inorganica Chim. Acta *298*, 97–102.
6. Romero, N.A., and Nicewicz, D.A. (2016). Organic Photoredox Catalysis. Chem. Rev. *116*, 10075–10166.
7. Rehm, D., and Weller, A. (1970). Kinetics of Fluorescence Quenching by Electron and H-Atom Transfer. Isr. J. Chem. *8*, 259–271.
8. Tolbert, L.M., Nesselroth, S.M., Netzel, T.L., Raya, N., and Stapleton, M. (1992). Substituent effects on carbanion photophysics. 9-Arylfluorenyl anions. J. Phys. Chem. *96*, 4492–4496.
9. Legros, B., Vandereecken, P., and Soumillion, J.P. (1991). Electron transfer photoinduced from naphtholate anions: anion oxidation potentials and use of Marcus free energy relationships. J. Phys. Chem. *95*, 4752–4761.
10. Vásquez-Céspedes, S., Chepiga, K.M., Möller, N., Schäfer, A.H., and Glorius, F. (2016). Direct C–H Arylation of Heteroarenes with Copper Impregnated on Magnetite as a Reusable Catalyst: Evidence for CuO Nanoparticle Catalysis in Solution. ACS Catal. *6*, 5954–5961.
11. Yu, X., Park, E.-J., Kondratyuk, T.P., Pezzuto, J.M., and Sun, D. (2012). Synthesis of 2-arylindole derivatives and evaluation as nitric oxide synthase and NFκB inhibitors. Org. Biomol. Chem. *10*, 8835.
12. Discekici, E.H., Treat, N.J., Poelma, S.O., Mattson, K.M., Hudson, Z.M., Luo, Y., Hawker, C.J., and de Alaniz, J.R. (2015). A highly reducing metal-free photoredox catalyst: design and application in radical dehalogenations. Chem. Commun. *51*, 11705–11708.
13. Yamada, S., Flesch, K.N., Murakami, K., and Itami, K. (2020). Rapid Access to Kinase Inhibitor Pharmacophores by Regioselective C-H Arylation of Thieno[2,3-*d*]pyrimidine. Org. Lett. *22*, 1547–1551.
14. Pospech, J., Tlili, A., Spannenberg, A., Neumann, H., and Beller, M. (2014). Regioselective Ruthenium-Catalyzed Carbonylative Direct Arylation of Five-Membered and Condensed Heterocycles. Chem. Eur. J. *20*, 3135–3141.
15. Mäsing, F., Mardyukov, A., Doerenkamp, C., Eckert, H., Malkus, U., Nüsse, H., Klingauf, J., and Studer, A. (2015).

Controlled Light-Mediated Preparation of Gold Nanoparticles by a Norrish Type I Reaction of Photoactive Polymers. Angew. Chem. Int. Ed. *54*, 12612–12617.
16. Chen, X., Yin, Y., Tanaka, K., Kita, H., and Okamoto, K.-I. (2006). Synthesis and Characterization of Novel Sulfonated Polyimides Derived from Naphthalenic Dianhydride. High Perform. Polym. *18*, 637–654.
17. Zhang, X., Zhang, W.Z., Shi, L.L., Guo, C.X., Zhang, L.L., and Lu, X.B. (2012). Silver(I)-catalyzed carboxylation of arylboronic esters with CO_2. Chem. Commun. *48*, 6292–6294.
18. Meyers, A.I., and Higashiyama, K. (1987). Asymmetric Additions to Chiral Naphthalenes. 4. An Asymmetric Synthesis of the AB-Ring of Aklavinone. J. Org. Chem. *52*, 4592–4597.
19. Berger, P., Bessmernykh, A., Caille, J.C., and Mignonac, S. (2006). Palladium-catalyzed hydroxycarbonylation of aryl and vinyl bromides by mixed acetic formic anhydride. Synthesis *2006*, 3106–3110.
20. Nemoto, K., Yoshida, H., Egusa, N., Morohashi, N., and Hattori, T. (2010). Direct Carboxylation of Arenes and Halobenzenes with CO_2 by the Combined Use of $AlBr_3$ and R_3SiCl. J. Org. Chem. *75*, 7855–7862.
21. Mori, S., Simkhada, D., Zhang, H., Erb, M.S., Zhang, Y., Williams, H., Fedoseyenko, D., Russell, W.K., Kim, D., Fleer, N., et al. (2016). Polyketide Ring Expansion Mediated by a Thioesterase, Chain Elongation and Cyclization Domain, in Azinomycin Biosynthesis: Characterization of AziB and AziG. Biochemistry *55*, 704–714.
22. Suerbaev, K.A., Aldabergenov, M.K., and Kudaibergenov, N.Z. (2015). Carboxylation of hydroxyarens with metal alkyl carbonates. Green Process. Synth. *4*, 91–96.
23. Wang, S., Dupin, L., Noël, M., Carroux, C.J., Renaud, L., Géhin, T., Meyer, A., Souteyrand, E., Vasseur, J.-J., Vergoten, G., et al. (2016). Toward the Rational Design of Galactosylated Glycoclusters That Target Pseudomonas aeruginosa Lectin A (LecA): Influence of Linker Arms That Lead to Low-Nanomolar Multivalent Ligands. Chem. Eur. J. *22*, 11785–11794.
24. Abarbri, M., Thibonnet, J., Bérillon, L., Dehmel, F., Rottländer, M., and Knochel, P. (2000). Preparation of new polyfunctional magnesiated heterocycles using a chlorine-, bromine-, or iodine-magnesium exchange. J. Org. Chem. *65*, 4618–4634.
25. Chalker, J.M., Wood, C.S.C., and Davis, B.G. (2009). A convenient catalyst for aqueous and protein Suzuki-Miyaura cross-coupling. J. Am. Chem. Soc. *131*, 16346–16347.
26. Kaizerman, J.A., Gross, M.I., Ge, Y., White, S., Hu, W., Duan, J.X., Baird, E.E., Johnson, K.W., Tanaka, R.D., Moser, H.E., et al. (2003). DNA binding ligands targeting drug-resistant bacteria: Structure, activity, and pharmacology. J. Med. Chem. *46*, 3914–3929.
27. Dai, J.J., Xu, W.T., Wu, Y.D., Zhang, W.M., Gong, Y., He, X.P., Zhang, X.Q., and Xu, H.J. (2015). Silver-Catalyzed $C(sp^2)$-H Functionalization/C-O Cyclization Reaction at Room Temperature. J. Org. Chem. *80*, 911–919.
28. Kilbinger, A.F.M., Schenning, A.P.H.J., Goldoni, F., Feast, W.J., and Meijer, E.W. (2000). Chiral aggregates of α,ω-disubstituted sexithiophenes in protic and aqueous media. J. Am. Chem. Soc. *122*, 1820–1821.
29. Hagishita, S., Yamada, M., Shirahase, K., Okada, T., Murakami, Y., Ito, Y., Matsuura, T., Wada, M., Kato, T., Ueno, M., et al. (1996). Potent inhibitors of secretory phospholipase A2: Synthesis and inhibitory activities of indolizine and indene derivatives. J. Med. Chem. *39*, 3636–3658.
30. Frizler, M., Schmitz, J., Schulz-Fincke, A.C., and Gütschow, M. (2012). Selective nitrile inhibitors to modulate the proteolytic synergism of cathepsins S and F. J. Med. Chem. *55*, 5982–5986.
31. Podlesný, J., Pytela, O., Klikar, M., Jelínková, V., Kityk, I. V., Ozga, K., Jedryka, J., Rudysh, M., and Bureš, F. (2019). Small isomeric push-pull chromophores based on thienothiophenes with tunable optical (non)linearities. Org. Biomol. Chem. *17*, 3623–3634.
32. Baillie, S.E., Bluemke, T.D., Clegg, W., Kennedy, A.R., Klett, J., Russo, L., De Tullio, M., and Hevia, E. (2014). Potassium-alkyl magnesiates: Synthesis, structures and Mg-H exchange applications of aromatic and heterocyclic substrates. Chem. Commun. *50*, 12859–12862.
33. Shang, R., Ilies, L., and Nakamura, E. (2016). Iron-Catalyzed Ortho C-H Methylation of Aromatics Bearing a Simple Carbonyl Group with Methylaluminum and Tridentate Phosphine Ligand. J. Am. Chem. Soc. *138*, 10132–10135.
34. Paridala, K., Lu, S.M., Wang, M.M., and Li, C. (2018). Tandem one-pot CO_2 reduction by PMHS and silyloxycarbonylation of aryl/vinyl halides to access carboxylic acids. Chem. Commun. *54*, 11574–11577.
35. Kubota, K., Hayama, K., Iwamoto, H., and Ito, H. (2015). Enantioselective Borylative Dearomatization of Indoles through Copper(I) Catalysis. Angew. Chem. Int. Ed. *54*, 8809–8813.
36. Magalhães, J., Franko, N., Annunziato, G., Welch, M., Dolan, S.K., Bruno, A., Mozzarelli, A., Armao, S., Jirgensons, A., Pieroni, M., et al. (2018). Discovery of novel fragments inhibiting O-acetylserine sulphhydrylase by combining scaffold hopping and ligand–based drug design. J. Enzym. Inhib. Med. Chem. *33*, 1444–1452.
37. Bettinetti, L., Schlotter, K., Hübner, H., and Gmeiner, P. (2002). Interactive SAR studies: Rational discovery of super-potent and highly selective dopamine D3 receptor antagonists and partial agonists. J. Med. Chem. *45*, 4594–4597.
38. Takaya, J., Tadami, S., Ukai, K., and Iwasawa, N. (2008). Copper(I)-catalyzed carboxylation of aryl- and alkenylboronic esters. Org. Lett. *10*, 2697–2700.

39. Nogi, K., Fujihara, T., Terao, J., and Tsuji, Y. (2015). Cobalt- and Nickel-Catalyzed Carboxylation of Alkenyl and Sterically Hindered Aryl Triflates Utilizing CO_2. J. Org. Chem. *80*, 11618–11623.
40. Liu, R., Yang, Z., Ni, Y., Song, K., Shen, K., Lin, S., and Pan, Q. (2017). Pd(II)/Bipyridine-Catalyzed Conjugate Addition of Arylboronic Acids to α,β-Unsaturated Carboxylic Acids. Synthesis of β-Quaternary Carbons Substituted Carboxylic Acids. J. Org. Chem. *82*, 8023–8030.
41. Fogg, G.T., P. (1992). Carbon Dioxide in Non–Aqueous Solvents At Pressures Less Than 200 KPA. In IUPAC Solubility Data Series 50, J. W. Lorimer, H. L. Clever, and C. L. Young, eds. (Pergamon Press), p. 362.
42. Grimme, S., Antony, J., Ehrlich, S., and Krieg, H. (2010). A consistent and accurate ab initio parametrization of density functional dispersion correction (DFT-D) for the 94 elements H-Pu. J. Chem. Phys. *132*, 154104.
43. Becke, A.D. (1993). Density-functional thermochemistry. III. The role of exact exchange. J. Chem. Phys. *98*, 5648–5652.
44. Marten, B., Kim, K., Cortis, C., Friesner, R.A., Murphy, R.B., Ringnalda, M.N., Sitkoff, D., and Honig, B. (1996). New model for calculation of solvation free energies: Correction of self-consistent reaction field continuum dielectric theory for short-range hydrogen-bonding effects. J. Phys. Chem. *100*, 11775–11788.
45. Bochevarov, A.D., Harder, E., Hughes, T.F., Greenwood, J.R., Braden, D.A., Philipp, D.M., Rinaldo, D., Halls, M.D., Zhang, J., and Friesner, R.A. (2013). Jaguar: A high-performance quantum chemistry software program with strengths in life and materials sciences. Int. J. Quantum Chem. *113*, 2110–2142.